

Studies of Deposition on Cooled Tubes with
Special Reference to Coal-Fired Boilers.

K. R. CLIFFE.

A thesis submitted to the
University of Aston in Birmingham
for the degree of Doctor of
Philosophy.

November, 1969

130960

SUMMARY

The present work is concerned with the formation of alkali-matrix deposits on superheater tubes of coal-fired boilers arising from the combustion of high alkali content coals. The main contribution to the problem of these deposits is through mass transfer studies.

Four salts, namely sodium chloride, potassium chloride, sodium sulphate and calcium chloride were investigated in a model combustor containing a single tube. The rates of deposition to the surface of the tube and the morphology of the deposits were studied with surface temperature, concentration of vapour and mainstream velocity as parameters. Flow model studies in a wind tunnel showed that at the Reynolds numbers under investigation, a laminar boundary layer formed on the front of the tube separating to give a turbulent wake.

The deposition rates of sodium chloride and potassium chloride were found to be predicted well by a heat/mass transfer analogy for the area beneath the laminar boundary layer. The nature of the two salts was found to be temperature dependent and the fusion temperatures were up to 200°C below their respective melting points.

With sodium sulphate it was found that there was a 19% discrepancy between experimental and theoretical results calculated using a heat/mass transfer analogy for the area beneath the laminar boundary layer. The nature of the deposit was found to be dependent upon concentration as well as surface temperature. Fused deposits were obtained at temperatures up to 350°C below the melting point of the

deposits.

The observed condensation points for the three salts agreed well with previous workers' values. Deposition rates of the three salts in the turbulent wake were considerably less than was to be expected from a heat/mass transfer analogy.

The results for calcium chloride indicated that it is unlikely to play any part in the formation of alkali-matrix deposits.

ACKNOWLEDGEMENTS

The author wishes to thank Dr. B. Gay for supervision of the topic and help with preparing the thesis. He also wishes to acknowledge the valuable assistance given by Dr. R. J. Bishop, Wolverhampton College of Technology, both in producing the photographic plates and designing the apparatus. He also wishes to thank Mr. T. Langford, Wolverhampton College of Technology, for help with the construction and maintenance of the apparatus, and producing the photographic plates.

Thanks are also due to Mr. B. Vokes, Wolverhampton College of Technology, for help with the computer program for evaluating the results. The author further wishes to thank his wife for reproduction of the drawings.

Finally, he wishes to thank the British Coal Utilisation Research Industrial Laboratories who financed the project and, in particular, Mr. D. C. Davidson who made their appropriate facilities available.

List of ContentsPage
Number

	Summary.	i
	Acknowledgements.	iii
	List of Figures, Tables and Plates.	iv
	Nomenclature.	xvii
1.	<u>Introduction.</u>	1
2.	<u>Fouling Characteristics of Coal.</u>	3
2.1	Bonded Deposits in Boilers.	3
2.1.1	Occurrence of Alkalis and Chlorine in Coal.	3
2.1.2	Nature of Deposit.	4
2.1.3	Problems caused by Alkali-Matrix Deposits.	13
2.1.4	Theories Predicting Fouling Characteristics of Coal.	14
3.	<u>Transport Phenomena in Deposition.</u>	18
3.1	Aerodynamic Conditions around Boiler Tubes.	18
3.1.1	Operating Conditions in a Boiler.	18
3.1.2	Aerodynamic Conditions around a Single Tube.	18
3.2	Initial Stages of Deposition.	19
3.2.1	Theories of Deposition.	19
3.2.2	Mechanisms of Deposition.	20
3.2.2.1	Inertial Impaction.	21
3.2.2.2	Concentration Diffusion.	23
3.2.2.3	Thermal Diffusion.	31
3.2.2.4	Electrostatic Precipitation.	35
3.3	Methods for Determining Deposition Rates.	36
3.3.1	General Approach.	37
3.3.2	Calculation of Concentration Diffusion Rates through a Laminar Boundary Layer.	37
3.3.2.1	Use of Heat/Mass Transfer Analogy.	37
3.3.2.2	More Exact Methods.	39
3.3.3	Estimation of Magnitude of Thermal Diffusion.	41

3.4	Heat Transfer to a Tube in Cross-Flow.	42
3.4.1	Heat Transfer to a Single Tube under Channel Blockage Conditions.	42
3.4.1.1	Average Heat Transfer Coefficients.	42
3.4.1.2	Local Heat Transfer Coefficients.	44
3.4.2	Effect of Turbulence on Heat Transfer.	44
3.4.2.1	Intensity of Turbulence.	44
3.4.2.2	Scale of Turbulence.	47
3.4.3	Corrections for High Temperature Difference.	48
3.5	Calculation of the Alkalis released from the Combustion of Coal.	49
4.	<u>Reappraisal of the Deposition Problem.</u>	51
4.1	Previous Research.	51
4.2	An Experimental Programme.	53
5.	<u>Design and Construction of Combustor.</u>	57
5.1	Description of Combustor.	57
5.1.1	Design Criteria.	57
5.1.2	Design Calculations.	58
5.1.3	Input to the Combustion Chamber.	60
5.1.3.1	Air.	60
5.1.3.2	Town Gas.	60
5.1.3.3	Propane.	60
5.1.3.4	Salt.	61
5.1.4	Combustion Chamber and Intermediate Duct.	63
5.1.5	Target Section.	63
5.1.6	Exhaust Section.	64
5.1.7	Instrumentation.	65
5.1.7.1	Temperature Measurement.	65
5.1.7.2	Flow Measurement.	66
5.1.7.3	Analysis of Flue Gases.	66

6.	<u>Flow Model Studies.</u>	69
6.1	Experimental Method.	69
6.1.1	Consideration of Similarity.	69
6.1.2	Apparatus.	69
6.1.2.1	General Arrangement of Flow Model.	69
6.1.2.2	Measurement of Air Flow Rates.	70
6.1.2.3	Measurement of Static Pressure.	70
6.2	Experimental Runs.	70
6.2.1	Pressure Distribution Test Runs.	70
6.2.2	Effect of Surface Roughness upon Static Pressure Distribution around a Tube.	70
6.3	Results.	71
6.3.1	Variation of Static Pressure at the Tube Surface with Angular Position.	71
6.3.2	Calculation of the Dimensions of the Velocity Boundary Layer.	71
6.3.3	Calculation of Separation Point.	75
7.	<u>Combustor Tests.</u>	76
7.1	Preliminary Test on the Combustor.	76
7.1.1	Variation of Oxygen and Carbon Dioxide Concentrations.	76
7.1.2	Transverse and Longitudinal Variation of Temperature in the Settling and Target Sections.	76
7.1.3	Peripheral Variation in Surface Temperature.	77
7.1.4	Effect of Ceramic Coating upon Surface Temperature.	77
7.1.5	Difficulties of Vaporisation.	78
7.1.6	Reactions of Sodium Chloride with Combustor Walls.	78
7.1.7	Separation Lines.	78
7.2	Description of Tests.	79

7.2.1	Conditions Investigated.	79
7.2.2	Test Procedure.	81
7.2.3	Sampling Procedure.	82
8.	<u>Results of Combustor Tests.</u>	84
8.1	Deposition of Sodium and Potassium Chlorides.	84
8.1.1	Under Conditions of Incomplete Vaporisation.	84
8.1.2	Under Conditions of Complete Vaporisation.	84
8.1.2.1	Effect of Run Duration upon Deposit Weight.	84
8.1.2.2	Effect of Variation of Surface Temperature, Gas Velocity and Concentration of Salt Vapour.	85
8.1.2.3	Condensation Points.	88
8.1.3	Analysis of Deposits.	88
8.2	Deposition of Sodium Sulphate.	92
8.2.1	Effect of Run Duration upon Deposit Weight.	92
8.2.2	Effect of Variation of Surface Temperature, Gas Velocity, and Concentration of Salt Vapour.	92
8.2.3	Condensation Points.	96
8.2.4	Analysis of Deposits.	96
8.3	Deposition of Calcium Chloride.	98
8.3.1	General Characteristics.	98
9.	<u>Discussion of Results.</u>	102
9.1	Deposition of Sodium Chloride and Potassium Chloride.	102
9.1.1	Deposition by Impaction and Diffusion.	102
9.1.2	Deposition by Diffusion.	102
9.1.3	Physical Characteristics of Deposited Salt.	106
9.2	Deposition of Sodium Sulphate.	110
9.2.1	Difficulties of Vaporisation.	110
9.2.2	Deposition by Diffusion.	110
9.2.3	Physical Characteristics of Deposited Salt.	111

9.3	Calcium Chloride.	112
10.	<u>Conclusions.</u>	115
	References.	118
Appendix 1	Calculation of the Range of Velocities possible in the Target Section.	124
Appendix 2	Formulae for Computer Programme.	127
Appendix 3	Method for Calculating the Dimensions of the Laminar Boundary Layer.	131
Appendix 4	Method for Calculating the Separation Point.	134
Appendix 5	The Contribution of Thermal Diffusion to the Total Mass Transfer through the Laminar Boundary Layer.	135
Appendix 6	Solution of the Boundary Layer Equations for Mass Transfer when Vapour Diffusion is the Sole Mechanism of Transfer.	141
Appendix 7	Theoretical Calculation of the Mass Transfer Rate for Sodium Chloride, Potassium Chloride and Sodium Sulphate.	149
Appendix 8	Results.	162

Figure Number	<u>List of Figures</u> Title	Position in Text, following Page Number
2.1	Four Zones of a Boiler Tube.	7
2.2	Section through a Corroded Boiler Tube.	12
3.1	Flow Conditions in a Staggered Tube Bank.	17
3.2	Flow Conditions around a Tube at a Reynolds Number of 3,500.	17
3.3	Concept of Impaction Efficiency.	20
3.4	Variation of Impaction Efficiency with Particle Parameter.	21
3.5	Average Blockage Corrections of Reynolds Numbers for Tube Blockage in a Channel.	43
3.6	Comparison of Heat Transfer Data for a Single Tube in Cross-Flow.	44
3.7	Stagnation Point Heat Transfer Coefficients against Corrected Reynolds Number for varying Turbulence Intensities.	46
5.1	Internal Dimensions of Combustor.	57
5.2	Input to Combustor.	59
5.3	Cross-Section of Burner.	60
5.4a	Original Design of Probe.	61
b	Modified Design of Probe.	61
5.5	General Arrangement of Combustor.	62
5.6	Target Tube Assembly.	62
5.7	Enlarged Diagram of the End Section of the Combustor.	64
5.8	Calibration Graph for Thermocouple	

Figure Number	Title	Position in Text, following Page Number
5.8	(Continued) Measuring Temperature of Main Gas Stream.	64
5.9	Calibration Graph for the Pitot Tube.	65
6.1	Flow Model in Wind Tunnel (Photograph).	68
6.2	Variation in Static Pressure at Tube Surface with Angular Position.	70
6.3	Variation in Static Pressure at Tube Surface with Angular Position for Extreme Sizes of Grit Paper used.	70
6.4	Velocity at Edge of Boundary Layer versus Distance along Tube from Forward Stagnation Point.	72
6.5	Relationship between Reynolds Number and Distance from Stagnation Point.	74
7.1	Temperature Profiles across Combustor.	75
7.2	Longitudinal Variation of Temperature along Central Axis of Combustor.	75
7.3	Peripheral Temperature Distributions at Surface of Target Tube.	76
7.4	Flow Separation Line (Photograph).	77
8.1	Molten Streaks of Sodium Chloride (Photograph).	83
8.2	Variation of Deposition Rate with Surface Temperature (Incomplete Vaporisation).	83
8.3	Dependence of Deposit Weight upon Time of Exposure.	

Figure Number	Title	Position in Text, following Page Number
8.3	(Continued)	
	a. Sodium Chloride.	83
	b. Potassium Chloride.	83
8.4	Dendrites of Sodium Chloride (Photograph).	
	a. Plan View.	84
	b. Side View.	84
8.5	Elongate Crystals of Sodium Chloride, Plan View (Photograph).	84
8.6a	Partially Disturbed Deposit of Elongate Crystals of Sodium Chloride (Photograph).	84
b	Two Elongate Crystals from the Deposit (Shown in Fig. 8.6a). (Photograph).	84
8.7	Fused Deposit of Sodium Chloride with Crystallisation occurring (Photograph).	84
8.8	Dendrites of Sodium Chloride growing within the Area beneath the Turbulent Wake (Photograph).	85
8.9	Dendrites of Potassium Chloride, Plan View (Photograph).	85
8.10	Elongate Crystals of Potassium Chloride, Plan View (Photograph).	85
8.11	Variation of Deposition Rate with Surface Temperature.	
	a. Sodium Chloride Concentration, 0.055 torr.	86
	b. Sodium Chloride Concentration, 0.110 torr.	86

Figure Number	Title	Position in Text, following Page Number
8.11	(Continued)	
	c. Sodium Chloride Concentration, 0.250 torr.	86
8.12	Variation of Deposition Rate with Surface Temperature.	
	a. Potassium Chloride Concentra- tion, 0.035 torr.	86
	b. Potassium Chloride Concentra- tion, 0.065 torr.	86
	c. Potassium Chloride Concentra- tion, 0.125 torr.	86
	d. Potassium Chloride Concentra- tion, 0.250 torr.	86
8.13	Dependence of Deposit Weight upon Time of Exposure, Sodium Sulphate.	91
8.14	Deposit of Sodium Sulphate Collected when Impaction was occurring (Photograph).	91
8.15	Dendrites of Sodium Sulphate, Plan View (Photograph).	91
8.16	Variation of Deposition Rate with Surface Temperature.	
	a. Sodium Sulphate Concentration, 0.0055 torr.	95
	b. Sodium Sulphate Concentration, 0.0110 torr.	95
8.17	Dependence of Deposit Weight upon Time	

Figure Number	Title	Position in Text, following Page Number
8.17	(Continued) of Exposure, Calcium Chloride.	97
8.18	Dendrites of Calcium Chloride (Photograph).	97
8.19	Variation of Deposition Rate with Surface Temperature.	
	a. Concentration of Calcium Chloride, 0.007, 0.014 torr.	97
	b. Concentration of Calcium Chloride, 0.030, 0.056 torr.	97
9.1	Vapour Pressure of the Four Salts Investigated as a Function of Temperature.	109
A.1.1	Velocity of Flue Gases in the Target Section at 1,100°C against Nett Heat with Excess Air and Propane Feed Rate as Parameters.	123
A.6.1	Control Volume enclosing the Phase Interface.	142

List of Tables

Table Number	Title	Page Number
2.1	Variation of Alkalis in a Selection of Mainly East Midlands Coals as used by Bishop (1967).	5
2.2	Variation of Alkalis in a Selection of Coals.	6
2.3	Average Enrichment Ratios of Sodium and Potassium in Deposits formed from Burning Coals given in Table 2.1.	10
2.4	Compounds Identified in Deposits Formed from Burning the Coals given in Table 2.1.	11
3.1	Target Efficiencies of Various Size Fractions of Fly-Ash from Cliff-Quay Power Station.	24
6.1	Variation in Static Pressure at Tube Surface with Angular Position.	72
6.2	Quantities derived during calculation of the Thickness of the Boundary Layer.	74
8.1	Determined Condensation Points for Sodium Chloride.	89
8.2	Determined Condensation Points for Potassium Chloride.	90
8.3	Comparative Analysis of Injected Salts and Deposit.	93
8.4	Fusion Temperatures at the Concentrations Investigated.	95
8.5	Determined Condensation Points for Sodium Sulphate.	97

Table Number	Title	Page Number
8.6	Comparative Analysis of Injected Salt and Deposit.	99
8.7	Analysis of Deposits from Injection of Calcium Chloride into Combustor.	101
9.1	Comparison with the Results of Jackson & Duffin.	109
9.2	The Crystalline Forms of Sodium Sulphate.	113
A.5.1	The Amount of Mass Transferred by Thermal Diffusion compared with that Transferred by Concentration Diffusion for the Salts Sodium Chloride, Potassium Chloride and Sodium Sulphate.	139
A.5.2	The Amount of Energy Transferred due to Mass Transfer compared with that Transferred due to Heat Transfer for the Salts Sodium Chloride, Potassium Chloride and Sodium Sulphate.	140
A.7.1	Diffusivities of the Three Salts as a Function of Temperature.	151
A.7.2	Evaluation of the Conductance 'g' as a Function of Surface Temperature and Gas Velocity.	153
A.7.3	(a) Evaluation of the Driving Force 'B' as a Function of Surface Temperature for Sodium Chloride.	157
	(b) Evaluation of the Driving Force 'B' as a Function of Surface Temperature for Potassium Chloride.	158

Table Number	Title	Page Number
A.7.3	(Continued)	
	(c) Evaluation of the Driving Force 'B' as a Function of Surface Temperature for Sodium Sulphate.	159
	(d) Evaluation of the Driving Force 'B' as a Function of Surface Temperature for Potassium Chloride.	160

NOMENCLATURE

<u>Symbol</u>	<u>Significance</u>	<u>Dimensions</u>
A	Cross-sectional area of duct	L^2
A_{mean}	Arithmetic mean cross-sectional area of duct	L^2
A_0	Constant used in defining a_p , see equation 3.8.	-
B	Mass transfer driving force, see equation 3.28.	-
B_a	Mass transfer driving force at any point in the boundary Layer, see equation 3.33.	-
B_0	Constant used in defining a_p , see equation 3.8.	-
C	Constant, see appendix 6.	-
C_D	Drag coefficient.	-
C_0	Constant used in defining a_p , see equation 3.8.	-
$D_{1,2}$	Molecular diffusivity.	$L^2 t^{-1}$
D_T	Thermal diffusivity.	$L^2 t^{-1}$
E	Correction factor for atmospheric pressure, see appendix 2.	-
E_p	A correction function, see equation A 3.2.	-
F	Thermal diffusive force on a particle.	MLt^{-2}
F_b	A function representing the growth rate of momentum thickness, $\frac{u_g}{\nu} \frac{d\delta_b^2}{dx}$	-
F_Δ	A function representing the growth rate of conduction thickness, $\frac{u_g}{\nu} \frac{d\Delta^2}{dx}$	-

<u>Symbol</u>	<u>Significance</u>	<u>Dimensions</u>
G	Mass flow rate	$ML^{-2}t^{-1}$
H_a	Ratio of thermal diffusion flux to concentration diffusion flux.	-
H_b	Ratio of heat energy due to mass transfer with that due to heat transfer.	-
I	Impact number, see equation 3.2.	-
J	Unit force, an additional term arising from the average balance of forces in the laminar boundary layer, see equation 3.44.	Lt^{-2}
K	Boltzmann constant.	$ML^2t^{-2}T^{-1}$
K_a	Measure of the inertia of a particle, $\frac{\rho_1 d_1^2 u}{\mu d_c}$	-
L	Scale of turbulence, see equation 3.45.	-
M	Molecular weight	-
M_{air}	Molecular weight of air, see appendix 7.	-
M_{salt}	Molecular weight of salt, see appendices 2 and 7.	-
N	Exponent.	-
N_{Le}	Lewis number, $\frac{\text{Prandtl number}}{\text{Schmidt number}}$	-
N_{Pr}	Prandtl number, $\frac{c\mu}{k}$	-
N_{Re}	Reynolds number, $\frac{du\rho}{\mu}$	-
N_{Sc}	Schmidt number, $\frac{\mu}{\rho D_{1,2}}$	-
N_{st}	Stanton number, $\frac{h}{u\rho c}$	-
P	Pressure	$ML^{-1}t^{-2}$

<u>Symbol</u>	<u>Significance</u>	<u>Dimensions</u>
$P_a, P_b, P_c,$ P_{salt}	Pressure measurements, see appendix 2.	$M L^{-1} t^{-2}$
Q	Collision integral obtained when transport coefficients are expressed in terms of the Sonine polynomial expansion coefficient.	-
Q_1, Q_2 Q'	Functions of the collision integral. A factor analogous to the collision integral dependent on the collision pattern.	-
$Q_I, Q_{Prop},$ $Q_{Air}, Q_{Solvent},$ Q_{Salt}, Q_{Total}	Flow rates, see appendix 2.	$L^3 t^{-1}$
$R(y)$	A correlating coefficient, see equation 3.46.	-
S_1, S_2	Functions of the collision integral, see equation 3.17.	-
T	Temperature.	T
T_a, T_b, T_c	Temperature measurements, see appendix 2.	T
V V_{salt}	Molecular Volume. Volume fraction of salt vapour in wet flue gases.	L^3
W	Height of duct.	L
X	Mole concentration in condensed phase.	-
Y	Mole concentration in vapour phase.	-
Z	Intensity of Turbulence, see equation 3.43.	-
a_a	Constant, see equation 3.6.	-

<u>Symbol</u>	<u>Significance</u>	<u>Dimensions</u>
a_b	Constant, see equation 3.8.	-
a_c	Constant, see equation 3.13.	-
a_d	Constant, see equation 3.22.	-
a_e	Constant, see equation 3.32.	-
a_f	Constant, see equation 3.38.	-
a_g	Constant, see equation A.1.3.	-
a_h	Constant, see equation A.1.2.	-
a_i	Constant, see equation A.1.3.	-
a_j	Constant, see equation A.1.2.	-
a_k	Constant, see equation A.1.5.	-
a_m	Constant, see equation A.1.5.	-
a_n	Constant, see equation A.1.8.	-
a_o	Constant, see equation A.1.8.	-
b	Conserved property either mass or enthalpy.	-
c	Specific heat capacity.	$L^2 t^{-2} T^{-1}$
d	Diameter.	L
d'	Limiting width of the flow lines between which all particles collide with the tube.	L
d_{12}	Collision diameter.	L
e	Constant, see equation A.3.2.	-
e_x	Percentage excess air, see appendix 1.	-
$f()$	Function of.	-
g	Gravitational constant.	$L t^{-2}$
g_i	Mass transfer conductance, see equation A.7.11.	$ML^{-2} t^{-1}$
g_h	Heat transfer conductance, see equation A.7.16.	$ML^{-2} t^{-1}$

<u>Symbol</u>	<u>Significance</u>	<u>Dimensions</u>
h	Heat transfer coefficient.	$Mt^{-3}T^{-1}$
Δh	Water differential across orifice, see appendix 2.	L
i	Enthalpy.	ML^2t^{-3}
i_{gas}	Nett enthalpy of combustion gases, see appendix 1.	ML^2t^{-3}
j	Constant, see equation A.3.2.	-
k	Thermal conductivity.	$MLt^{-3}T^{-1}$
k_T	Thermal diffusion ratio, see equation 3.15.	
l_{Pr}	Prandtl mixing length, see equation 3.12.	L
m	Mass.	M
m_1, m_2	Mass concentration of substances 1,2 in a mixture.	
\dot{m}	Mass flux.	$ML^{-2}t^{-1}$
n	Number density, the number of particles per unit volume.	
p	Vapour pressure.	$ML^{-2}t^{-2}$
q	Mobility, $\frac{kT}{D_{1,2}}$	Mt^{-2}
r	Radius.	L
s	The fraction of gas molecules whose collisions with larger molecules are diffuse but elastic, Mason-Chapman collision pattern.	-
t	The fraction of gas molecules whose collisions with larger molecules are diffuse and inelastic, Waldmann collision pattern.	-

<u>Symbol</u>	<u>Significance</u>	<u>Dimensions</u>
u	Velocity in x-direction.	Lt^{-1}
v	Velocity in y-direction.	Lt^{-1}
w	Velocity in z-direction.	Lt^{-1}
$\bar{u}, \bar{v}, \bar{w}$ u', v', w'	Time average of the three fluctuating velocity components, u', v', w' .	$L^2 t^{-2}$
x, y, z	Rectangular coordinates.	L
Γ	Thermal exchange coefficient, $\frac{k}{c}$.	$ML^{-1}t^{-1}$
Δ	Conduction thickness, $\frac{k}{h}$.	L
Λ	Shape factor for laminar flow, $\frac{\delta^2}{\nu} \frac{du}{dx}$	-
ξ	Stream function defined by $u = \frac{\partial \xi}{\partial x}$ and $v = \frac{\partial \xi}{\partial y}$.	$L^2 t^{-1}$
Ω	Distance coordinate, $y \left[\left(\frac{du_g}{dx} \right) \left(\frac{1-N/2}{\nu} \right) \right]^{\frac{1}{2}}$	-
ψ	Prandtl or Schmidt number, see equation 3.32.	-
α	Thermal diffusion factor, see equation 3.16.	-
γ	Mass exchange coefficient, $\rho D_{1,2}$.	$ML^{-1}t^{-1}$
δ	Boundary layer thickness.	L
δ_a	Displacement thickness, $\int_0^\infty \left(1 - \frac{u \rho}{u_\infty \rho_\infty} \right) dy$.	L
δ_b	Momentum thickness, $\int_0^\infty \frac{\rho u}{\rho_\infty u_\infty} \left(1 - \frac{u}{u_\infty} \right) dy$	L
$\epsilon_{1,2}$	Energy of molecular interaction.	$ML^2 t^{-2}$
η	Efficiency of interception, see equation 3.1.	-
ζ	A dimensionless stream function, ξ / u_g $\sqrt{\left[\frac{du_g}{dx} \left(\frac{1-N/2}{\nu} \right) \right]}$	-

<u>Symbol</u>	<u>Significance</u>	<u>Dimensions</u>
θ	Angle from forward stagnation point.	-
λ	Mean free path.	L
μ	Absolute viscosity.	$ML^{-1}t^{-1}$
ν	Kinematic viscosity.	L^2t^{-1}
ρ	Density.	ML^{-3}
ϕ	Parameter used by Langmuir and Blodgett, $\frac{g}{4} \cdot \frac{\rho^2 d_c u}{\mu \rho}$	-
φ	Either Γ or γ .	$ML^{-1}t^{-1}$
σ	Molecular diameter.	L
ω	Second order corrections in the Chapman-Enskog kinetic theory.	-

Subscripts

<u>Symbol</u>	<u>Significance</u>	<u>Dimensions</u>
c	Based on tube.	-
g	The state at the local main stream condition.	-
h	In the presence of heat transfer.	-
i	In the presence of mass transfer.	-
m	Arithmetic mean value.	-
o	At the phase interface immediately before the substance has changed phase.	-
t	The state in the transferred state just beyond the phase boundary.	-
v	In the vapour phase.	-

SECTION 1

Introduction

As the efficiency of pulverised coal-fired boilers is of great importance in the present-day competition between fuels, the periods for which the boiler is out of service are of considerable significance.

Boilers have to be taken out of service because of :-

- (a) The 'bridging effect' between the tubes caused by deposits growing out from the surface and joining.
- (b) A corroded tube.

Both these phenomena are caused by the mineral matter in the coal depositing onto the tube surface.

The main type and most troublesome of these deposits arising from the combustion of coal is called an alkali-matrix. Although the chemical and physical characteristics of such deposits are extremely complicated, the deposits can be conveniently visualised as fine-grained aggregates of inert particulate matter, (comprising alumino-silicates, quartz, iron oxides, glass etc.) bonded by a cementing matrix rich in normal and complex sulphates of sodium, potassium and calcium. It is this bonding matrix which is thought to be the cause of corrosion, and bridging, by cementing the particles together. The chemical and physical aspects of these deposits have been the subject of the majority of previous research into deposit formation, while relatively little attention has been given to the mode of transport of the depositing material from the bulk gas stream to the tube surface. Hence it is considered appropriate to reappraise the problem of boiler fouling and to devise an experimental approach which would :-

- (a) Widen our understanding of the mechanism of deposition involved, and
- (b) provide quantitative data on the deposition rates of the alkali-metal salts to the tube surface which are likely to be of use to the operators and designers of boilers using deposit-forming fuels.

SECTION 2

Fouling Characteristics of Coal

2.1 Bonded Deposits in Boilers

2.1.1 Occurrence of Alkalies and Chlorine in Coal

The quantity and mode of occurrence of the alkali cations sodium, potassium and calcium, and of sulphur and chlorine in coals, is believed to be the prime factor in the formation of alkali-matrix deposits. Sulphur occurs in pyritic and organic forms in coal, and during combustion, appears as sulphur oxides in the gaseous phase.

As the sodium content is not wholly water-soluble it has been proposed that sodium is associated partly with the chlorine in the coal substance and partly with ash-forming constituents (Crumley & McCamley 1958). Using statistical analysis of data for East Midland coals, these workers demonstrated that potassium is almost entirely associated with adventitious shales (complex alumino-silicates). Confirmation of this relationship is given by Bishop, Cliffe & Langford (1967) who plotted the mean potassium contents of various coals used in deposition studies in a pilot-scale combustor against the corresponding ash values. The reasonable agreement between the results and the original curve of Crumley & McCamley shows that a direct relationship between potassium and ash contents is not confined to coals from the East Midlands and is probably true for most British coals. It is also probable that calcium occurs in the form of alumino-silicates though this has not been confirmed.

The amounts of these substances found in coals vary considerably from coalfield to coalfield. Tables 2.1 and 2.2 give an indication of this variation and the proportion of

these elements that are present. Table 2.1 shows a comparison of mainly East Midland coals, as selected by Bishop (1967). These coals were originally selected for as varied an ash/S/Cl content as possible.

Daybell (1967), Durie (1963), and Boll & Patel (1960) have also given analyses of coal. Table 2.2 shows a selection of their results. Daybell was concerned with coals in the East Midland and Leicestershire coalfield, Durie with Australian Brown Coals, while Boll & Patel dealt with central Illinois coals.

In both Tables 2.1 and 2.2, the ash content has been included to give an idea of the relative proportions of solid material going into the combustion products. It should be pointed out that some of the highest and lowest chlorine, sulphur and alkali content coals have been selected from the extensive results of Daybell, while Table 2.1 contains average colliery figures, (extremely high or low chlorine, sulphur and alkali content seams can be found in collieries where the average content is much different).

2.1.2 Nature of Deposit

As mentioned in the introduction, the type of deposit that forms the subject of this thesis is classified as alkali-matrix.

This type of deposit is the most troublesome one to be found on the fireside of boilers and consists essentially of fly-ash particles bonded together with sodium and potassium sulphates. However, with Australian Brown Coal deposits, calcium sulphate (found in the form of anhydrite) seems to be one of the bonding materials (Proctor & Taylor 1966). Anhydrite has also been found in British coal deposits by

Coal	Ash Content	Calcium	Sodium	Potassium	Chlorine	Sulphur
Ollerton	6.9	0.206	0.2	0.1	0.62	1.1
Langwith	6.8	0.165	0.1	0.1	0.29	2.4
Rothwell	23.7	0.466	0.2	0.7	0.22	3.5
Hem Heath	16.2	0.635	0.2	0.2	0.7	2.6
High Ash Thoresby	17.9	0.73	0.3	0.5	0.83	1.2
Low Ash Thoresby	5.0	0.25	0.26	0.04	0.9	0.9
Birch Coppice	10.8	0.208	0.07	0.12	0.1	4.3
Welbeck	22.7	0.83	0.3	0.6	0.74	1.0

Table 2.1

Variation of Alkalis in a Selection of Mainly East Midlands

Coals as used by Bishop (1967)

(% by weight)

Coal	Ash	Calcium	Sodium	Potassium	Chlorine	Sulphur
Leicester-shire	5.8	Analysis not carried out	0.184	0.890	0.320	Analysis not carried out
Leicester-shire	27.5	Analysis not carried out	0.062	0.030	0.130	Analysis not carried out
Notts & N. Derby	8.6	Analysis not carried out	0.044	0.154	0.056	1.86
Notts. & N. Derby	1.7	Analysis not carried out	0.261	0.000	0.943	0.000
Pana (American)	12.1	Analysis not carried out	0.46	0.191	0.66	4.5
Wright (American)	11.4	Analysis not carried out	0.03	0.21	0.01	4.9
Morwell (Austrian)	4.5	0.48	0.34	0.00	0.27	1.02
Yallown (Austrian)	1.6	0.13	0.06	0.00	0.07	0.18

Table 2.2

Variation of Alkalis in a selection of coals

(% by weight)

Bishop (1967), using X-ray analysis on the water soluble portion of the deposits. For a compound to be detected by X-ray analysis, it must be present in an amount greater than 5% by weight. As alkali and alkali earth salts are more loosely bonded than other compounds in coal, then they will dissolve preferentially in water, so giving a more concentrated solution. Hence, it means that the anhydrite found by Bishop was in an amount less than 5% of the deposit, but greater than 5% of the water soluble portion.

In boilers, these deposits were found to be mostly reddish brown in colour and had a layered structure with an inner layer yellowish white in colour up to $\frac{1}{4}$ " thick. Analysis of these deposits showed them to be mainly composed of complex aluminosilicates and iron oxides.

However, it is difficult to obtain a true analysis of the deposits, because

- (a) The varying conditions under which a boiler is fired.
- (b) Analysis techniques are not sensitive for detecting compounds.
- (c) Alkalis react slowly with the fly ash so there is little chance of them being found in boiler deposits. This is why deposits obtained from boilers are termed "fossil deposits".

One factor that did emerge from analyses of boiler deposits was that the inner layer was found to be richer in alkalis than the outer one, which suggested that the initial deposition process was the most important. (The higher the alkali content, the more severe the deposit, as regards corrosion and bridging the tubes). This led Bishop (1966) & Bishop, Cliffe & Langford (1967) to study the initial deposits

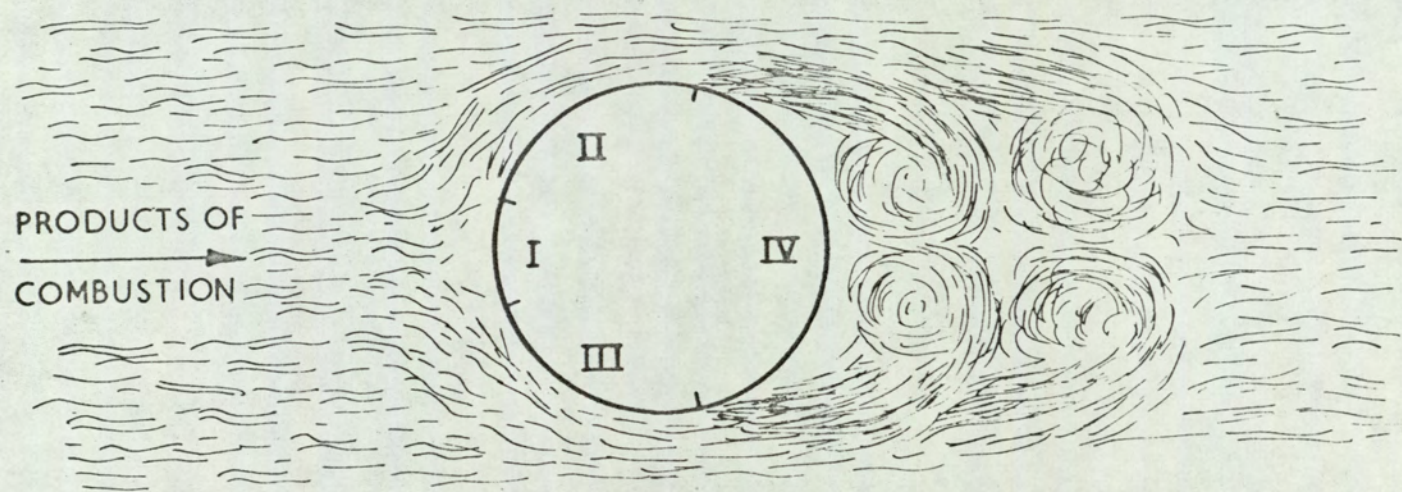


FIG 2-1 FOUR ZONES OF A BOILER TUBE (BISHOP 1966)

from burning those coals mentioned in Table 2.1 under controlled conditions in a pilot scale combustor, burning at the rate of 10 kg/hr.

It is proposed to discuss these results in some detail, as they provide an indication of the chemical and physical nature of the initial deposit, with reference to sodium and potassium salts.

Bishop collected deposits on a 5.1 cm. O.D. tube, which could be split up into four zones circumferentially according to the amount of deposit present as shown in Fig. 2.1. The deposit on Zone I was found to be mainly composed of fly-ash, with a particle size range from 10 - 100 microns. This material was loosely adhering and could easily be brushed off, leaving clear boundaries with Zones II and III. This area is where the majority of the fly-ash impacts, so preventing any alkalis from condensing on to the surface.

The deposit on Zones II and III consisted of a tenacious layer of material, covered with a thin layer of fly-ash. The majority of the particles in the tenacious layer were generally less than 1 micron in size. Between these Zones and Zone IV, were marked separation lines due to the aerodynamical conditions around the tube (see Section 3.1). On Zone IV, the deposit was similar to that on Zones II and III. However, the weight of deposit was considerably less, under a third of the total weight of Zones II and III.

The chemical analysis of the deposit from Zone I showed little or no alkali enrichment, mainly because it was fly-ash. Analysis of deposits from Zones II, III and IV showed that there was an enrichment of sodium and potassium compared with amounts present in laboratory prepared ash. However, it was

surprising to find that there was no enrichment of calcium in the deposits. Table 2.3 shows the average enrichment ratio for sodium and potassium obtained with each coal.

From Table 2.3, it will be noticed that for low-ash Thoresby, two layers are indicated, also that enrichment ratios for the primary layer are far greater than for any other coal. With this coal, a dark brown glossy fused layer of deposit was observed close to the surface, which was termed the primary layer, and on top of this layer was an unfused less tenacious secondary layer. Incidentally, no primary layer was observed with the other coals tried.

Analysis of the primary layer showed the following amounts of alkali salts to be present, assuming that all the chlorine was combined as sodium chloride, and that all potassium was combined as sulphate.

Sodium sulphate	51 - 55 %
Sodium chloride	5 - 8 %
Potassium sulphate	8 - 9 %

This assumption had to be made because chemical analysis of deposits only gave the cations and anions present. X-ray analysis had to be used to determine which compounds were present. Table 2.4 gives a list of compounds found in deposits from which it will be noticed that potassium salts were not found in deposits even on low ash Thoresby, which means that if they were present, there was less than 5%. Also anhydrite was found in the water soluble portion of the deposits of certain coals. Water soluble samples were not taken for low ash Thoresby deposits.

Anhydrite has also been observed in British boiler deposits by other workers. Carlile (1952) noted that some

COAL	ENRICHMENT RATIO ^x			
	Potassium		Sodium	
	Primary Layer	Secondary Layer	Primary Layer	Secondary Layer
Low-Ash Thoresby	5.0	3.8	4.0	2.4
	Total		Total	
Ollerton	2.9		3.0	
Langwith	1.3		2.3	
Rothwell	1.0		2.0	
Hem-Heath	1.5		2.4	
High-Ash Thoresby	2.5		3.2	
Birch Coppice	1.8		1.7	
Welbeck	2.5		3.1	

^x Enrichment ratio is defined as the amount of Alkali cation in the deposit compared with that in a sample of laboratory prepared ash.

Table 2.3

Average Enrichment Ratios of Sodium and Potassium
in Deposits formed from burning coals given in Table 2.1

Coal	Compounds Formed
Ollerton	Mullite, Fe_2O_3 , Na_2SO_4
Langwith	Fe_2O_3 , Fe_3O_4
Rothwell	Mullite, Fe_2O_3
Hem Heath	Mullite, Fe_2O_3 , Anhydrite (water soluble)
High-Ash Thoresby	Mullite, quartz, Anhydrite (water soluble)
Low-Ash Thoresby	Fe_2O_3 , Na_2SO_4 , NaCl
Birch Coppice	Mullite, Fe_2O_3 , Anhydrite (water soluble)
Welbeck	Mullite, quartz, Anhydrite (water soluble)

Table 2.4

Compounds Identified in Deposits Formed from
Burning the Coals given in Table 2.1

deposits appear to be bonded by calcium sulphate rather than by sodium and potassium sulphate. Grumley et al (1955) supported this and provided the following extreme analysis of a pulverised-coal-fired boiler deposit showing the amount of calcium present:

% CaO	%(Na,K) ₂ O	%SO ₃
31.9	4.2	30.7

They postulated that calcium chloride was formed in the gas phase from hydrochloric acid and calcium carbonate. It was then sulphated in the combustion gases, whence it would easily condense on to the tube. Due to the high calcium content (compared with sodium and potassium) of Australian Brown coals, calcium seems to form an important part in boiler deposits. Brown & Swaine (1964) found calcium and sodium enrichment in Brown coals. In a more rigorous analysis, Procter & Taylor (1966), using various microscopic techniques, found anhydrite (CaSO₄), and Thenardite (Na₂SO₄) as thin films around fly-ash particles. They suggested that the calcium sulphate came from the fly-ash particles as the calcium content in the flue gas was very small.

Enrichment of sodium and potassium has also been obtained in American coals. Anderson & Diehl (1955) examined deposits from Central Illinois coals, and came to the conclusion that the inner layer was a mixture of alkali sulphates with potassium aluminium sulphate, KAl(SO₄)₃, and sodium ferri sulphate, Na₃Fe(SO₄)₃. They suggest that these were formed by a gas phase reaction of sulphur oxides with fly-ash. Adams & Raask (1963) have also shown these compounds to be present in British boiler deposits, together with potassium ferri sulphate, K₃Fe(SO₄)₃.



FIG. 2-2 SECTION THROUGH A CORRODED BOILER TUBE

A reason for potassium salts appearing in boiler deposits, i.e. enrichment occurring despite non-volatile forms, was suggested by Jackson & Ward (1956), and Jackson & Duffin (1963). They proposed that an exchange reaction between complex potassium alumino silicates (shales) and sodium chloride vapour resulted in the formation of condensable potassium chloride vapour. It must be remembered, as pointed out earlier, that most of the chlorine in coal is thought to be associated with the sodium.

2.1.3 Problems caused by Alkali-matrix deposits

These deposits have three deleterious effects:

- (a) They interfere with heat transfer to the tube.
- (b) They cause a bridging effect between tubes, so increasing the pressure drop through a tube bundle.
- (c) They corrode the tube walls and support. (An example of corrosion caused is shown in Fig. 2.2 of a section through a boiler tube. The preferential corrosion on the upstream side is due to the increased deposition which is in turn due to the aerodynamic conditions, see Section 3.1).

It is reasonable that these problems are related to the alkali content of the coal, i.e. the higher the alkali content, the more severe are all three effects. The effect of calcium content is less well defined, although it is thought (Anderson & Diehl 1955) that it could strengthen the bonded deposit. The sodium and potassium content is also believed to help strengthen the deposit, and so cause a bridging effect.

Bishop (1966) notes that three main theories have been proposed to explain the corrosive action of these deposits. These are :-

- (a) That alkali pyrosulphates occur in deposits, and corrode steel tubes above 595°C (Crossley 1955, 1963).
- (b) That alkali sulphates and small amounts of sodium chloride condensing on the tube will corrode it. (Sykes & Shirley, 1952; Edwards et al, 1962).
- (c) That molten complex sulphates, such as $\text{Na}_3\text{Fe}(\text{SO}_4)_3$ and $\text{K}_3\text{Fe}(\text{SO}_4)_3$ form within deposits and migrate to the tube surface which they attack (Nelson & Cain 1959).

All three theories place importance on the presence of alkali sulphates whether normal or complex, and the existence of a sticky, molten film. Deposit build up and corrosion will be greater, of course, with a molten film. Chlorides are inferred to play an important part in the corrosion and deposition process, as they can condense on to the tubes at normal superheater tube temperatures. Their conversion to sulphates explains some of the sulphates found on tube surfaces.

Of the three theories mentioned above, the first one is least likely to be true, as it has not yet been proved that alkali pyrosulphates can exist in high temperature deposits.

2.1.4 Theories Predicting Fouling Characteristics of Coal

As inferred previously, alkali chlorides appear to play an important part in the formation of alkali-matrix deposits. This is because being more volatile than sulphates, they are formed in the gas-phase whence they can be converted to sulphates in the gas-phase or condense on to the tube surface where the sulphation takes place.

Crossley (1948, 1952) first recommended the use of the chlorine content of coal as an approximate index on which the fouling properties of coal could be based. Marskell & Miller

(1956) questioned this to some extent, having found that the addition of hydrogen chloride to a pulverised-coal-fired combustor increased the rate of fouling. They suggested that this showed compounds other than alkalis were involved.

For the chlorine index to give an accurate indication of the amount of alkalis present (i.e. the fouling characteristics), the ratio of chlorine to water soluble sodium or potassium should be approximately constant. It was found that this was not the case both by Boulton & Taylor (1963), and more recently by Daybell (1967), who found considerable variation in a representative cross-section of East-Midland coals. Similar evidence has also been provided from studies of American coals by Barnhart & Williams (1955) and by Abernathy, Gibson & Frederic (1965). However in one study Gluskster & Rees (1964) established that there was a direct relationship between the chlorine-content and total alkali content of Illinois coals; that is, a high alkali metal content is associated with a high chlorine content.

Crumley & McGamley (1958) proposed that the chlorine/ash ratio was better index of fouling than the chlorine index of Crossley. This was confirmed by Jackson & Ward (1956) who found that coals containing more than 0.5% chlorine are liable to cause fouling, particularly if less than 15% ash was present.

The ratio of soluble sodium/ash has proved to be a useful criterion of fouling for Leigh Creek brown coals in South Australia (C.S.I.R.O. 1966).

The idea of considering fouling in terms of the sulphur/chlorine ratio evolved during studies by Crumley, Fletcher & Wilson (1955) of the possible contribution of calcium compounds

to deposit growth. It was reasoned that sulphur and chlorine compete within the products of combustion from coal-firing for sodium and potassium, as well as for calcium, hence the sulphur/chlorine ratio of the coal is likely to influence the relative amounts of sodium, potassium and calcium sulphate and chlorides in initial deposits.

Bishop, Cliffe & Langford (1967) in pilot scale combustion studies found that corrosion worsened with the following contents of coal :

- (1) Increasing soluble sodium content.
- (2) Increasing soluble potassium content.
- (3) Increasing chlorine content.
- (4) Decreasing sulphur content.
- (5) Decreasing sulphur/chlorine ratio.
- (6) Increasing chlorine/ash ratio.
- (7) Increasing soluble sodium/ash ratio.

Their explanation of these variations were that a coal with a high soluble sodium content and/or soluble potassium content, both of which are broadly related to the chlorine content, will produce relatively large amounts of condensable potentially corrosive salts during combustion. A high sulphur content or high sulphur/chlorine ratio, indicated that the concentration of sulphur oxides in the flue gases would be high, thereby favouring the conversion of alkali-metal chlorides to sulphates, either within the gaseous phase or the deposits. The chlorine/ash ratio was originally derived from a consideration of the distribution of sodium in coal (Crumley & McCamley 1958); however, it may also be regarded as an approximate measure of the ratio of volatilised sodium per unit weight of mineral matter. The relative proportions

of bonding material to comparatively inert, particulate matter in the deposits are indicated by the sodium/ash ratio of the coal. The calcium content of coals was not considered in their work.

From this brief survey it can be concluded that no one ratio or content can determine the fouling and hence corrosive effect of coal. However, all the proposed theories tend to emphasise the formation of alkali-metal halides and their transfer to the tube surface.

SECTION 3

Transport Phenomena in Deposition

3.1 Aerodynamic Conditions around Boiler Tubes

The flow patterns around the tubes play an important part in the amount and type of deposit formed. However it is difficult to state what these patterns are for a bank of tubes. Fig. 3.1 shows that after the first row there is considerable interaction between the turbulent wakes. Hence only the front row of a tube bank and even more specifically, a single tube in that bank will be considered as flow conditions are similar around each tube in that row.

3.1.1 Operating Conditions in a Boiler

The combustion gases approaching a bank of superheater tubes have a velocity of about 7-10 m/s and temperature of 1100°C. The diameter of the superheater tubes is 5.1 cm. which gives a Reynolds number of about 3,000-3,500. The intensity and scale of turbulence are unknown but could well be high.

3.1.2 Aerodynamic Conditions around a Single Tube

At a Reynolds number based on the tube of about 3,500 the flow conditions will be as in Fig. 3.2. A laminar boundary layer will be formed on the front of the tube and will separate at a certain angle θ , varying from 80°-110° dependent on turbulence, Reynolds number (Galloway & Sage 1967) and channel blockage conditions (Perkins & Leppert 1966) to give a turbulent wake.

The intensity of turbulence affects transition from a laminar to a turbulent boundary layer; the higher the value, the earlier the transition at a specific Reynolds number. However, it has been found (Knudsen & Katz 1958a) that even

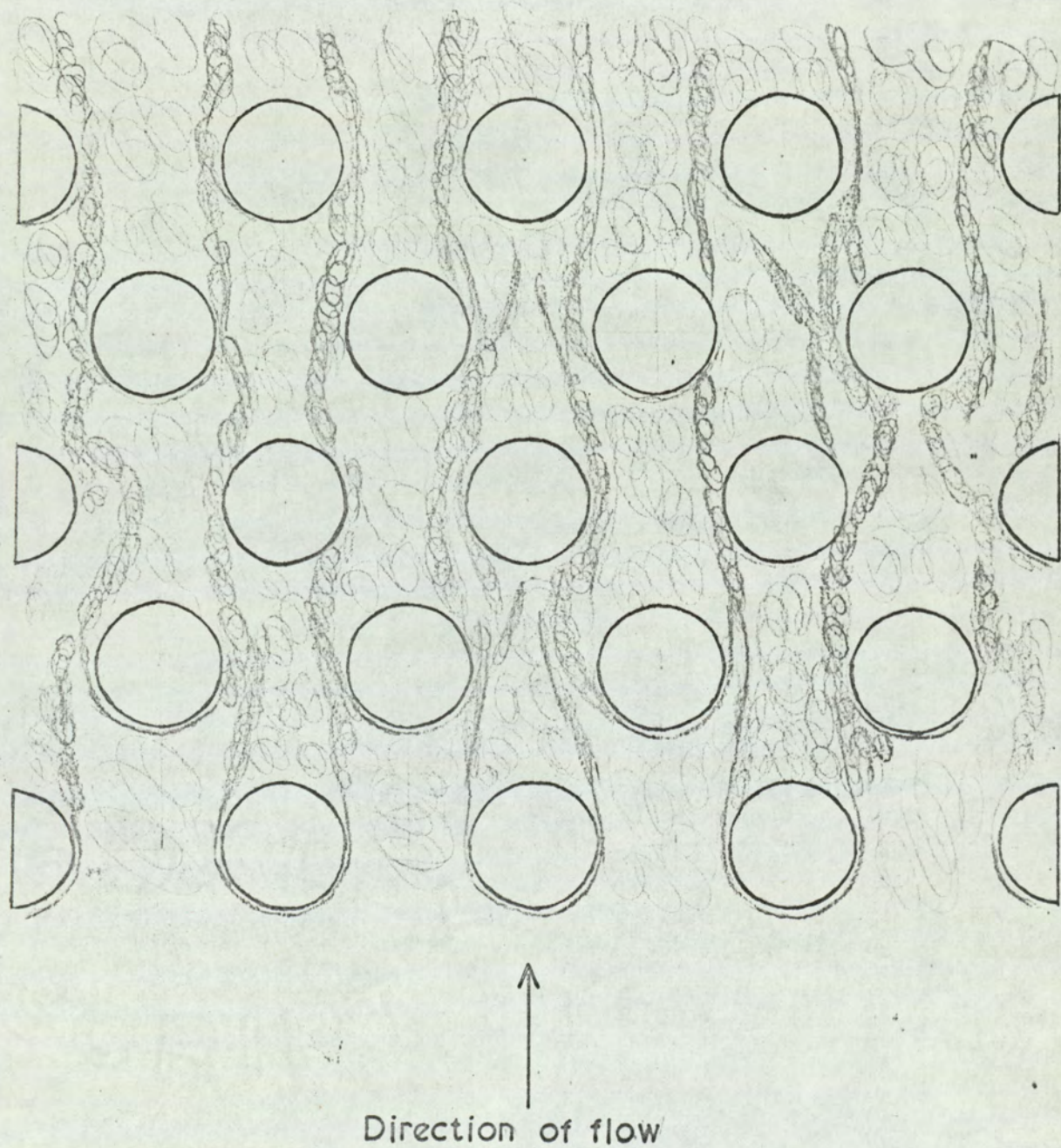


FIG. 3-1 FLOW CONDITIONS IN A STAGGERED TUBE BANK

(Taken from a photograph in McAdams, 1954.)

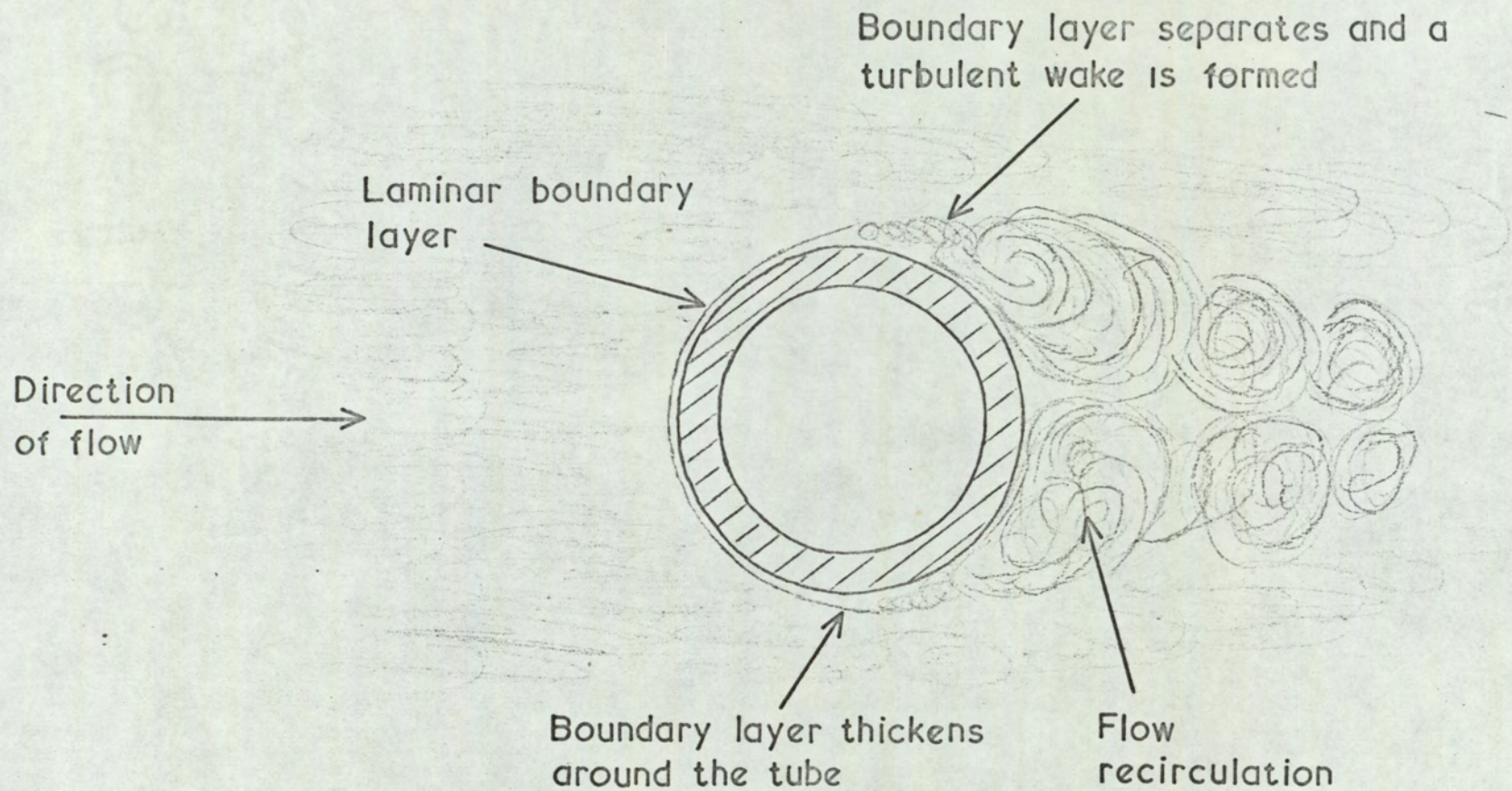


FIG. 3-2 FLOW CONDITIONS AROUND A TUBE AT A REYNOLDS NUMBER OF 3,500

with an intensity of turbulence of 11.5% and a Reynolds number of 39,000, the boundary layer was still laminar up to an angle of 90° from the forward stagnation point. An intensity of turbulence of 11.5% is unlikely to be exceeded in the region of superheater tubes in boilers.

Scale of turbulence does not alter the flow conditions, in particular it will not affect the transition from a laminar to a turbulent boundary layer or the point of separation of the boundary layer (Hegge Zijnen 1958).

3.2 Initial Stages of Deposition

From Section 2 it can be concluded that alkali-matrix deposits are a matrix of condensed alkali vapours and fly-ash particles. The essence of the problem now is how do these vapours and solid particles arrive at the surface. This section reviews the possible mechanism of deposition together with theories of deposition that have already been proposed.

3.2.1 Theories of Deposition

Numerous theories have been postulated for the initial stages of deposition. These have been summarised by Bishop (1966) as follows :-

1. That the initial deposit consists of powdery fly-ash; alkalis and sulphur oxides diffuse through the fly-ash to the tube surface and eventually form the inner layer (Anderson & Diehl 1955).
2. The initial deposit consists of molten and partially-molten particles of fly-ash, which have been impacted on to the tube (Jonakin, Rice & Reese 1959).
3. The alkali oxides ($\text{Na}_2\text{O}, \text{K}_2\text{O}$) condense on to the tubes and are converted to sulphates and pyrosulphates by sulphur

oxides in the gas stream.

4. Sulphates and pyrosulphates condense on to the tubes to form a molten matrix, which collects the impacting particles of fly-ash (Crone 1945; Carlile 1952).
5. That there are two distinct stages in the formation of deposits. The first is the process by which particles cohere to form composite airborne aggregates or deposits on boiler tubes. The second is the process of growth of anhydrite and thernardite around and between fly-ash particles, especially those lodged on boiler tubes (Proctor & Taylor 1966).

All of these theories explain the chemistry of the formation of deposits but do not explain the actual mechanism of transfer to the surface other than by impaction.

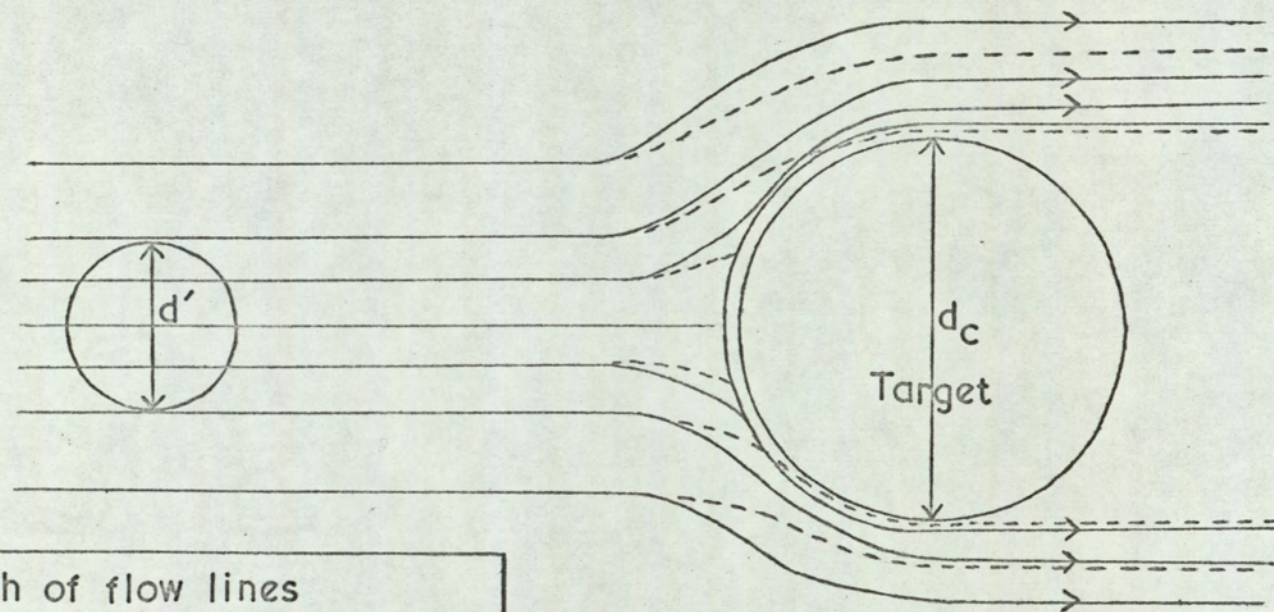
3.2.2 Mechanisms of Deposition

There are four principal mechanisms for the deposition of particles and vapours onto a cooled surface. These are:-

1. Inertial Impaction.
2. Concentration Diffusion.
3. Thermal Diffusion.
4. Electrostatic Precipitation.

There are also two other possible mechanisms of deposition: pressure diffusion and forceddiffusion, both of which are unlikely to contribute to the formation of boiler deposits. Pressure diffusion only occurs under a very great pressure gradient, while forceddiffusion only occurs in ionic systems (Bird et al 1960). Neither of these conditions are likely to occur in the vicinity of boiler tubes.

Only binary vapour mixtures are considered in the following review as the flue gas from the combustion of coal contains



- | | |
|-------|---|
| —→ | Path of flow lines |
| ----- | Path of heavy particles |
| d_c | Diameter of tube |
| d' | Diameter of impactation zone
for one particle size |

FIG 3.3 CONCEPT OF IMPACTION EFFICIENCY

extremely small amounts of condensable vapour (approx. 0.2% by weight). This point has particular relevance in the sections on concentration and thermal diffusion.

3.2.2.1 Inertial Impaction

This mechanism is due to the inertia of the particles, which causes them to deviate from the flow lines around a tube and impact on it.

The efficiency of impaction is defined as the ratio of the number of particles of the same size striking the surface of the obstacle to the number of particles that would strike it if the flow lines were not diverted by the obstacle. This concept is illustrated in Fig. 3.3. For a tube, the efficiency is equal to $\frac{d'}{d_c}$ where d' is the limiting width of the flow lines between which all particles of the same size collide with the tube, and d_c is the diameter of the tube. However, this concept is rather difficult to use mathematically because of trouble in calculating d' . A more convenient function called the impact number, I , first introduced by Sell (1931) is usually used for correlating impaction efficiencies. The impact number being dimensionless provides a better means of comparing the behaviour of particles in different systems. It is obtained from solution of the equations of motion of the particle around the tube. (In the case of a tube, this is an approximate solution).

In the region of the stagnation point, there exists a limiting solution which specifies a minimum value for I of $\frac{1}{8}$ for a finite efficiency of impaction. This critical value of I means that there will be a lower limit on the size of particles reaching the surface. However, the condition is

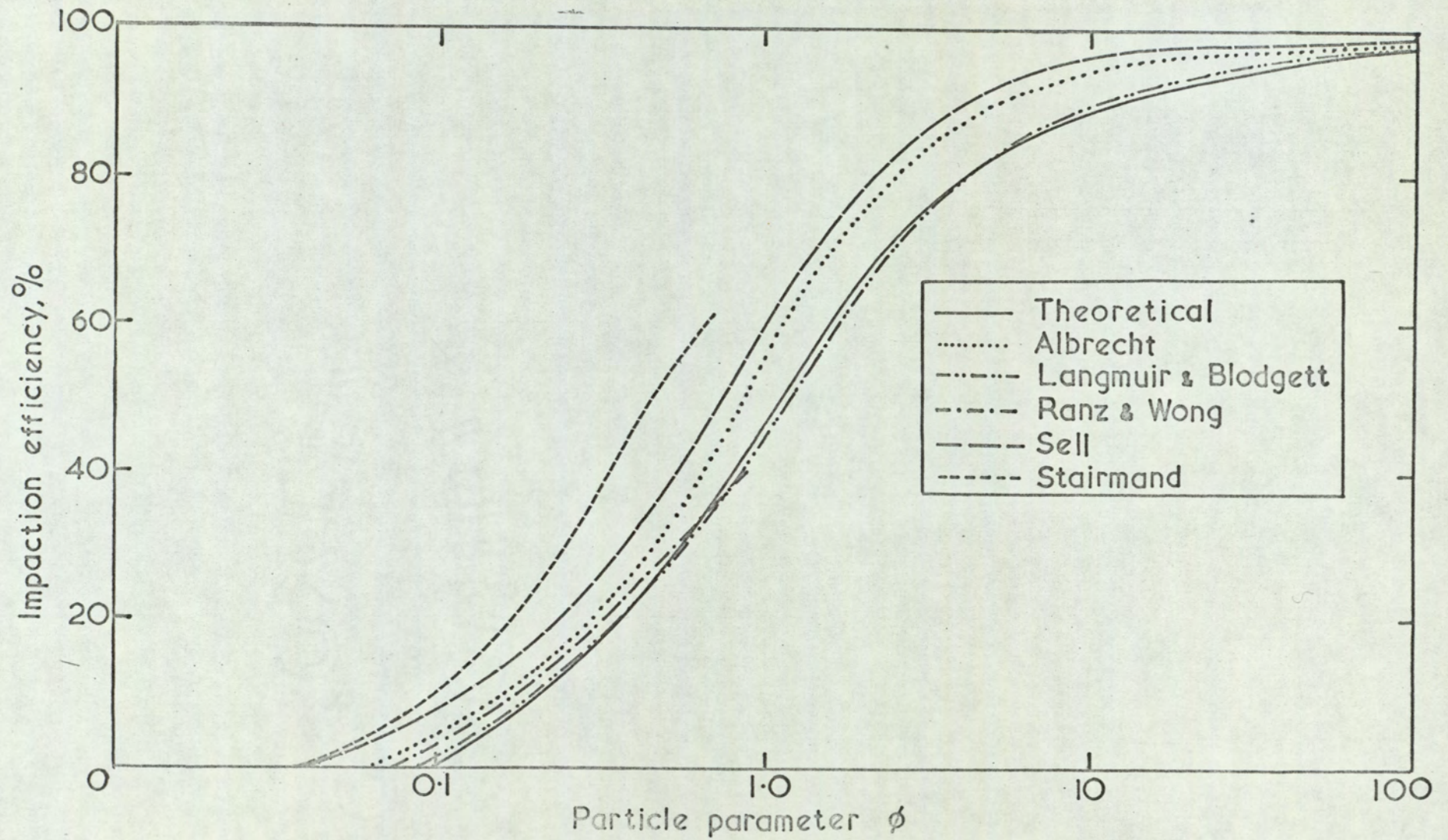


FIG. 3.4 VARIATION OF IMPACTION EFFICIENCY WITH PARTICLE PARAMETER

not entirely true because particles have a finite size and impact whenever their trajectories approach within a distance of $d_1/2$ of the collector surface. The effect is called "interception" and is only large when the collector size is small. The magnitude of interception can be calculated using the following equation of Chen (1955) :-

$$\eta = \left(1 + \frac{d_1}{d_c} \right) - \left(\frac{1}{1 + \frac{d_1}{d_c}} \right) \quad 3.1$$

The impact number can most conveniently be expressed in the following form, given by Taylor (1940) :-

$$I = \frac{8}{9} \frac{\rho_1}{\rho_2} \left(\frac{d_1}{d_2} \right)^2 N_{Re,c} \quad 3.2$$

Although other forms are quoted in the literature, they can usually be converted into this dimensionless form.

In Fig. 3.4 the experimental results of Sell (1935), Albrecht (1931), Ranz & Wong (1952), Stairmand (1950), and Langmuir & Blodgett (1944) are compared with the theoretical results of Langmuir & Blodgett (1944). It should be mentioned that in Sell's theoretical analysis, he obtained a critical impact number of zero due to the fact that he took no account of the boundary layer.

Langmuir & Blodgett (1944) calculated and measured experimentally the impaction efficiencies of small water droplets in air moving at high velocities across a tube. The real value of their extensive calculations is that they present graphs of θ , the angle from the forward stagnation point beyond which no impaction occurs as a function of a variable K_a for various values of a dimensionless parameter ϕ where

$$\phi = \frac{9}{4} \frac{\rho \frac{2}{2} d_c u}{\mu \rho_1} \quad : \quad K_a = \frac{1}{9} \frac{\rho_1 d_1^2 u}{\mu d_c}$$

Hence the amount and distribution of particles that impact over the surface of a tube can be calculated for given concentrations in the main stream. They also give graphs of overall efficiency of impaction as a function of K_a for values of the parameter ϕ , and efficiency at the stagnation point as a function of K_a for a number of values of ϕ .

Bishop (1967) considered the inertial impaction of fly-ash particles from the combustion of coal onto a cooled tube using the critical impaction number curve of Langmuir & Blodgett (1944). He used the data obtained by Thorne & Watt (1962) for ash from Cliff Quay Power Station to provide the size distribution of fly-ash in the flue gas. Table 3.1 gives the overall impaction efficiency for a number of actual size fractions of the fly-ash. As can be seen, anything less than 20 micron will not impact. Bishop's calculations were carried out for typical conditions around a superheater tube, namely

Gas velocity : 7.2 m/s
 Gas temperature : 1000°C
 Tube diameter : 5.1 cm.

No mention has been made of impaction in viscous flow (low Reynolds number), as this type of flow is never encountered in boilers.

3.2.2.2 Concentration Diffusion

This mechanism sometimes referred to as ordinary diffusion drives a species from a region of high concentration to one of low concentration due to the concentration gradient. Although concentrations of the diffusing substances are likely to be

Size Distribution of Cliff-Quay Fly-Ash		Target ¹ Efficiency (from Langmuir & Blodgett's curve)	% w/w x Target Efficiency
Size (Micron)	Amount of size fractions (% w/w of total amount of fly-ash)		
2.3			
	2.7	0	0
3.3			
	4.3	0	0
4.7			
	3.6	0	0
6.6			
	7.5	0	0
9.4			
	9.5	0	0
13			
	12.0	0	0
19			
	14.0	0.1	1.4
27			
	14.0	0.27	3.8
37			
	16.0	0.45	7.2
53			
	5.8	0.55	3.2
76			
	3.9	0.77	3.0
104			
	4.1	0.86	3.5
152			
	0.8	0.93	0.8
211			
	Total 98.2		Total 22.9

1. Target efficiency is defined as the fraction of the particles in the system that impact onto the tube.

Table 3.1

Target Efficiencies of Various Size Fractions of Fly-Ash from Cliff-Quay Power Station

small in a boiler, particularly of condensable vapours, the concentration gradient will occur across the concentration boundary layer which will be of similar proportions to the velocity boundary layer. For a laminar boundary formed on the front of a tube in typical boiler conditions the velocity boundary layer has been found to be of the order of 1 mm. thick (see Appendix 3). Hence high concentration gradients will occur in the tube banks of a boiler.

The discussion of this mechanism will be divided into three parts reviewing diffusion of vapours in laminar flows, diffusion of particles in laminar flows and the diffusion in turbulent flows respectively.

(a) Laminar Diffusion (Vapours)

The mass flux for diffusion of vapours is given by Fick's law which for a one dimensional system can be formulated as,

$$\dot{m}'' = \rho D_{1,2} \frac{dc}{dy} \quad 3.3$$

The diffusivity $D_{1,2}$ can be calculated from the kinetic theory. Gilliland (1934) derived the following equation from a simplified kinetic theory assuming perfectly elastic, rigid spheres :-

$$D_{1,2} = 0.0043 \frac{T^{3/2}}{P(v_1^{1/3} + v_2^{1/3})^2} \sqrt{\left(\frac{1}{M_1} + \frac{1}{M_2}\right)} \quad 3.4$$

A more rigorous equation given by Hirschfelder, Curtiss & Bird (1954) takes into account the attractive and repulsive forces between molecules. To a first approximation the result is,

$$D_{1,2} = 5.26 \times 10^{-3} \frac{T^{3/2} \sqrt{\left(\frac{1}{M_1} + \frac{1}{M_2}\right)}}{P d_{1,2} Q} \quad 3.5$$

where

$$d_{1,2} = \frac{d_1 + d_2}{2}$$

The collision integral Q is a function of $\frac{KT}{\epsilon_{1,2}}$. Both of these flux terms can be evaluated for a limited number of elements and compounds using the tables of Hirschfelder, Curtiss & Bird (1954).

Wilke & Lee (1955) gave the following improved form of equation 3.5

$$D_{1,2} = \frac{2a_a T^{3/2} \sqrt{\left(\frac{1}{M_1} + \frac{1}{M_2}\right)}}{P d_{1,2} Q} \quad 3.6$$

where,

$$a_a = \left[10.7 - 2.46 \sqrt{\left(\frac{1}{M_1} + \frac{1}{M_2}\right)} \right] \times 10^{-4}$$

The modification takes into account the dependence of diffusivity on molecular weight.

(b) Laminar Diffusion (Particles)

Very small particles less than 5 microns will also diffuse along a concentration gradient in a similar manner to the vapour. This diffusion is sometimes known as Brownian Motion due to the fact that it was first noticed by Robert Brown in 1827.

These small particles can be considered as exceptionally large and massive molecules, hence Fick's law can be applied to the calculation of the mass flux. The problem is then reduced to the calculation of the diffusivity $D_{1,2}$.

Einstein (1905) applying Stokes' law obtained the following equation for diffusivity :-

$$D_{1,2} = \frac{KT}{3\pi\mu d_1} \quad 3.7$$

He assumed that the particle under consideration is large compared with the mean free path of the gas molecules, hence the gas can be treated as a continuous medium. Stokes' law

is only strictly applicable to particles greater than 3 microns in size. For smaller particles the Cunningham correction factor has to be used to account for discontinuities.

Equation 3.7 becomes :-

$$D_{1,2} = \frac{KT (1 + 2a_p \lambda / d_1)}{3 \pi \mu d_1} \quad 3.8$$

where,

$$a_p = A_0 + B_0 \rho e^{(-Cd/2 \lambda)}$$

A_0 , B_0 , and C are constants (Knudsen & Weber 1911). Several investigators have measured A , B and C (Millikan 1923 a & b, Maltauch 1925, Mönch 1923) and the mean values have been deduced from their results by Langmuir (1942). Langmuir's values have been corrected to the present accepted value by Green & Lane (1964). Using these corrected values, Samms & Watt (1966) gave the values shown in Table 3.2 for the function $(1 + 2a_p \lambda / d_1)$ against various ratios of particle diameter to mean free path.

Using these values of $(1 + 2a_p \lambda / d_1)$, the validity of equation 3.8 has been demonstrated by Samms & Watt (1966) who calculated the diffusivity from this equation and the diffusivity from the kinetic theory for a specific collision diameter. It was found that the diameter of the particle was approximately twice the collision diameter when the two diffusivities were equal.

For small particles when the mean free path is large compared with the size of the particles, a more exact approach is to use the kinetic theory of Chapman and Enskog (Chapman & Cowling 1952). Using his theory Chapman (1962) and Chapman & Mason (1963) considered a gas mixture composed of particles of highly unequal masses in which the lighter

Ratio:						
$\frac{\text{Particle Diameter}}{\text{Mean Free Path}}$	0.001	0.01	0.1	1.0	10	100
$(1 + 2a\lambda/d_p)$	3,380	339	34.3	4.01	1.25	1.025

Table 3.2

Variation of the function $(1 + 2a\lambda/d_p)$ with
Particle Diameter

particles were in large excess. This type of mixture is named Quasi-Lorentzian (Mason 1957) and approximates to the case when a small concentration of minute particles is diffusing through a gas. For a Quasi-Lorentzian mixture the transport properties can be expressed in relatively simple terms.

If the collisions are perfectly elastic the following equation describes the diffusivity of the particle :-

$$D_{1,2} = \frac{3}{2n} \left(\frac{\pi K T}{2M_2} \right)^{\frac{1}{2}} \frac{1}{\pi d^2 Q} \quad 3.9$$

Chapman and Mason assumed that a fraction f of the colliding molecules rebounded diffusely, only the direction, not the speed, being altered, the rest rebounded specularly. For this model they showed that the collision integral reduced to :-

$$Q = 1 + \frac{4f}{9} \quad 3.10$$

Waldmann (1959) treated the problem of small particle diffusion differently. Using an earlier approach of Epstein (1924) he calculated in detail the force on a particle by adding up all the impulses transferred to it by the colliding gas molecules using the known Chapman-Enskog velocity distribution for a gas not in equilibrium. The main difference between Waldmann's and Epstein's work was that Epstein treated the collisions as being diffusely elastic, whereas Waldmann supposed that a fraction of the molecules, a , were diffusely reflected with a random distribution of speeds, the rest being specularly reflected.

Waldmann's treatment gives a similar result for the diffusivity as that of Chapman and Mason, the only difference being in the value of the collision integral Q .

For Waldmann's approach :-

$$Q = 1 + \frac{\pi t}{8} \quad 3.11$$

When all the collisions are specular ($s = 0$, $t = 0$), the collision integrals are the same. The two values differ slightly for equal values of s and t between 0 and 1; however, Chapman & Mason (1963) found that the maximum difference was only 3.7%.

Waldmann's treatment is the more exact and is confirmed by the experimental results of Schmidt (1959). However, Chapman & Mason (1963) considered that their method was more convenient because of the complicated evaluation of Waldmann's collision integral.

(c) Turbulent Diffusion (Eddy Diffusion)

It is not proposed to discuss this mechanism in great detail because as it will be shown later, the emphasis of this thesis will be based on transfer through a laminar boundary layer. Also, the discussion will be mainly concerned with vapours, as little work has been done on the eddy diffusion of particles.

The rate of eddy diffusion can be much larger than that due to laminar diffusion under similar circumstances and has been found to be as great as 100 times (Sherwood & Woertz 1939). Eddy diffusion depends on the nature of the flow, the type of substance involved, and the concentration gradient. Hence the intensity and scale of turbulence of the flow are important. Inclusion of the nature of flow into the mechanism renders the mathematical approach more difficult, consequently most of the theoretical approaches have been obtained with the help of analogies. The basis of these is

that the eddies transferring mass also cause transfer of heat and momentum.

Two of the more accurate analogies have been formulated by Prandtl & Taylor and Deissler (Bird et al. 1960).

Prandtl & Taylor obtained the following equation, based on the model of eddies moving around in a fluid similar to molecules moving about in a gas :-

$$\dot{m}'' = -l_{Pr}^2 \left| \frac{du}{dy} \right| \frac{dc}{dy} \quad 3.12$$

where l_{Pr} is termed a mixing length and is analogous to the mean free path used in the kinetic theory.

The main resistance to eddy diffusion is a thin layer of fluid near the wall, termed the laminar sublayer because flow in it is assumed to be mainly laminar. Deissler proposed the following equation for transfer in this region:-

$$\dot{m}'' = -a_c^2 u y \left[1 - \exp\left(\frac{-a_c^2 u y}{\nu}\right) \right] \frac{dc}{dy} \quad 3.13$$

where a_c is a constant determined empirically by Deissler as 0.124.

3.2.2.3 Thermal Diffusion

Thermal diffusion is the mechanism which drives small particles and vapours along a temperature gradient due to differential bombardment. This mechanism will be of relevance for mass transfer to boiler tubes as severe temperature gradients exist in their neighbourhood. As the thermal gradient will exist across thermal boundary layer which is of similar magnitude to the velocity boundary layer, gradients of the order of 500°C/mm can be found.

Enskog (1911) and Chapman (1912) independently established a general theory of thermal diffusion and obtained a law similar to that of Fick's for concentration diffusion to

describe the mass transfer rate namely :-

$$\dot{m}'' = \frac{\rho D_T}{T} \frac{dT}{dx} \quad 3.14$$

where D_T is the thermal diffusion coefficient.

In practice D_T is replaced by the thermal diffusion ratio k_T , which is defined as :-

$$k_T = \frac{D_T}{D_{1,2}} \quad 3.15$$

As in a mixture of substances the thermal diffusion ratio k_T , is strongly dependent on the product $n_{1,0} n_{2,0}$ (for a binary mixture), a new term, the thermal diffusion factor, has been introduced which for a binary mixture is :-

$$\alpha = \frac{k_T}{n_{1,0} n_{2,0}} \quad 3.16$$

The thermal diffusion factor is still dependent on the relative proportions of the components present but to a much lesser extent than is k_T .

Thermal diffusion is mathematically the most complicated of the gas transport phenomena due to the dependence of the direction of the relative motion on the nature of the molecular collisions. In general the heavier molecules or particles diffuse down the temperature gradient. Exceptions arise when the mass difference between the two species is small, then the extension of the molecular fields can become the dominating factor resulting in the heavier molecules diffusing up the temperature gradient. Such a reversal has only been observed with components of close molecular weight, for example a neon-ammonia mixture (Grew 1944).

(a) Evaluation of ' α ' for Vapours

The theoretical expressions for ' α ' are complicated even to a first approximation. However for three types of gas

mixture the theory is less complex than in the general case. The simplest of the three mixtures is an isotopic mixture in which the interactions of like and unlike molecules obey the same law.

Chapman & Cowling (1952) gave the following first approximation of α for an isotopic mixture of rigid elastic spheres:-

$$\alpha = \frac{S_1 n_{1,0} - S_2 n_{2,0}}{Q_1 n_{1,0}^2 + Q_2 n_{2,0}^2 + Q_{12} n_{1,0} n_{2,0}} \quad 3.17$$

where $n_{1,0}$, $n_{2,0}$ are the volume fractions of the two components and the quantities S and Q are as follows:-

$$S_i = \frac{1}{5} \left\{ 2^{3/2} \frac{M_i}{M_j} \left(\frac{\sigma_i}{\sigma_{12}} \right)^2 - M_j \left(15 M_j - 7 M_i \right) \right\}$$

$$Q_i = M_j^2 \left\{ \frac{2}{25} \left(\frac{2}{M_j} \right)^{1/2} \left(\frac{\sigma_i}{\sigma_{12}} \right)^2 \right\} \left\{ 13 \left(M_{ij} \right)^2 + 16 M_{ji} + 30 \right\}$$

$$Q_{12} = M_2^2 \left\{ \frac{39}{5} \left(M_{12} - 1 \right)^2 + \frac{344}{25} M_2 + \frac{16}{25} M_{12} \left(\frac{\sigma_1 \sigma_2}{\sigma_{12}} \right)^2 \left(\frac{1}{M_1 M_2} \right)^{3/2} \right\}$$

and $j = 1$ or 2 when $i = 2$ or 1 respectively.

σ is the molecular diameter.

The second type of gas mixture for which the theory simplifies is named a Lorentzian mixture in which the mass of one species is very large compared with that of the other, and at the same time either the proportion of the heavier species or its relative size is very large. This means that collisions between lighter molecules are negligible. Although evaluation of α is possible the formulae are far more complicated than in the isotopic case and must be evaluated in successive steps. These formulae given by Chapman & Cowling (1952) are not stated here because their complexity renders them less useful than the equation obtained from the third type of gas mixture. This type of mixture is named

Quasi-Lorentzian and has been mentioned previously in Section 3.2.2.2. It can be shown (see Appendix 5) that by using the method of Chapman (1962), α is given to the second approximation as:-

$$\alpha = \frac{5}{16\sqrt{2}} \left(\frac{d_1}{d_2}\right)^2 \left(\frac{M_1}{M_1 + M_2}\right)^{\frac{1}{2}} \quad 3.18$$

for the case of rigid elastic spheres.

A gas containing a small concentration of a polyatomic gas is the closest approximation to a Quasi-Lorentzian mixture, though any gas mixture in which the lighter molecules are in large excess can be better considered as a Quasi-Lorentzian mixture than either an isotopic or a Lorentzian mixture.

(b) Evaluation of α for Small Particles

Chapman (1962) and Chapman & Mason (1962) calculated the thermal diffusive force on small particles using a similar approach to the calculations of the concentration diffusive force of particles. Again they used the model of a Quasi-Lorentzian gas which gives the thermal diffusion factor as:-

$$\alpha = \frac{5}{16\sqrt{2}} \left(\frac{d_1}{d_2}\right)^2 \quad 3.19$$

Waldmann (1962) applied his approach (see Section 3.2.2.2) to the calculation of the thermal diffusive force on small particles. Both his, and Chapman's and Mason's equations were similar, namely:-

$$F = -\frac{2}{15} \frac{k_2 d_1^2 Q}{Q'} \left(\frac{2\pi M_2}{K+T}\right)^{\frac{1}{2}} \frac{dT}{dx} \quad 3.20$$

In Waldmann's derivation the factor $\frac{Q}{Q'}$ is equal to unity, whereas in the Mason-Chapman derivation it is equal to $(1 + \omega)(1 + 4s/9)$. Although $\omega \leq \frac{1}{42}$ (Chapman 1962), this ratio can differ significantly from unity if s is not small.

Whereas the Waldmann and Mason-Chapman collision patterns give

closely similar results for concentration diffusion of particles, the difference when thermal diffusion is taking place can be large. This difference arises because thermal diffusion, as mentioned previously, depends on the precise nature of the interactions at collision.

When the diameter of the particles becomes greater than the mean free path of the molecules of the surrounding gas, the particles cannot be treated as large molecules. For this case the thermal diffusive force can be calculated from a solution of the hydrodynamical and convective diffusion equations. Epstein (1927) obtained the following relationship for the thermal force on a particle:-

$$F = -17.9 \frac{d_1 \rho \lambda}{T} \left(\frac{k_1}{2k_1 + k_2} \right) \frac{dT}{dx} \quad 3.21$$

Equation 3.21 takes into account both the kinetic and hydrodynamic consequences of heat transfer through the particle. General agreement with the expression has been found experimentally by Saxton & Ranz (1952) and Rosenblatt & La Mer (1946).

Using the fact that $u = qF$ where q is the mobility of the particle $q = \frac{kT}{D_{1,2}}$, the mass flux can be found by substituting for F in Equation 3.21 to obtain the velocity of the particles and then multiplying by $\frac{4\rho}{\pi d_1^2}$, the result being :-

$$\dot{m}'' = - \frac{1.5\lambda^2 d_1^2 (1 + 2ad\lambda/d_1)}{\mu T} \left(\frac{k_1}{2k_1 + k_2} \right) \frac{dT}{dx} \quad 3.22$$

3.2.2.4 Electrostatic Precipitation

Electrostatic precipitation arises due to the attraction and repulsion of electrostatic charges on particles. Haase (1962) and Min et al (1963) have shown that charges can be built

up on clouds of particles in motion. However little work has been done to determine their effect on causing boiler deposits. Only Gabler (1963) has made a detailed study in a boiler, and although he found large positive potentials could be obtained, he was unable to show that they were one of the mechanisms of the deposition process mainly because he could not find any charge on the flue gas in the immediate vicinity of the superheater. This suggested that the conductivity of the gas (highly ionised at high temperatures) prevented the build up of any potential and hence no attractive forces could arise.

A more direct test of the possible magnitude of electrostatic precipitation effects was carried out by Pereles (1958), investigating the deposition of dust in mine galleries. He showed that at a distance of 1 cm. electrostatic forces could only contribute 1% of the total deposition under his conditions.

3.3 Methods for Determining Deposition Rates

In this section methods are reviewed for assessing the important mechanisms of deposition quantitatively with special reference to the flow conditions that can be defined in a boiler tube bank.

3.3.1 General Approach

From section 3.2 it can be concluded that there are three principle mechanisms for the transfer of vapours and particles to the surface of a tube namely, inertial impaction, concentration diffusion and thermal diffusion.

As no existence of appreciable potentials have been found in the neighbourhood of boiler tubes it is assumed that electrostatic precipitation will contribute little to the total deposition rate.

Particles which are transferred to the tube surface by inertial impaction can be calculated from a known size distribution of fly-ash in the flue gas and use of the graphs presented by Langmuir & Blodgett (1944). The mass flux of particles small enough to be considered as large molecules, and vapours reaching the surface by concentration and thermal diffusion can be calculated for a two-dimensional laminar or turbulent boundary layer. However the solution of the relevant equations is extremely complicated if coupling of the fluxes is assumed, so a simpler approach is to consider the two diffusion mechanisms separately. The solution of the equations describing thermal diffusion is still complicated, hence as concentration diffusion is the dominating force, an approach used by Baron (1958) will be reviewed in which the magnitude of the thermal diffusive flux compared with the concentration diffusive flux is evaluated and the concentration diffusive flux is obtained from solution of the mass transport equations.

Emphasis is placed on an evaluation of the flux rates for a laminar boundary layer because the only definable flow conditions in a boiler exist in the front row of the tube bank where a laminar boundary layer is formed on the front of the tube separating to give a turbulent wake.

It is not possible to solve the partial differential equations describing the concentration diffusive flux and thermal diffusive flux in the turbulent wake of a tube because of flow recirculation in that region.

3.3.2 Calculation of Concentration Diffusion Rates through a Laminar Boundary Layer

3.3.2.1 Use of Heat/Mass Transfer Analogy

If constant properties are applicable, Spalding (1960) has

shown that every mass transfer problem can be expressed by a relation of the 'ohms law' type, namely:-

$$\dot{m}'' = g_i B \quad 3.23$$

where g_i is a surface conductance dependent only on aerodynamic factors and B is a dimensionless driving force dependent on the thermodynamic properties of the layer of fluid in contact with the phase boundary and the so called transferred substance on the tube surface. Equation 3.23 is derived in Appendix 6.

The conductance g_i can be calculated from the following equation:-

$$g_i = N_{st,i} G \quad 3.24$$

In fact data are not usually available for evaluation of the mass transfer Stanton number. Hence Spalding (1960) proposed calculating the Stanton number for heat transfer and making corrections for the fact that heat transfer is only analogous to mass transfer under certain conditions. Two basic assumptions are made in this analogy:-

(1) That the thermal diffusion ($\frac{k}{c}$) coefficient is equal to the mass diffusion coefficient ($\rho D_{1,2}$) for the same system. The following correction compensates for the case when the Lewis number does not equal unity:-

$$N_{st,i} = (N_{st,h}) (N_{Le})^{2/3} \quad 3.25$$

(2) The mass diffusivity ($D_{1,2}$) is independent of concentration gradient. Spalding (1951) and Evans (1961) showed that this dependence followed the same pattern for most cases; namely, $N_{st,i}$ falls below $N_{st,h}$ when B is positive (evaporation), and rises above it when B is negative (condensation).

From these results Spalding & Evans (1961) proposed the following correction factor:-

$$N_{st,i} = N_{st,h} (1+B)^{-0.4} \quad 3.26$$

Therefore equation 3.24 becomes:-

$$G_i = N_{st,h} G(N_{Le})^{2/3} (1+B)^{-0.4} \quad 3.27$$

The mass transfer driving force B is defined as:-

$$B = \frac{b_g - b_o}{b_o - b_t} \quad 3.28$$

where subscript g is the local main stream condition

o is the state just inside the phase boundary,
i.e. for a vapour the state immediately before
it has condensed; for a particle the state
immediately before it has deposited.

t is the condition in the transferred state beyond
the phase boundary, i.e. the state on the surface
of the tube.

This method is valuable in solution of laminar boundary layer problems for small mass transfer rates as in the present work.

3.3.2.2 More Exact Methods

The basic problem of calculating the transfer through a laminar boundary layer is in the solution of the equation,

$$\rho u \frac{\partial b}{\partial x} + \rho v \frac{\partial b}{\partial y} - \frac{\rho}{\rho} \frac{\partial^2 b}{\partial y^2} = 0 \quad 3.29$$

which is derived from the mass and energy equations for transfer in the laminar boundary layer (Spalding 1960) and is given in Appendix 6. The velocity components 'u' and 'v' come from a solution of the corresponding momentum and continuity equations,

$$u \frac{\partial u}{\partial x} + v \frac{\partial u}{\partial y} - \frac{\mu}{\rho} \frac{\partial^2 u}{\partial y^2} = \frac{-g_c}{\rho} \frac{dP}{dx} \quad 3.30$$

and

$$\frac{\partial u}{\partial x} + \frac{\partial v}{\partial y} = 0 \quad 3.31$$

Spalding & Patanker (1967) have developed a numerical method of solving these equations using a combined parametric - integral

and finite - difference approach. The solution is also applicable for turbulent boundary layers and is given in the form of a computer program written in 'Fortran IV'.

Two earlier methods have been developed for solution of equation 3.29, mainly of use where computer facilities are not available.

(1) Spalding & Evans (1961) showed that under conditions of 'similar' velocity distributions, that is the mainstream velocity profile obeying the relation:

$$\frac{du_g}{dx} = a_e u_g^N \quad 3.32$$

Equation 3.29 can be reduced to:-

$$B_a'' + \psi \xi B_a' = 0 \quad 3.33$$

with boundary conditions:-

$$\text{at } \Omega = 0; \quad B_a = 0, \quad B_a' = B_o' = -\psi \xi_o$$

$$\text{at } \Omega = \infty; \quad B_a = B$$

where ψ = Prandtl or Schmidt number

Ω = a dimensionless distance coordinate

namely,

$$y \left[\left(\frac{du_g}{dx} \right) \left(\frac{1 - \frac{N}{2}}{\nu} \right) \right]^{\frac{1}{2}}$$

ξ = a dimensionless stream function which depends only on Ω and,

$$\xi = \frac{\xi}{u_g} \sqrt{\left(\frac{du_g}{dx} \right) \left(\frac{1 - \frac{N}{2}}{\nu} \right)}$$

and ξ is the conventional stream function defined by

$$u \equiv \frac{\partial \xi}{\partial x} \quad \text{and} \quad v = -\frac{\partial \xi}{\partial y}$$

The functions Ω and ξ enable reduction from the partial differential equation 3.29 to the ordinary differential equation 3.33. This equation can be solved by a quadrature procedure using values of $f(\Omega)$ and ψ given by Spalding & Evans (1961).

(2) A more general method not dependent on similar flows is given by Spalding & Chi (1963) using dimensionless analysis. The solution of equation 3.29 can be written in the form:-

$$\frac{u_g}{\nu} \frac{d\Delta^2}{dx} = F_{\Delta} \left(\frac{\Delta^2}{\nu} \frac{du_g}{dx}, B, \psi \right) \quad 3.34$$

which is evaluated by the standard methods of numerical analysis e.g. Runge-Kutta referring to tables given by Spalding & Chi (1963) for values of F_{Δ} as functions of B and ψ .

Of the three more exact methods reviewed, that of Spalding & Patanker (1967) is the more accurate and easiest to apply if computing facilities are available. The other two methods were developed before the advent of large digital computers.

3.3.3 Estimation of Magnitude of Thermal Diffusion

Baron (1958) compares the ratio of the thermal diffusive flux to the concentration diffusive flux for a one dimensional system, and suggests that it is a reasonable estimation for a two dimensional system.

The ratio of the thermal diffusive flux H is:-

$$H_a = \frac{\alpha m_1 m_2 \frac{\partial \ln T}{\partial y}}{\frac{\partial m_1}{\partial y}} \quad 3.35$$

Assuming that the temperature and concentration gradients are linear and taking a mean value of the diffusing substance across the boundary layer, equation 3.35 becomes :-

$$H_a \approx \frac{\alpha \left(\frac{m_{1,\infty} + m_{1,w}}{2} \right) m_2 \left(\frac{T_{\infty} - T_w}{\delta} \right)}{\left(\frac{T_w + T_{\infty}}{2} \right) \left(\frac{m_{1,\infty} - m_{1,w}}{\delta} \right)} \quad 3.36$$

For small concentrations of diffusing material $m_2 \rightarrow 1$

$$H_a \approx \alpha \left(\frac{T_{\infty} - T_w}{T_{\infty} + T_w} \right) \left(\frac{m_{1,\infty} + m_{1,w}}{m_{1,\infty} - m_{1,w}} \right) \quad 3.37$$

3.4 Heat Transfer to a Tube in Cross-Flow

The simplest method of calculating vapour and particle deposition rates through a laminar boundary layer is by using the heat/mass transfer analogy (Section 3.3.2.1), particularly as very small concentrations of substances are involved. Hence the deposition rate can readily be calculated if heat transfer data is available.

The heat transfer to a single tube in the front row of a tube bank is affected by the proximity of the tubes either side. No correlations have been given in the literature for average and local heat transfer coefficients to a single tube under these conditions. However there are several correlations for heat transfer to a tube under channel blockage conditions, which can be taken as approximations for the actual case. These correlations are reviewed with particular emphasis on the effect of main-stream turbulence.

3.4.1 Heat Transfer to a Single Tube under Channel Blockage Conditions

3.4.1.1. Average Heat Transfer Coefficients

Several workers have proposed correction factors for the Reynolds number to account for the higher heat transfer obtained as the channel blockage ratio ($\frac{d}{W}$) approaches one.

Knudsen & Katz (1958b) first suggested that the average Nusselt number should be corrected by a factor of $\sqrt{[1 + (d/W)]}$ to account for the blockage condition; however, this factor has had no direct experimental verification. Robinson et al (1951) empirically determined the following correction from local heat transfer data for tubes with non-isothermal surfaces:-

$$N_{Nu} = a_f N_{Re}^n \left[1 + \sqrt{(d/W)} \right] \frac{1}{N} \quad 3.38$$

They found that using their data N varied from 0.53 to 0.806. Perkins & Leppert (1964) determined heat transfer coefficients between a tube and water, and found that their results varied considerably from those predicted using the correction of Robinson et al.

Vliet & Leppert (1961) proposed a mean area concept for correcting heat transfer coefficients under blockage conditions. This was:-

$$A_{\text{Mean}} = \frac{\text{Channel Volume} - \text{Tube Volume}}{\text{Tube Diameter}} \quad 3.39$$

A_{Mean} was defined as the ratio of the flow volume in the channel at the location of the body to the body height. For a tube, the ratio of the area of the tube to the mean area becomes:-

$$\frac{A}{A_{\text{Mean}}} = \frac{4W}{(4W - d_{\text{ou}})} \quad 3.40$$

Pope (1954) suggested correcting for both 'solid blocking' and 'wake blocking' and gave the following correction to the Reynolds number:-

$$N_{\text{Re, corrected}} = N_{\text{Re}} \left[1 + 0.822 \left(\frac{dc}{W} \right)^2 + \frac{C_D}{4} \left(\frac{dc}{W} \right) \right] \quad 3.41$$

where the second term corrects for 'solid blocking' and the third term for 'wake blocking'. This form of correction was based on the results of potential flow theory using the method of images.

A graph taken from Perkins & Leppert (1964) comparing the various blockage correction factors for the Reynolds number mentioned with the experimental results of Perkins & Leppert is shown in Fig. 3.5.

The correction factor of Knudsen & Katz has been included, and it can be seen that it compares favourably with the other correction factors.

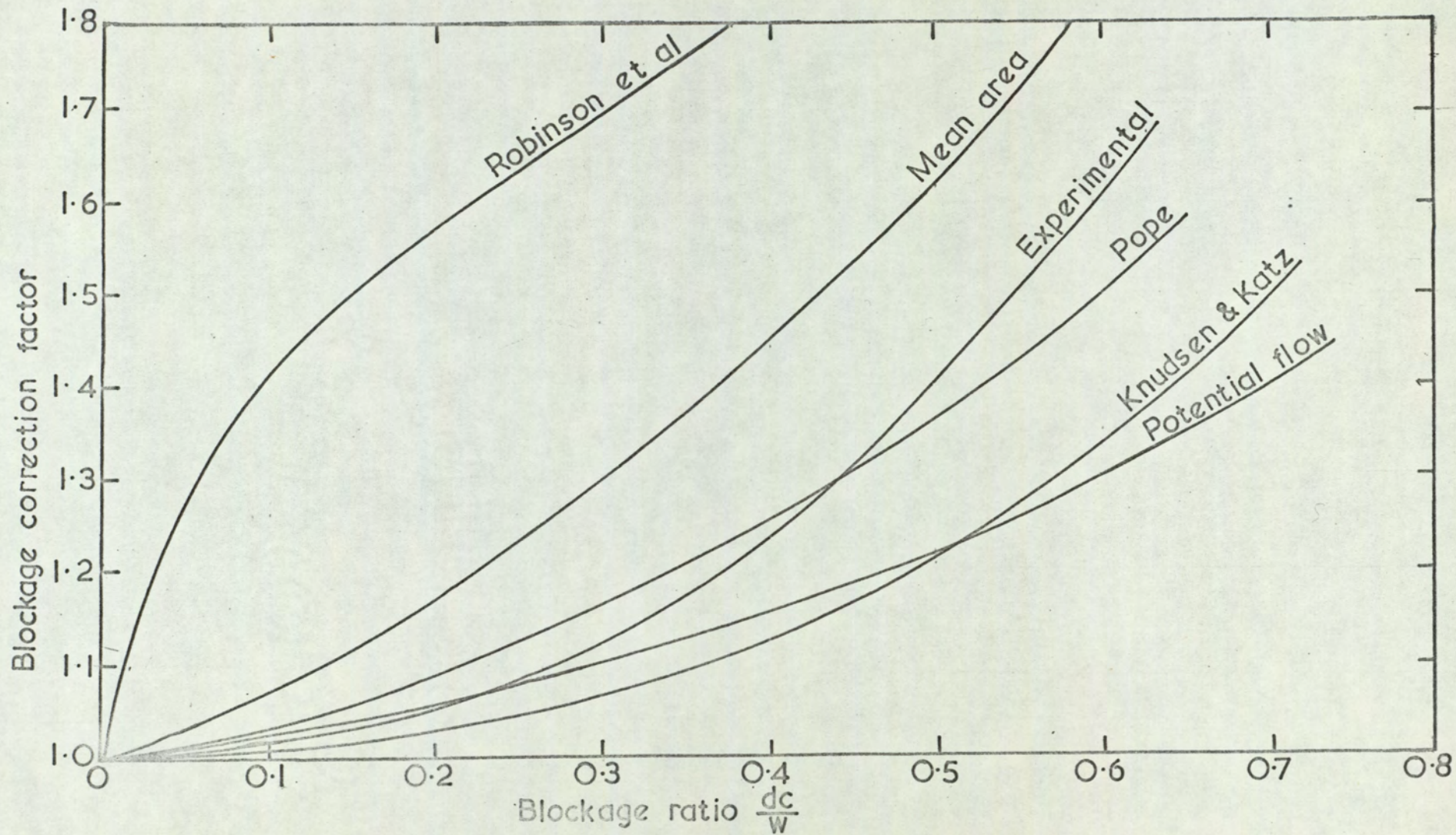


FIG. 3.5 AVERAGE BLOCKAGE CORRECTIONS OF REYNOLDS NUMBERS FOR TUBE BLOCKAGE IN A CHANNEL

3.4.1.2 Local Heat Transfer Coefficients

Two main approaches have been made to correct local heat transfer coefficients. Robinson et al (1951) determined an empirical correction factor $1 + (d/W)$ for the Reynolds number at the forward stagnation point by correlating their results to those predicted by Squire (1938) at various blockage ratios ($0.25 < \frac{d}{W} < 0.75$).

The second approach of Vliet & Leppert (1961) obtained a new Reynolds number to correlate the blockage effect. They presented the corrected Reynolds number as:-

$$N_{Re, \text{ corrected}} = \frac{N_{Re} \ u(\theta) \ \text{finite blockage}}{u(\theta) \ \text{zero blockage}}$$

Perkins & Leppert found that their experimental work confirmed this second result.

3.4.2 Effect of Turbulence on Heat Transfer

There are two factors of free stream turbulence that can affect the average and local heat transfer coefficients to or from a tube in cross flow, namely:-

- (1) Intensity of turbulence.
- (2) Scale of turbulence.

3.4.2.1 Intensity of Turbulence

This is a measure of the amplitude of random oscillation of the flow under consideration. If turbulence is taken into consideration then the dimensionless heat transfer equations (local and average) become :-

$$\begin{aligned} N_{Nu} &= f_a(N_{Re}, N_{Pr}, Z) \\ N_{Nu, m} &= f_b(N_{Re}, N_{Pr}, Z) \end{aligned} \quad 3.42$$

Mathematically, the intensity of turbulence Z is:-

$$Z = \frac{1}{3} \frac{(\bar{u}'^2 + \bar{v}'^2 + \bar{w}'^2)}{u_\infty} \quad 3.43$$

The effect of turbulence on heat transfer cannot be

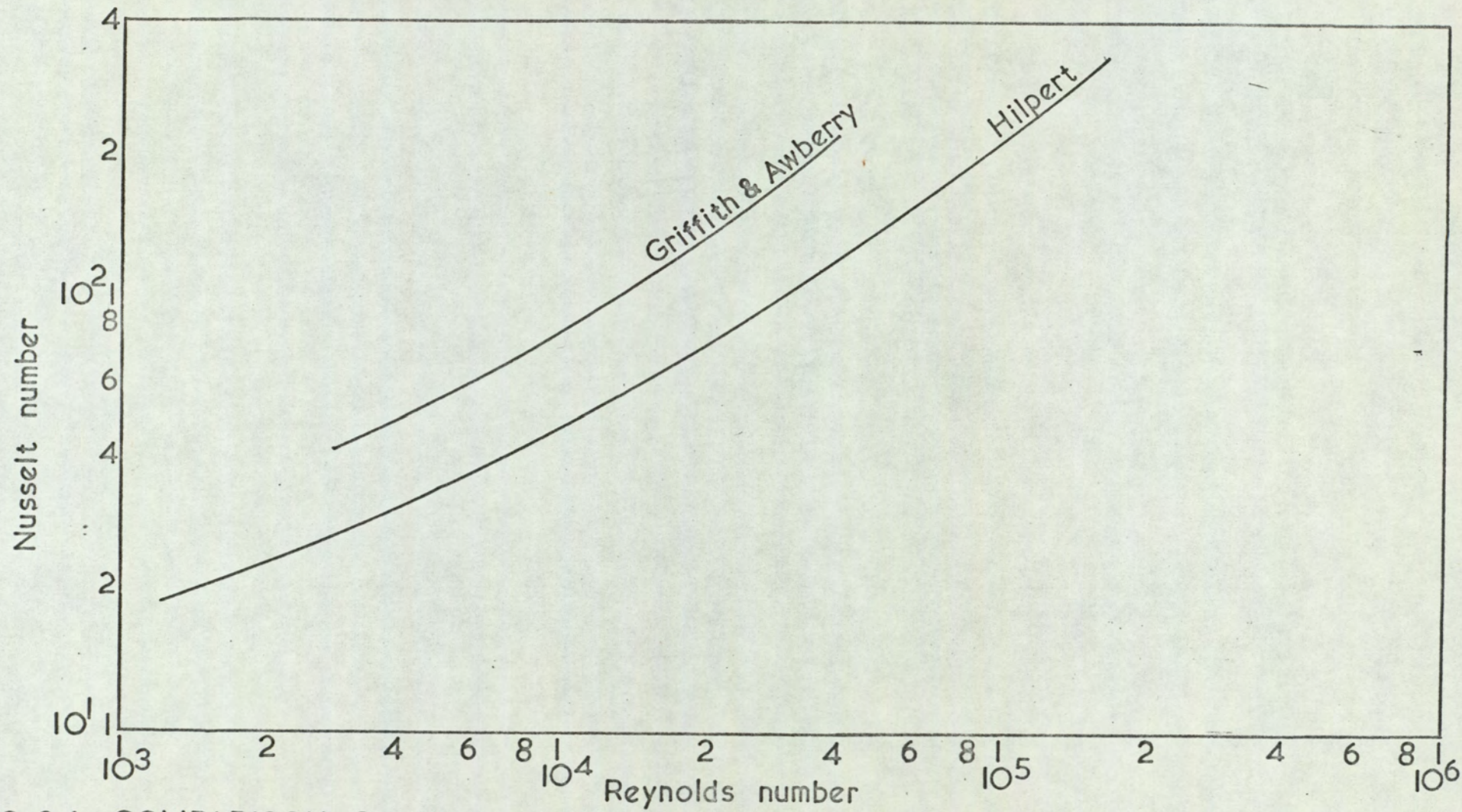


FIG. 3.6 COMPARISON OF HEAT TRANSFER DATA FOR A SINGLE TUBE IN CROSS-FLOW

determined theoretically, due to the difficulty in mathematically handling random fluctuations, so it has to be determined experimentally. Its existence can be seen in Fig. 3.6 in which a graph is drawn of Hilpert's (1933), and Griffiths & Awbery's (1933) heat transfer results to a tube in cross flow. The difference between the curves is too large to be explained by consideration of their experimental techniques.

Comings et al (1948) were among the first to obtain experimental results for the effect of intensity of turbulence. For a Reynolds number of 5,800, they varied the intensity of turbulence from 1.8% to 21.6% and found that over this range, the heat transfer increased by 10% with the majority of the increase of heat transfer being in the range 1.8% to 8% turbulence. Kestin, Maeder & Wang (1961) showed that imposing a pressure gradient on a flat plate restored the influence of turbulence intensity, and hence concluded that intensity of turbulence only affected local rates of heat transfer in the presence of a pressure gradient. Schlichting (1962) showed that the interdependence between pressure gradient and turbulence intensity could be understood qualitatively using the theory of Lins (1957) for non-steady boundary layer flows in which the average balance of forces in the laminar boundary layer involved an additional term J , of the form

$$J = \frac{1}{2} u_g \frac{du_g}{dx} f\left(\frac{y}{\delta}\right) \quad 3.44$$

for the case of a harmonic oscillation $u_\infty(x) \sin nt$ superimposed on an average velocity $\bar{u}_\infty(x)$. In this example the amplitude u has the same effect as the intensity of turbulence which is a measure of the r.m.s. of the amplitude of random

oscillations. The term J vanishes when the rate of change of amplitude $\frac{du}{dx} = 0$. According to this reasoning strong deceleration and subsequent acceleration of a stream as occurs in the neighbourhood of the stagnation point on a tube will cause the rate of change of the intensity of turbulence to become large, hence the effect on heat transfer will be greatest at this point. This has been confirmed experimentally by Seban (1960), Kestin, Maeder & Sogin (1961), Sogin & Subramanian (1961) and Perkins & Leppert (1964).

All these results, together with the extensive local heat transfer measurements of Zapp (1950) and Geidt (1951), now form a reasonably comprehensive set of results upon which a basis can be set up to rationalise all future heat transfer work on tubes. This was basically the idea of Talmor (1966), who used the data of Zapp, Kestin, Maeder & Sogin, Schmidt & Wenner (1947) and Geidt, together with his own work essentially in the supercritical range in correlating :-

$\frac{N_{Nu}}{(N_{Pr})}$ (average) Versus N_{Re} (corrected for blockage) and

$\frac{N_{Nu}}{(N_{Pr})}$ (stagnation point) Versus N_{Re} , with turbulence as a parameter.

He found that the curves obtained were accurate enough to obtain the intensity of turbulence of the flow from heat transfer data. It was found that the intensity of turbulence for Schmidt & Wenner's work was 1%, not zero, as they inferred, and that four of Geidt's zero intensity of turbulence results were obtained at a value of 3%.

However, Talmor did not use all the local heat transfer coefficient data available which could easily be converted to average heat transfer coefficients, namely that of Seban (1960), Sogin & Subramanian (1961), Perkins & Leppert (1964) and all

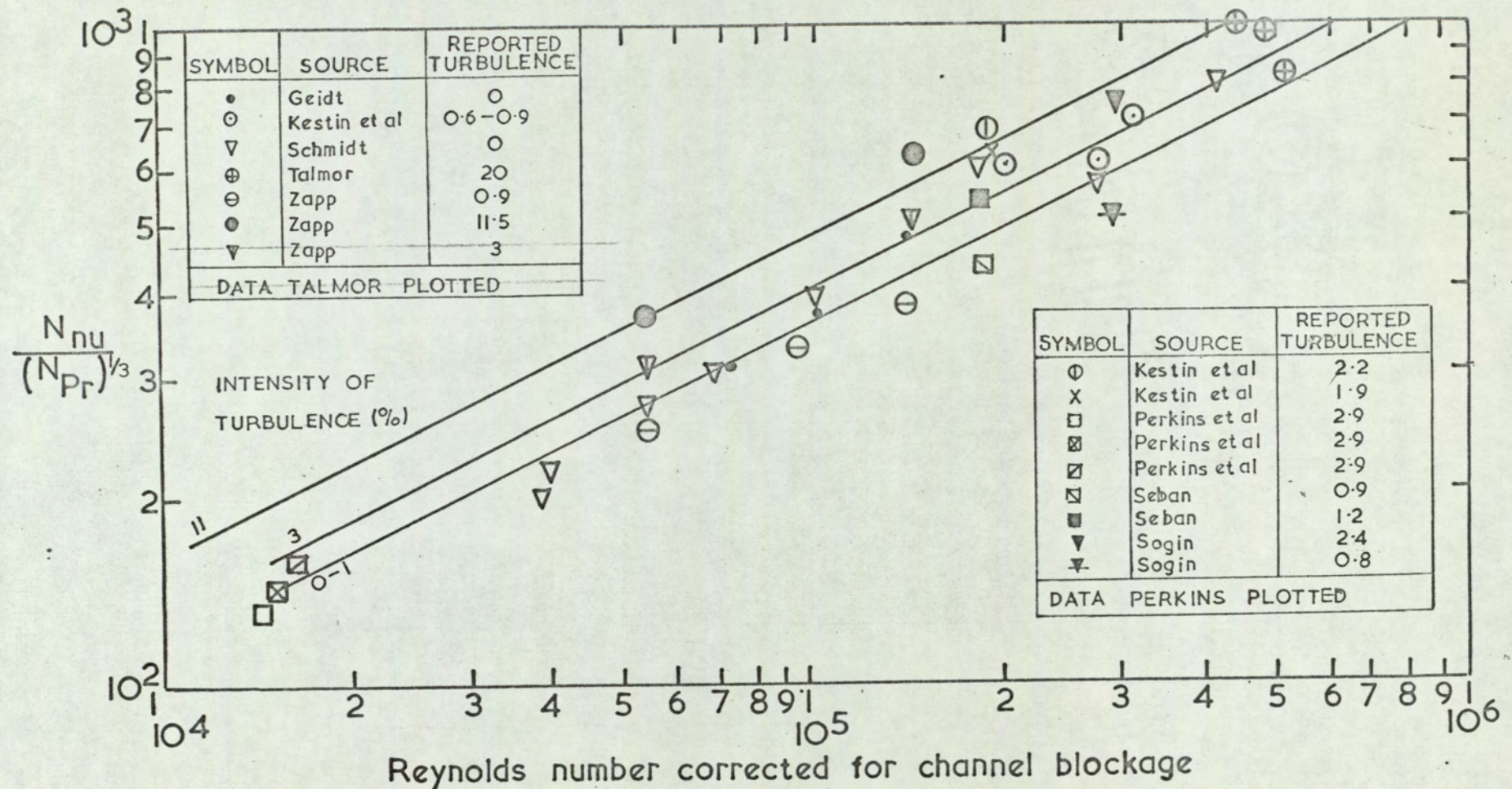


FIG. 3.7 STAGNATION POINT HEAT TRANSFER COEFFICIENTS AGAINST CORRECTED REYNOLDS NUMBER FOR VARYING TURBULENCE INTENSITIES

the available results from the work of Kestin, Maeder & Sogin (1961). Perkins & Leppert (1964) plotted these workers' data together with that of Zapp (1950) with turbulence as parameter and found some discrepancy which could not be explained when both channel blockage conditions or intensity of turbulence were taken into account. Fig. 3.7 compares the stagnation point heat transfer correlations (as a function of turbulence) of Talmor (1966) with the data that Perkins & Leppert (1964) plotted.

3.4.2.2 Scale of Turbulence

The scale of turbulence is a measure of the size of individual eddies and is defined by a characteristic length, L where,

$$L = \int_0^{\infty} R(y) dy \quad 3.45$$

$R(y)$ is a correlating coefficient of longitudinal fluctuations u'_1, u'_2 at two points whose transverse distance is y , namely,

$$R(y) = \frac{\overline{u'_a u'_b}}{\sqrt{u'^2_a} \sqrt{u'^2_b}} \quad 3.46$$

The effect of scale of turbulence upon heat transfer has been the subject of fewer investigations than intensity of turbulence. The most comprehensive experimental study has been carried out by Hegge Zijnen (1958) who measured rates of heat transfer from wires and tubes for Reynolds numbers of between 60 - 25,800 and ratios of scale of turbulence to tube diameter $\frac{L}{d_c}$ of between 0.31 - 240. Results showed that at constant Reynolds number and intensity of turbulence, heat transfer increased with increasing scale ratio to a maximum when the ratio $\frac{L}{d_c}$ was about 1.5 - 1.6, and then steadily decreased. Most of the increase in heat transfer occurred in

the range of scale of turbulence 0.5 - 7.

Hegge Zijnen (1958) explained this variation by assuming that the effective frequency of turbulence was proportional to $\frac{u_\infty}{L}$, and equalled the frequencies of eddies shed by the tube (Strouhal effect) over the range of $\frac{L}{d}$ of 1.5 - 1.6 (the value of maximum effect on heat transfer).

3.4.3 Corrections for High Temperature Difference

Douglas & Churchill (1956) re-examined data and correlations for convective heat transfer for gases flowing across a tube, particularly with respect to large temperature differences between the gas and surface. The object of the work was to provide the most satisfactory method for obtaining correlations from available data.

They reviewed three methods of correlating heat transfer data. These were:-

- (1) Evaluating thermal conductivity and absolute viscosity at the mean film temperature, i.e. $0.5 (T_\infty + T_w)$ and plotting N_{Nu} against N_{Re} . It was found that correlations obtained by McAdams (1954b) using this method did not adequately fit the high-temperature difference data.
- (2) Evaluating thermal conductivity and kinematic viscosity at the mean film temperature. Douglas & Churchill (1956) found that a satisfactory correlation could be obtained for both heating and cooling when this method was used.
- (3) Using a method in which the resistance to heat transfer between a gas stream and a tube can be considered as two resistances in parallel, one corresponding to the laminar boundary layer over the front part of the tube and the other corresponding to the turbulent wake region. The

thermal resistance in the region within the laminar boundary layer can be taken as inversely proportional to $u_{\infty}^{\frac{1}{2}}$ and the resistance in the turbulent wake as inversely proportional to u_{∞} . Using these two assumptions, Douglas & Churchill (1956) found the following correlation fitted the data available :-

$$N_{Nu,m} = 0.46 N_{Re,m}^{\frac{1}{2}} + 0.00128 N_{Re,m} \quad 3.47$$

Methods (2) and (3) are both satisfactory for evaluating high temperature difference heat transfer data but as the resistance method is more complicated to apply, method (2) will be used to evaluate heat transfer data in the present work.

3.5 Calculation of the Alkalies Released from the Combustion of Coal

In the previous section methods have been presented to calculate the mass transfer conductance. Before this coefficient can be used to determine the mass transfer rate to the tube surface, the driving force across the boundary layer has to be calculated which means that the concentration in the bulk gas stream must be known. As there are a great number of unknown constituents passing into the vapour phase on the combustion of coal, the problem has to be greatly simplified. At present, methods are only available for calculating the constituent vapours and condensed phases present, not any particulate matter formed on the combustion of coal.

Boll & Patel (1960) calculated the concentrations at equilibrium for the combustion gases of two Illinois coals with emphasis on the sodium and potassium salts obtained. They assumed that twenty-nine gaseous and five condensed constituents containing seven elements were present in the

gas phase which was the maximum number of constituents that the store of the computer used could accommodate. Boll & Patel calculated the amount of volatile matter passing into the gas phase from the ultimate coal analysis and ash analysis assuming that the only volatiles in the ash were sodium and potassium. The percentages of these elements and the amount of sulphur¹ passing into the vapour phase were called 'appearance factors' and were estimated from data obtained with an experimental cyclone furnace. The procedure to determine the composition of the gas phase involved the simultaneous solution of the equations representing all the thermodynamic equilibria possible in the gas for the chosen constituents. Use was made of a simplifying assumption of Brinkley (1947) to reduce the number of equilibria possible for the selected compounds.

Cliffe (1967) calculated the equilibrium concentrations obtained from the combustion of the coals named in Table 2.1, again with emphasis on the sodium and potassium salts. The method used was similar to that of Boll & Patel but utilised an improved computer programme (Raynor 1964) which allowed up to fifty compounds containing ten elements to be present in the combustion gases. The 'appearance factors' were calculated by assuming that the water-soluble portion of the sodium and potassium content in the coal passed into the gas phase and used the data of Cutler (1963) for the amount of sulphur volatilised.

1. Some of the sulphur will be absorbed by the ash,

SECTION 4

Reappraisal of the Deposition Problem

It can be concluded from Section 1 that there is a considerable amount of evidence to show that the behaviour of alkali-metal compounds plays an important part in the build up of tenacious and potentially corrosive deposits. Hence a method of limiting or preventing alkali-metal compounds in the flue gas from reaching the tubes would help to solve both fouling and corrosion problems.

To achieve this objective an experimental programme is proposed in this Section which should provide quantitative data of deposit formation under conditions that bear a close relationship to those in a tube bank of a boiler.

4.1 Previous Research

There has been little research done to determine quantitatively the mechanisms of deposit formation on boiler tubes from the combustion of coal. Bishop (1966) and Bishop, Gliffe & Langford (1967) measured deposition rates from the combustion of the coals given in Table 2.1 in a small pilot scale combustor. However it was not possible to obtain the rates of deposition due to a specific mechanism from their results.

A laboratory scale model study into the condensation of sodium chloride from a moving gas stream with reference to deposit formation in boiler tubes has been carried out by Jackson & Duffin (1963). Their combustor was fired with a 'clean' fuel in which known concentrations of the pure salt were injected. The salt was condensed onto a single tube and deposition rates were determined as a function of surface temperature. Two conclusions were drawn from this work:

firstly, that for constant mainstream velocity, the deposition rate was proportional to the mainstream concentration of salt vapour when the surface deposit did not exert an appreciable vapour pressure, and secondly, that the effective vapour pressure of the salt in the flue gas was much higher than in nitrogen or 'in vacuo', probably due to the presence of water vapour.

In this research, no attention was given to consideration of flow conditions in a boiler tube bank when constructing the apparatus, which resulted in the low Reynolds number of 21 based on tube diameter being attained compared with 3,000 in an actual boiler; nor was any attention given to the theoretical prediction of the deposition rate. However, at a later date, Brown (1966) calculated these theoretical deposition rates using a heat/mass transfer analogy approach (Section 3.3.2.1) and found that the theoretical deposition rates were 30% higher than the experimental results for the region where the surface deposit did not exert an appreciable vapour pressure.

Shuttleworth (1964) and Brown (1966) have carried out pilot scale model deposition studies with specific reference to oil-fired boilers. The deposition problem in oil-fired boilers is similar to the one found in coal-fired boilers, the main differences being that vanadates are the major cause of corrosion and that the ash content of the oil is considerably less than coal, hence impaction is not such an important mechanism of deposition. In this work known amounts of sodium sulphate and vanadium pentoxide were injected into a kerosine-fired combustor and collected on a single tube. Using the deposition rate results obtained, an attempt was

made to assess quantitatively the mechanisms of deposition but the analysis was far from rigorous as the effect of the flow conditions around the collection tube on mass transfer were not fully realised. Little agreement occurred between experimental and theoretical results.

Recently Goldberg, Gallagher & Orning (1967) made a laboratory study of the sulphation of sodium chloride and potassium chloride and tried to relate it to the corrosion on fireside surfaces of coal-fired boilers. The work was very qualitative in nature but did show that the surface sulphation proceeded at a faster rate than the vapour phase reaction for both salts, the sulphation of sodium chloride being faster than the sulphation of potassium chloride. However, no mention was made in their work of residence time which will be of some importance for the gas phase reaction.

4.2 An Experimental Programme

In deciding upon an experimental system, a suitable collection surface has to be chosen onto which the deposit can be collected and the deposition rate determined. The flow conditions around this collecting surface must be known and bear some relation to those found in the tube bank of a boiler. A suitable collecting surface is a single tube which can be considered as representing one of the tubes in the front row of a tube bank. Under typical boiler operating conditions a laminar boundary layer exists on the front of one of these tubes which means that it is possible to calculate the mass flux due to concentration diffusion and thermal diffusion through the layer.

The next decision to be made is whether to have a coal-fired experimental system or to use a model technique. The

principal advantages of a coal-fired system can be summarised as follows :-

- (1) The products of combustion are complicated in character, comprising mixtures of gases, vapours, solid particles and liquid droplets, thus are difficult to simulate in model experiments.
- (2) A working combustor of appropriate size was available having been used for more qualitative studies previously (Bishop 1966; Bishop, Cliffe & Langford 1967).
- (3) Certain aspects could be compared with the previous work on this combustor.

However, there are numerous difficulties inherent in this type of system, namely:-

- (1) It is not easy to decide the chemical or physical characteristics which should be used in the selection of the test coal.
- (2) The errors in calculating the vapour phase concentration of condensable salt are large.
- (3) The vapour phase and surface sulphation rates are unknown.
- (4) A deposit contains more than one salt, so to evaluate the effective vapour pressure exerted by a salt at a particular temperature, Henry's law constant has to be known. This constant is unknown for any of the salt mixtures possible.
- (5) The effect of particles on the condensation of vapours is unknown.
- (6) Quantitative analysis of the deposit is only possible for the cations and anions present. The actual compounds in the deposit can only be determined qualitatively, hence several assumptions have to be made to assess the actual composition of a deposit.

It can be concluded that these numerous difficulties prevent quantitative data on mechanisms of deposition being obtained from a coal-fired system, hence it was proposed to use a model technique which could be made progressively more complicated until an accurate simulation of the deposition characteristics of coal could be achieved. The basic assumption made in this model approach is that a deposit consists of a matrix of inert fly-ash particles cemented together by alkali-metal salts. The only chemical reaction that is assumed to take place is the sulphation of the chloride both in the vapour phase and on the surface of the tube. In essence the model places emphasis on the condensation of alkali-metal salts and influence of particles on this condensation.

The model system chosen involved a combustor fired with a clean fuel into which the salts, sodium chloride, potassium chloride, sodium sulphate and calcium chloride, together with sulphur dioxide and particles would be injected in the following stages:-

- (1) The salts would be injected individually into the combustor, in order to compare the experimental and theoretical deposition rates.
- (2) Several mixtures of salts would be injected to obtain Henry's law constant.
- (3) A study of the sulphation process by injecting sulphur dioxide and the salts used in stage (1) individually, then injecting sulphur dioxide and mixed salts as used in stage (2). As this will only give the overall kinetics, both in the gas phase and on the surface of the tube of the sulphation process, a further series of

tests would be carried out to find the magnitude of the individual sulphation rates. The surface sulphation rate could be obtained by injecting and condensing the salt onto the tube, then injecting the sulphur dioxide.

- (4) A study of the influence of solids on condensation and the sulphation of the chlorides by injecting known size fractions of solids into the combustor and repeating stages (1) - (3).

The main parameters used in this model would be surface temperature, velocity of bulk gas flow and concentration of injecting species.

SECTION 55.0 Design and Construction of Combustor

The combustor was designed on a similar scale to the one that had been used for previous research at Wolverhampton (Bishop 1966; Bishop, Cliffe & Langford 1967). The reasons for this decision were:-

- (1) That the target section in the combustor already simulated a single boiler tube in the front row of a tube bank with appropriate channel blockage conditions.
- (2) Combustion was efficient in the combustor.
- (3) A wind tunnel of similar dimensions to the proposed target section was available for flow studies.
- (4) That this size of combustor was the maximum that could be accommodated.

5.1 Description of Combustor5.1.1 Design Criteria

The combustor was designed on six criteria, namely:-

- (1) A gas temperature of at least 1000°C should be attained in the target section. This is in line with normal boiler running conditions and ensures that all the alkali salts are volatilised.
- (2) A wide range of velocities (about 4 or 5 to 1) including a velocity of 10 m/s (normal boiler running conditions) should be obtained.
- (3) The gases are completely burned well before the target tube so ensuring that flow conditions and transport properties are constant in the target section.
- (4) The intensity and scale of turbulence would be as low as possible in the region of the target tube because heat

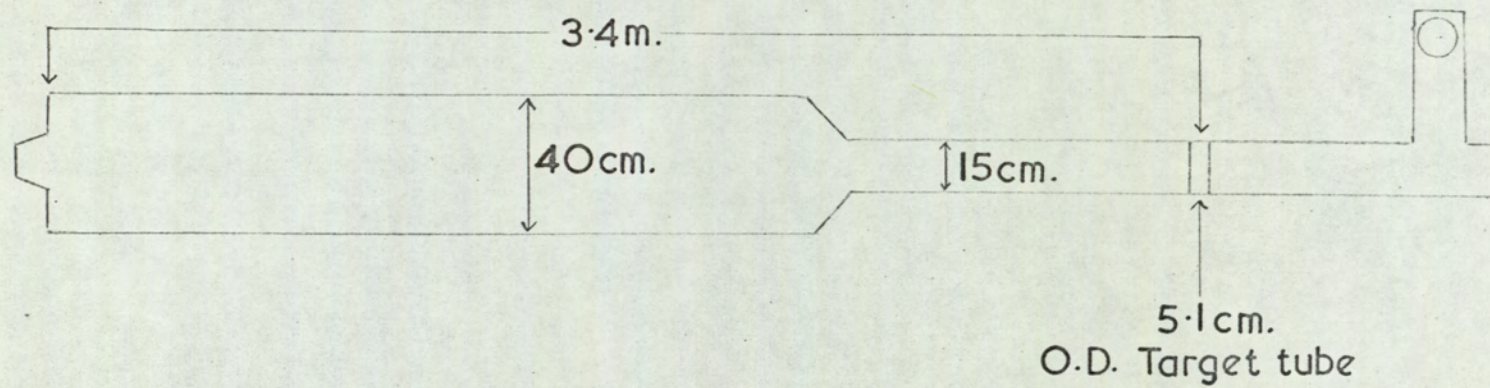


FIG.5.1 INTERNAL DIMENSIONS OF COMBUSTOR

transfer data used to estimate mass transfer rates was calculated from simulated flow conditions.

- (5) For reasons of safety, a 3% excess of oxygen was required.
- (6) A target section with a height of at least 10 cm. was required in order that a 5 cm. diameter target tube could be fitted into the duct with similar boundary conditions to those in the neighbourhood of an actual boiler tube.

Propane was selected as the fuel for the combustor because it was readily available in a high-purity form, it was more flammable than liquid fuel (e.g. kerosine) and a burner of relatively simple design was available which facilitated the introduction and mixing of the injected salt solution. Due to economic reasons, it was decided to use town gas for pre-heating the combustion chamber before each test.

5.1.2 Design Calculations

An outline of the combustor giving the relative dimensions is shown in Fig. 5.1. These dimensions were derived as follows:-

The target had similar dimensions to the one in the previous combustor, namely 10 cm. high by 15 cm. wide. By incorporating a 5 cm. diameter tube into the 10 cm. high duct, a channel blockage ratio of 0.5 is obtained, this is approximately the blockage ratio formed between two tubes in a tube bank. A 5 cm. diameter tube is the minimum diameter from which a reasonable sample could be collected without having an excessive length to target tube. Bishop (1966) showed that with a width of 15 cm. the temperature gradient across a 2.5 cm. length of 5 cm. diameter tubing in the centre of the duct was constant.

As the combustor was to be built on a similar scale to

that of Bishop's (1966), his heat input figure to obtain a target section gas temperature of $1,100^{\circ}\text{C}$ was used to calculate the range of velocities possible in the vicinity of the target tube. As shown in Appendix 1, velocities between 7.5 - 30 m/s were possible which was satisfactory because a range of velocities of $\frac{1}{4}$ to 1 and a velocity of 10 m/s were obtainable.

A round combustion chamber was chosen in preference to a square one because although a square one had superior burning characteristics, it was far more difficult to construct. The diameter of the combustion chamber was made 40 cm. which was similar to the previous combustor. In this combustor, a 1.3 m. long combustion chamber was satisfactory for a velocity of 10 m/s, so in order to facilitate the high velocities, it was increased to 2.1 m. There is no direct method of calculating flame length without knowing the variation of gas composition along the combustor, particularly carbon dioxide, hence the length was estimated from the previous work which used a different fuel (coal). With a combustion chamber of these dimensions, a contraction ratio of 8 to 1 resulted between it and the target section. A settling section was included upstream of the target section to steady the flow after the contraction. Using the data of McPhail (1940) it was estimated that a 0.9 m. long settling duct would be satisfactory for smoothing the flow.

The actual contraction between the combustion chamber and settling section was made 30 cm. long and smooth (i.e. a gradual reduction, not a step), as it has been found that a smooth contraction produced a flat velocity distribution at the exit (Pankhurst & Holder 1953).

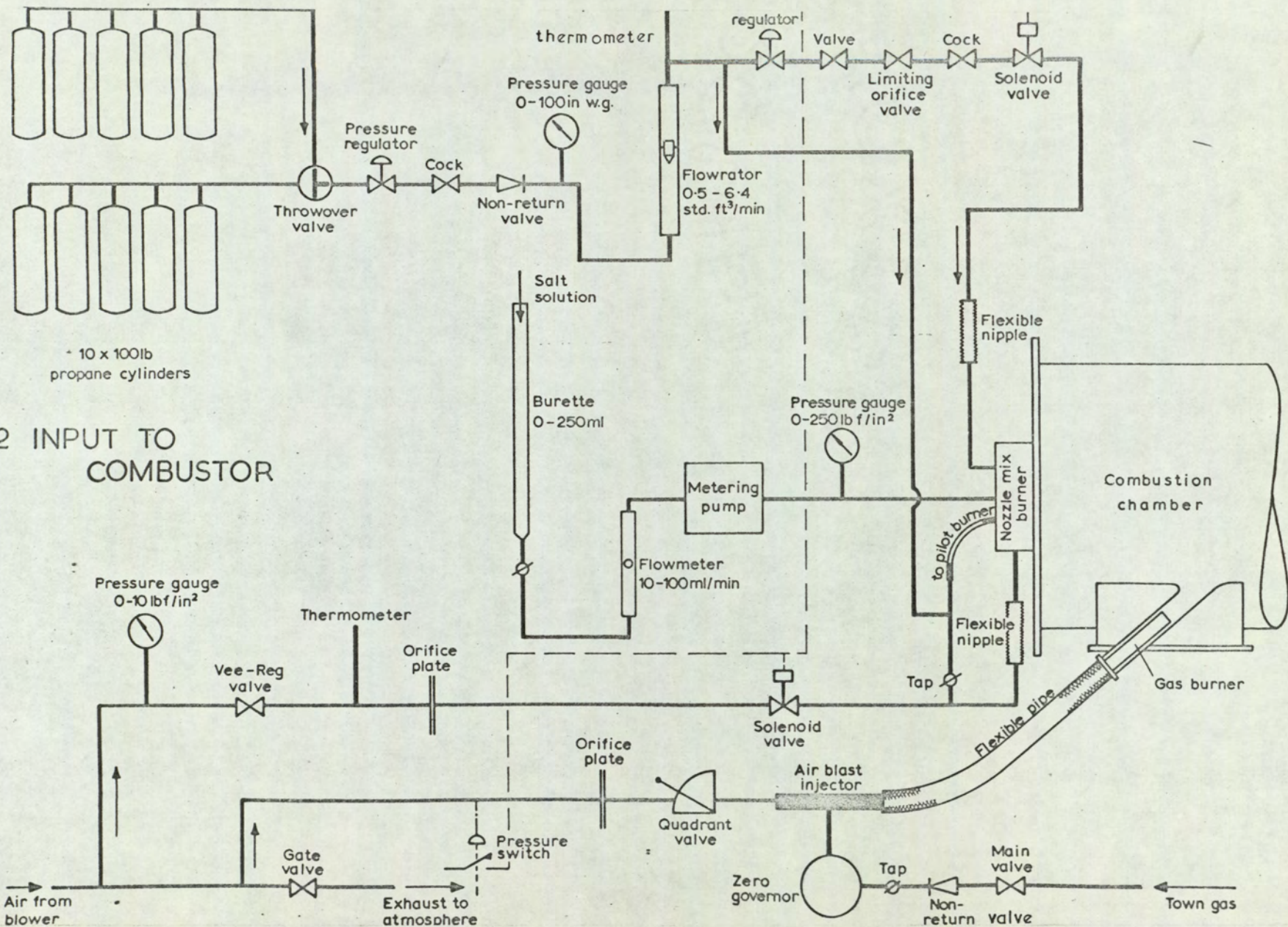


FIG. 5.2 INPUT TO COMBUSTOR

The whole combustor was designed to be placed horizontal because of ease of accessibility and increased constructional difficulties in building a vertical one.

5.1.3 Input to the Combustion Chamber

5.1.3.1 Air

A forced draught of air was supplied to the burner by a Rootes-type blower (Holmes 6 in. x 10 in. RBS). Compression in the blower raises the temperature of the air to approximately 50°C . The air in the main supply pipe from the blower was usually maintained at a pressure of approximately 42 kN/m^2 by manual adjustment of a gate valve which allowed air to be bled off to atmosphere (see Fig. 5.2). Limitations of space did not permit the inclusion of a damping chamber in the main pipe and the air pressure was subject to fluctuations of high frequency and low amplitude; however, these variations in pressure were not serious. In the event of the air pressure falling below normal operating values (e.g. a power failure), a pressure switch caused solenoid valves to close both town gas and propane lines.

5.1.3.2 Town Gas

The combustion chamber was preheated for approximately two hours by burning town gas. Supply arrangements for this gas are shown in Fig. 5.2. A Keith Blackman type 66 air blast burner in conjunction with a regulator was used, mainly on economic considerations.

5.1.3.3 Propane

Propane gas was obtained from one of two banks of 5 x 45.4 kg (100 lb.) cylinders and passed to the burner through a 2.5 cm. B.S. pipe (Fig. 5.2). Five cylinders have sufficient evaporative capacity to maintain a steady flow of

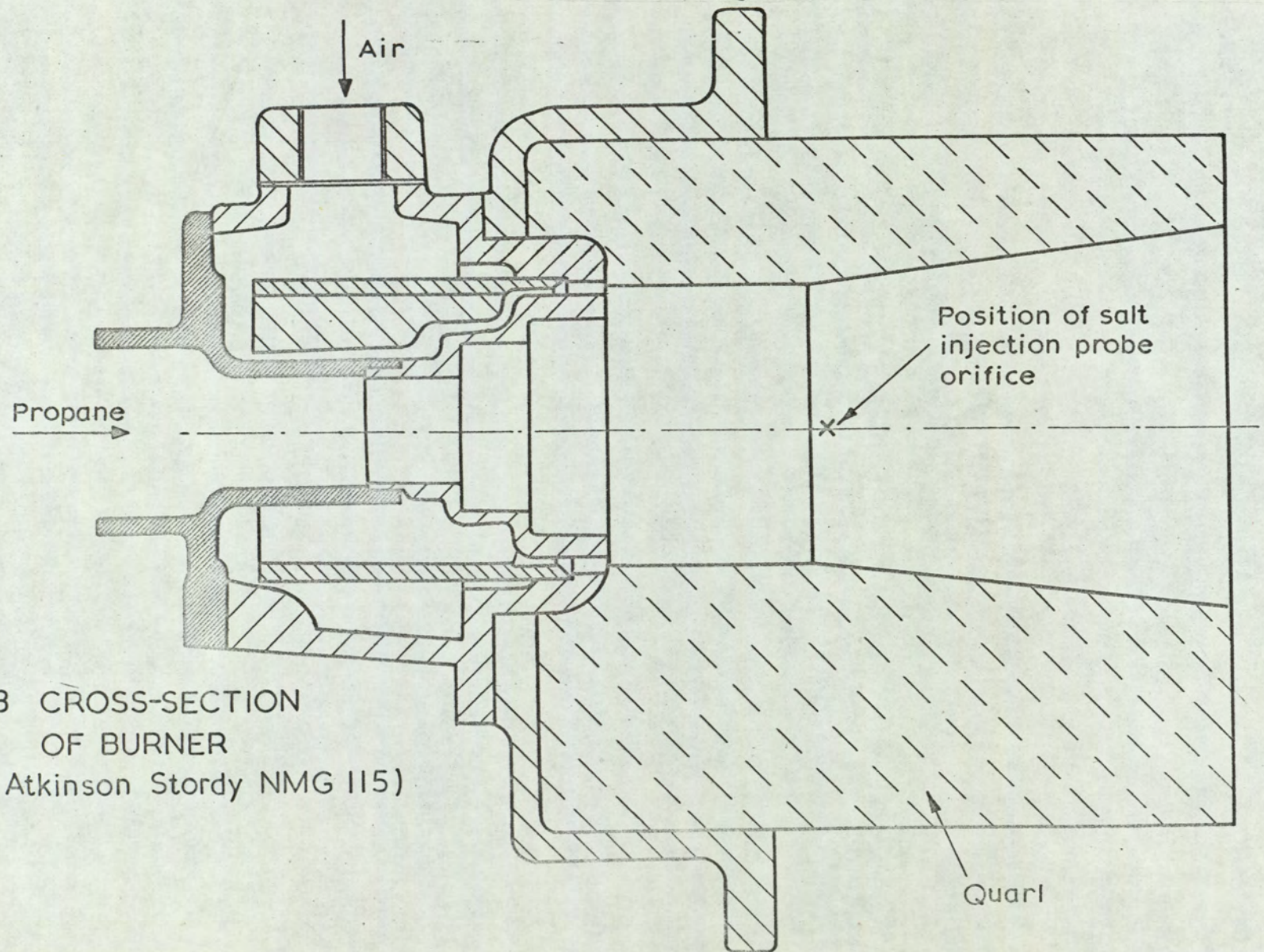


FIG. 5-3 CROSS-SECTION
OF BURNER
(Stein Atkinson Stordy NMG 115)

up to 18 kg/h (40 lb./h). Cylinders were chosen, rather than a single tank, because of the comparatively simple safety precautions. A two-stage system reduced the pressure of propane from cylinder pressure (about 690 N/m²) to 70 cm. w.g. and finally to about 15 cm. w.g. A two-stage system was used to obtain a steady flow.

The most suitable type of burner was found to be the Sturdy-Hauck N.M.G. nozzle mix burner, shown in Fig. 5.3. It was extremely flexible, cheap, and salts could be injected through its back.

5.1.3.4 Salt

Salt was injected along the axis of the burner in the form of an aqueous solution. The desired partial pressure of salt vapour in the gaseous phase was obtained by varying either the solution strength or the pumping rate. This method enabled the input of salt to be measured accurately but relied upon complete vaporisation of the salt in the flame zone. The introduction of water was acceptable because much larger amounts of water vapour are formed during the combustion of propane. (Alternative methods for introducing salts into a high temperature system have been summarised by Fells & Harker 1967).

The supply arrangements for the salt solution are shown in Fig. 5.2. A peristaltic pump (Watson Marlow Ltd., model MHRE) was originally used to inject the salt solution into the combustion chamber. Modifications to the probe nozzle, however, necessitated higher solution pressures and the peristaltic pump was replaced by a metering pump. The average rate of flow of the salt solution was obtained by using a 250 ml. burette as a reservoir for the standard salt solution and

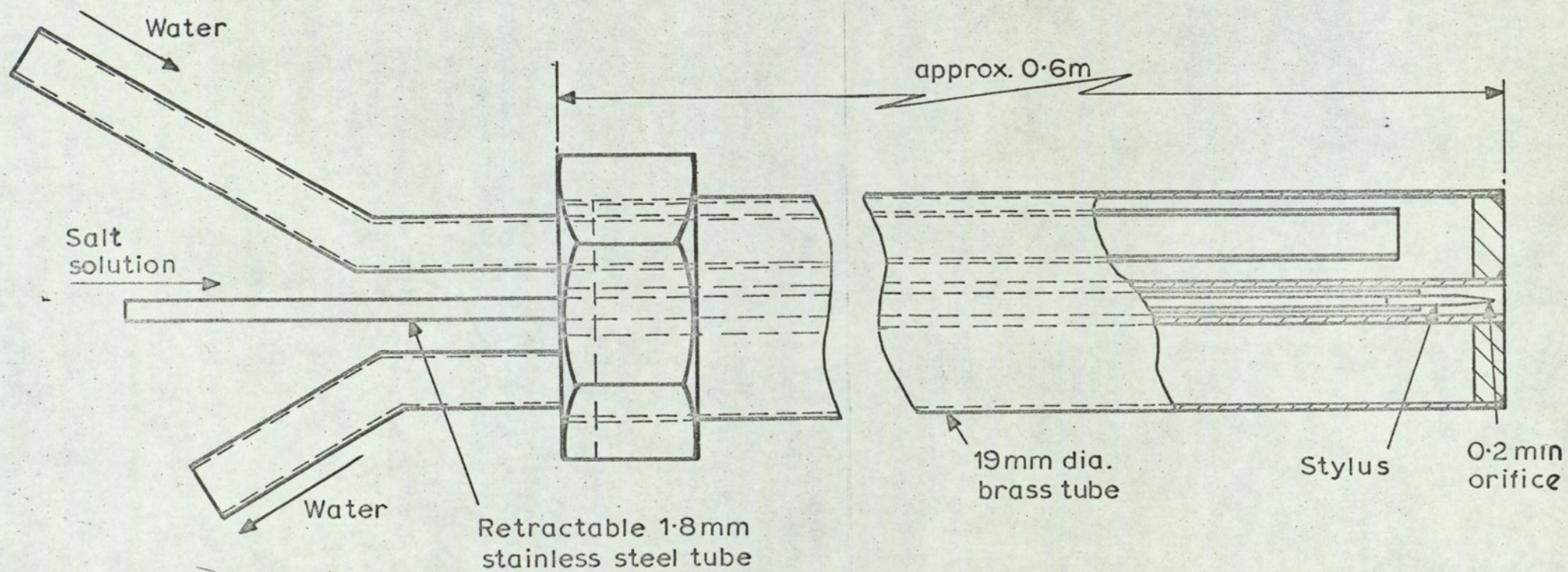


FIG 5.4a ORIGINAL DESIGN OF PROBE

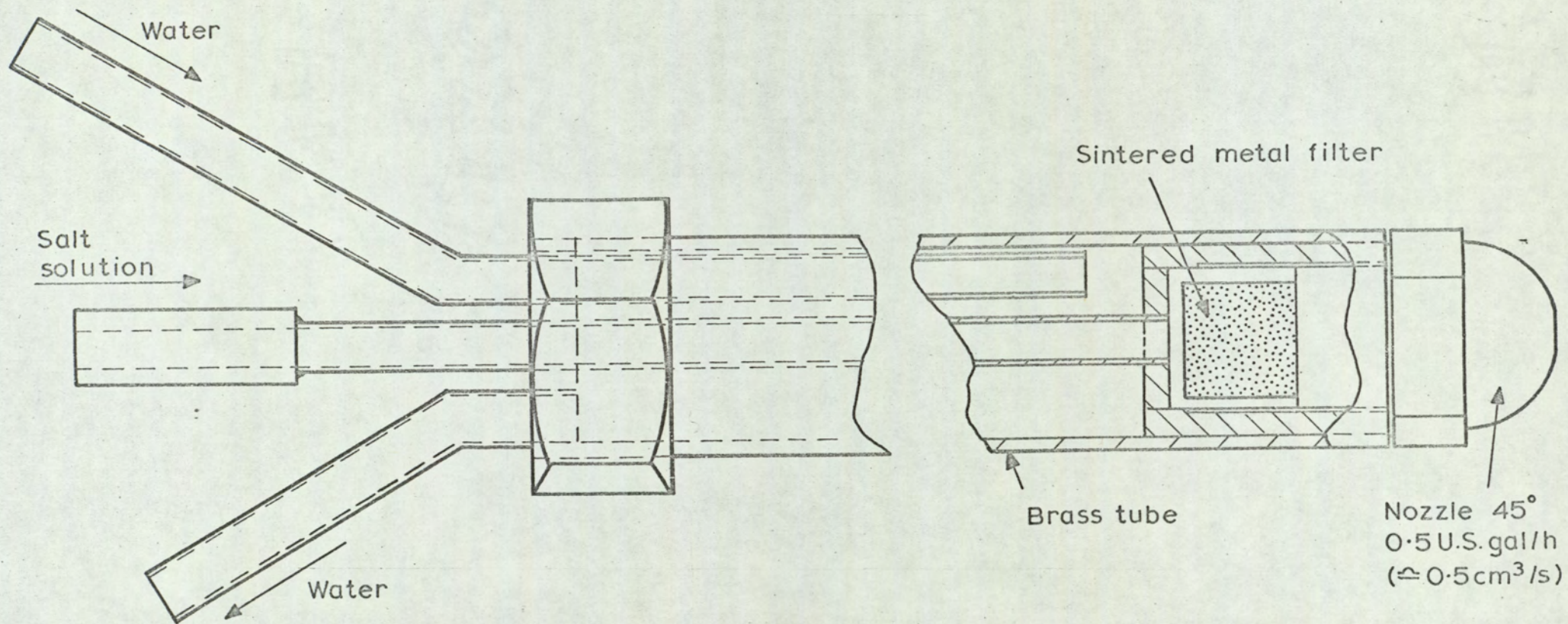


FIG.5.4b MODIFIED DESIGN OF PROBE

determining the rate at which the meniscus fell. The pressure of the pumped solution was about 55 kN/m^2 ; fluctuations in the flow were damped by having a small air pocket in the line to the pressure gauge.

Considerable difficulty was experienced in achieving complete vaporisation of the injected salt. The main features of the two types of water-cooled probes developed are shown in Fig. 5.4a and b. The jet of the first design of probe (Fig. 5.4a) was made from a stainless steel stylus which had a round and smooth 0.20 mm. diameter orifice. (Hypodermic needle tubing was unsatisfactory because the bore was less regular, causing drops of solution to accumulate slowly at the probe tip and/or the jet to become skew). Although the jet of solution from the probe shown in Fig. 5.4a reached the flame, the salt was not wholly vapourised and the minute droplets of salt which survived impacted onto the target tube. Reproducibility of results was poor and salt glaze formed in small regions on the refractory lining in the combustion chamber. Little or no free chloride was detectable at the refractory surface after tests.

These difficulties were overcome by fitting an oil burner nozzle (Monarch) to the end of the probe (Fig. 5.4b). No sign of impaction was found on the target tube indicating that the injected salt was completely vaporised in the combustion chamber. The nozzles which were used were designed for oil flow rates of 0.5 and 0.6 u.s. gal/h and project a spray with an apex angle of 45° . During a test, the nozzle, made of ferritic steel, became hot and was corroded by the solution of sodium chloride at a slow but tolerable rate. The nozzle was water washed and dried after each test run.

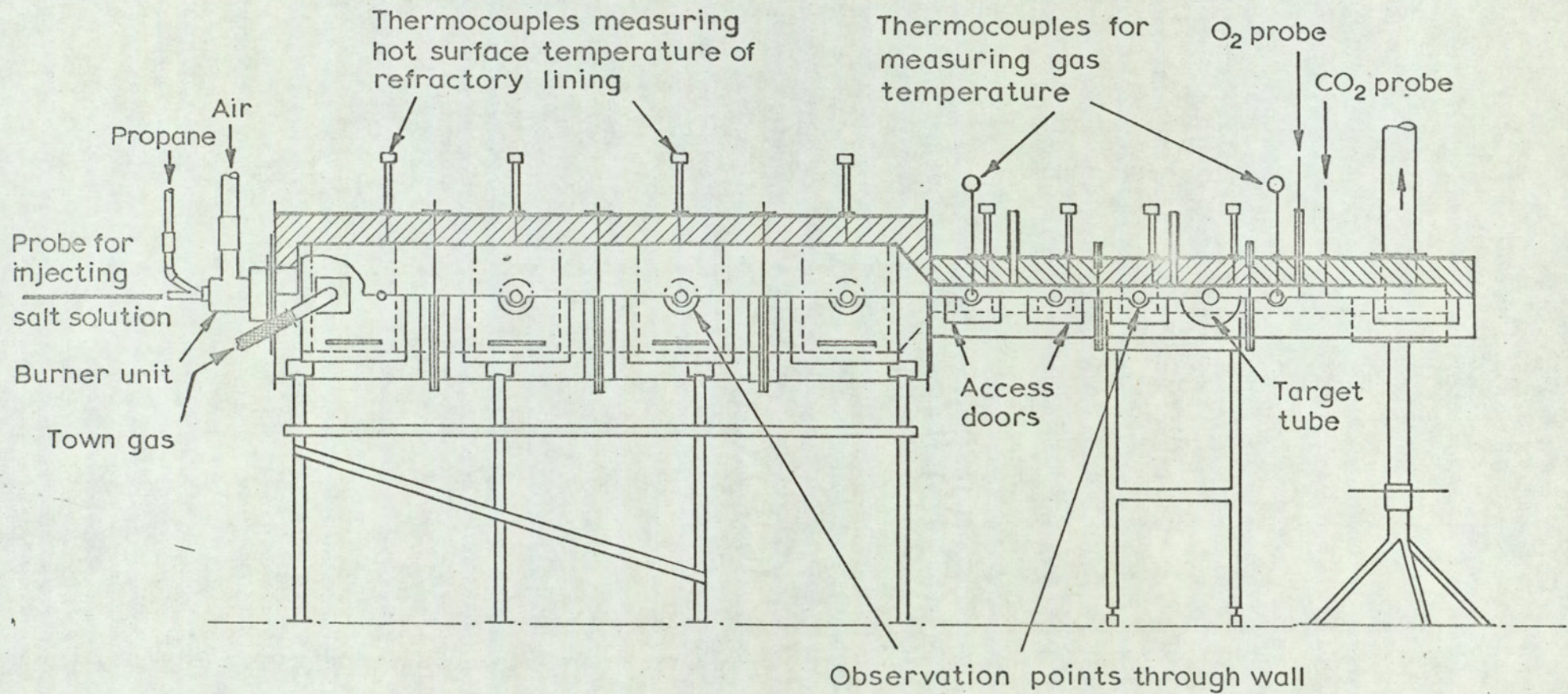


FIG. 5-5a GENERAL ARRANGEMENT OF COMBUSTOR

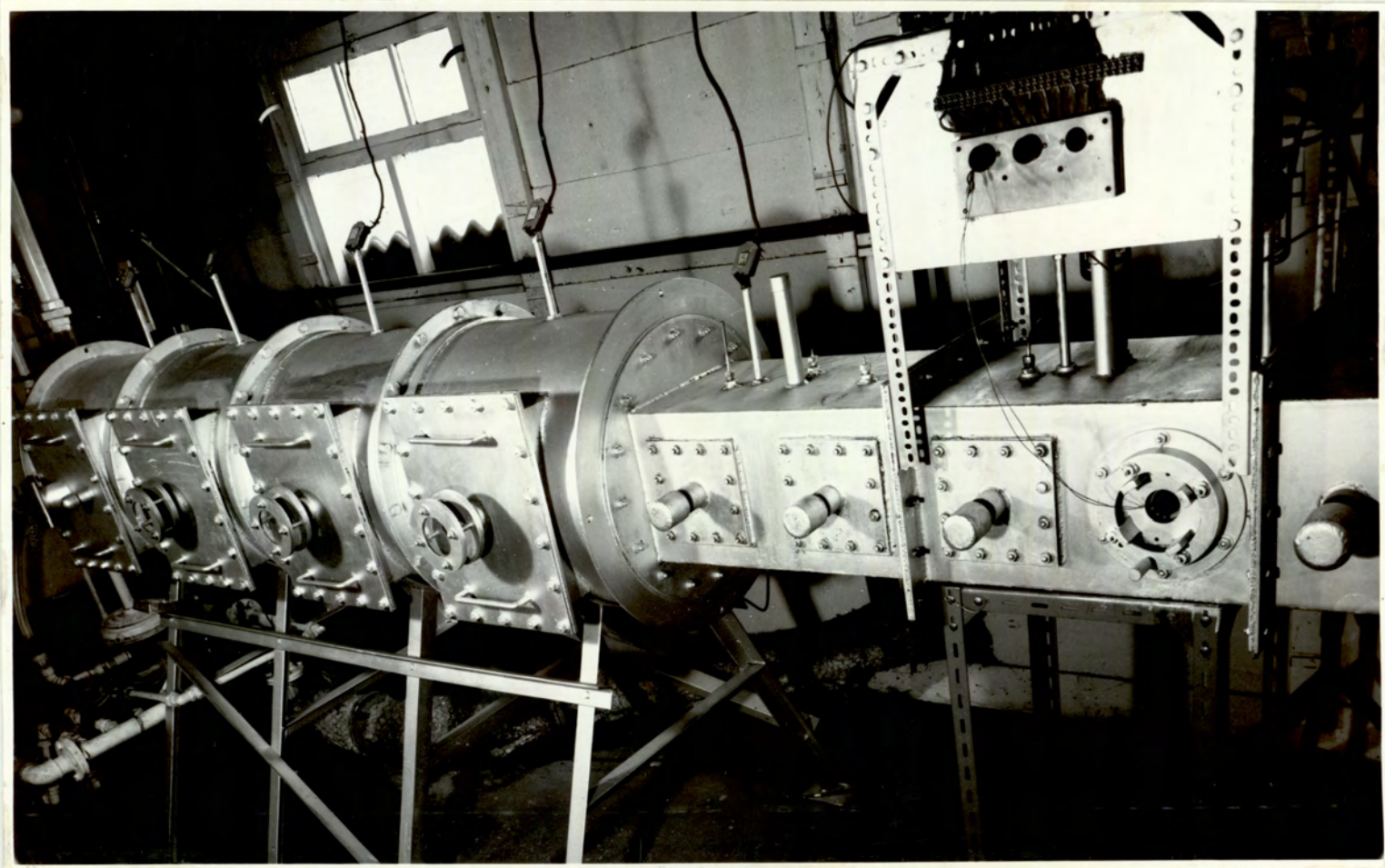


FIG 5-5b COMBUSTOR

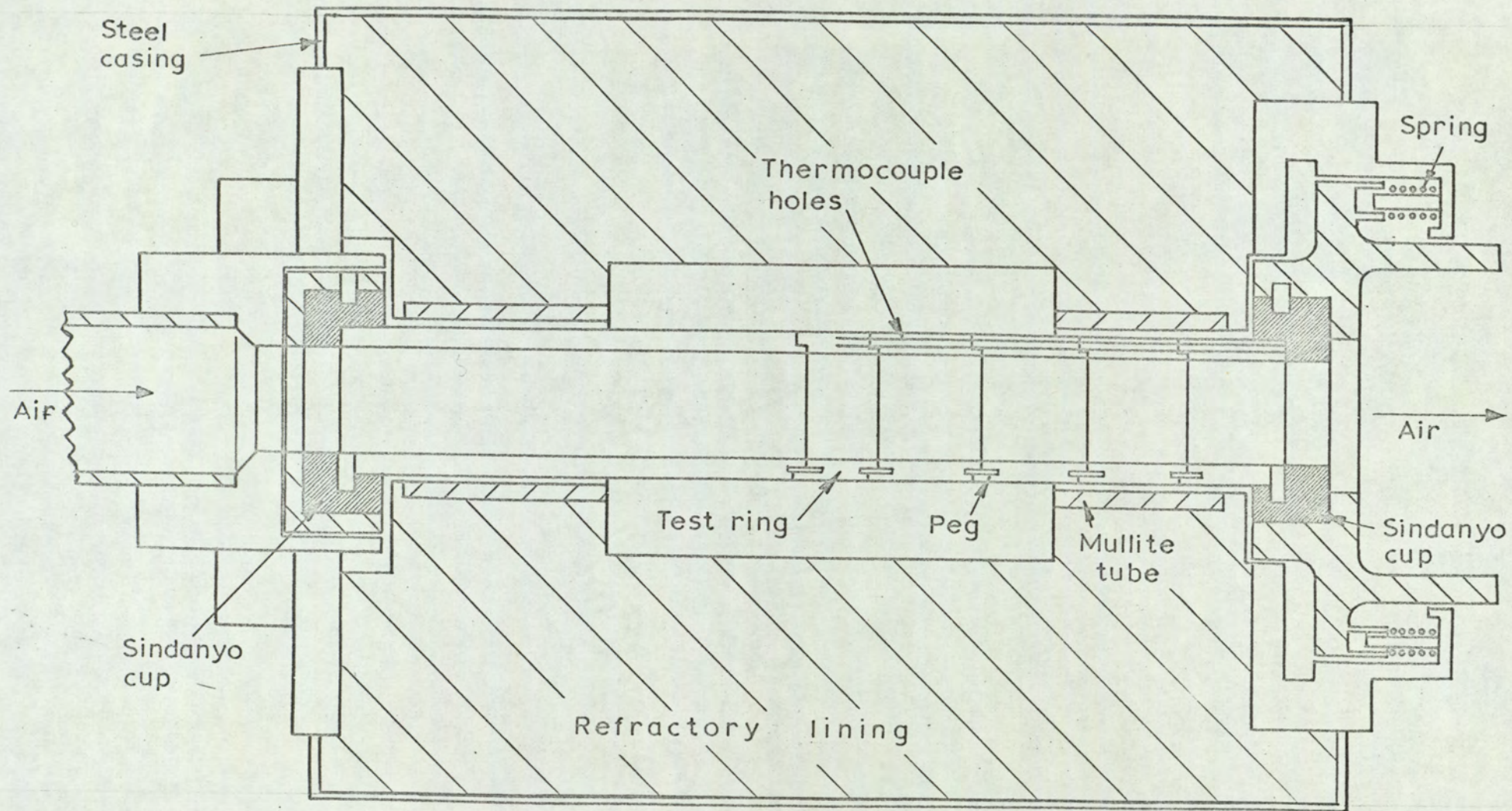


FIG 5-6a CROSS-SECTION OF TARGET SECTION

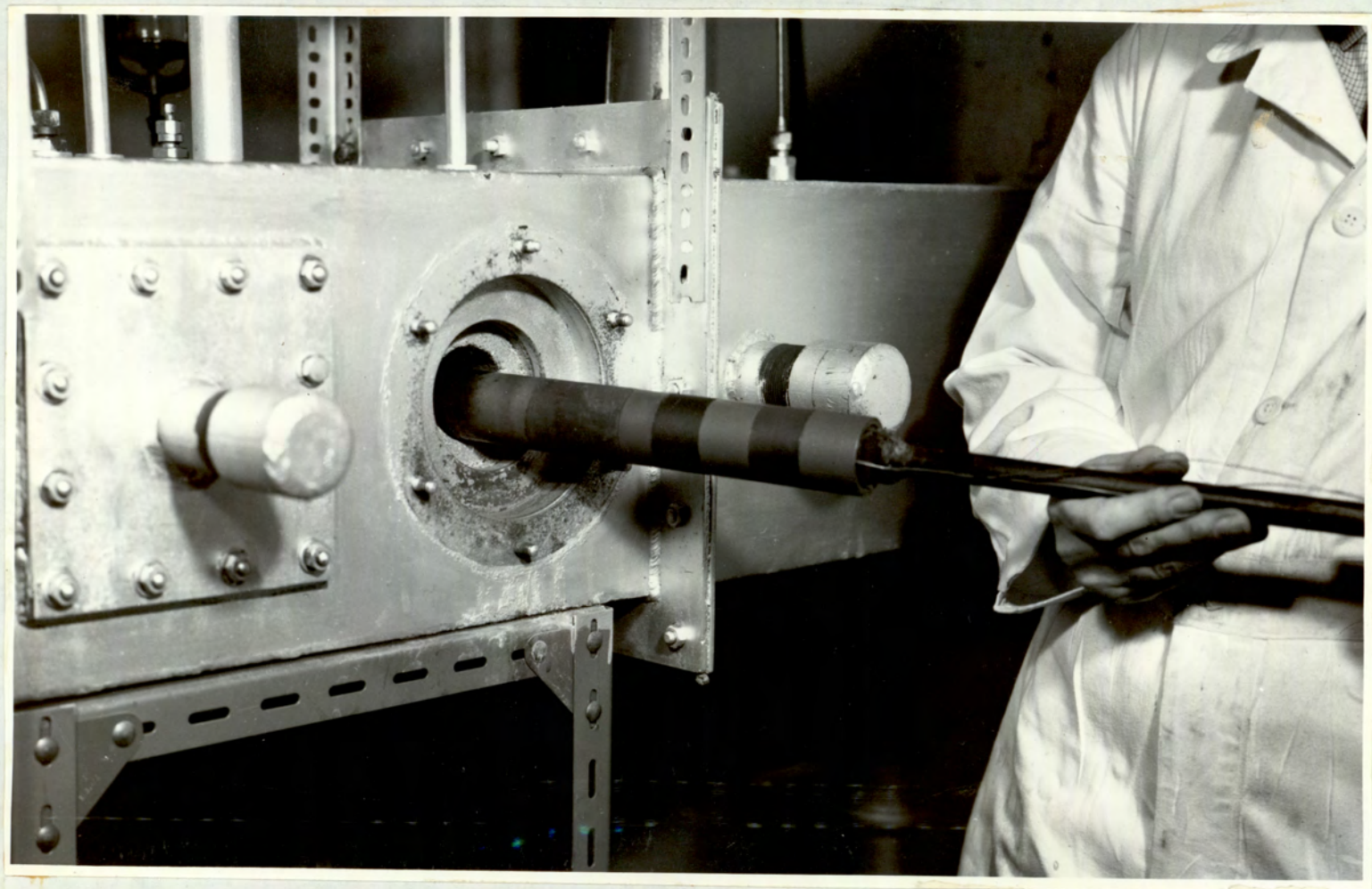


FIG. 5-6b TARGET SECTION

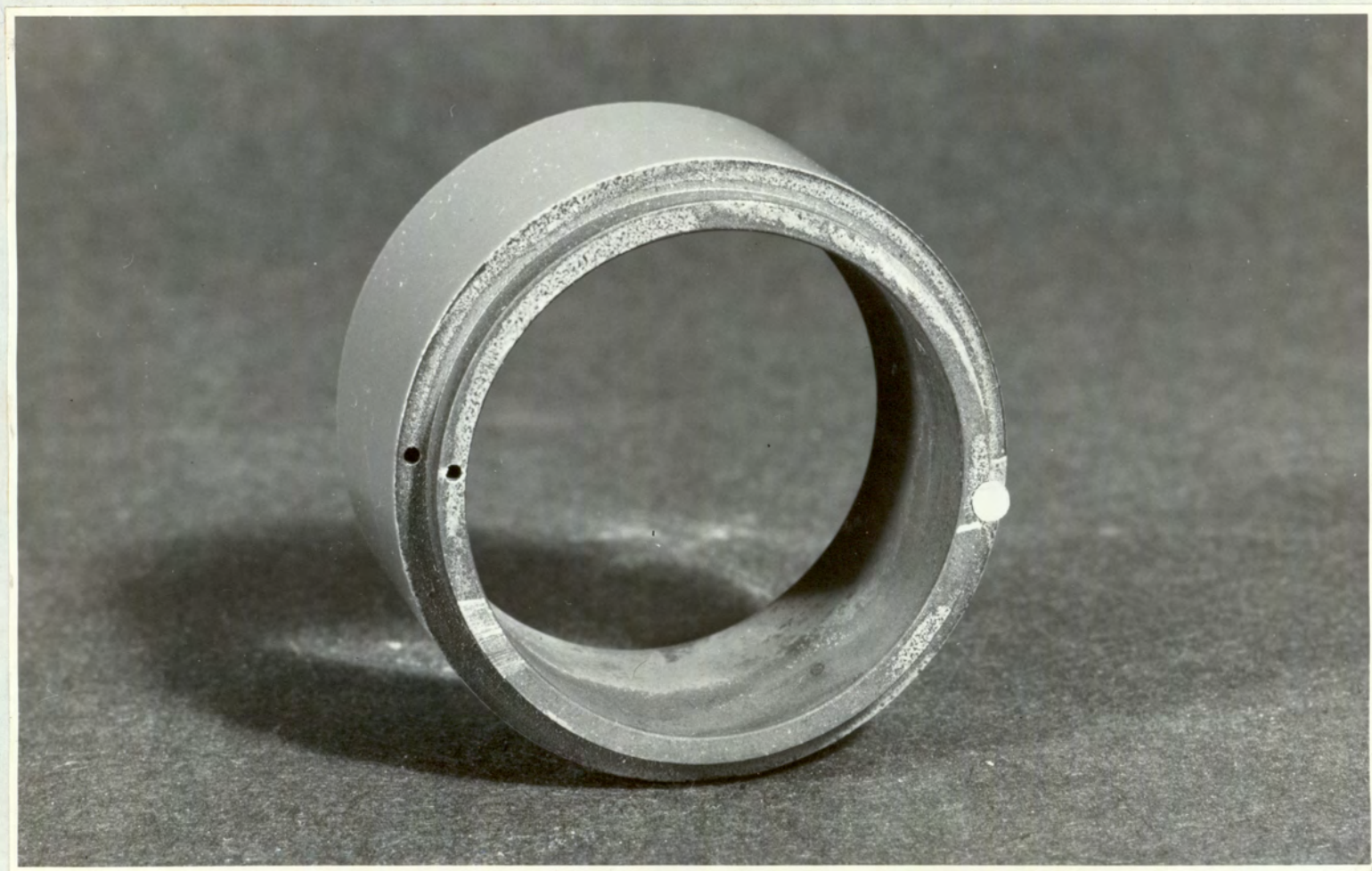


FIG. 5-6c TEST RING

5.1.4 Combustion Chamber and Intermediate Duct

The combustion chamber and the duct leading to the target section consisted of an outer shell of mild steel with a 10 cm. thick refractory lining (Fig. 5.5). The lining comprised of a 6 cm. thick hot-face layer of Plancrete/Molochite and a 4 cm. thick outer insulating layer of Plancrete/Vermiculite. With this thickness of lining, the greater part of the inner face operated at above 800°C, hence condensation in the combustor was unlikely.

Access doors with either safety windows of mica and perspex or covered tubular ports were provided along the length of the combustor. The central portion of the target tube was observed directly during tests through an obliquely located sight glass in the target section.

5.1.5 Target Section

This is shown in Fig. 5.6. The 5 cm. target tube consisted of spigotted support tubes and a central test ring, 2.5 cm. long, from which deposit was sampled after each test. Each section of the target tube was coated with a hard, inert and spall-resistant coating of enamel¹. The thin coating survived short-term exposures to the salt-laden gases and, by preventing oxidation of the underlying steel, facilitated sampling of the deposits. The target tube was machined from 12% chromium steel tubing in the fully softened condition. Although the choice of ferritic steel had the disadvantage that the enamel coating had to be fired in an inert atmosphere to prevent scaling, it facilitated the drilling of pairs of

1. Applied by Ferro Enamels Ltd., Wombourne, Nr. Wolverhampton, and fired by the author in an argon atmosphere.

clearance holes for 1.05 mm. diameter thermocouples along the tube wall parallel to the major axis of the target tube. The alternative use of an austenitic alloy, preferable for the enamel coating process, posed severe problems for drilling.

The various component tubes were held together temporarily by a central tie rod when fitting the assembled target tube into the test section. After careful insertion through a circular hole in one side of the target section duct, location of the target tube assembly in two Sindanyo cups and fastening of the circular end plates, the tie rod was unscrewed and withdrawn. The Sindanyo cups have a low thermal conductivity and reduce the lengthwise loss of heat from the tube assembly. During heating, the tube assembly expanded lengthwise against a set of coil springs. This arrangement prevented the considerable expansion stresses from distorting the spigot joints of the target tube. The entire tube assembly could be rotated through 30° increments and firmly pegged in each position, thus enabling the temperature distribution around the tube periphery to be determined under various conditions of operation.

The surface temperature at the forward stagnation point was controlled within the range 520° - 900°C by varying an internal flow of air from a blower (Keith Blackman centrifugal compressor); the maximum delivery of the blower was approximately $77 \text{ Std dm}^3/\text{s}$ ($160 \text{ Std ft}^3/\text{min}$) measured by a Dall tube.

5.1.6 Exhaust Section

Initially, a nimonic alloy cyclone was fitted downstream of the target section in preparation for tests with injected solid particles (see Section 4.3). However, difficulties were encountered with the pressure drop at velocities above

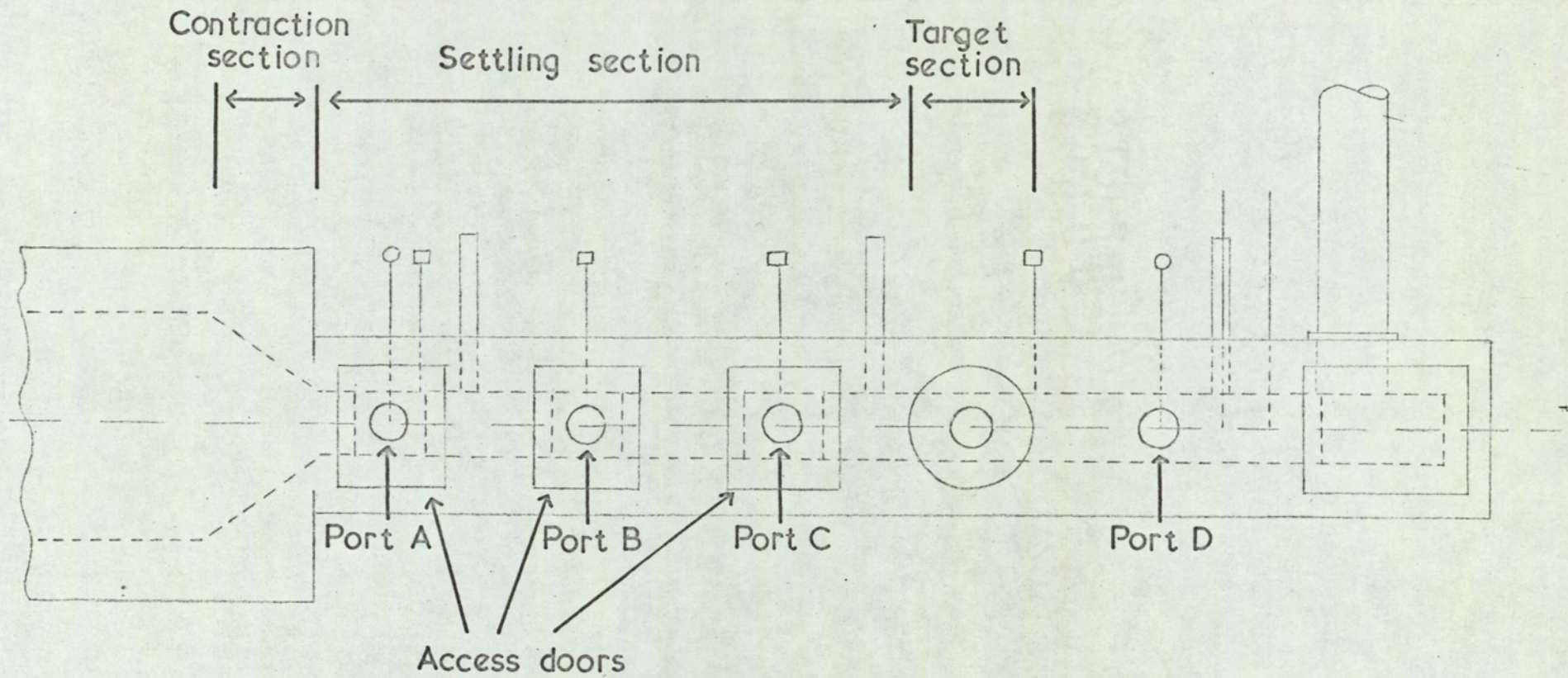


FIG.5-7 ENLARGED DIAGRAM OF THE END SECTION OF THE COMBUSTOR

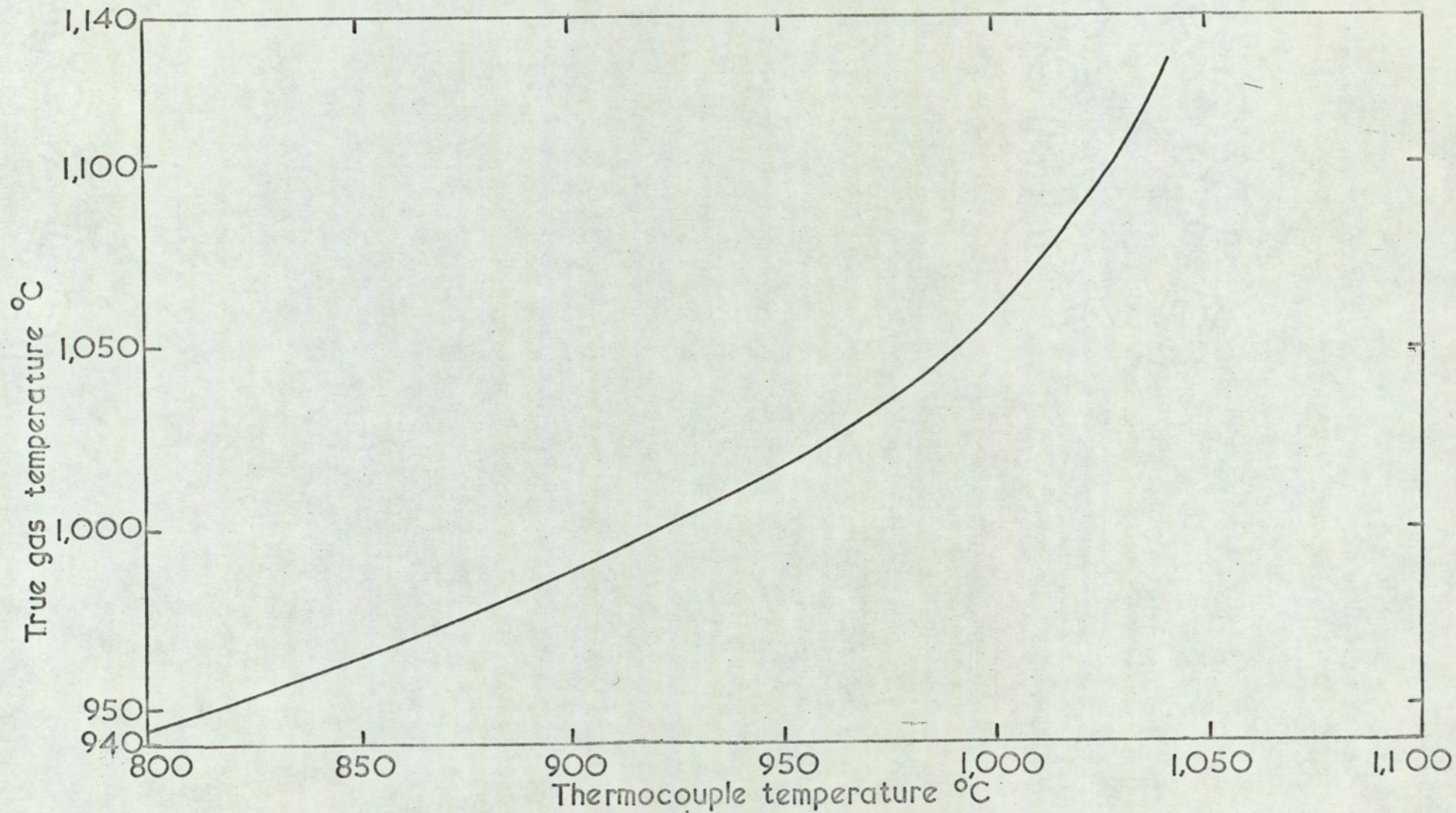


FIG. 5-8 CALIBRATION GRAPH FOR THERMOCOUPLE MEASURING TEMPERATURE OF MAIN GAS STREAM

11 m/s, also the entry part became red-hot under typical operating conditions. Accordingly the cyclone unit was replaced with a refractory-lined duct. Two 90° changes in direction were included for collection of solid particles in later tests. The salt vapours exhausted to atmosphere on leaving the chimney.

5.1.7 Instrumentation

5.1.7.1 Temperature Measurement

All thermocouples were of the mineral-insulated, stainless steel sheathed type (Pyrotenax Ltd., HT2/NC - NA/BJ).

The following measurements were made during each test run:-

- (1) The temperature just below the hot face of the refractory lining at eight points along the length of the combustor (Fig. 5.5) using 3.2 mm. diameter thermocouples.
- (2) The gas temperature downstream of the target tube, using a 3.2 mm. diameter thermocouple in a 6.4 mm. diameter sheath (Fig. 5.7). The relationship between this reading and the gas temperature immediately upstream of the target tube was obtained by interpolating from calibration graphs of gas stream temperatures at positions A, B, C and D (Fig. 5.8). These temperatures were measured by temporarily inserting a suction pyrometer through the portholes at these positions.
- (3) The wall temperature of the target tube at 30° intervals around the periphery, using 1.05 mm. diameter thermocouples. The 1.32 mm. diameter clearance holes for these thermocouples were parallel to the major axis of the target tube and decreased to 1.09 mm. diameter at the bottom so that the hot junction of each thermocouple made a good thermal contact. Each pair of hot junctions

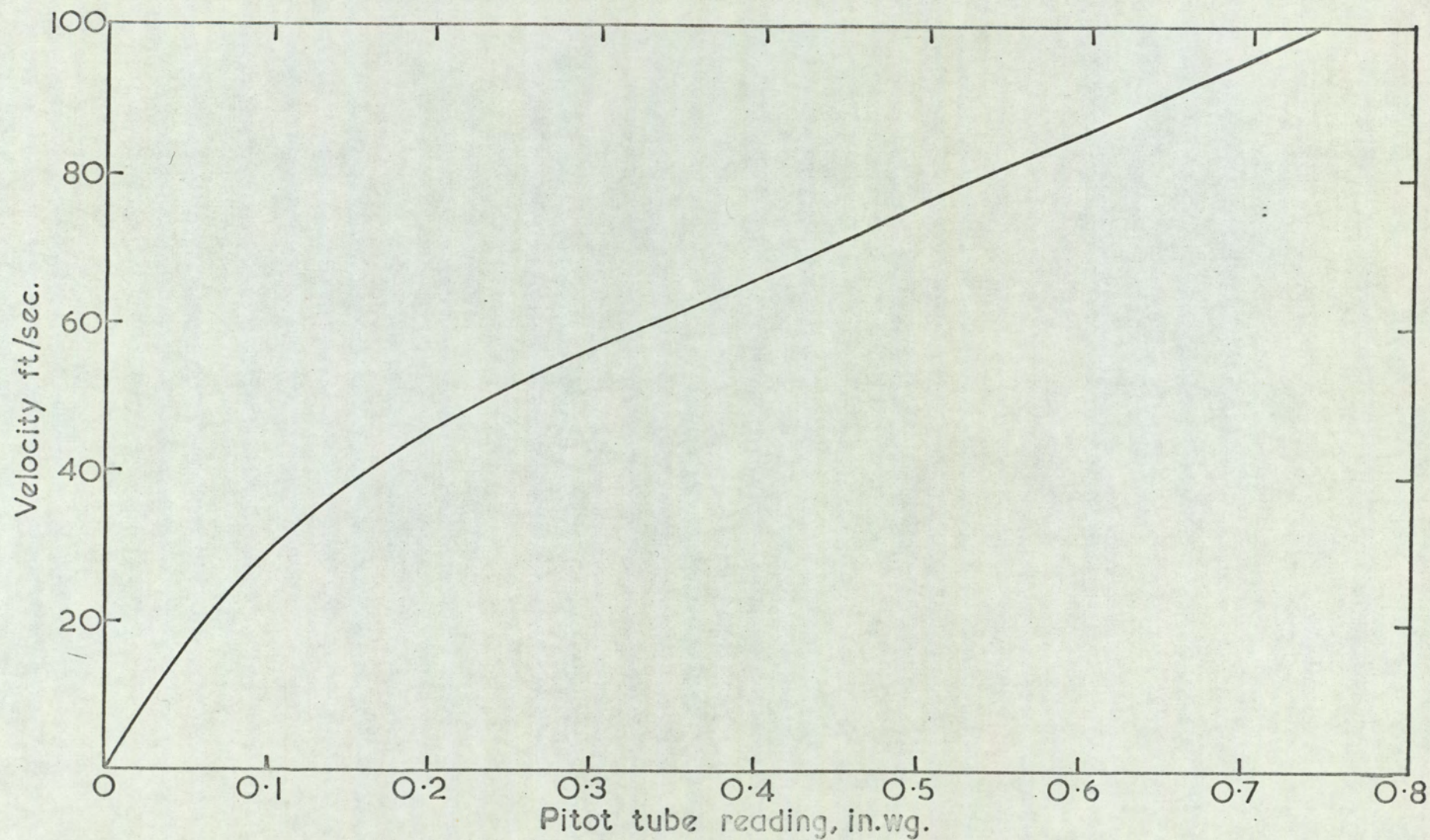


FIG.5-9 CALIBRATION GRAPH FOR THE PITOT TUBE

lay on the same radius. The readings obtained were shown to be true surface temperature readings (Section 7.1.4). Thus by taking readings from a single pair of thermocouples, in the middle of the centre test ring and rotating the whole target tube through 30° increments between readings, it was possible to obtain the temperature distribution around the periphery of the collecting surface.

5.1.7.2 Flow Measurement

The following measurements were made during each run:-

- (1) The flow of air through a 5.1 cm. diameter pipe to the burner, using either 2.5 cm. or 3.75 cm. orifice (dependent on the flow rate) which satisfied the requirements of B.S. 1042:1943.
- (2) The flow of propane to the burner, using a flowrater with a range of 0.24 - 3.0 Std dm^3/s (0.5-6.4 Std ft^3/min).
- (3) The flow of standard salt solution to the water-cooled injection probe, by taking readings from the supply burette at various periods. A 'MeTeRoTe' flowmeter with a range of 10 - 100 ml/min gave an instantaneous indication of the flow rate.
- (4) The flow of cooling air with a 'Dall' tube.
- (5) An indication of the mean velocity of hot gases with a pitot tube in the vertical offtake which leads to the chimney. The tube was calibrated against the calculated throughput and the result is shown in Fig. 5.9.

5.1.7.3 Analysis of Flue Gases

Samples for analysis were withdrawn at two points downstream of the target tube in order to avoid any interference with the gases approaching the target tube (Fig. 5.7).

The oxygen content of the flue gases was determined with a Kent paramagnetic analyser. The carbon dioxide content was determined with an Elliot Duplex 'Mono' analyser. The response time of this instrument was much larger than that of the paramagnetic analyser; consequently the carbon dioxide content was used as a check on the accuracy of the oxygen content. Observed and computed values of the oxygen content did not usually differ by more than 1% v/v.

The alkali-metal content of the flue gases was deduced from the known input of salt solution to the burner. Direct analysis of the flue gas was tried but proved unsuccessful. Sodium chloride was the only salt tried in both methods; in the first one (Shotter 1965), continuously aspirated flue gases were brought into contact with a constant flow of distilled water in two impacting chambers in order to dissolve the salt. The sodium content of the flowing water was then measured with sodium sensitive glass electrodes. Condensation of sodium chloride between the combustor and the impactors caused low readings to be obtained. The second method used a modified flame photometer (Ounsted 1958). Salt condensed between the combustor and the multijet burner of the photometer, sometimes blocking the orifice which measured the flow aspirated gases. Some improvement resulted from electric resistance heating of most of the tubing upstream of the photometer and step-changes were evident when the tube was freshly cleaned. However, condensation was not entirely prevented and it was decided that available resources did not permit further attention to the development of a direct method of measurement.

Summarising, the need to maintain the metallic tube which

conveyed the flue gases from the combustor to the measuring device above $700-800^{\circ}\text{C}$ was the main obstacle to this method. A second one was that an improved method of measuring the gas flow to the photometer was needed.

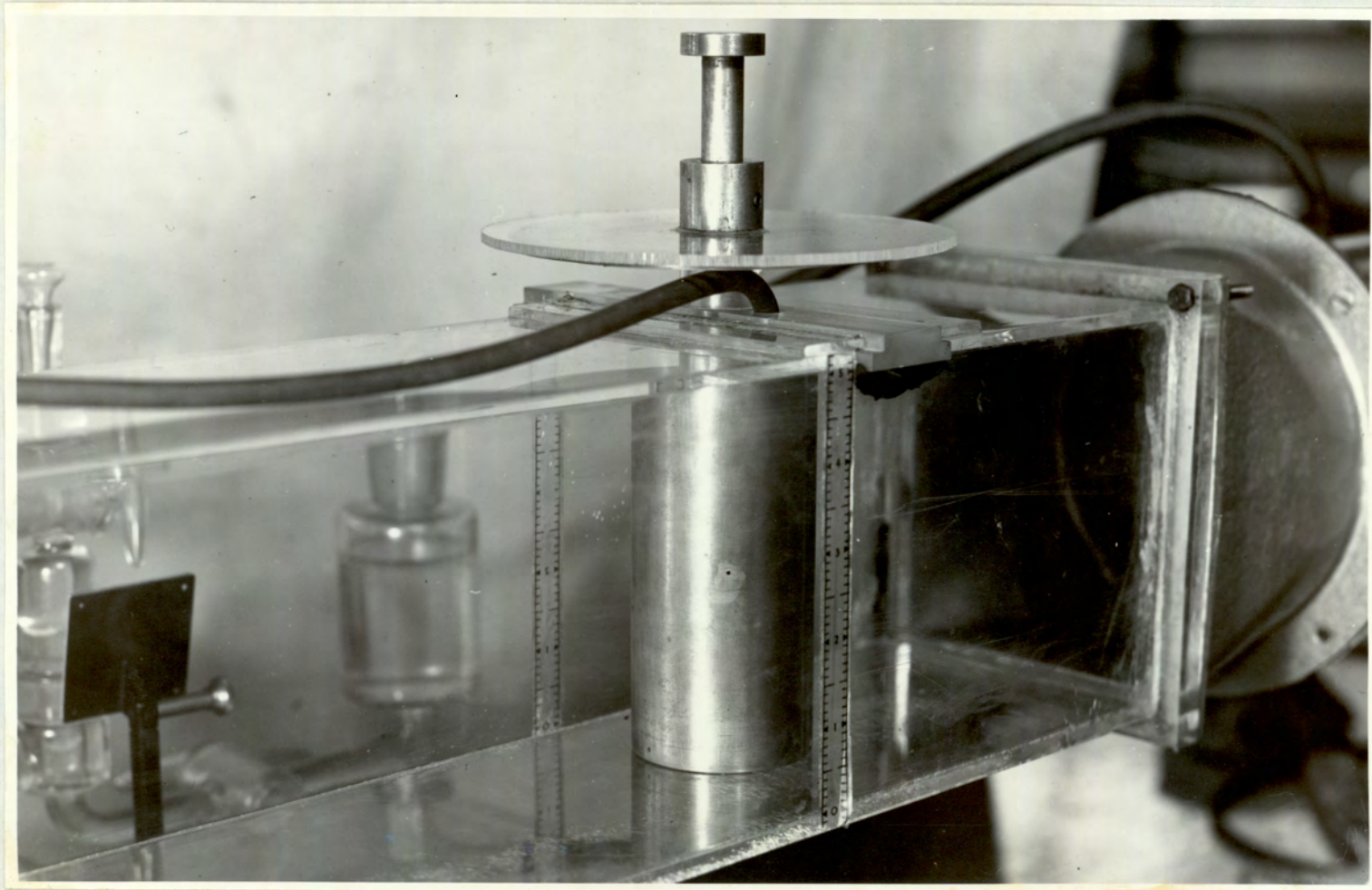


FIG. 6.1 FLOW MODEL IN WIND TUNNEL

SECTION 6

Flow Model Studies

In order to investigate the flow characteristics around the target tube model studies were carried out. In particular the effect of Reynolds number and roughness of deposit on the boundary layer dimensions were investigated.

6.1 Experimental Method

6.1.1 Consideration of Similarity

In order to simulate the target section, certain geometric and kinematic conditions had to be satisfied. The available wind-tunnel had a test section which was almost identical in size to the prototype in the combustor. The tube dimensions were chosen so that the channel blockage ratio was 0.5 as in the test section of the combustor. This was the criterion of geometrical similarity.

The Reynolds number was used as the criterion of kinematic similarity on the basis of the following assumptions:-

- (1) That there was no interaction between the momentum (velocity), thermal and concentration boundary layers.
- (2) That the density of the gases was constant.
- (3) That the intensity of turbulence of the flow had little effect upon the boundary layer dimensions.

6.1.2 Apparatus

6.1.2.1 General Arrangement of Flow Model

Fig. 6.1 shows the flow model in the transparent test section of the wind tunnel. The tube of the flow model was constructed from mild steel with a single pressure tapping flush with the external surface. It was held in the wind tunnel by a slide, the protractor attached to it being used as a reference with its 0-180° line parallel to flow.

6.1.2.2 Measurement of Air Flow Rates

The flow rate of air through the wind tunnel was controlled by a damper. A cone entry (B.S. 726, 1957) in the inlet duct and a venturi meter down-stream of the cylindrical tube were used to measure the rate of air flow through the wind tunnel.

6.1.2.3 Measurement of Static Pressure

It was necessary to measure the difference between the static pressure P_θ at the tube surface for a particular angle θ and a reference static pressure tapping P in the duct upstream of the tube. As the Reynolds number was low, the pressure difference $P - P_\theta$ was small despite the channel blockage condition. In order to increase this difference for ease of measurement, a reference tapping downstream of the tube was used in the test duct and the values were converted to the corresponding upstream values. A Chattock-Fry manometer, with a sensitivity of 0.005 in wg. was used to measure the pressure difference.

6.2. Experimental Runs

6.2.1 Pressure Distribution Test Runs

Flow rates were selected which corresponded to the range of Reynolds numbers of between 2,500-10,000 (7.5 m/s to 30 m/s). The smooth tube was then fixed at various angular positions, and readings of the pressure difference were taken every 10° from 0° to 70° , and from 90° to 110° . Around the minimum pressure position, readings were taken every 5° from 70° to 90° . The barometric pressure was noted during each test.

6.2.2 Effect of Surface Roughness upon Static Pressure Distribution around a Tube

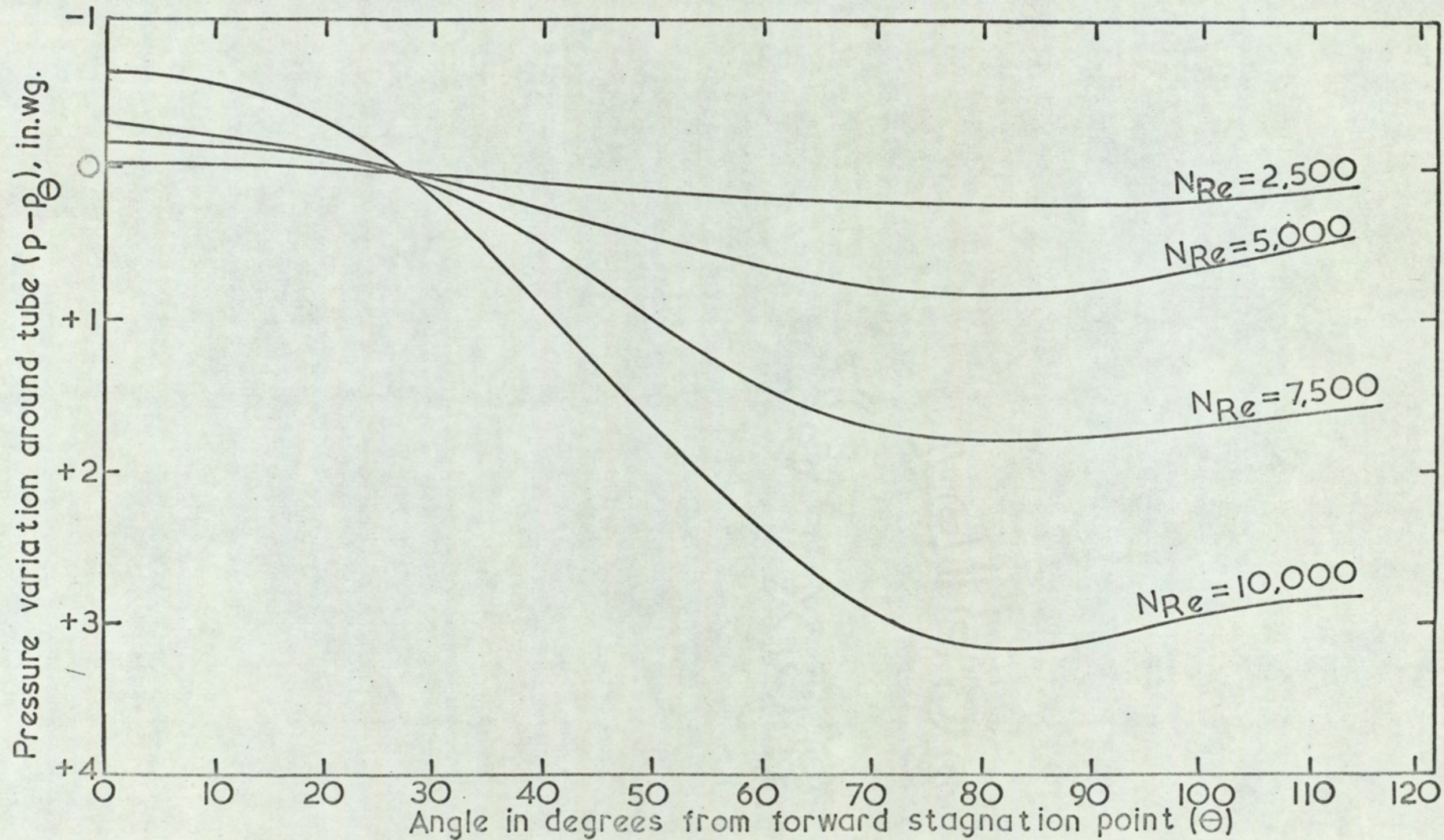


FIG. 6-2 VARIATION IN STATIC PRESSURE AT TUBE SURFACE WITH ANGULAR POSITION

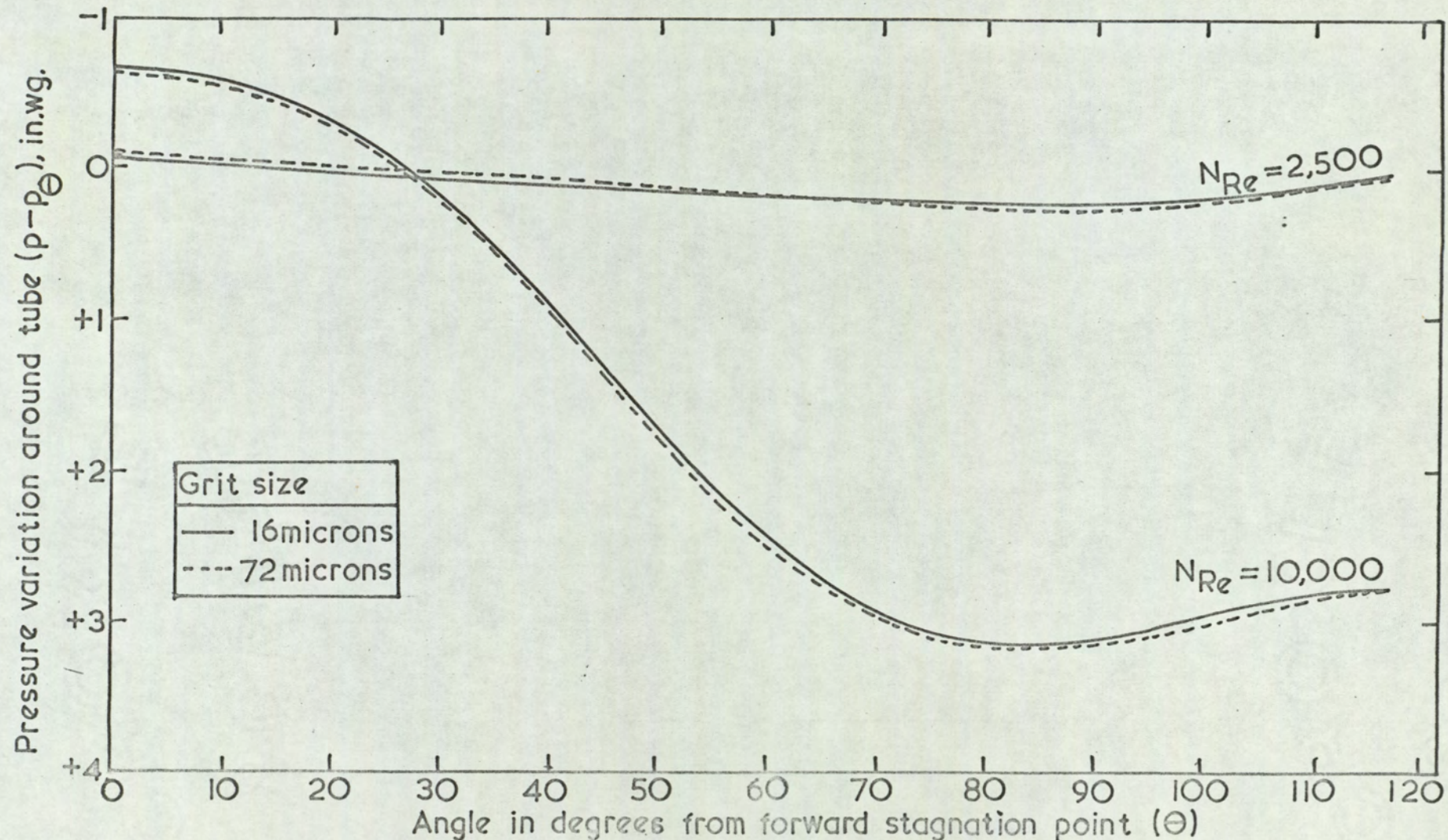


FIG. 6-3 VARIATION IN STATIC PRESSURE AT TUBE SURFACE WITH ANGULAR POSITION FOR EXTREMES OF GRIT SIZE USED

As material deposits onto a clean tube surface, the roughness of the surface will increase. Assuming that particle size is a direct measure of the roughening then the effect upon the pressure distribution can be investigated by wrapping various grades of grit paper around the tube. The grit papers used were as follows:-

<u>Reference</u>	<u>Average Size of Grit (micron)</u>
800	15
600	25
400	37
240	72

The largest grit size investigated was greater than particles found in initial boiler deposits. As the layer of fly-ash on boiler tubes, which prevents alkalis from condensing directly on them, increases with time, it was considered that the initial deposit formation was most important.

6.3 Results

6.3.1 Variation of Static Pressure at the Tube Surface with Angular Position

The variation of pressure at the smooth tube surface with angular position is shown in Fig. 6.2 and Table 6.1. From the results it was concluded that, as expected, a laminar boundary layer formed on the front of the tube which separated to give a turbulent wake.

Increasing the roughness of the tube over the particle size range from 16 microns to 72 microns had no measurable effect upon the pressure distribution. The results for the extreme size grit papers and Reynolds numbers used are shown in Fig. 6.3.

6.3.2 Calculations of the Dimensions of the Velocity (Cont'd)

Reynolds Number	2500	5000	7500	10000
Angle subtended between stagnation point and measurement point (degrees)	Pressure Variation around tube ($P-P_\infty$) (in w.g.)			
0	-0.040	-0.165	-0.370	-0.660
10	-0.035	-0.145	-0.315	-0.560
20	-0.015	-0.070	-0.155	-0.275
30	0.010	0.045	0.110	0.195
40	0.060	0.230	0.515	0.920
50	0.100	0.400	0.910	1.605
60	0.145	0.580	1.300	2.360
70	0.195	0.760	1.705	3.010
75	0.200	0.790	1.780	3.205
80	0.205	0.795	1.780	3.250
85	0.200	0.792	1.778	3.210
90	0.195	0.775	1.740	3.180
100	0.190	0.755	1.700	3.100
110	0.175	0.715	1.685	2.910

Temperature of air = 60°F (520°R)

Density of air = 0.0715 lbf/ft³

TABLE 6.1

Variation in static pressure at tube
surface with angular position

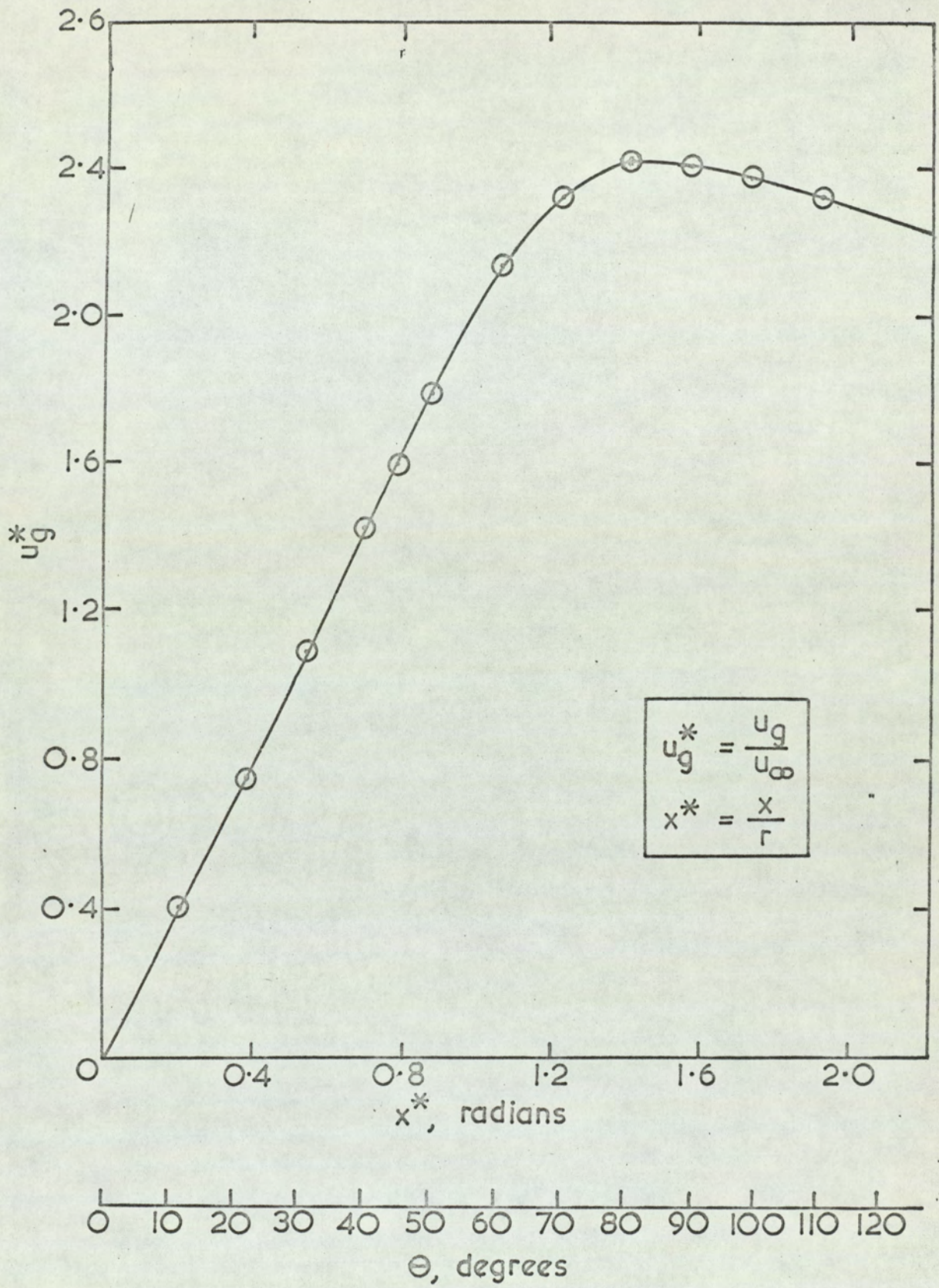


FIG. 6.4 VELOCITY AT EDGE OF BOUNDARY LAYER (RELATIVE TO MAIN STREAM VELOCITY) VERSUS DISTANCE ALONG TUBE FROM FORWARD STAGNATION POINT

(Cont'd) Boundary Layer

Firstly the pressure data was converted to velocities at the outer 'edge' of the boundary layer by using Bernoulli's equation,

$$P_{\infty} + \frac{\rho u_{\infty}^2}{2g_c} = P_g + \frac{\rho u_g^2}{2g_c} \quad 6.1$$

Equation 6.1 can be rearranged to give the following form:-

$$u_g = u_{\infty} \sqrt{\left(\frac{2g_c(P_g - P_{\infty})}{\rho u_{\infty}^2} + 1 \right)} \quad 6.2$$

Fig. 6.4 shows the variation in velocity with distance around the upstream surface of the tube. For convenience velocity and distance are given in dimensionless forms signified by superscript x . As there was negligible variation in the relative velocity, u_g^x , for the four Reynolds numbers investigated, the curve applies over all the range. Values of the derivative $\frac{du_g^x}{dx^x}$ were obtained from Fig. 6.4 for various values of x^x and used in subsequent calculations.

The thickness of the laminar boundary layer was now calculated in terms of x by solution of the following differential equation representing the growth of the laminar boundary layer (Spalding 1961).

$$\frac{u_g}{\nu} \frac{d\delta_b^2}{dx} = F_b \left(\frac{\delta_b^2}{\nu} \frac{du_g}{dx}, \frac{v_o \delta_b}{\nu} \right) \quad 6.3$$

In dimensionless form this becomes:-

$$u_g^x \frac{d\delta_b^{x2}}{dx^x} = F_b \left(\delta_b^{x2} \frac{du_g^x}{dx^x}, v_o^x \delta_b^x \right) \quad 6.4$$

Equation 6.4 was solved using a quadrature procedure (see Appendix 3). Table 6.2 shows values of the various quantities which were derived during successive stages of the calculations. As the range of Reynolds numbers investigated was small the variation in the thickness of the boundary

x^*	u_g^*	$\int_0^{x^*} \frac{0.441 u_g^{*4.164} dx^*}{u_g^{*5.164}}$ $= \delta_{b,I}^{*2} \times 10^2$	$\delta_{b,I}^{*2} \frac{du_g^*}{dx}$ $\times 10^2$	E_b $\times 10^3$	$\delta_{b,II}^*$	δ_b $\times 10^4$ (ft)	Λ	δ_a $\times 10^4$ (ft)	δ $\times 10^3$ (ft)
0	0	-	-	-	0.122	3.58	7.052	8.24	3.4
0.25	0.55	2.15	7.67	0.5	0.132	4.37	7.0	9.94	4.1
0.5	1.09	3.10	7.67	0.5	0.174	5.10	7.0	11.8	4.8
0.75	1.67	3.66	7.52	0.6	0.191	5.62	6.8	13.0	5.7
1.0	1.98	5.95	6.8	1.1	0.244	7.15	5.9	16.8	6.6
1.25	2.38	6.45	2.45	3.0	0.255	7.14	3.0	17.4	6.8
1.5	2.4	10.0	-2.5	-4.0	0.316	8.94	-1.8	23.6	7.35
1.75	2.36	16.1	-5.48	-18.0	0.402	11.4	-3.8	31.6	9.5
2.0	2.29	21.9	-9.4	-36.0	0.458	12.9	-6.5	38.3	11.6

TABLE 6.2

Quantities derived during calculation of
the thickness of the boundary layer

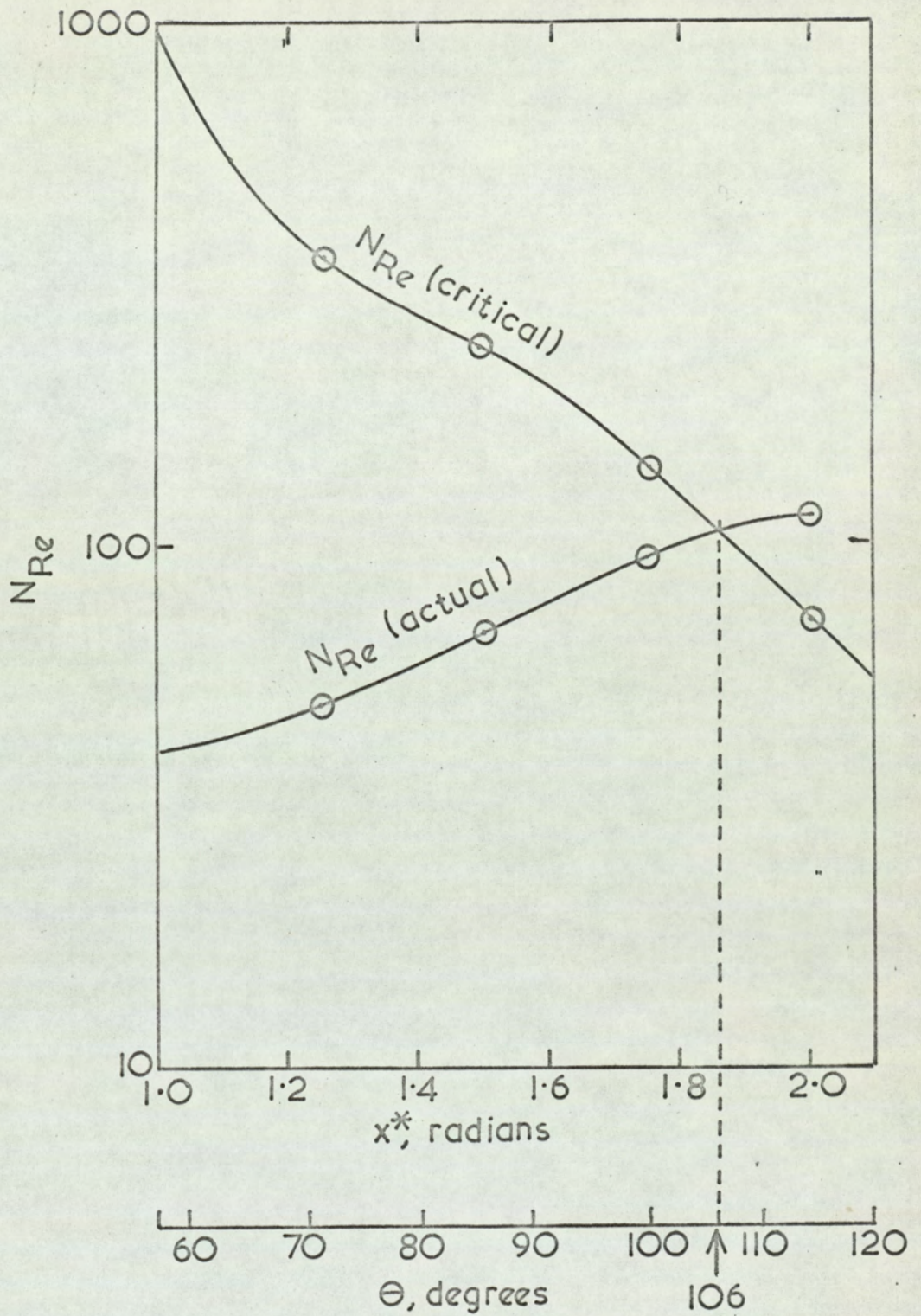


FIG. 6.5 RELATIONSHIP BETWEEN REYNOLDS NUMBER (CRITICAL AND ACTUAL) AND DISTANCE FROM STAGNATION POINT

layer with Reynolds number was negligible, hence in Table 6.2 results of boundary layer thickness are for the range of Reynolds numbers from 2,500-10,000. From this table it can be seen that the thickness of the velocity boundary layer is a minimum in the region of the stagnation point where it is approximately 1 mm. thick. As the largest grit size used was only 0.072 mm, then the grit particles were well within the boundary layer and so will not affect its dimensions. This is because for roughness to alter the flow conditions around an object, the roughness elements must be of a sufficient height to project beyond the laminar boundary layer and into the turbulent main stream. If this occurs there will be a turbulent wake behind each element which will cause turbulent eddies from the wake to penetrate the layer, and results in effectively thinning the laminar boundary layer.

6.3.3 Calculation of Separation Point

The relevant literature and method of calculation adopted are given in Appendix 4. Using the displacement thickness as the significant dimension, actual and critical Reynolds number were calculated and plotted against x^* as shown in Fig. 6.5. The intersection of the two curves represents the point of separation of the laminar boundary layer which occurred at an angle of 106° . This calculated value corresponds reasonably with a value of approximately 100° observed with coal firing in previous deposition studies in a similar flow configuration (Bishop, Cutler & Valance, 1963). The normal separation point at these Reynolds numbers of a tube in an infinite medium is about 80° ; however, due to the presence of the combustor wall, boundary layer separation is delayed to the angle of 106° for the present system with a channel blockage ratio of 0.5.

SECTION 7

Combustor Tests

7.1 Preliminary Tests on the Combustor

Before experimental work could proceed, combustor trials were carried out to show that design conditions were attainable.

7.1.1 Variation of Oxygen and Carbon Dioxide Concentrations

It was found that the oxygen and carbon dioxide contents of the flue gas were constant along the length of the combustor for the velocity range 7.5 m/s - 30 m/s and a gas temperature in the vicinity of the target tube of 1100°C. Hence combustion was completed well before the target tube.

However, when salt was injected at gas velocities above 20 m/s and salt concentrations above 0.2 torr, the propane flame failed and re-ignited spasmodically. This effect was detected by a variable and increased oxygen content, and decreased carbon dioxide content along the length of the combustor. Use of a pilot flame jet within the burner prevented this effect which was due to the presence of salt (Arthur & Wadsworth 1950).

7.1.2 Transverse and Longitudinal Variation of Temperature in the Settling and Target Sections

These temperature traverses were made with an Atkinson Suction Pyrometer positioned through the portholes A, B, C and D, as indicated in Fig. 5.7.

The results for the extreme velocities possible in the combustor (8 m/s and 30 m/s) are shown in Figs. 7.1 and 7.2. From Fig. 7.1 it can be seen that the transverse temperature profiles are flat topped, which signifies efficient turbulent mixing and a uniform temperature across the target section.

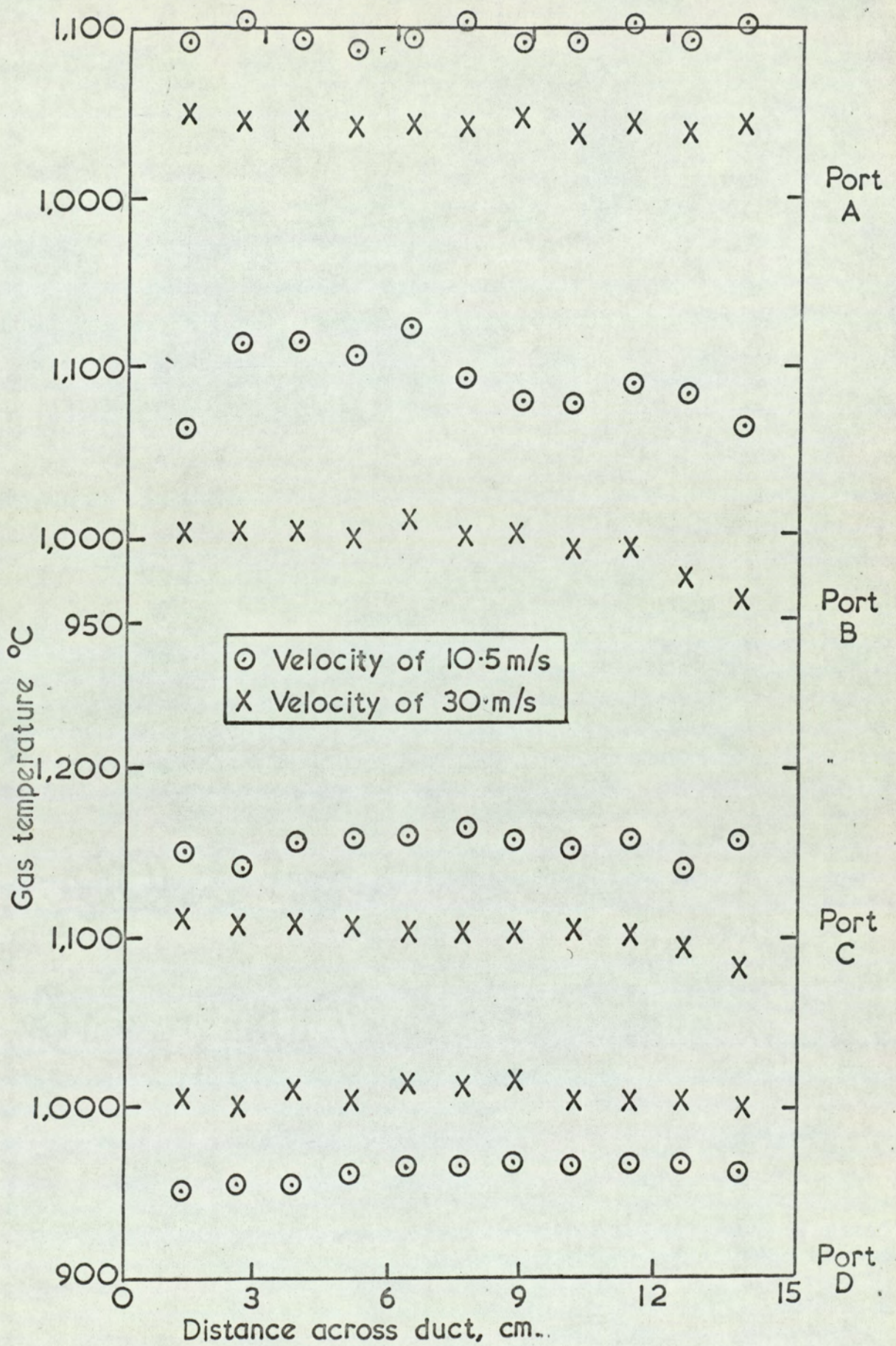


FIG. 7.1 | TEMPERATURE PROFILES ACROSS COMBUSTOR

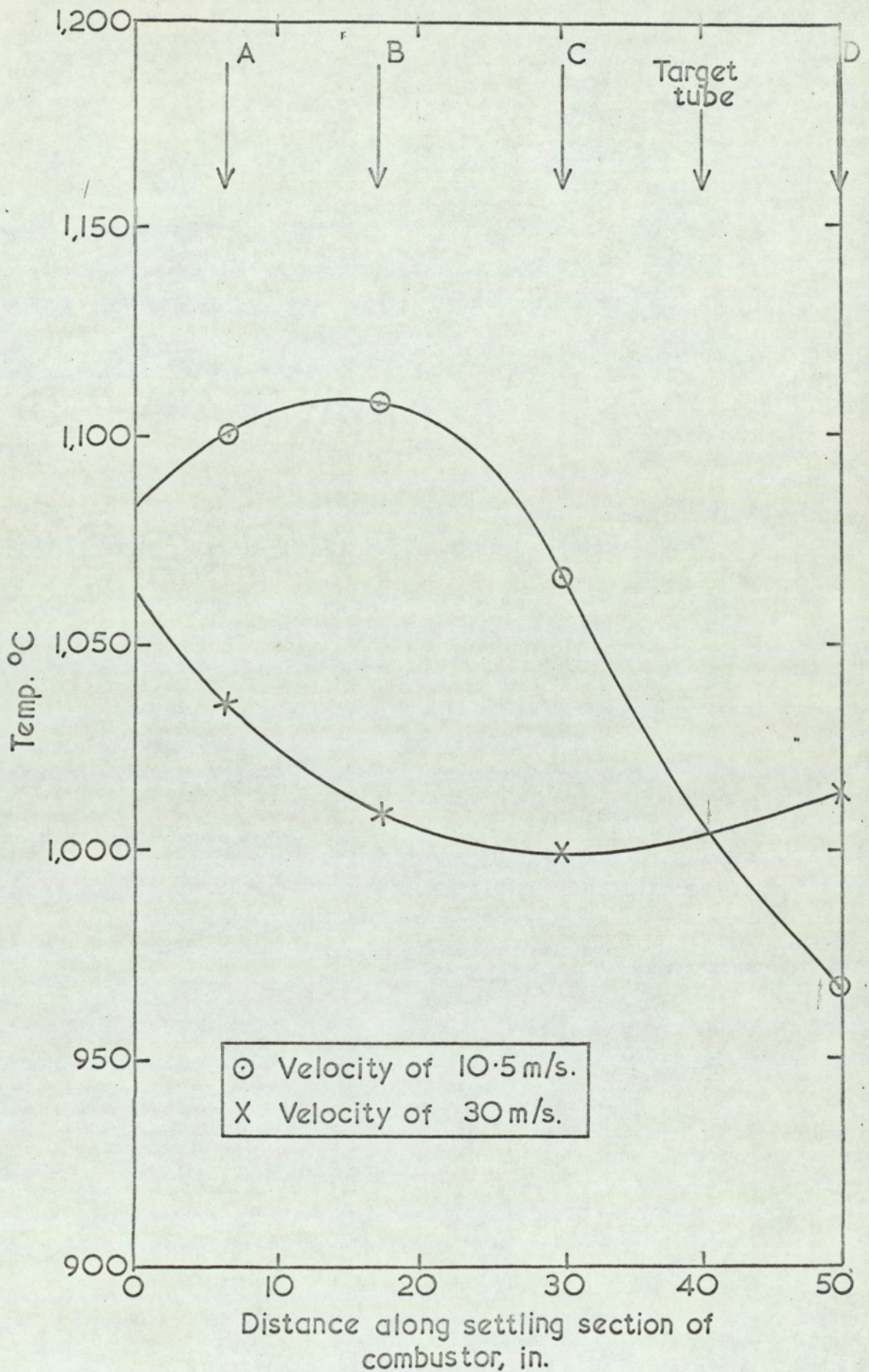


FIG. 7.2 LONGITUDINAL VARIATION OF TEMPEPERATURE ALONG CENTRAL AXIS OF COMBUSTOR

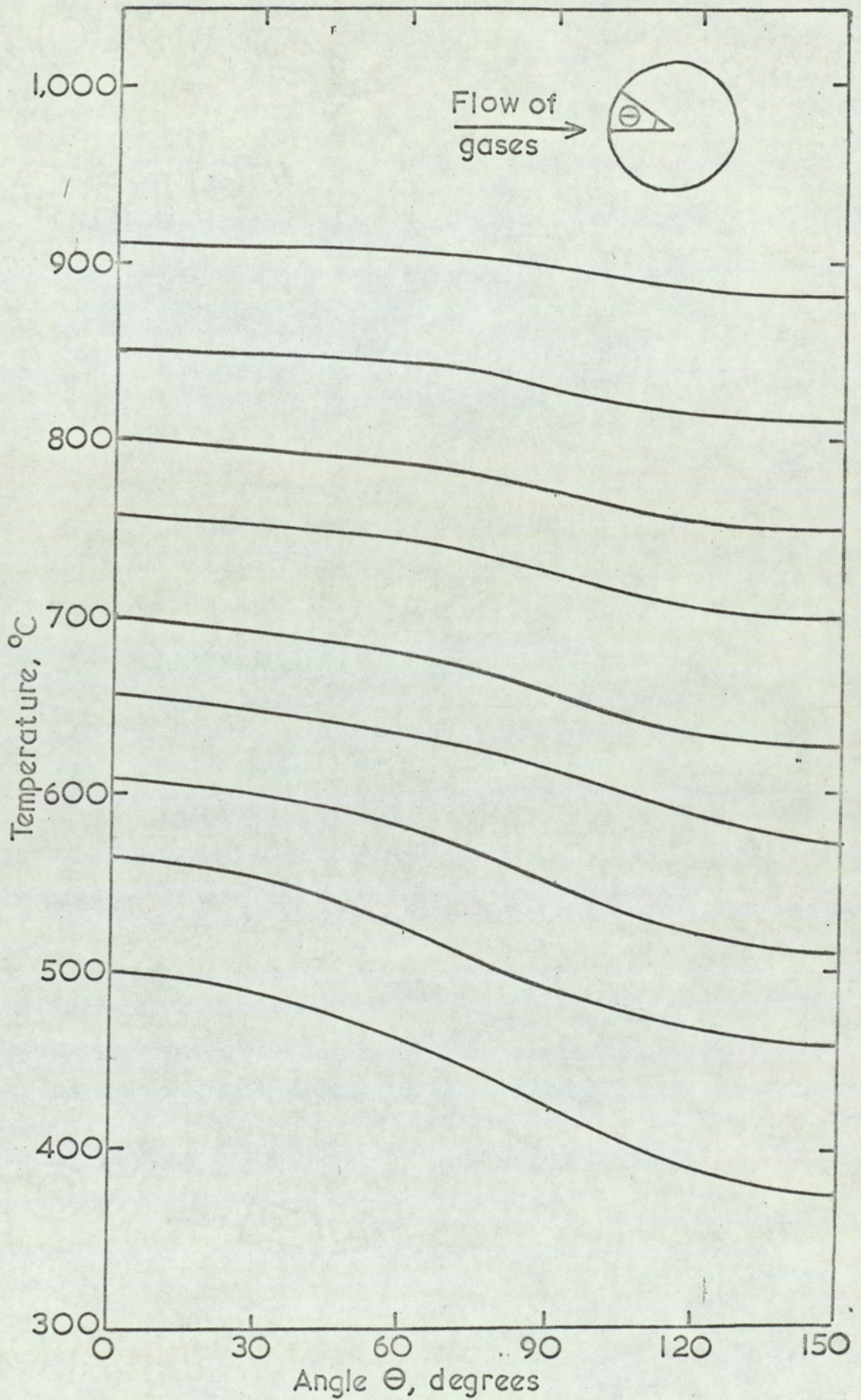


FIG.7-3 PERIPHERAL TEMPERATURE DISTRIBUTIONS AT SURFACE OF TARGET TUBE

The variation in the longitudinal temperature distribution is only 10% over a distance of 1.1 m. and as expected, is greatest at the lowest velocity. The reason why the temperatures at A, B, and C are less in the high velocity run is that both velocity runs were carried out at the same indicated temperature in the target section.

7.1.3 Peripheral Variation in Surface Temperature

Tests showed that on rotating the target tube through 30° intervals, the temperature distribution was symmetrical around the tube surface on either side of the front stagnation point. The distributions obtained over a range of stagnation point temperatures (500°C - 900°C) are shown in Fig. 7.3. Readings were not taken beyond an angle of 150° because the laminar boundary layer separated at approximately 100° . For similar stagnation point temperatures the surface temperature at an angle of 150° was only increased by 5°C on raising the flue gas velocity from 10.5 m/s to 30 m/s , therefore the temperature distributions shown in Fig. 7.3 can be considered as independent of flue gas velocity.

7.1.4 Effect of Ceramic Coating upon Surface Temperature

Two test rings of 12% chromium ferritic steel, one ceramic-coated and the other uncoated, were used in separate tests under similar conditions of combustion and target cooling. In each case, the surface temperatures at the forward stagnation point of the tube were obtained from the thermocouples mounted in the tube wall. It was found that the presence of the ceramic coating increased the surface temperature by less than 5°C , therefore the reading from the thermocouple nearest the outside wall of a ceramically coated ring could be taken as the surface temperature.

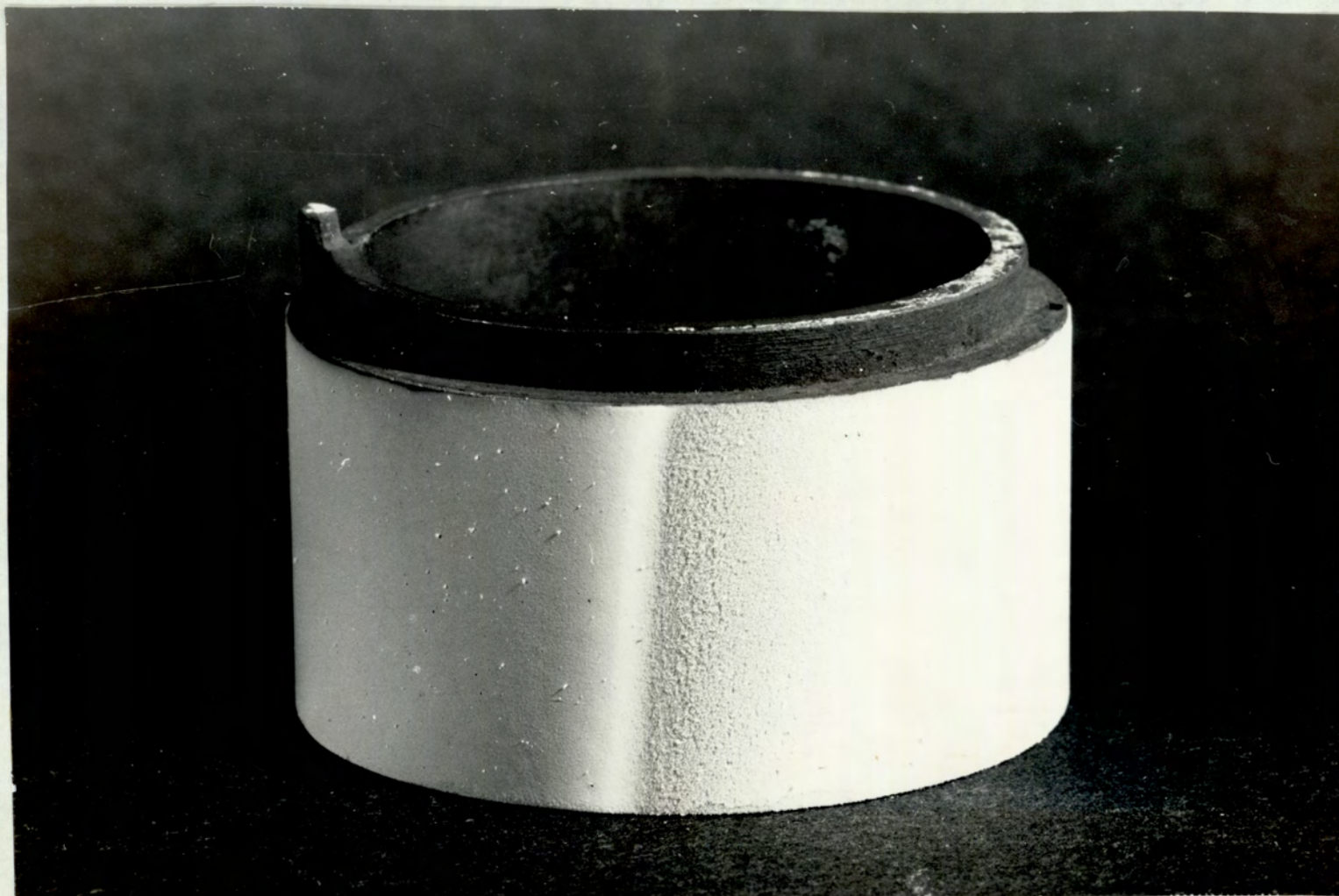


FIG. 7·4 FLOW SEPARATION LINE

7.1.5 Difficulties of Vaporisation

Initially, difficulties were experienced in obtaining the necessary complete vaporisation of the injected salt solution. Incomplete vaporisation enabled salt droplets to survive and impact upon the target tube. The problem was solved by injecting the salt through a modified probe containing an oil burner type of nozzle (see Section 5.1.3.4).

7.1.6 Reactions of Sodium Chloride with Combustor Walls

After runs with injection of sodium chloride totalling about 30 hours, a slight glaze appeared on the walls of the combustor. It was concluded that the glaze was a complex mixture of sodium silicates formed by the reaction between sodium chloride and the silica in the lining of the combustor. The reaction did not seem to affect either the rate of deposition, which was close to the predicted rate, or the reproducibility of results. Also no free chloride was ever found on the salt glaze or combustor walls which could re-evaporate in successive runs. Therefore the reaction was considered to be allowable.

7.1.7 Separation Lines

Two clear separation lines (Fig. 7.4) marked the boundary between the different types of deposit that formed beneath the laminar boundary layer and turbulent wake. The separation lines were at an angle of approximately 100° from the forward stagnation point. This angle was independent of which salt was injected, the concentration of the salt and the Reynolds number over the range investigated. These results show reasonable agreement with the flow model studies (Section 6), hence it can be concluded that the velocity and concentration boundary layers of the front of the tube are

similar.

7.2 Description of Tests

7.2.1 Conditions Investigated

It can be shown theoretically that for a constant Reynolds number the rate of deposition should be directly proportional to the bulk gas phase concentration and the square root of the gas velocity when the deposit at the tube surface is at a temperature low enough not to exert a significant vapour pressure. In order to demonstrate the validity of these relationships for the four salts used, the following tests were carried out:-

(1) Sodium Chloride

For this salt, nine sets of tests were made, involving three concentrations of sodium chloride in the gas phase, and three gas velocities. The principal test parameters were as follows:-

<u>Flue Gas Temperature:</u>	1,100°C
<u>Average Surface Temperature of Test Ring:</u>	500°C to temperatures in excess of theoretical condensation points.
<u>Main Stream Gas Velocity:</u>	10.5, 18.0 and 30.0 m/s.
<u>Partial Pressure of Sodium Chloride Vapour:</u>	0.055 torr, 0.110 torr and 0.250 torr.
<u>Period of Salt Deposition:</u>	10 - 50 min.

The highest partial pressure of salt vapour examined was similar in magnitude to the maximum theoretical value of the salt vapour obtained from the combustion of a high chlorine East Midland Coal (Bishop, Cliffe & Langford 1967). Test periods were adjusted according to the salt concentration and gas velocity. Thus collection of sufficient deposit for

analysis and weighing required a long exposure of 50 minutes when the partial pressure and gas velocity were relatively low.

(2) Potassium Chloride

A similar series of tests was carried out with this salt. Four concentrations were used to investigate the effect, if any, of water vapour on the vapour pressure exerted by the potassium chloride. The only vapour pressure data available for this salt was measured 'in vacuo'. The concentrations injected were of the same magnitude as theoretical amounts obtained from the combustion of a high chlorine East Midlands coal. Only two velocities were investigated because of the broad similarity between sodium and potassium chlorides.

The parameters used for the flue gas temperature, and range of average surface temperatures of the test ring, were the same as in previous tests; the other parameters were as follows:-

<u>Main Stream Gas Velocity:</u>	10.5 m/s and 18.0 m/s.
<u>Partial Pressure of Potassium Chloride Vapour:</u>	0.035 torr, 0.065 torr, 0.125 torr and 0.250 torr.
<u>Period of Salt Deposition:</u>	10 - 45 min.

(3) Sodium Sulphate

Considerable difficulty was encountered in vaporising sodium sulphate at concentrations above 0.1 torr and velocities above 10.5 m/s. At greater values of these parameters, inertial impaction occurred which resulted in a beard-shaped deposit building up at the stagnation point. Consequently, only one velocity was investigated at four concentrations below 0.1 torr.

The other four parameters were as follows:-

<u>Main Stream Gas Velocity:</u>	10.5 m/s.
----------------------------------	-----------

<u>Partial Pressure of Sodium Sulphate:</u>	0.0055 torr, 0.011 torr, 0.025 torr and 0.100 torr.
<u>Period of Salt Deposition:</u>	25 - 150 min.

(4) Calcium Chloride

As calcium chloride was also extremely difficult to completely vaporise, only the lowest velocity attainable in the combustor was investigated. Four concentrations of salt were used covering the range 0.007 torr to 0.056 torr. At concentrations greater than 0.06 torr, deposition by impaction occurred. Fewer runs were carried out with calcium chloride because the salt reacted with various components in the system. Consequently, the quantitative results obtained were of little value as reaction rates with these various compounds were unknown.

The parameters used for flue gas temperature, the range of average surface temperatures of the test ring and main stream gas velocity were the same as in the sodium sulphate experiments. The other test parameters were as follows:-

<u>Partial Pressure of Calcium Chloride Vapour:</u>	0.007 torr, 0.014 torr, 0.028 torr and 0.056 torr.
<u>Period of Salt Deposition:</u>	50 min. to 180 min.

7.2.2 Test Procedure

The principal steps in each test run were as follows:-

- (1) The target tube was assembled with a clean dry test ring, mounted on a tie rod and placed within the target section.
- (2) The leads from the thermocouples in the target tube were plugged into a multi-point recorder and cooling air passed through the target tube.
- (3) The main air blower was switched on. The town gas burner was ignited and inserted into the combustion chamber.

- (4) After 2-2 $\frac{1}{2}$ hrs., the town gas was shut off and propane was fed to the main burner.
- (5) Adjustments were made to the propane and air supplies until the gas velocity, as indicated by the pitot tube in the exhaust pipe, and the indicated gas temperature were correct.
- (6) The required surface temperature of the target tube was obtained by adjusting the flow of cooled air.
- (7) Having established the test conditions, the salt was pumped through the injection probe. The probe was then inserted along the burner axis and the salt solution sprayed into the combustion chamber for the test period.
- (8) During the test run, flow, temperature and pressure readings were taken, and, if necessary, the flow of cooling air through the target tube was adjusted.
- (9) At the finish of a test run the probe was removed from the burner, the propane and air supplies shut off, and the target tube removed from the target section with the aid of the tie rod. It was placed in a Sindanyo box and allowed to cool. The test ring was then put into a small dessicator.

7.2.3 Sampling Procedure

After obtaining the total weight of test ring and deposit, the weights of upstream and downstream salt deposits were determined separately. In the case of crystalline deposits formed at the lower surface temperatures, the two lines of flow separation clearly marked the boundaries between the two regions. The angular positions of these lines of flow separation were noted. Upstream and downstream samples for

analysis were scraped from the test ring with a scalpel and final traces of salt removed with moistened tissue. In the case of deposits which had fused completely, it was necessary to mark estimated lines of flow separation in the deposit before proceeding to separate upstream and downstream deposits.

The surface temperature decreased around the ring from the forward stagnation point to the rear of the ring, so in tests at a given salt concentration, it was possible for the surface temperature at the forward stagnation point to be above the condensation point of the salt and the surface temperature at the separation line to be below it. In such conditions, a line could be identified between the deposit free area and the area where deposit occurred. The two angular positions from the forward stagnation point at which this line appeared were measured. From curves of the known peripheral temperature distributions (Fig. 7.3), values of the surface temperature at the line, and hence the condensation point, were obtained.

Each deposit was examined microscopically 'in situ' on the test ring using oblique illumination. Representative deposits were photographed using a green filter and orthochromatic plates. Depth of focus limitations usually made it necessary to photograph at only moderate magnification and then obtain a final print by enlargement. Certain samples were subjected to X-ray diffraction analysis using the powder methods (cobalt radiation). The composition of some samples was checked by chemical analysis.

SECTION 8

Results of Combustor Tests

8.1 Deposition of Sodium and Potassium Chlorides

As the deposition characteristics of these two salts are similar, they will be discussed together.

8.1.1 Under Conditions of Incomplete Vaporisation

In the first series of test runs in which sodium chloride was injected through a probe shown in Fig. 5.4 inadequate dispersal and vaporisation of the injected salt solution caused droplets of molten salt to reach the tube surface by the unwanted processes of inertial impaction and particle diffusion. In these circumstances, molten streaks appeared in the upstream deposits and were particularly noticeable near the two lines of flow separation where the droplets approached the collecting surface at shallow angles of incidence (Fig. 8.1). Typical results for the variation of rates of deposition with surface temperature of the target tube are shown in Fig. 8.2. A characteristic plateau was visible but the deposition rates in this region were three to four times greater than the theoretical rate. The temperature at which the deposition rate falls to zero was about 50°C above the value obtained for complete vaporisation (Fig. 8.11).

8.1.2 Under Conditions of Complete Vaporisation

8.1.2.1 Effect of Run Duration upon Deposit Weight

At surface temperatures in the plateau range of deposition, the weight of the upstream salt deposit was directly proportional to the period of exposure for deposit weights up to about 100 mg. (Fig. 8.3 a & b show the curves for sodium chloride and potassium chloride respectively). At greater weights of deposit, the rate of deposition tended to decrease.

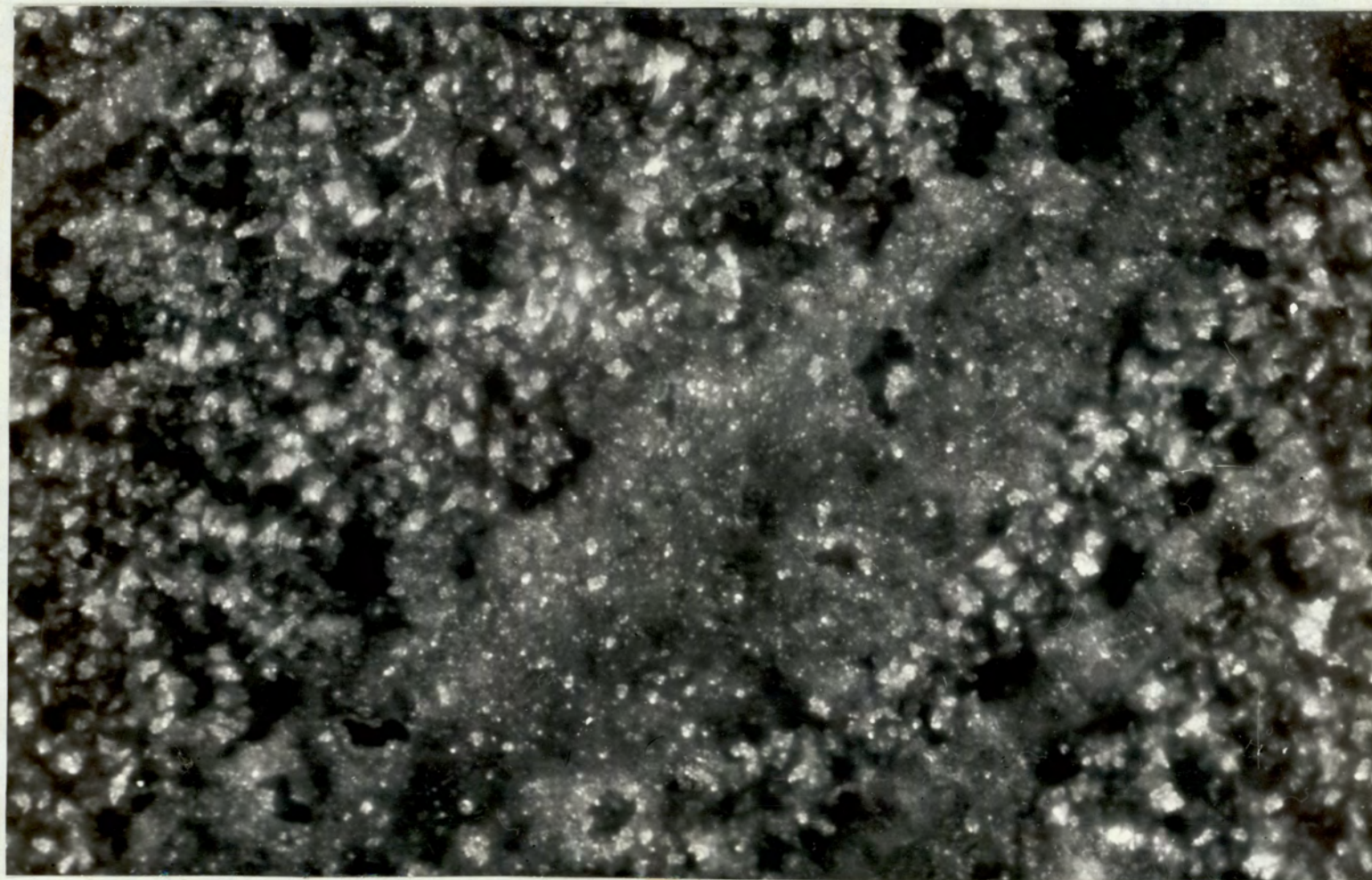


FIG. 8·1 MOLTEN STREAKS OF SODIUM CHLORIDE (MAGNIFICATION X150)

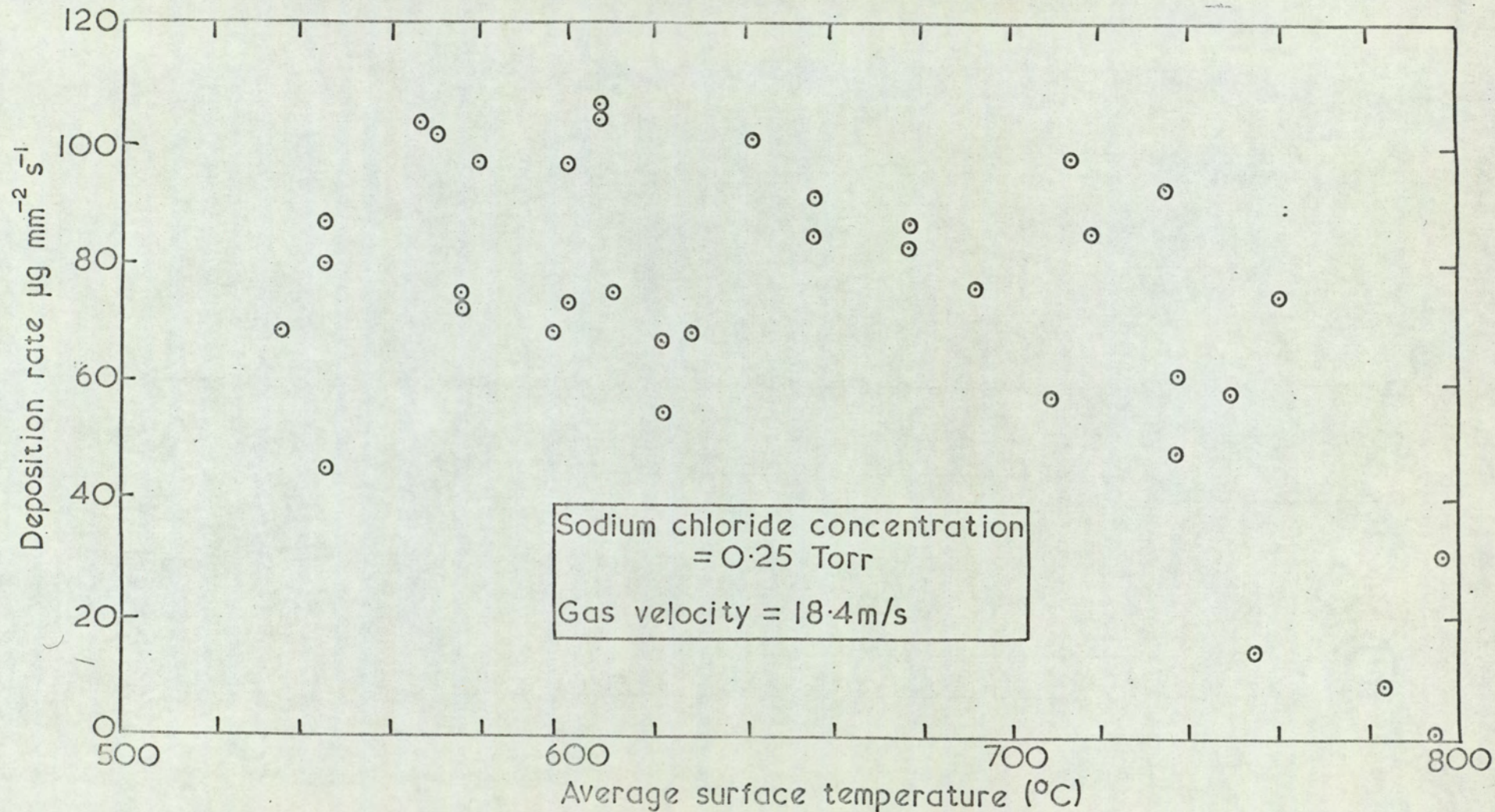


FIG 8.2 VARIATION OF DEPOSITION RATE WITH SURFACE TEMPERATURE
(INCOMPLETE VAPORISATION)

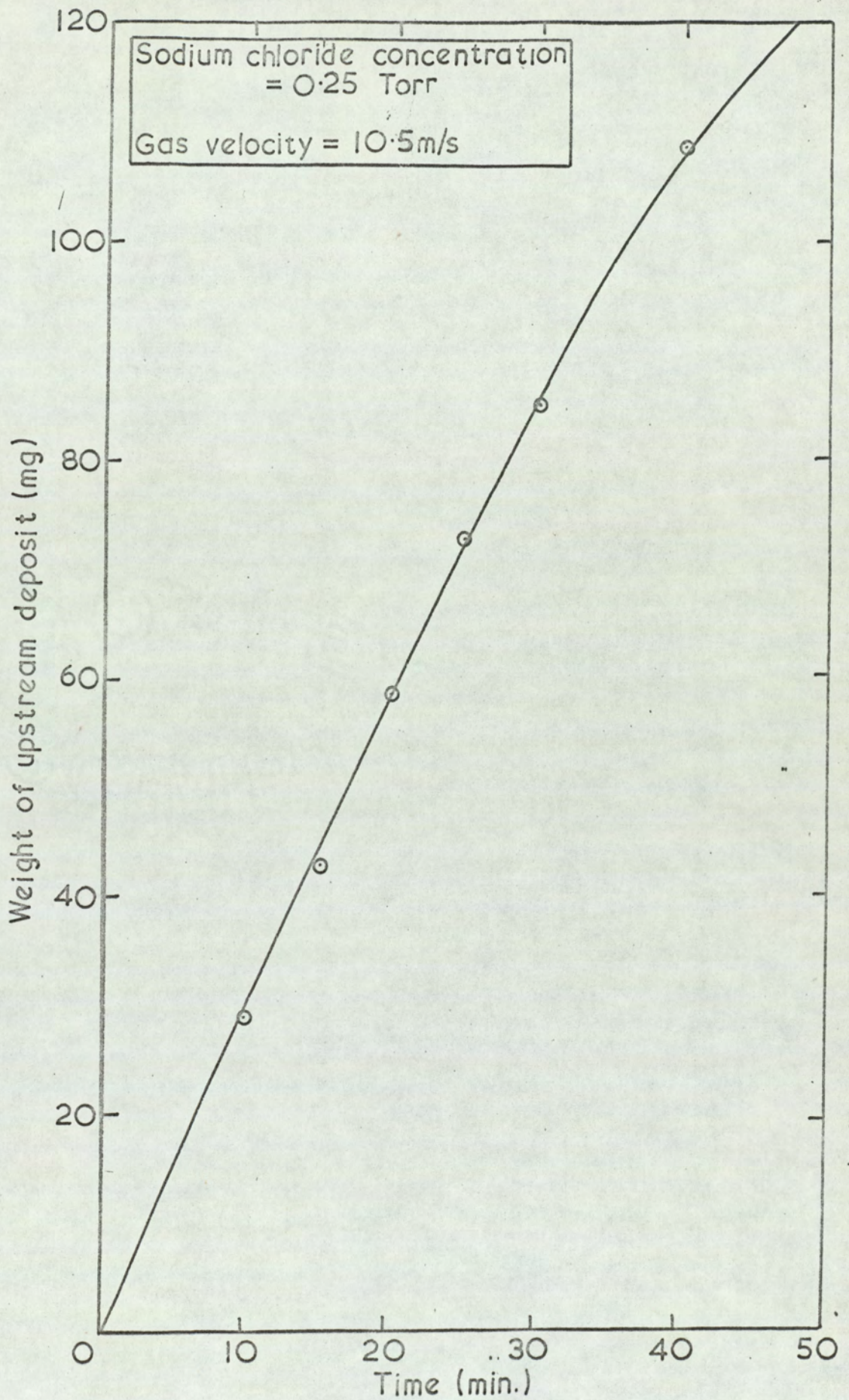


FIG. 8-3a DEPENDENCE OF DEPOSIT WEIGHT UPON TIME OF EXPOSURE

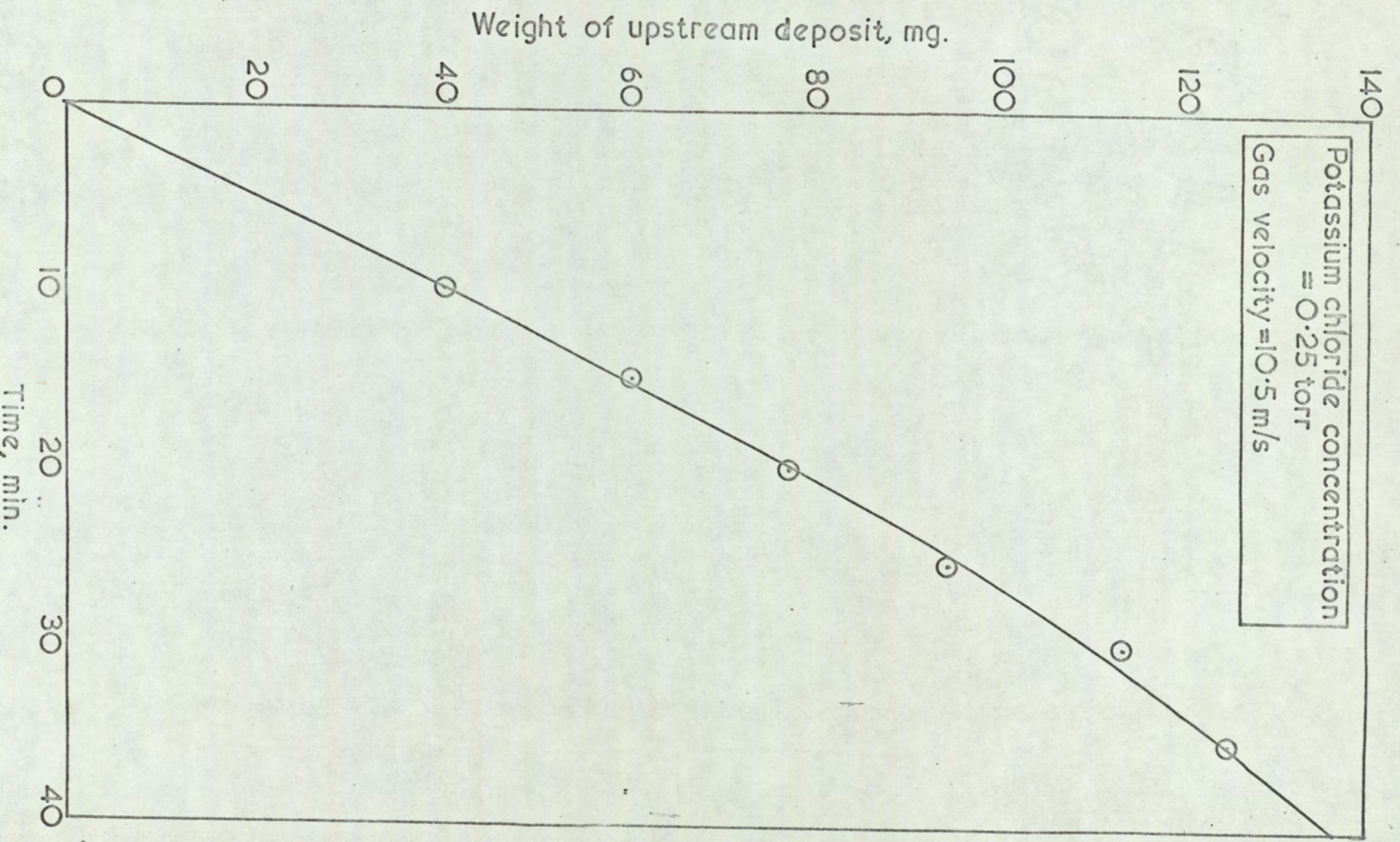


FIG. 8-3b DEPENDENCE OF DEPOSIT WEIGHT UPON TIME OF EXPOSURE

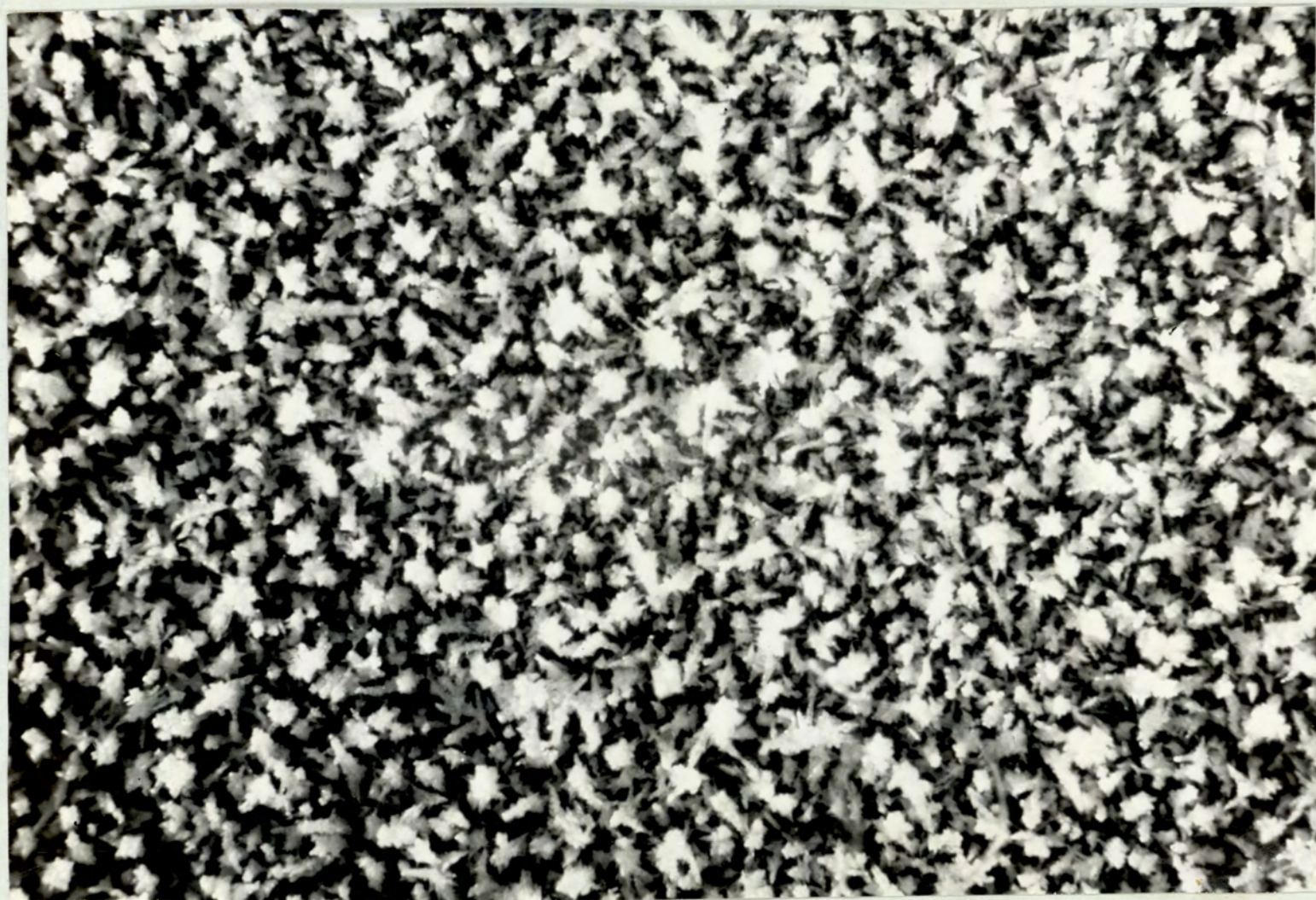


FIG. 8·4a DENDRITES OF SODIUM CHLORIDE, PLAN VIEW (MAGNIFICATION X350)

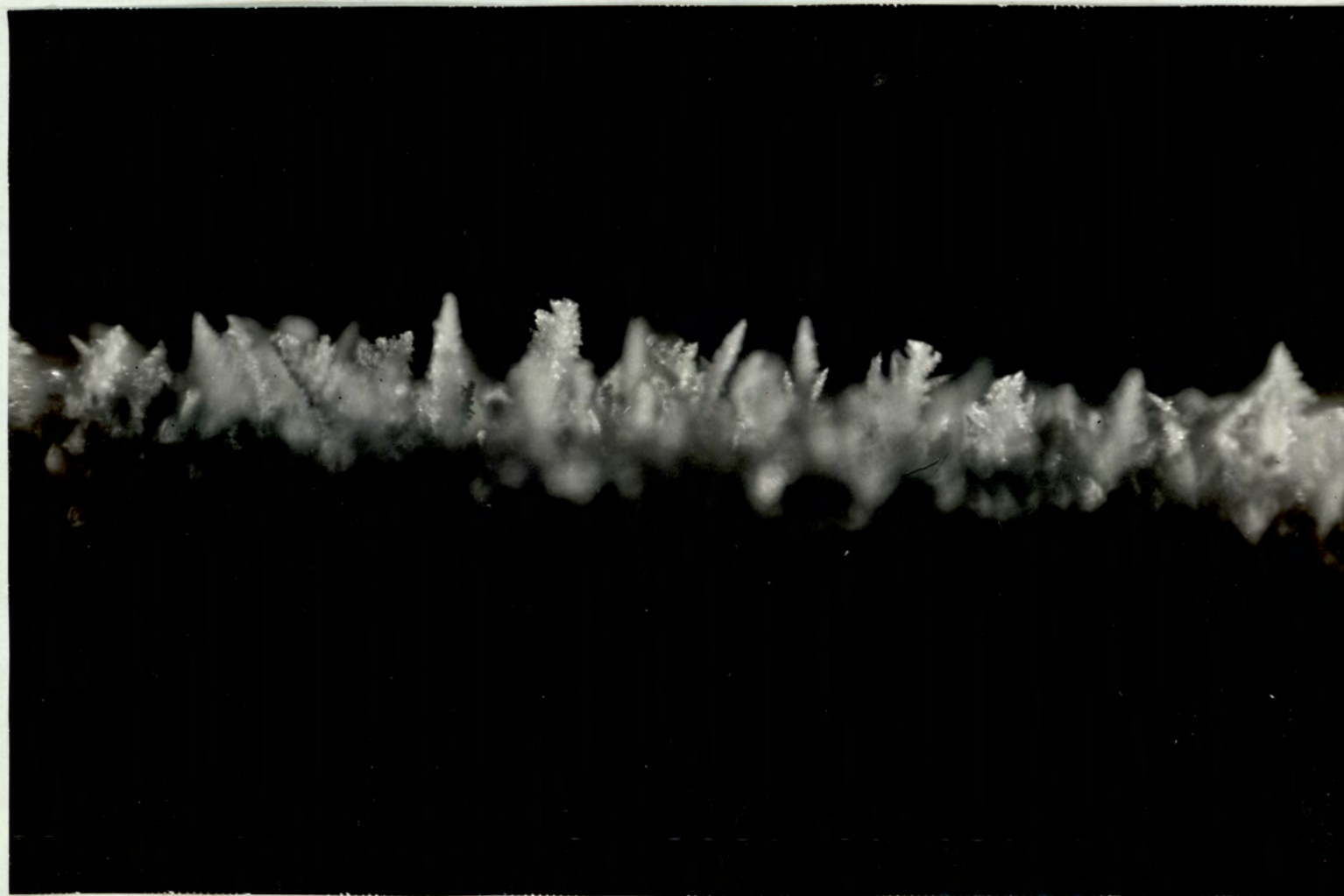


FIG. 8·4b DENDRITES OF SODIUM CHLORIDE, SIDE VIEW (MAGNIFICATION X500)

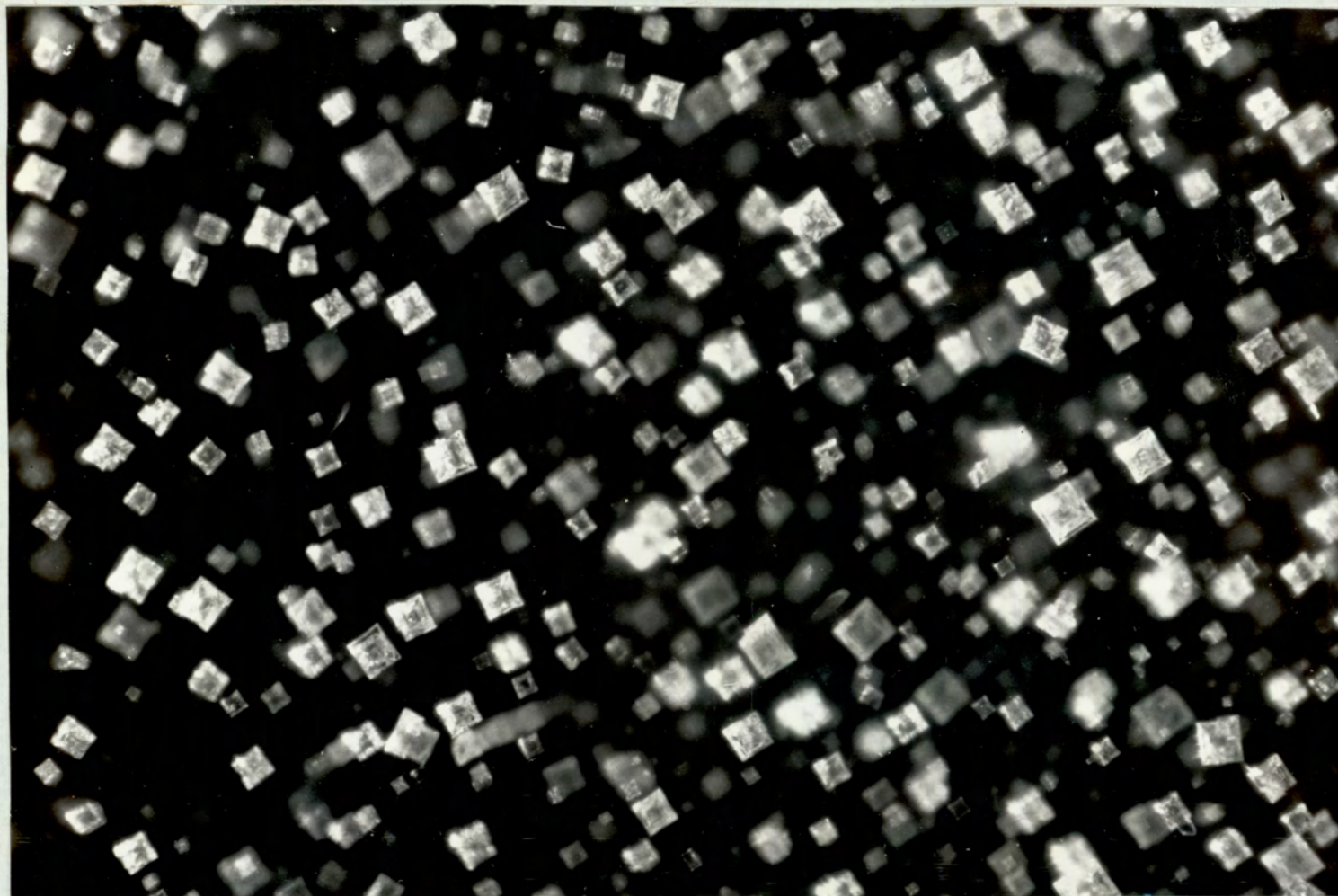


FIG. 8·5 ELONGATE CRYSTALS OF SODIUM CHLORIDE, PLAN VIEW
(MAGNIFICATION X350)

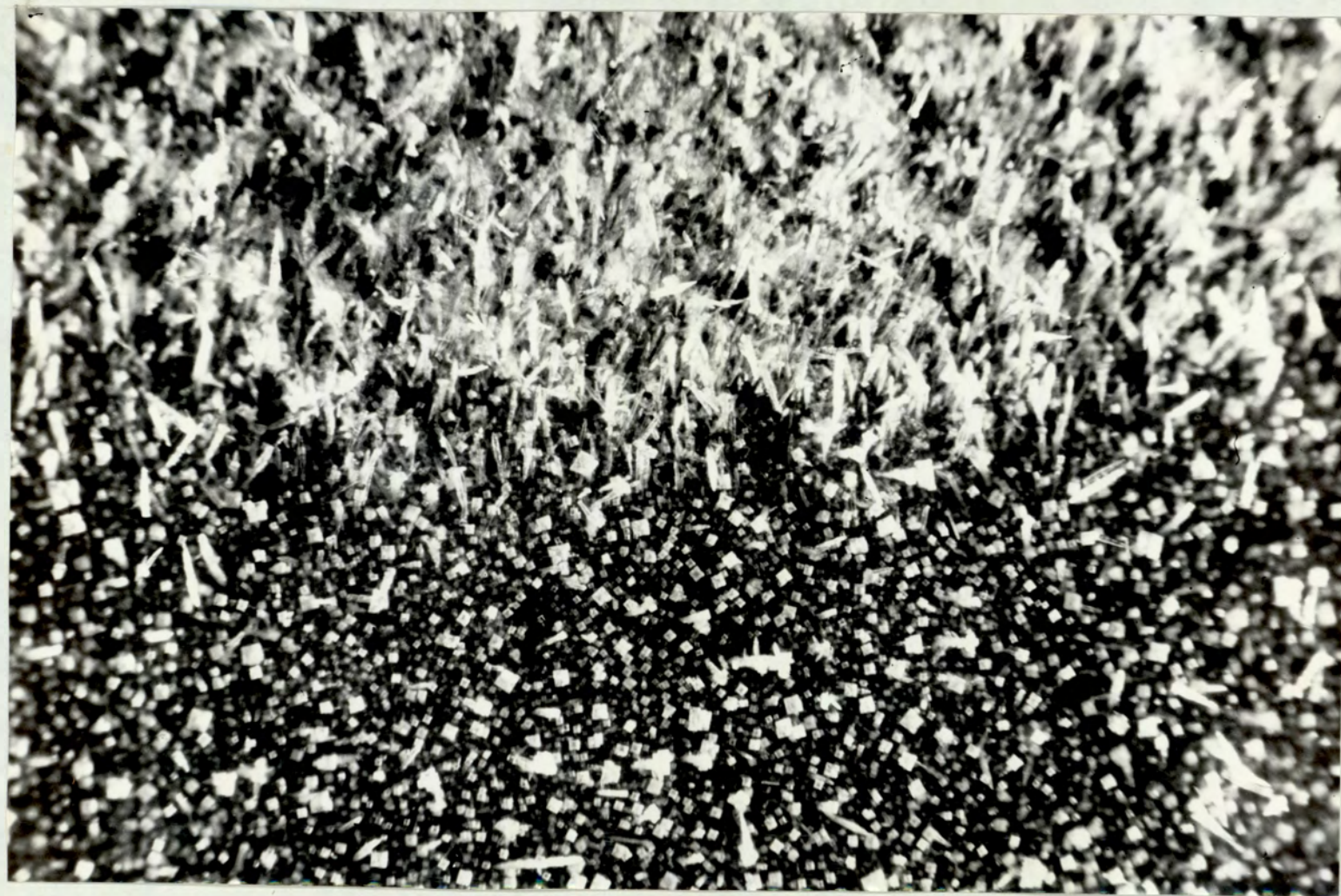


FIG. 8·6a PARTIALLY DISTURBED DEPOSIT OF ELONGATE CRYSTALS OF SODIUM CHLORIDE (MAGNIFICATION X120)

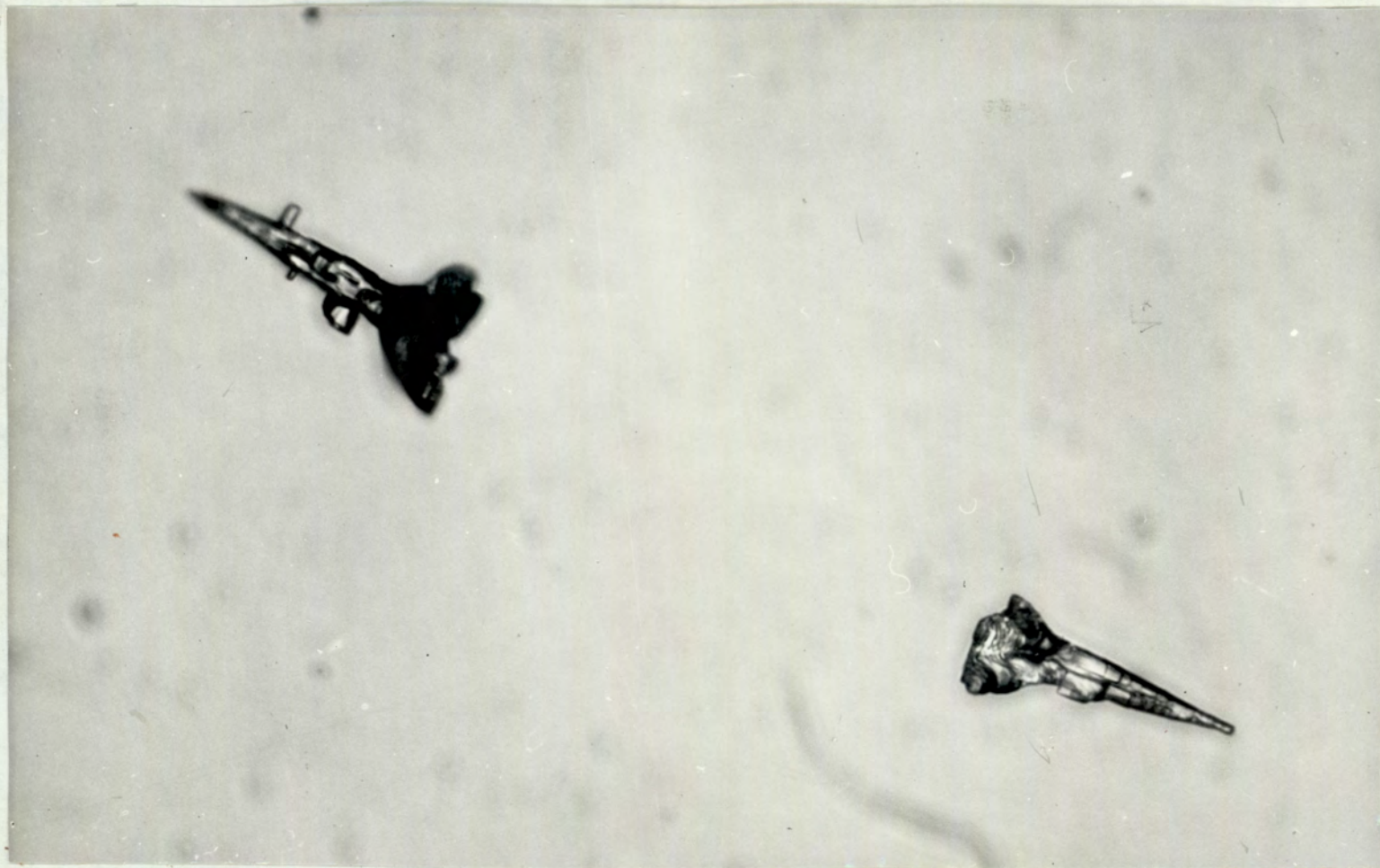


FIG. 8-6b TWO ELONGATE CRYSTALS FROM THE DEPOSIT SHOWN IN FIG. 8-6a
(MAGNIFICATION X1,000)

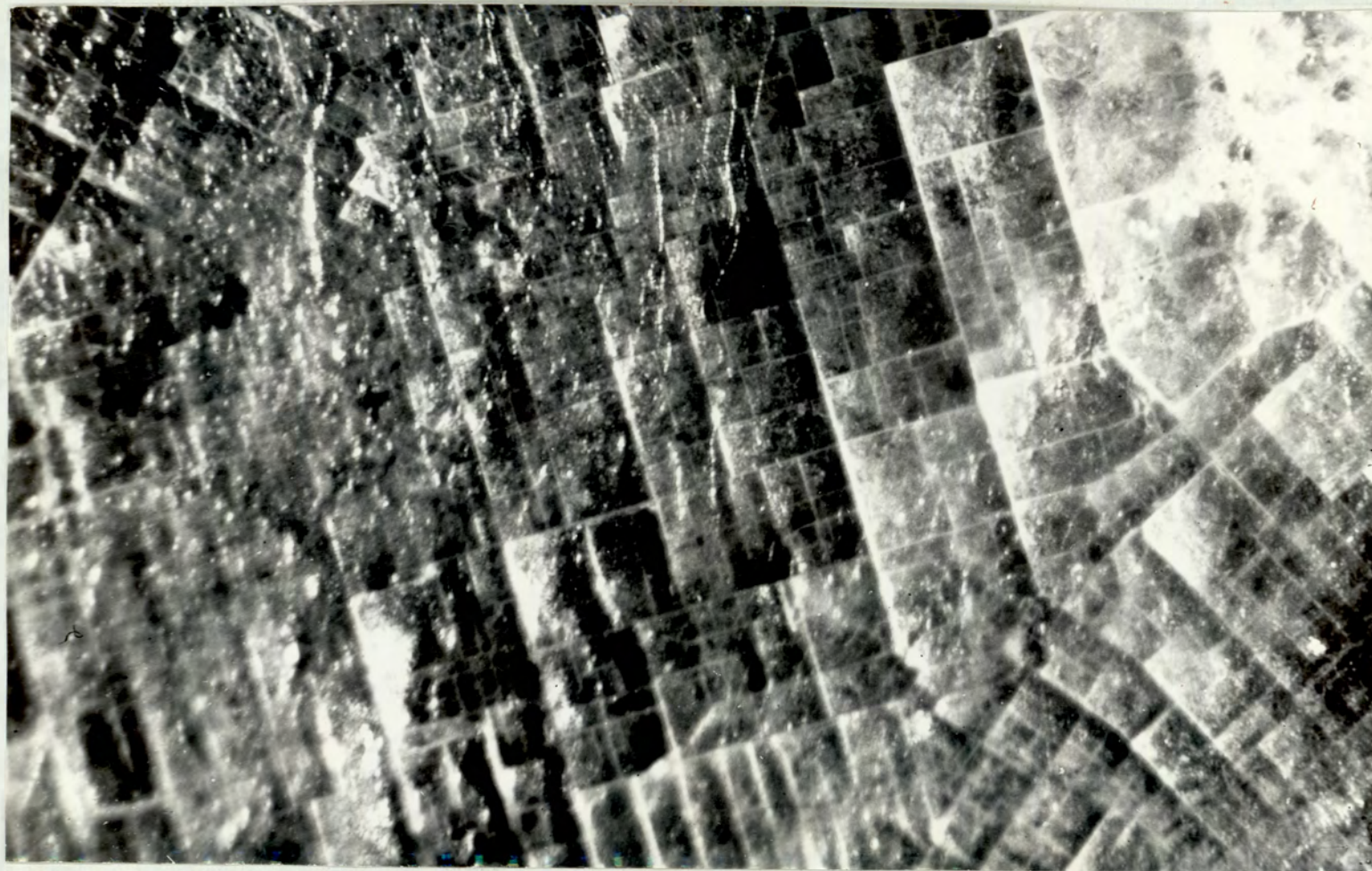


FIG. 8·7 FUSED DEPOSIT OF SODIUM CHLORIDE WITH CRYSTALLIZATION OCCURING
(MAGNIFICATION X350)

8.1.2.2 Effect of Variation of Surface Temperature, Gas Velocity and Concentration of Salt Vapour

(a) Physical Character of Deposited Salt

The nature of the deposited salt was unaffected by variation of the mainstream gas velocity or concentration of salt vapour, both in the region beneath the laminar boundary layer and the region beneath the turbulent wake. The mainstream velocity was varied over the range 10.5 - 30.0 m/s for sodium chloride and 10.5 - 18.0 m/s for potassium chloride while the mainstream concentration of salt vapour was varied over the range 0.055 - 0.25 torr for both salts.

However, the nature of both salts was found to be strikingly dependent upon the surface temperature of the target tube. Considering sodium chloride first; at the lowest upstream surface temperature examined, which was 440°C at the separation point of flow, dendrites of sodium chloride grew outwards from the upstream surface of the tube (Fig. 8.4 a & b). At 610°C the crystals were transformed from a dendritic growth to a seemingly cubic form when viewed in plan (Fig. 8.5); however, disturbance of the deposit revealed that the crystals were elongated with an increasing square cross section terminated with a flat topped cube (Figs. 8.6 a & b). Above 610°C the crystals became gradually smaller with increasing temperature and disappeared above a temperature of 640°C when the deposit was of a fully fused appearance. Fig. 8.7 shows a typical fused deposit which has crystallized from the melt during cooling to give a mosaic of cubic symmetry. The changes in orientation were postulated as corresponding to the impinging boundaries of the allotropic crystals. The appearance of fused salt deposits at temperatures of 190°C

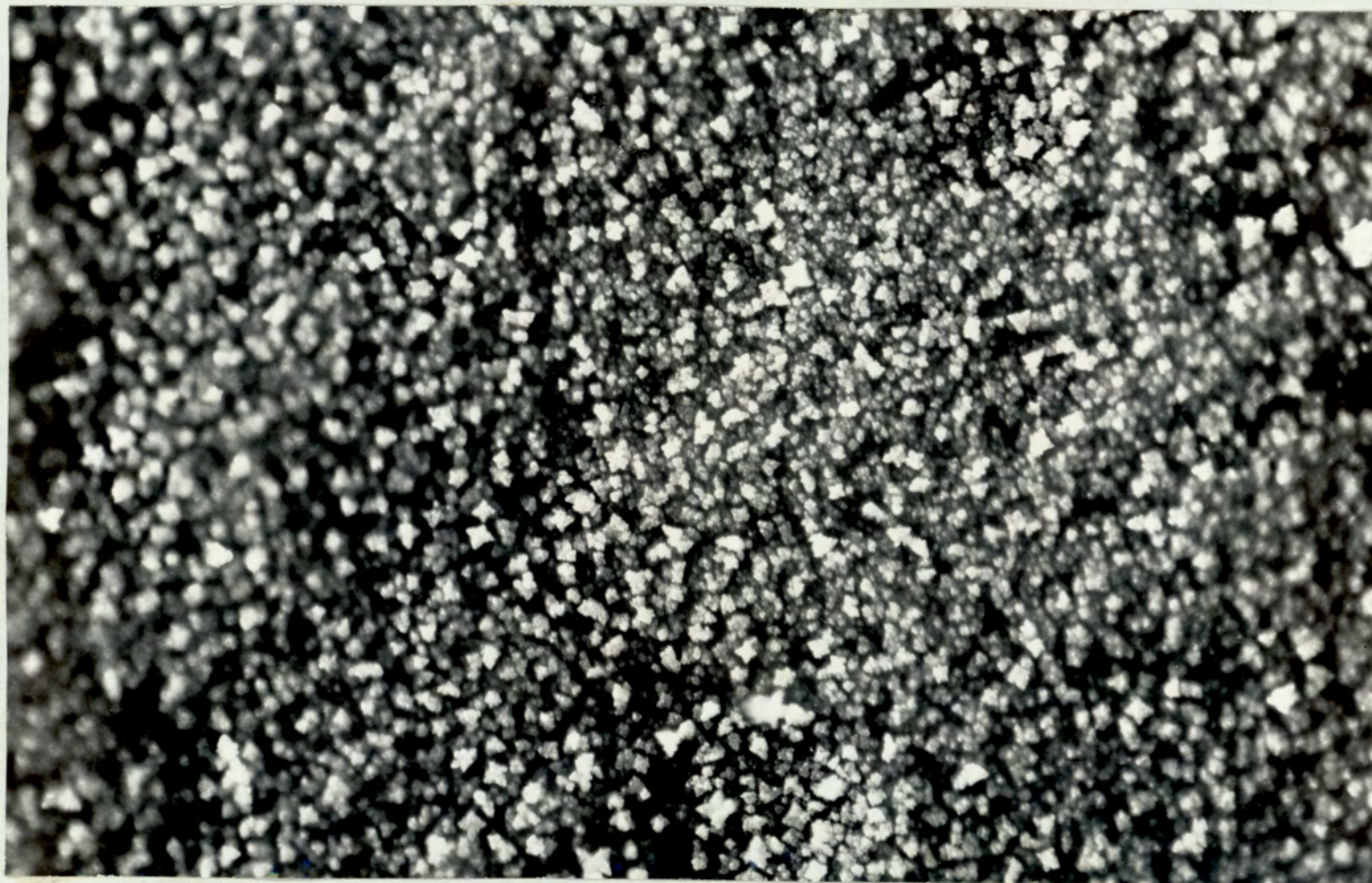


FIG. 8·8 DENDRITES OF SODIUM CHLORIDE GROWING WITHIN THE AREA BENEATH THE
TURBULENT WAKE (MAGNIFICATION X 350)

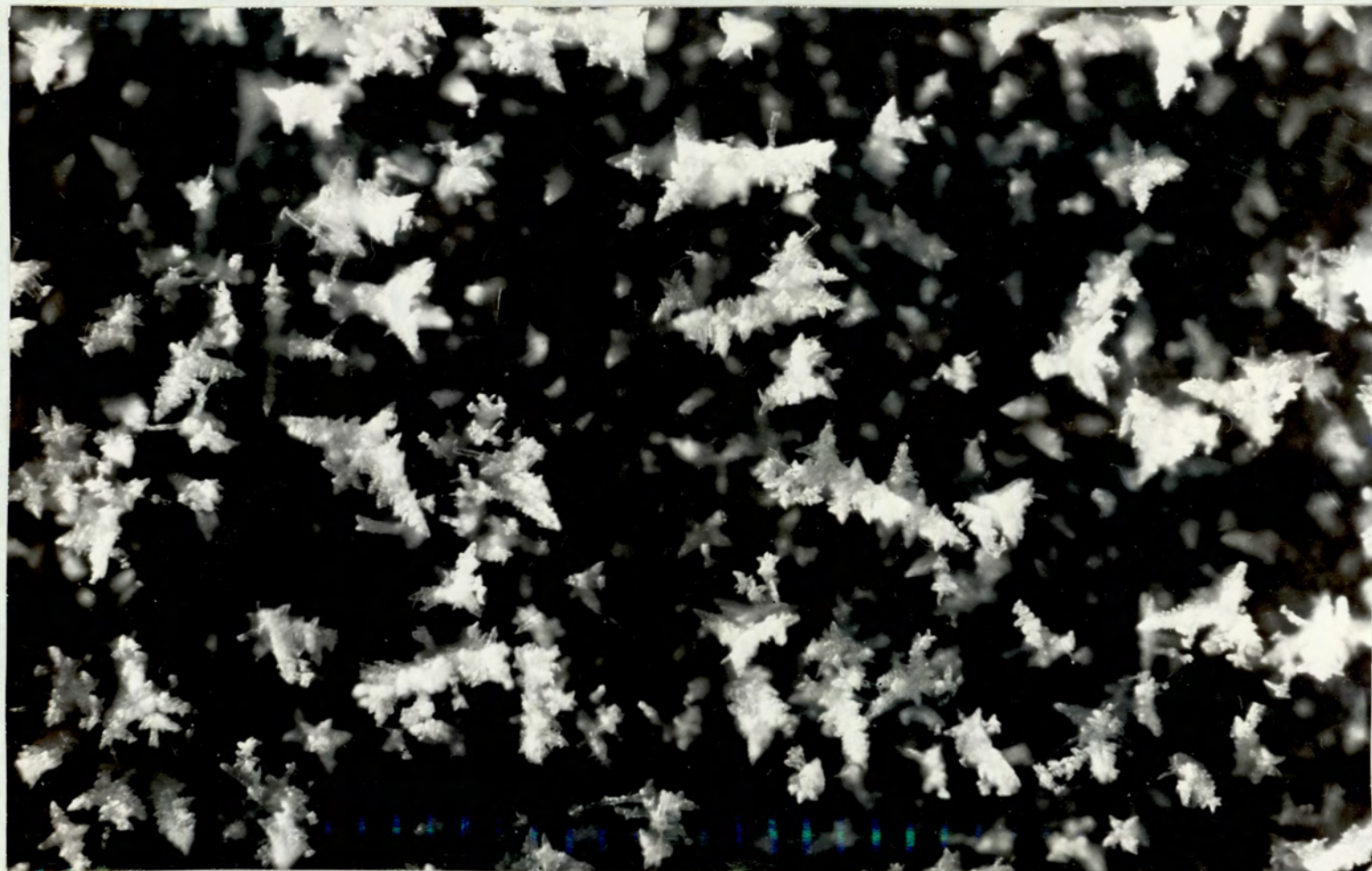


FIG. 8·9 DENDRITES OF POTASSIUM CHLORIDE, PLAN VIEW (MAGNIFICATION X400)

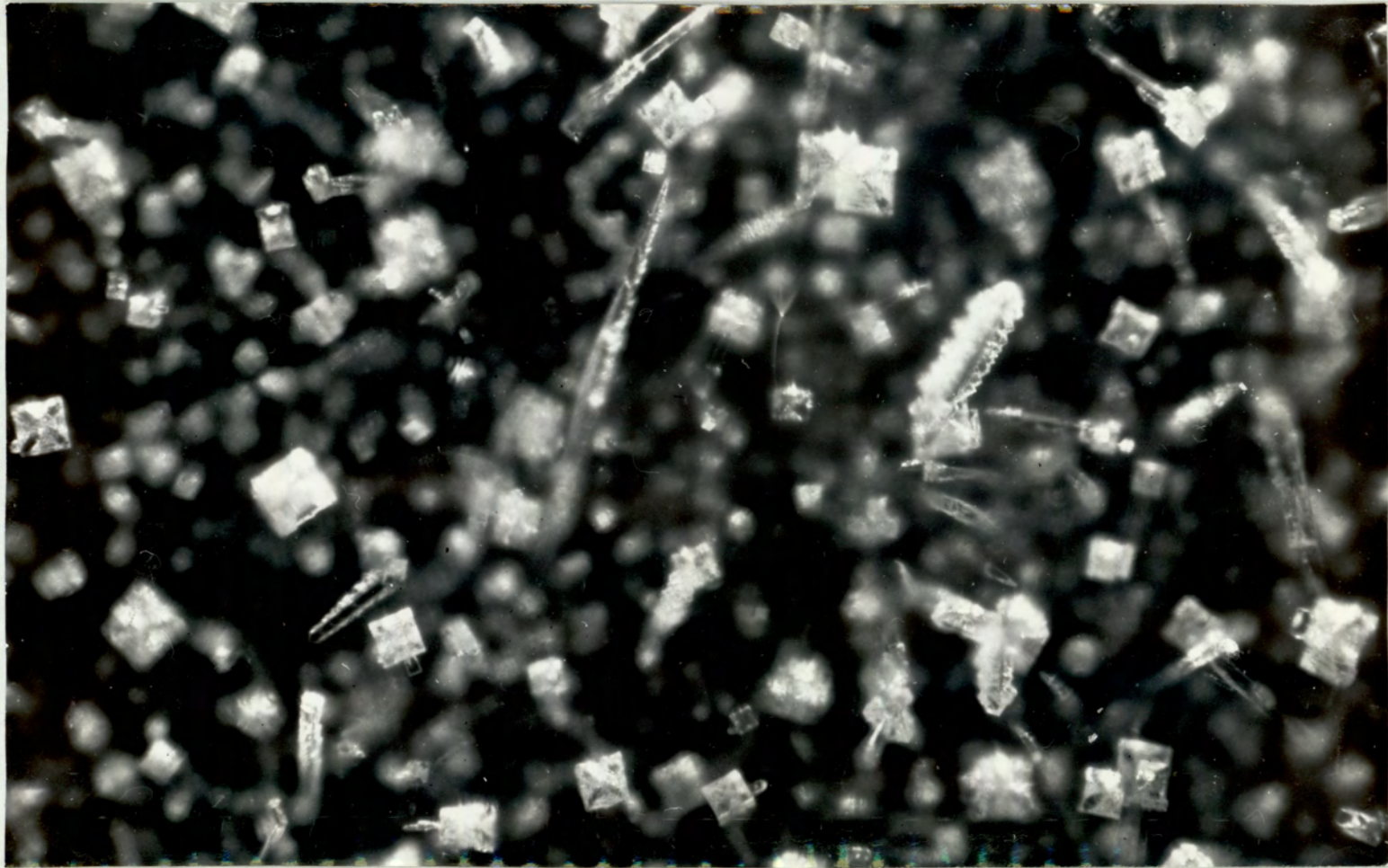


FIG. 8·10 ELONGATE CRYSTALS OF POTASSIUM CHLORIDE, PLAN VIEW
(MAGNIFICATION X400)

below the normal melting point of the salt (800°C) was regarded as a supercooling effect.

The downstream deposit beneath the turbulent wake was composed of very fine dendrites at surface temperatures of 400°C (Fig. 8.8). As the temperature was increased, the crystals became smaller until eventually complete fusion occurred over a temperature range of $610 - 640^{\circ}\text{C}$ which was similar to the transition range for the upstream deposit.

Potassium chloride behaved in a similar manner to sodium chloride. At the lowest temperature investigated within the laminar boundary layer, 430°C , dendrites of potassium chloride grew from the surface (Fig. 8.9). At 560°C there was nearly a complete transition to elongate crystals, but they did not all grow vertically from the surface as the sodium chloride crystals did (Fig. 8.10, cf. Fig. 8.5). Over the temperature range $560 - 585^{\circ}\text{C}$ the crystals gradually became smaller, until above 585°C the deposit was fully fused.

The nature of the downstream deposit showed the same variation with temperature as sodium chloride. The deposit became fully molten at 580°C .

(b) Rates of Deposition

Within the area of the laminar boundary layer the deposition rates (Appendix 8) were found to be :

- (1) Proportional to the concentration difference of salt vapour between the mainstream and tube surface.
- (2) Proportional to the square root of the mainstream velocity.

At temperatures above 660°C for sodium chloride and 620°C for potassium chloride, the deposits started to exert an appreciable vapour pressure so reducing the effective driving force for condensation. Hence in this region the deposition

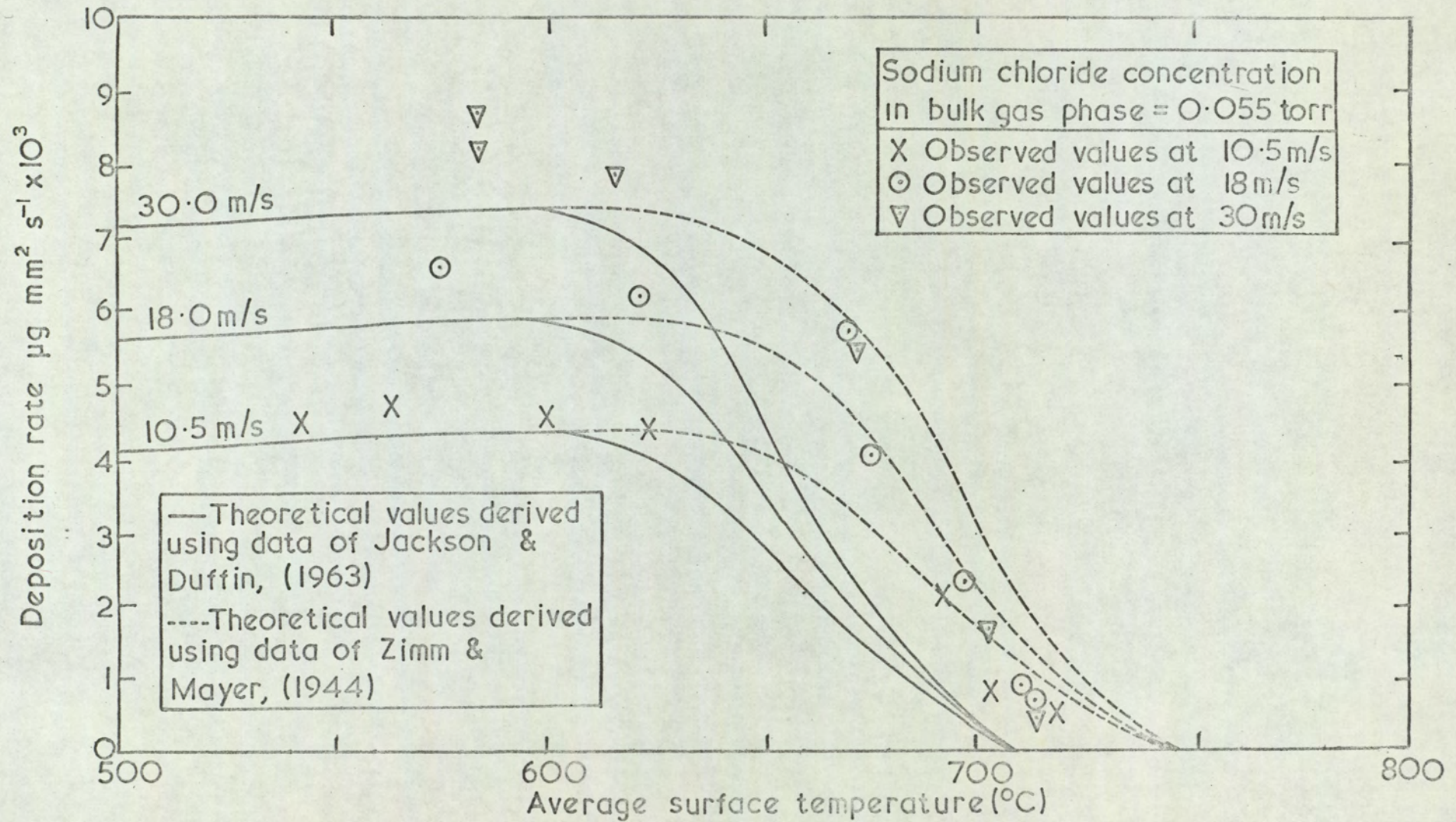


FIG 8.11a VARIATION OF DEPOSITION RATE WITH SURFACE TEMPERATURE

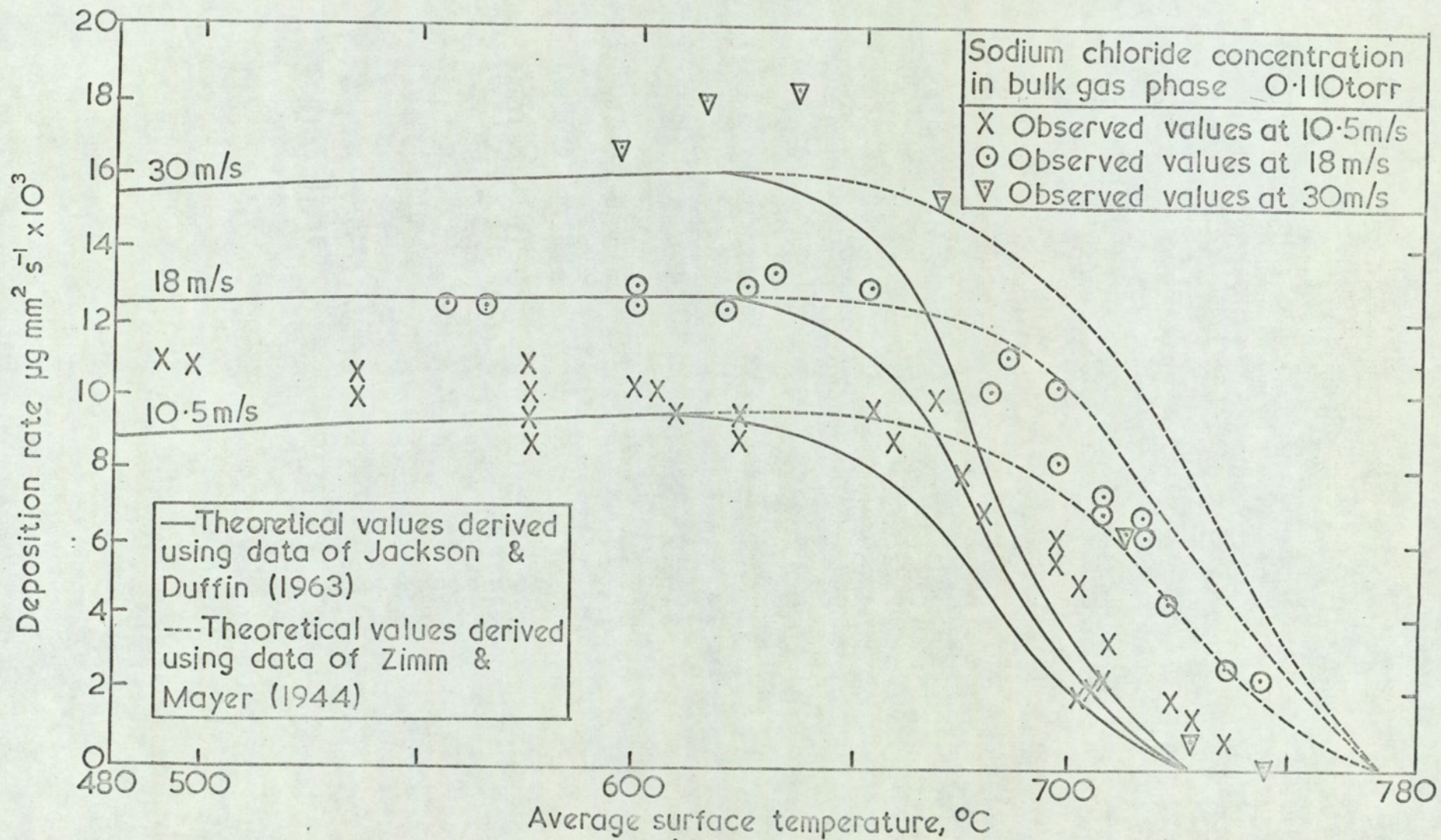


FIG.8-IIb VARIATION OF DEPOSITION RATE WITH SURFACE TEMPERATURE

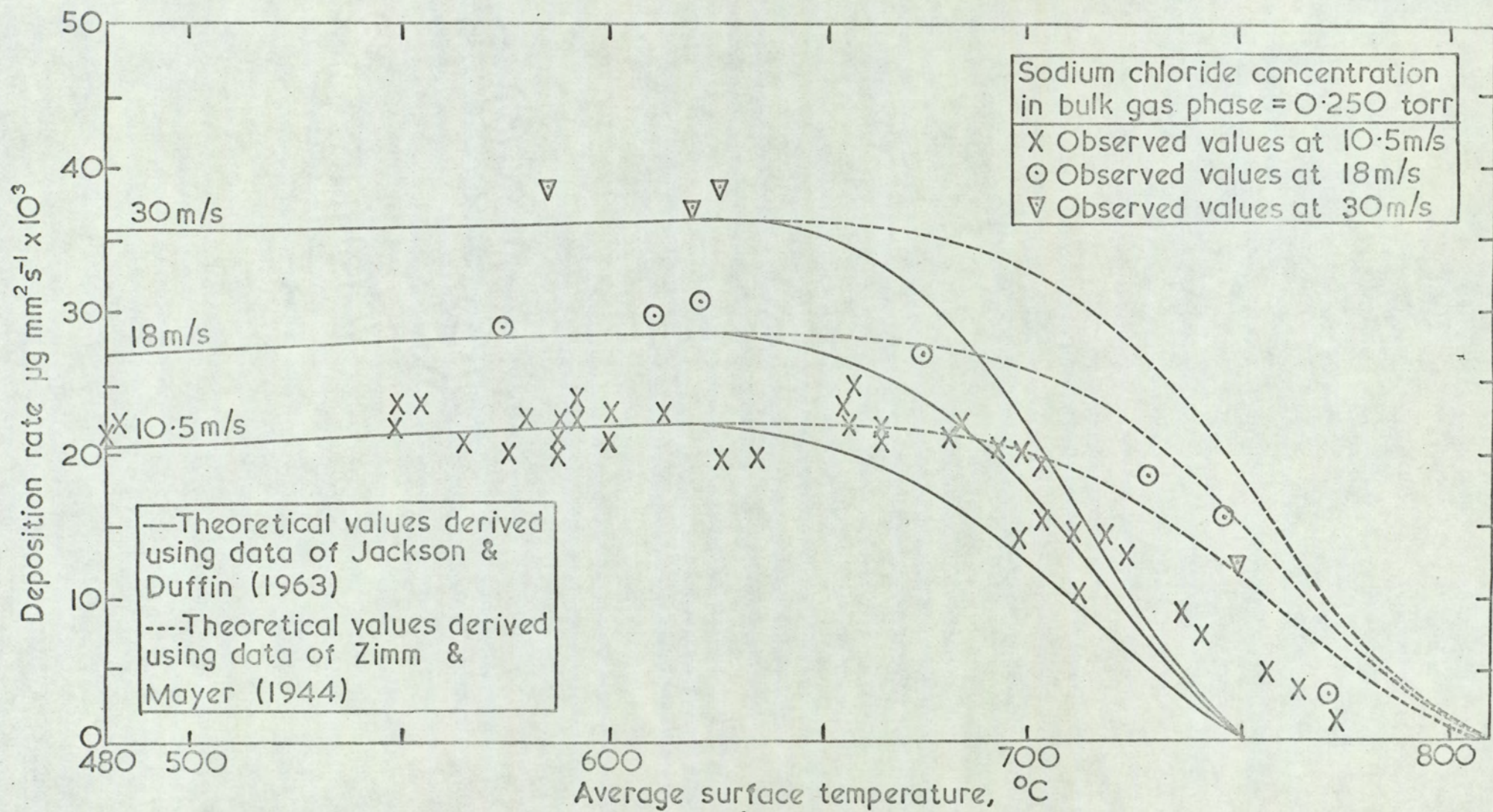


FIG.8-11c VARIATION OF DEPOSITION RATE WITH SURFACE TEMPERATURE

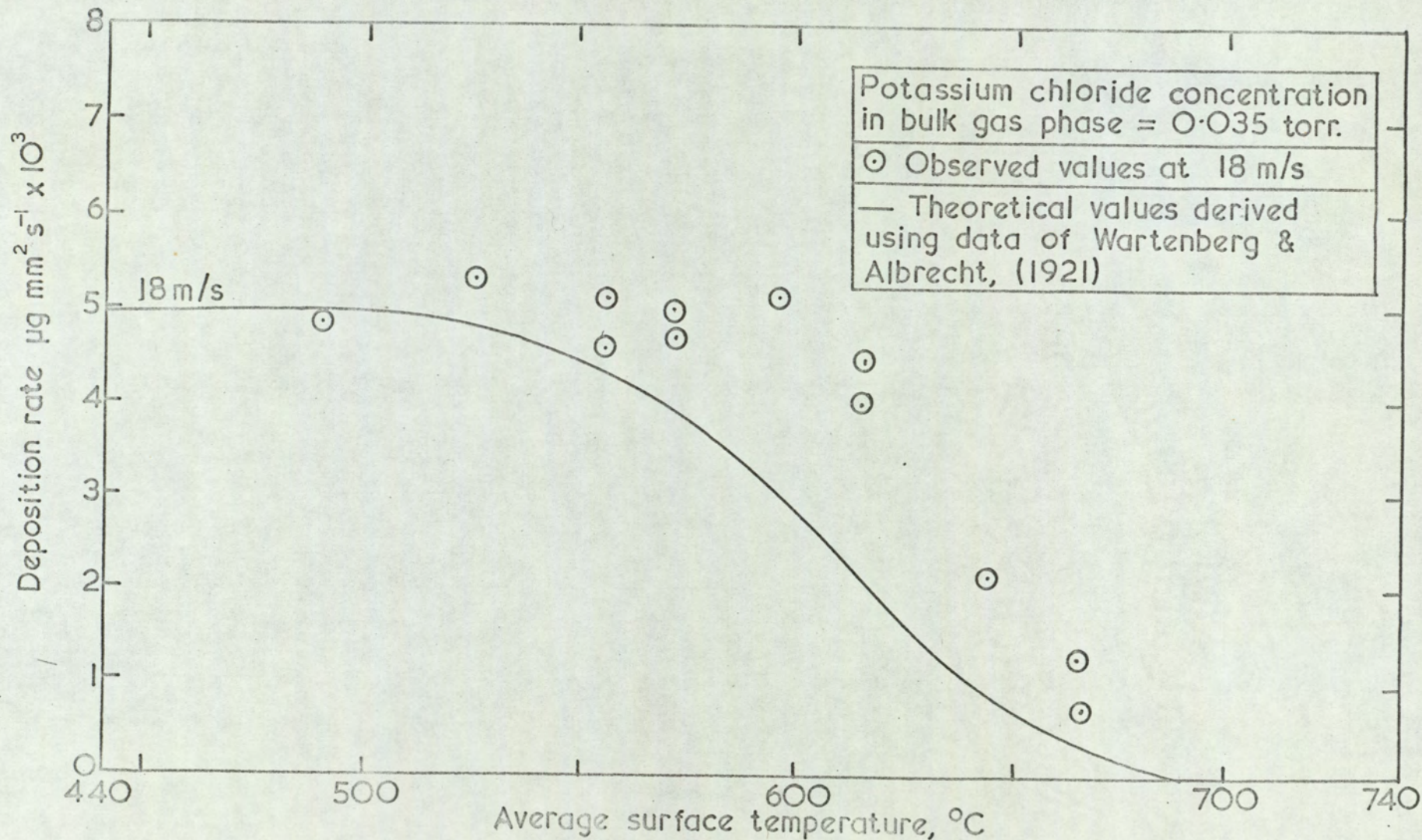


FIG. 8.12a VARIATION OF DEPOSITION RATE WITH SURFACE TEMPERATURE

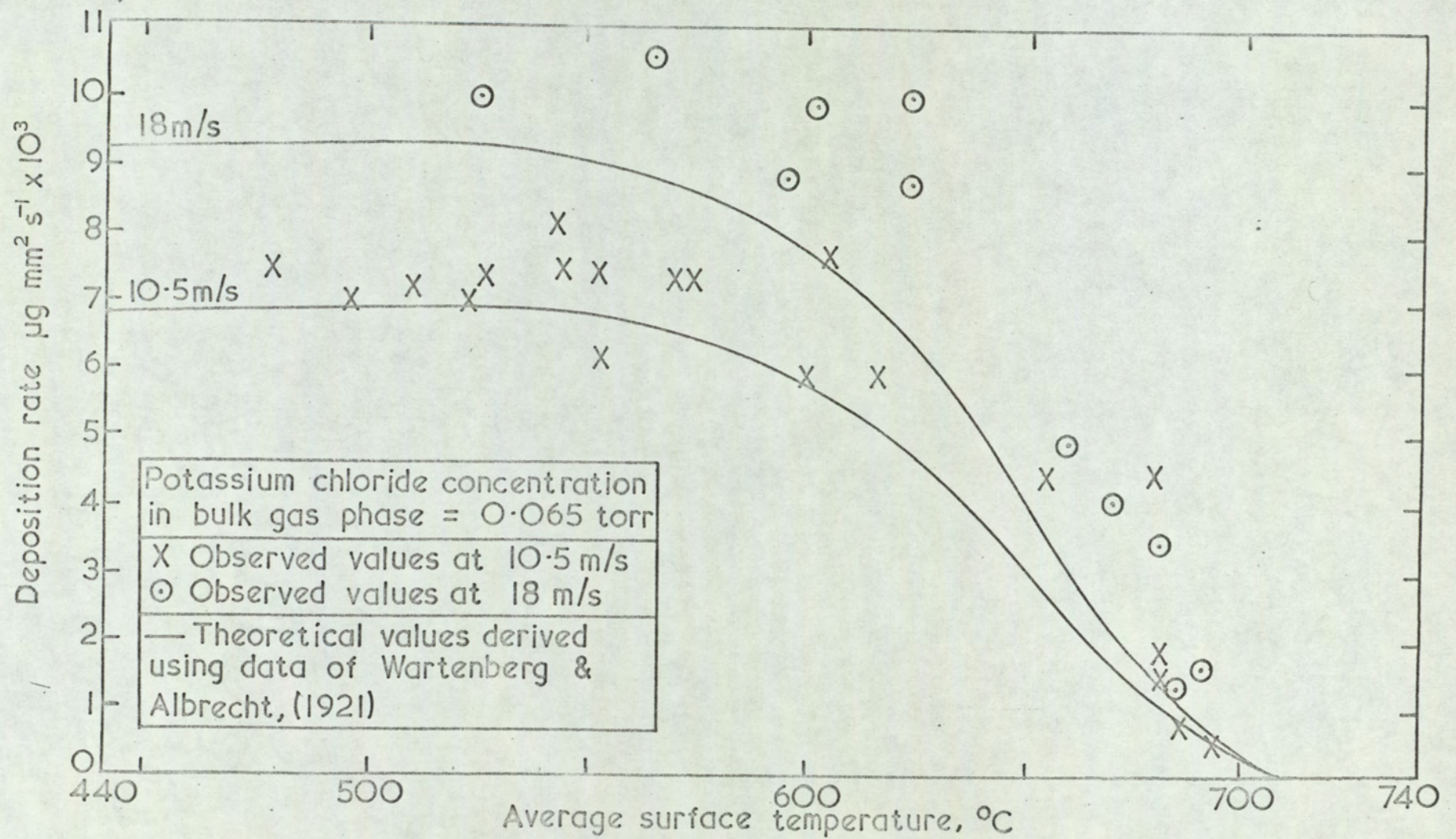


FIG. 8-12b VARIATION OF DEPOSITION RATE WITH SURFACE TEMPERATURE

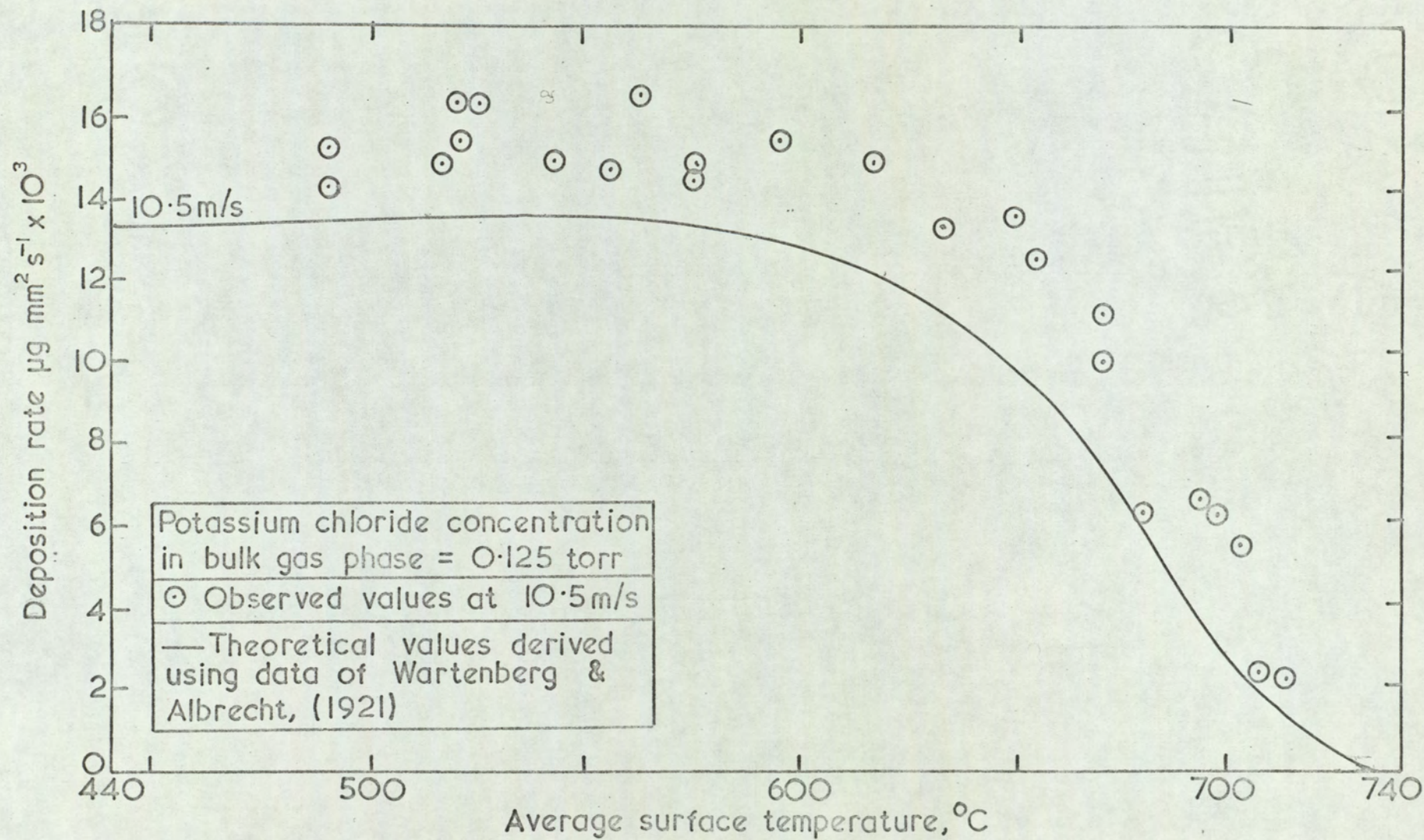


FIG.8-12c VARIATION OF DEPOSITION RATE WITH SURFACE TEMPERATURE

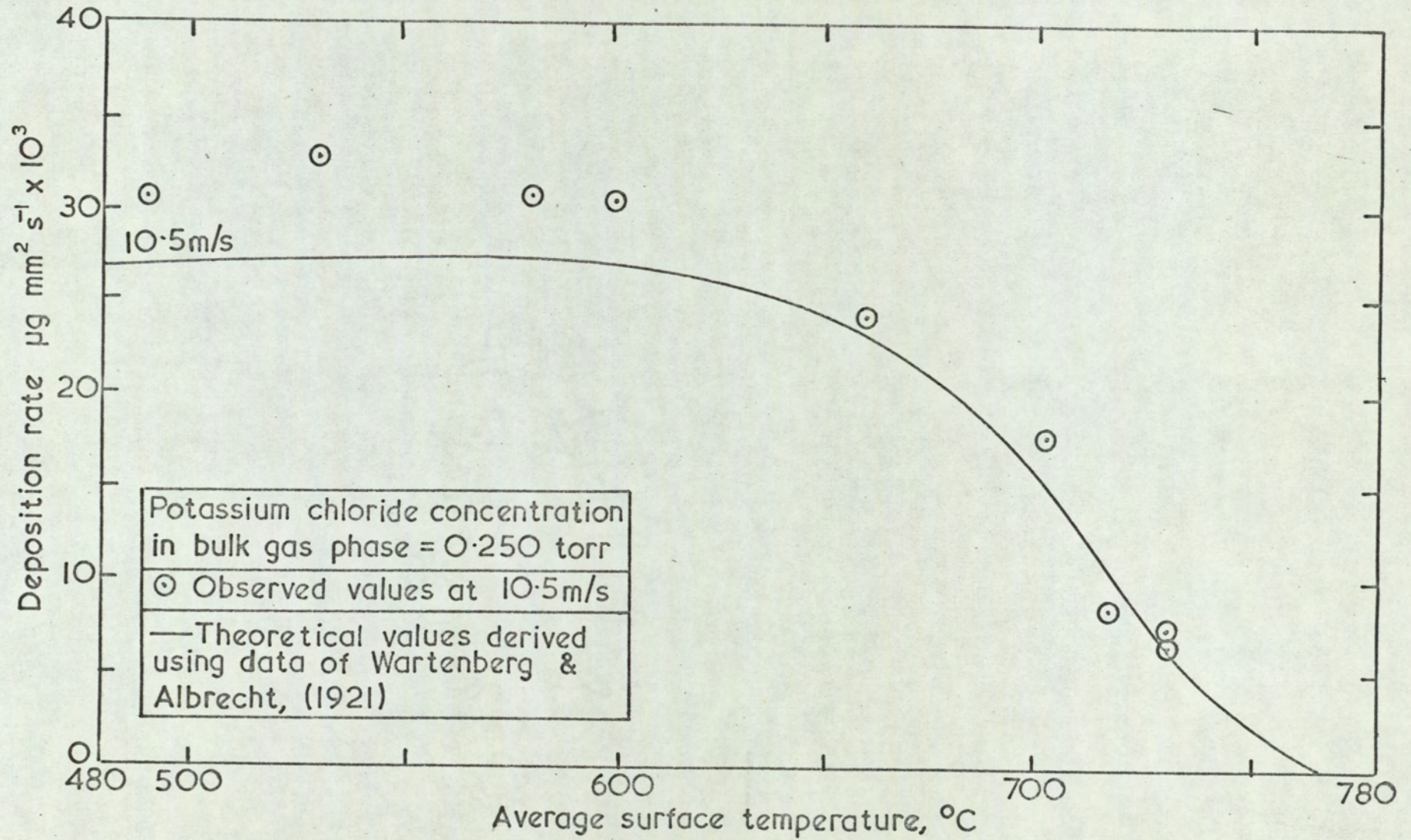


FIG. 8-12d VARIATION OF DEPOSITION RATE WITH SURFACE TEMPERATURE

rates were also dependent upon surface temperature.

It was not possible to obtain the exact velocity and concentration required for a particular run so in order that the deposition rate results could be plotted as a function of temperature for a specific concentration difference and gas velocity, they were corrected to one value assuming relationships (1) and (2). The deposition rate results plotted as a function of temperature with velocity as parameter are shown in Figs. 8.11 a-c & 8.12 a-d. The theoretical results (Appendix 7) are superimposed upon the experimental results. For sodium chloride the theoretical results have been calculated using the vapour pressure data of Zimm & Mayer (1944) measured 'in vacuo', and the data of Jackson & Duffin (1963) measured in the presence of water vapour. In the case of potassium chloride, the only available data was measured 'in vacuo'. Average surface temperatures were used in Figs. 8.11 & 8.12 because of the temperature distribution which existed around the ring.

The reproducibility of 90% of the experimental results was to within 10% on the plateau, but was less as the surface exerted an appreciable vapour pressure. This was due to the sensitivity of deposition rate upon surface temperature in this region.

On the plateau region of the curves the average deposition rates were 4% above the theoretical rate for sodium chloride and 8% above for potassium chloride. The agreement was again less when the surface deposit exerted an appreciable vapour pressure. However the slopes of the experimental curves were similar to the theoretical ones, and in the case of sodium

chloride, the results were closer to the theoretical ones using Zimm & Mayer's (1944) data. As water vapour is present in the system, one would have expected the experimental results to have been closer to the theoretical results evaluated using Jackson & Duffin's (1963) data.

The dependence of the rate of deposition in the turbulent wake downstream of the tube upon velocity and concentration was less well defined. In general, the rate was one third of the deposition rate at the upstream surface of the tube for both salts.

8.1.2.3 Condensation Points

Average temperatures of the upstream surface between the forward stagnation point and the separation lines are plotted in Figs. 8.11 & 8.12, so the temperature at which the rates of deposition are zero do not give values of the condensation points. As the surface temperature decreased from the forward stagnation point around the ring, zero deposition rate occurred on the upstream surface when the condensation point coincided with the surface temperature at the line of flow separation. In practice the condensation point for a particular concentration was obtained from the angle at which the condensation line appeared as described in section 7.2.3. Mean values for the condensation points as determined for various temperatures at the stagnation point are listed in Tables 8.1 & 8.2. The values obtained from previous workers' vapour pressure data are also included.

8.1.3 Analysis of Deposits

The sodium, potassium, chloride and sulphate contents of random samples of upstream deposits of both salts were determined. The chemical composition of the collected deposits

Concentration of sodium chloride, torr	Nominal main stream velocity m/s	Run No.	Temp. at stagnation point, °C.	Angle subtended at limit of deposition, degrees	Corresponding condensation point, °C.	Mean condensation point, °C.	Previously observed condensation points, °C.	
							Jackson & Duffin (1963)	Zimm & Mayer (1944)
0.055	10.5	D77	710	23	707	707	676	718
		D75	720	54	703			
		D76	735	64	712			
0.055	18.0	D110	725	59	706	707	676	718
		D124	720	44	708			
		D123	730	70	705			
0.110	10.5	D44	725	32	722	733	705	747
		D45	740	45	731			
		D48	750	69	732			
0.110	18.0	D94	735	30	730	733	705	747
		D92	740	33	735			
		D91	750	50	740			
0.110	30.0	D95	760	67	741	733	705	747
		D117	750	71	729			
0.250	10.5	D69	770	39	765	760	729	775
		D68	785	71	761			
0.250	18.0	D102	785	75	760	760	729	775
0.250	30.0	D128	765	55	754	760	729	775

TABLE 8.1

Determined Condensation Points for Sodium Chloride.

	Nominal main-stream velocity, m/s	Run No.	Temperature at stagnation point, °C.	Angle subtended at limit of deposition (degrees)	Corresponding condensation point °C.	Mean Condensation point, °C	Previously observed condensation point, °C. (Wartenberg & Albrecht 1921)
Nominal Concentration of Potassium Chloride = 0.0350 torr.	18	G 25	685	58	665	662	651
	18	G 77	670	46	661		
	18	G 78	685	68	659		
Nominal Concentration of Potassium Chloride = 0.0650 torr.	18	G 29	705	60	686	682	678
	18	G 30	700	47	688		
	18	G 36	710	70	682		
	10.5	G 54	700	60	681		
	10.5	G 57	710	77	675		

TABLE 8.2 Determined Condensation Points for Potassium Chloride.

Cont'd

	Nominal main-stream velocity, m/s	Run No.	Temperature at stagnat ⁿ ion point, °C.	Angle Sub- tended at limit of deposition (degrees)	Corres- ponding condensa- tion point, °C.	Mean Conden- sation point, °C.	Previously observed condensa- tion point, °C. (Wartenberg & Albrecht 1921)
Nominal Concentration of potassium Chloride = 0.125 torr.	10.5	G 39	720	44	708	706	708
	10.5	G 44	730	66	709		
	10.5	G 45	715	51	701		
	10.5	G 37	710	29	706		
Nominal Concentration of potassium Chloride = 0.250 torr.	10.5	G 59	735	36	730	733	742
	10.5	G 60	745	49	734		
	10.5	G 61	745	47	735		

TABLE 8.2 Determined Condensation Points for Potassium Chloride

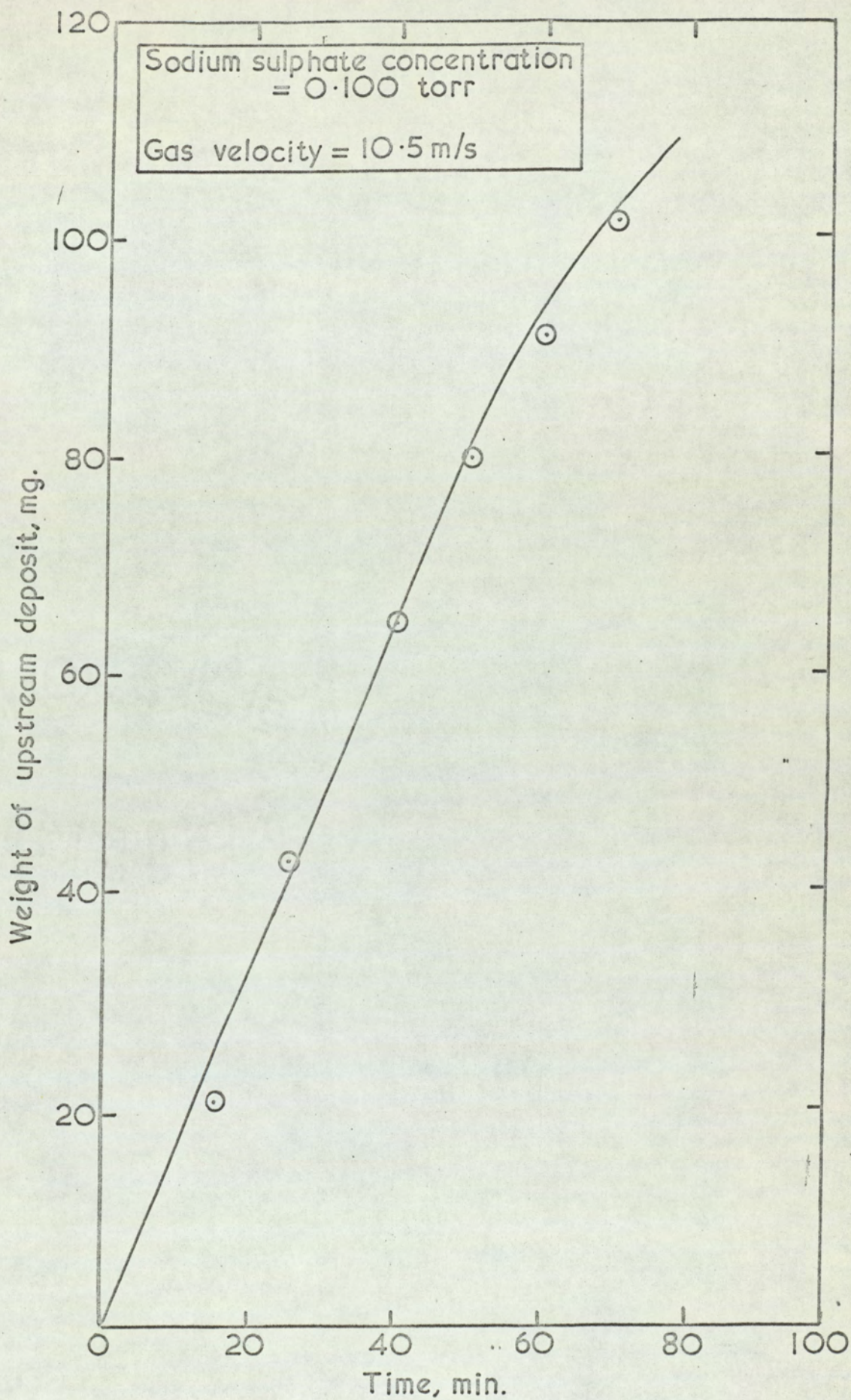


FIG.8-13 DEPENDENCE OF DEPOSIT WEIGHT UPON TIME OF EXPOSURE

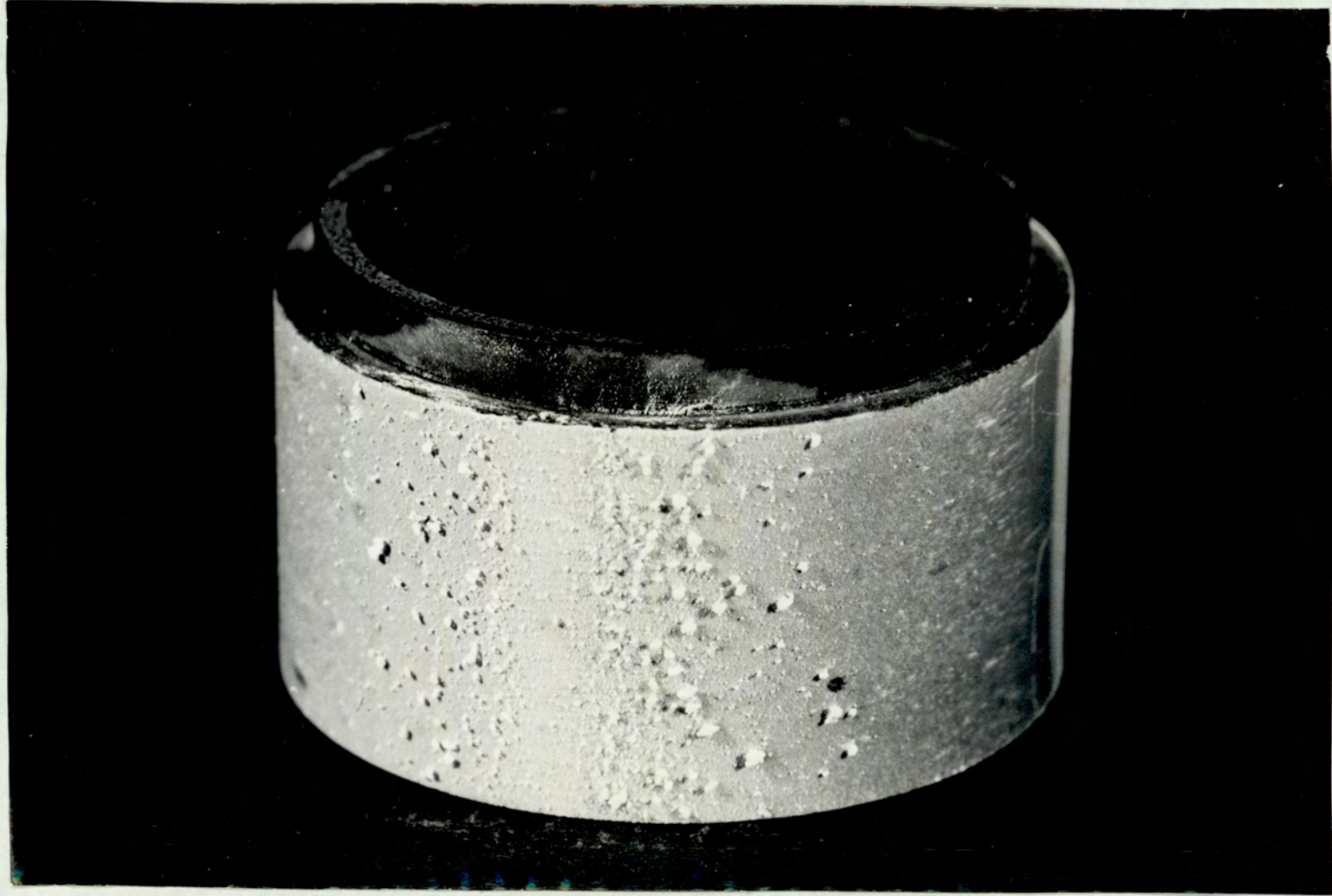


FIG. 8-14 DEPOSIT OF SODIUM SULPHATE COLLECTED WHEN IMPACTION WAS OCCURING

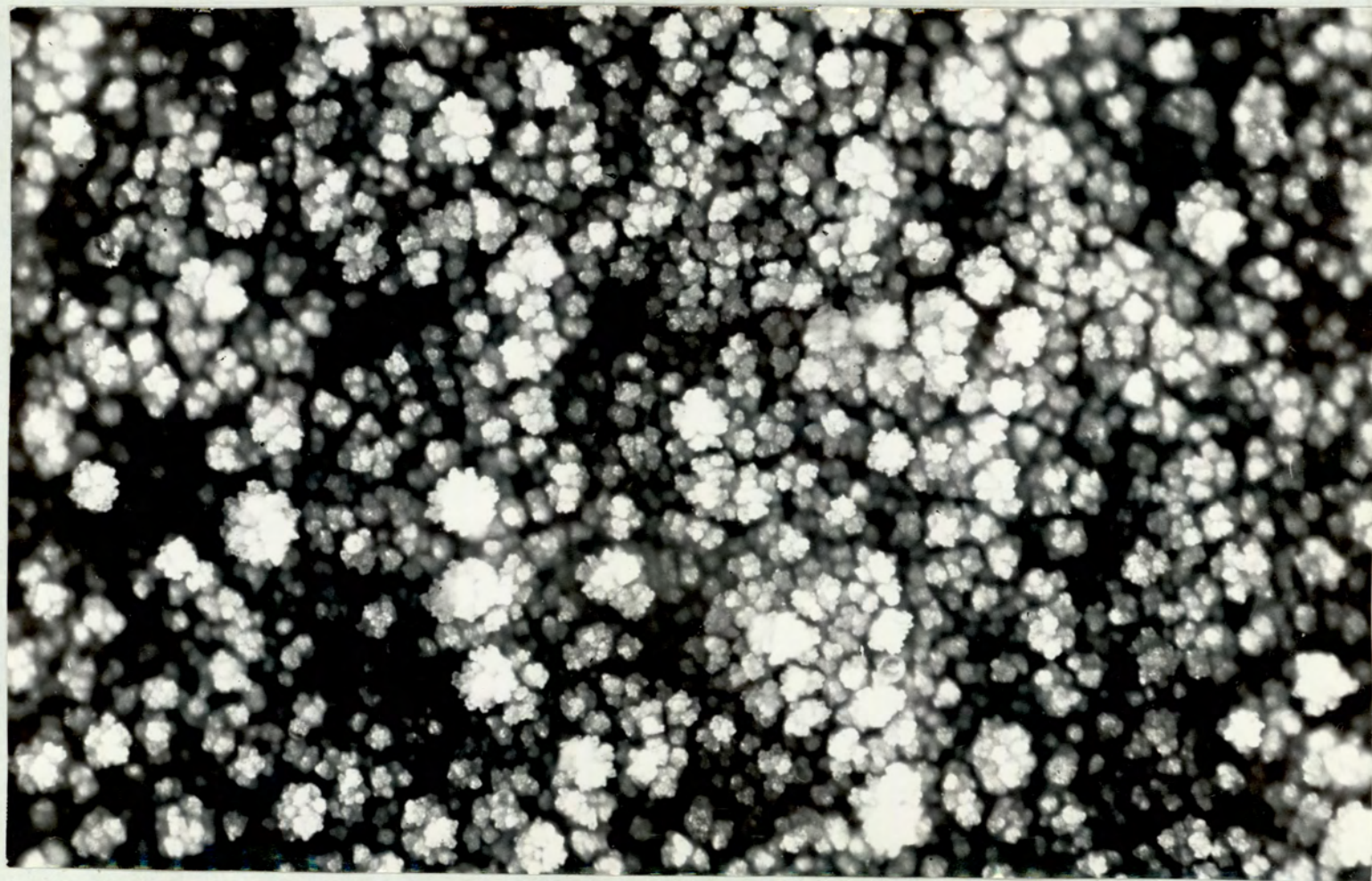


FIG. 8·15 DENDRITES OF SODIUM SULPHATE, PLAN VIEW (MAGNIFICATION X400)

differed little from the composition of the A.R. sodium chloride and potassium chloride used in preparing solutions for injection (Table 8.3 a & b). Samples of the deposits which had fused were subjected to X-ray analysis and it was confirmed that such deposits were essentially crystalline.

8.2 Deposition of Sodium Sulphate

8.2.1 Effect of Run Duration upon Deposit Weight

To find the maximum amount of deposit that could be collected on the ring before the deposition rate began to decrease, weights of deposits were collected for increasing run times. The surface temperature was kept below the fusion point of the sodium sulphate deposit. As can be seen from Fig. 8.13, the rate of deposition tended to decrease at weights above 150 mg.

8.2.2 Effect of Variation of Surface Temperature, Gas Velocity and Concentration of Salt Vapour

(a) Physical Character of Deposited Salt

Increasing the mainstream velocity above 10.5 m/s and concentration of salt above 0.1 torr caused only partial vaporisation of the salt and resulted in impaction occurring especially in a thin band around the stagnation point (Fig. 8.14). Hence, to prevent impaction occurring, only the lowest velocity obtainable in the combustor (i.e. 10.5 m/s) and small concentrations of the salt could be used.

As with the previous two salts the morphology of the sodium sulphate deposits was dependent upon surface temperature. At the lowest temperatures investigated (450°C) white dendritic crystals grew out from the surface (Fig. 8.15). However, the dendritic growth was less distinct and the crystal facets were not so clearly defined as the sodium chloride and potassium

(a)	A.R. Sodium chloride, w/w%.	Typical sample of upstream deposit, w/w%.
	38.6	38.2
	0.0	0.1
	60.5	59.7
	0.0	0.3
(b)	A.R. Potassium chloride, w/w%.	Typical sample of upstream deposit, w/w%.
	0.0	0.1
	52.2	51.1
	47.2	46.5
	0.0	0.4
	0.0	0.0

TABLE 8.3

Comparative Analysis of Injected Salts and
Deposit

chloride deposits. As the surface temperature was raised, the dendrites became gradually smaller and the deposit became fused. Small crystals continued to grow out of the melt even at high temperatures giving the molten deposit a white appearance.

Contrary to the results for the two previous salts, it was found that the morphology of sodium sulphate deposits was also dependent upon the concentration difference of salt vapour between the mainstream and tube surface. The effect of concentration gradient was to alter the temperature range over which the deposit became fused. These temperature ranges are given in Table 8.4. As with the previous two salts the fusion temperatures were well below the normal melting point of sodium sulphate indicating that supercooling occurred.

At low surface temperatures (450°C), the downstream deposit was composed of very fine dendrites of the same form as the upstream deposit. With increasing temperature, the crystals became smaller until complete fusion was evident over the range $530^{\circ}\text{C} - 550^{\circ}\text{C}$. This temperature range was independent of the concentration used.

(b) Rates of Deposition

Within the laminar boundary layer, the deposition rates were found to be independent of surface temperature until the surface deposit started exerting an appreciable vapour pressure.

Only at the lowest concentrations investigated was the deposition rate proportional to the concentration difference. Hence it was concluded that above a concentration of 0.011 torr, the salt was not fully vaporised. So that the results of the fully vaporised salt could be compared graphically with

Concentration of sodium sulphate in gas-phase, torr	Temperature range over which fused salt starts to appear, °C
0.100	660 - 680
0.0250	620 - 640
0.0110	540 - 560
0.0055	530 - 550

TABLE 8.4

Fusion temperatures at the concentrations
Investigated

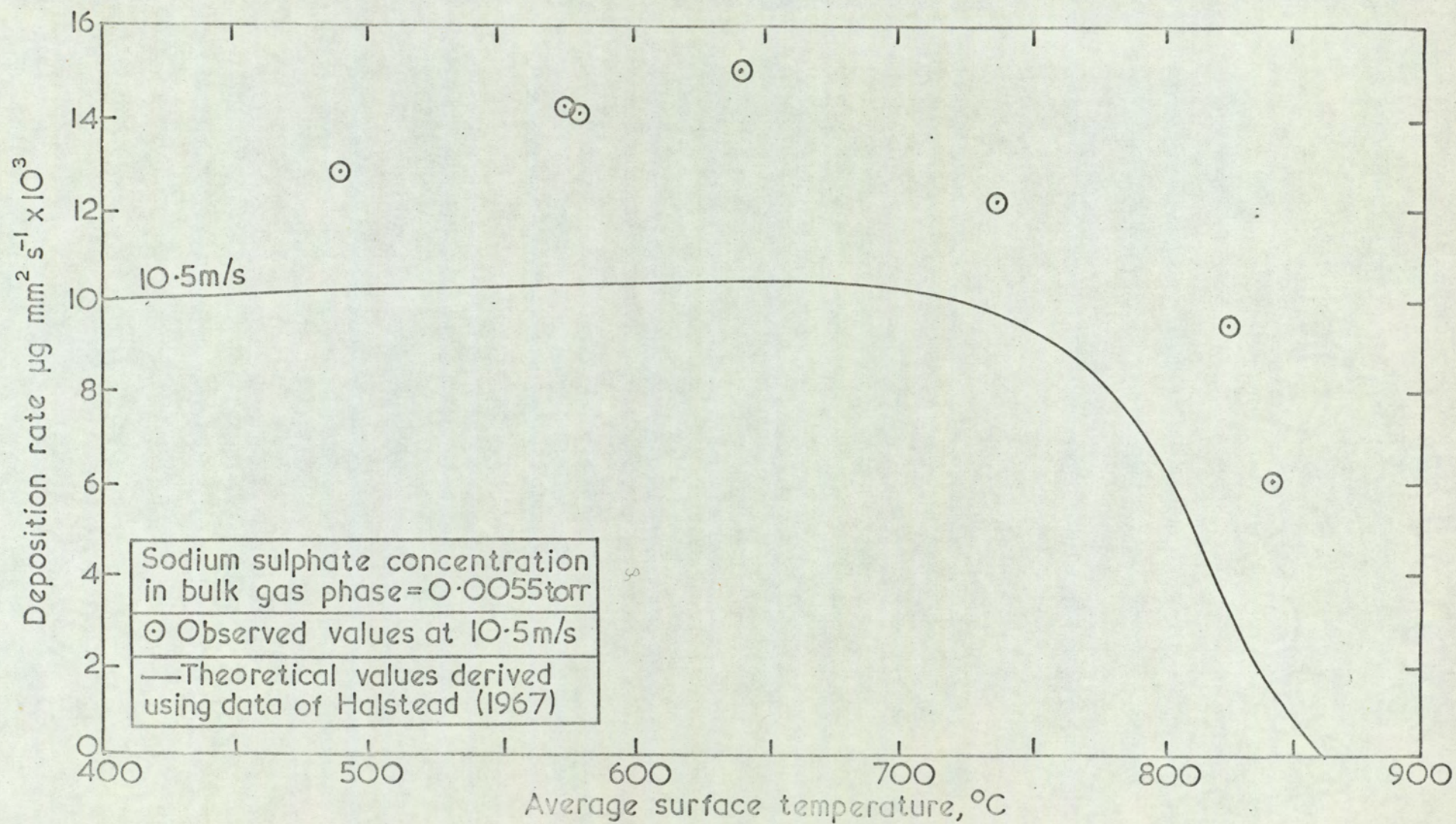


FIG. 8.16a VARIATION OF DEPOSITION RATE WITH SURFACE TEMPERATURE

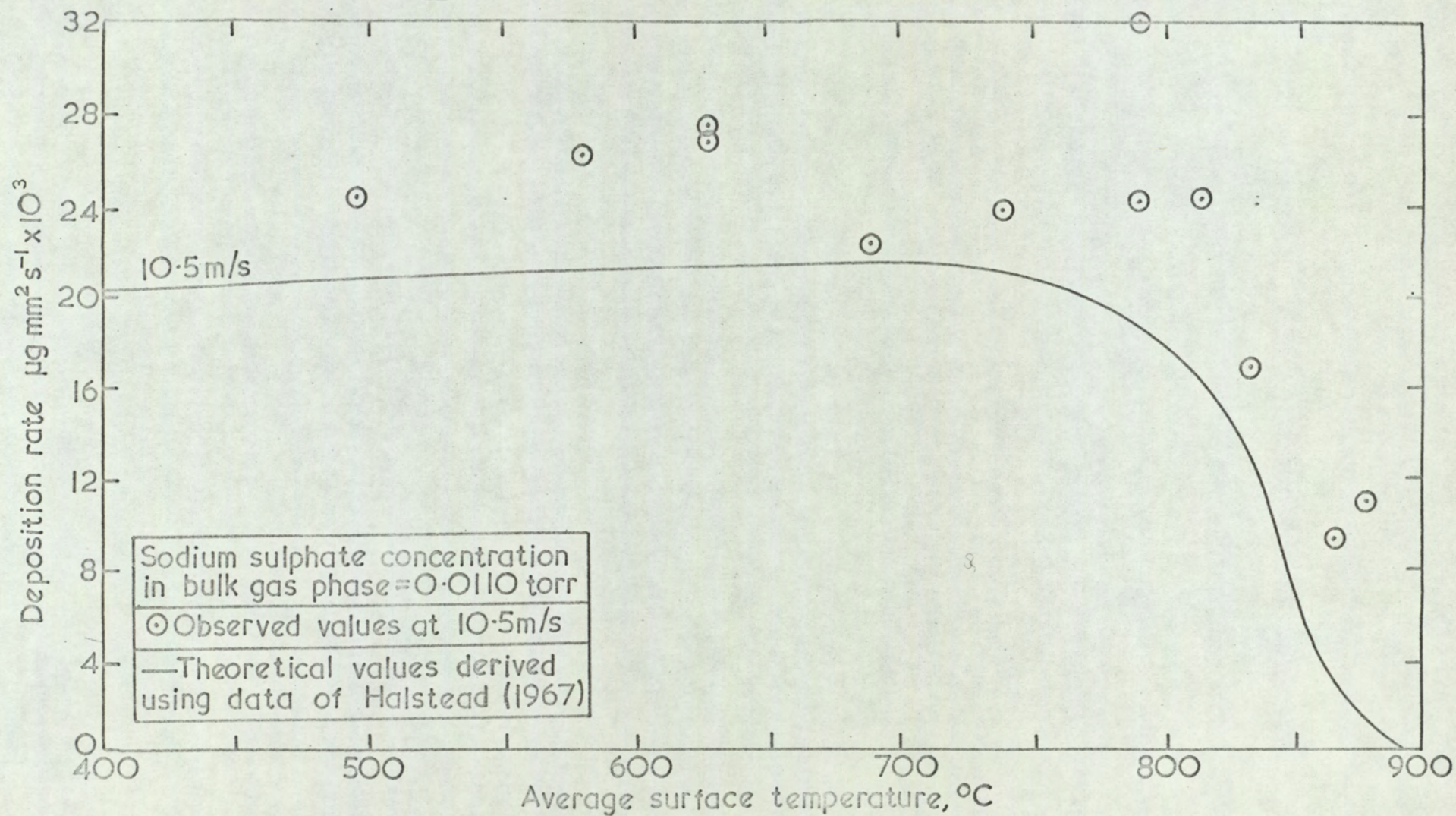


FIG. 8-16b VARIATION OF DEPOSITION RATE WITH SURFACE TEMPERATURE

the theoretical curve they were corrected to a specific concentration and velocity as were the sodium chloride and potassium chloride results. It was inferred that the rate of deposition of the fully vaporised salt would be proportional to the square root of the velocity although this could not be experimentally verified due to difficulties of vaporisation (Section 7.2.1).

The experimental results for concentrations of 0.011 torr and 0.060 torr together with the theoretical curves are shown in Fig. 8.16. The deposition rates on the plateau were approximately 30% above the theoretical rates. The discrepancy was similar when the surface deposit exerted an appreciable vapour pressure. The dependence of the rate of deposition in the turbulent wake upon surface temperature and concentration was less well defined, but in general was one fifth of the rate on the upstream surface of the tube.

8.2.3 Condensation Points

Condensation points were found as described in Section 7.2.3. As they were in the region of 900°C a platinum coated austenitic target ring was constructed and used at these high temperatures to determine the points. Although the platinum coating was superior to the ceramic coating at high temperatures, the cost prohibited more than one ring being made. The condensation points shown in Table 8.5 were only obtained for the two lowest concentrations where complete vaporisation was postulated as taking place. The points were difficult to determine due to the temperature variation around the ring being smaller at higher temperatures which meant the condensation line was less distinct.

8.2.4 Analysis of Deposits

	Run No.	Temperature of stagnation point, °C.	Angle subtended at limit of deposition (degrees)	Corresponding condensation point °C.	Mean Condensation point, °C.	Previously observed condensation point, °C. (Halstead, 1967)
Nominal Concentration of Sodium sulphate = 0.0110 torr and nominal main stream velocity = 10.5 m/s	E 51	870	69	860	859	867
	E 53	850	40	848		
	E 56	880	75	868		
Nominal Concentration of Sodium Sulphate = 0.0055 torr and nominal main stream velocity = 10.5 m/s	E 61	850	81	833	831	839
	E 73	835	52	829		

TABLE 8.5 Determined Condensation Points for Sodium Sulphate

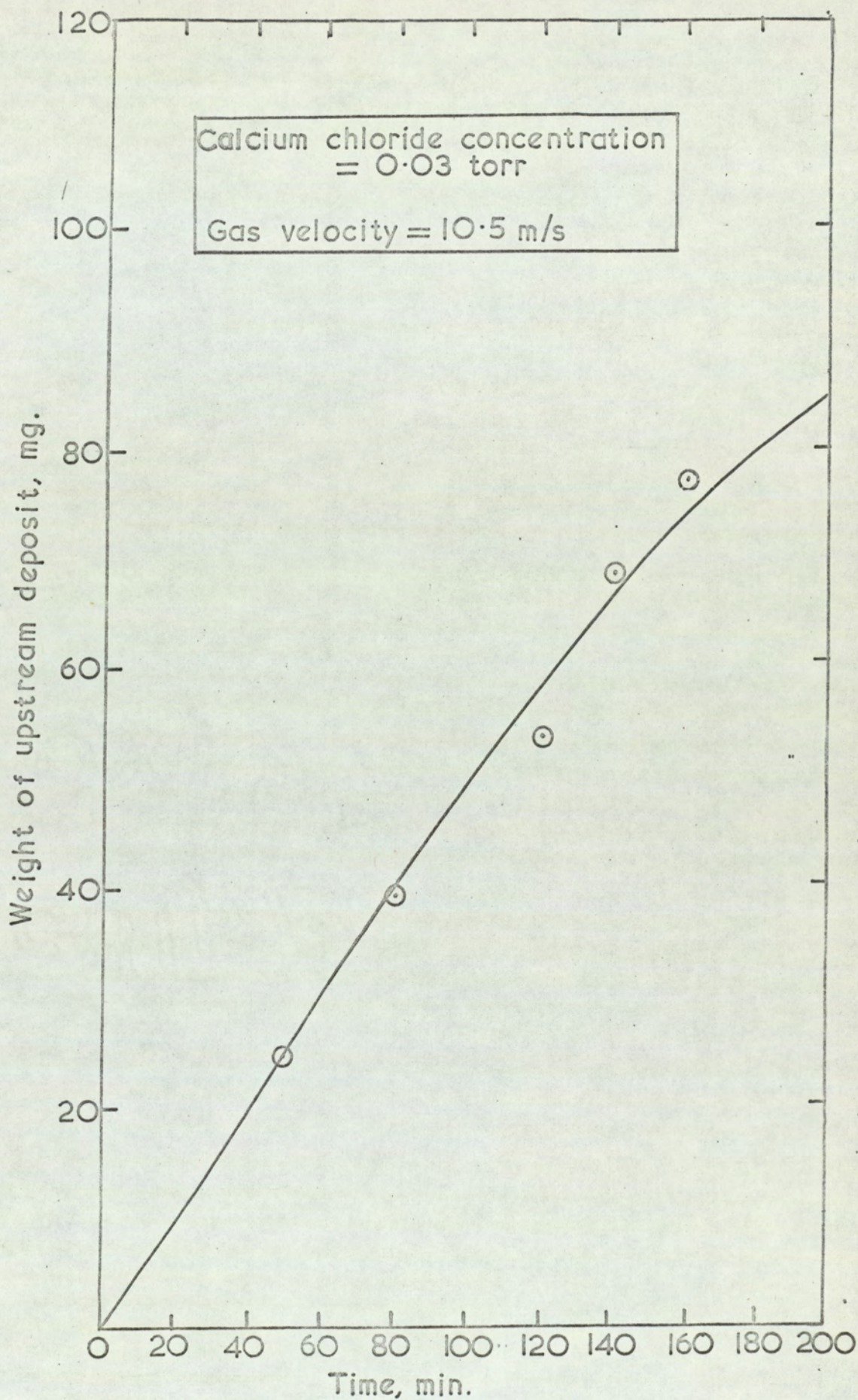


FIG.8.17 DEPENDENCE OF DEPOSIT WEIGHT UPON TIME OF EXPOSURE

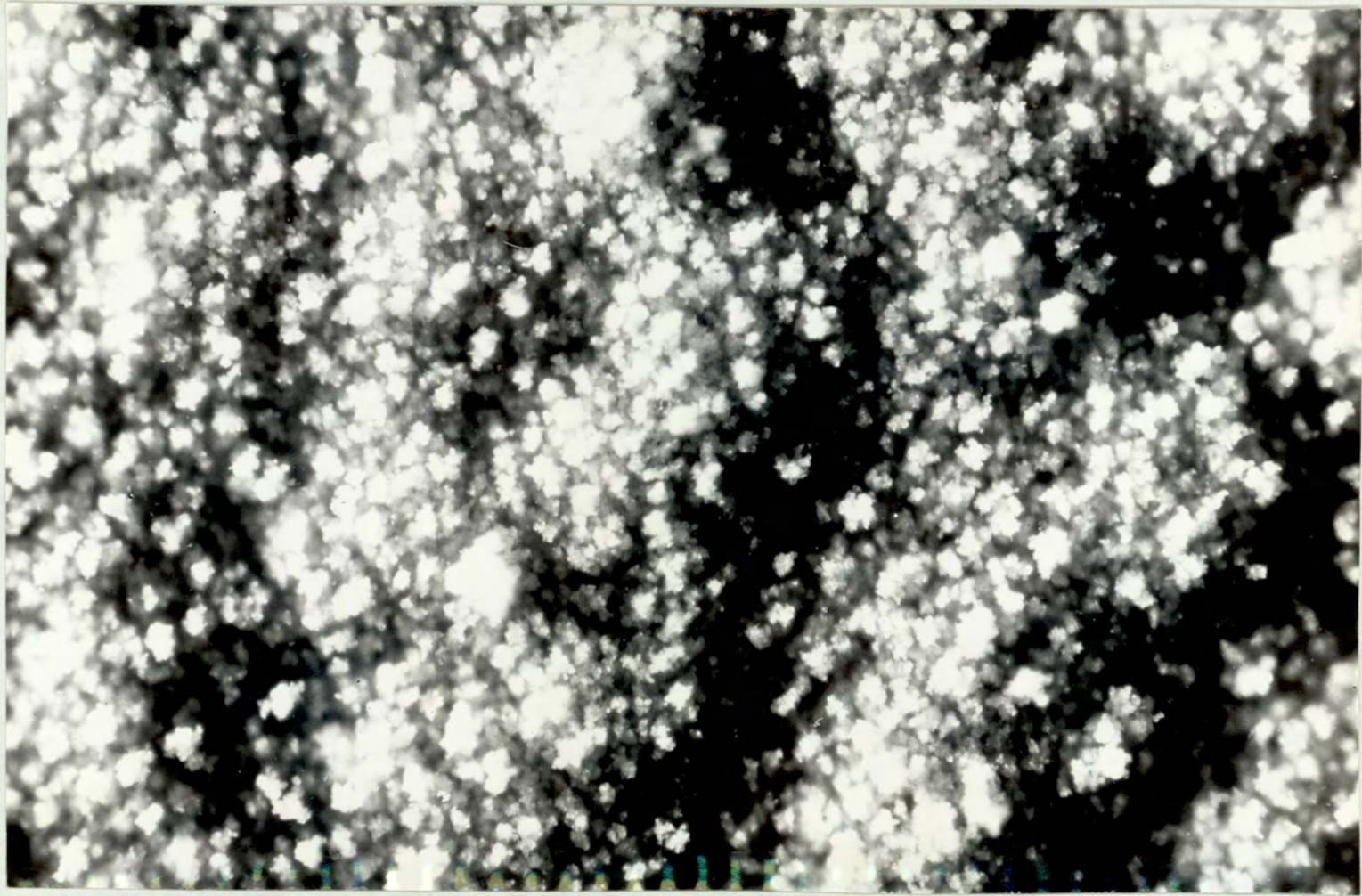


FIG. 8-18 DENDRITES OF CALCIUM CHLORIDE, PLAN VIEW (MAGNIFICATION X350)

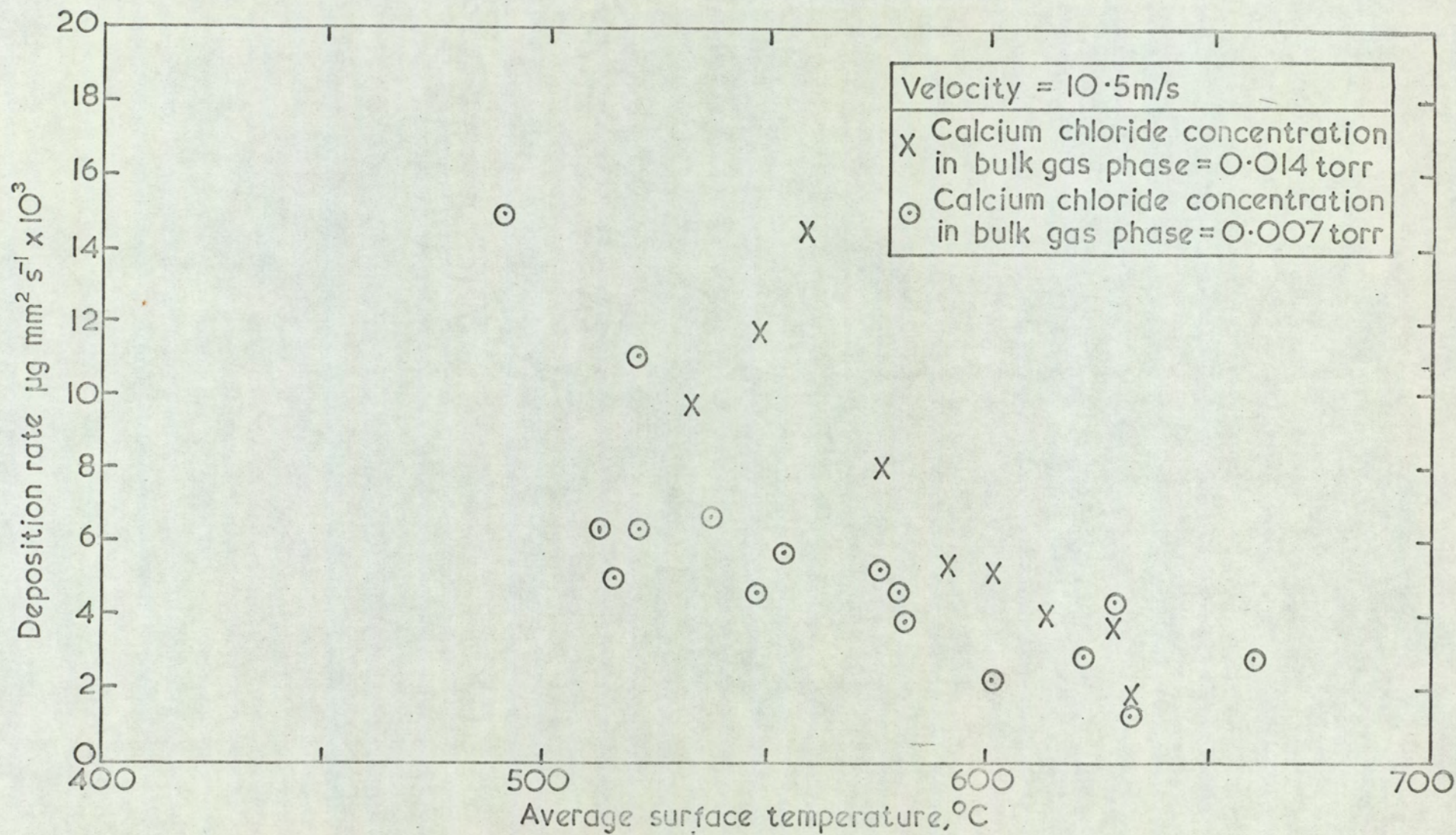


FIG. 8.19a VARIATION OF DEPOSITION RATE WITH SURFACE TEMPERATURE

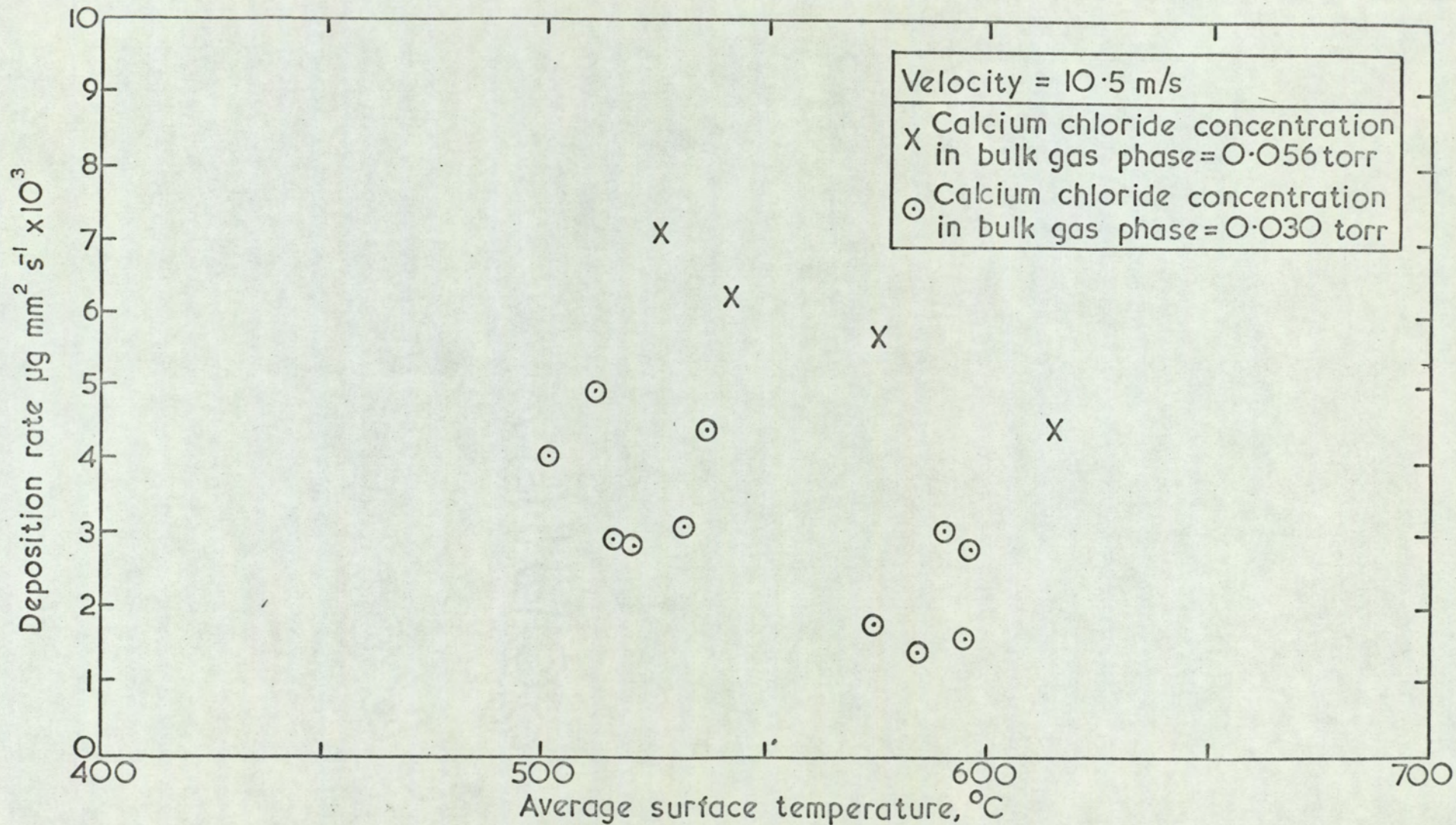


FIG. 8.19b VARIATION OF DEPOSITION RATE WITH SURFACE TEMPERATURE

Random samples of deposit were analysed for sodium and sulphate content. The results (Table 8.6) showed that the composition differed little from the A.R. sodium sulphate injected into the combustor.

Samples of the deposits, both crystalline and fused, were subjected to X-ray analysis. In all cases, it was found that Na_2SO_4 III was the only form of sodium sulphate present.

8.3 Deposition of Calcium Chloride

8.3.1 General Characteristics

As with the previous salts investigated, it was found that a weight of 100 mg of crystalline deposit could be collected on the ring before the rate of deposition began to decrease (Fig. 8.17).

Above velocities of 10.5 m/s and concentrations of 0.060 torr deposition by impaction as well as diffusion occurred. Below concentrations of 0.060 torr deposition was entirely by diffusion. At low surface temperatures (520°C) dendrites grew outwards from the upstream surface beneath the laminar boundary layer (Fig. 8.18). These dendrites were of similar form to the sodium sulphate crystals but were larger for the same weight of deposit collected. As the temperature was increased, the dendrites decreased in size until the deposit was completely fused. The fusion point was independent of concentration and occurred over the range $580^\circ\text{C} - 590^\circ\text{C}$.

Discrepancies between rates of deposition in similar runs were as high as 50%; however, even with this poor reproducibility, deposition rates decreased markedly above a temperature of 600°C (Fig. 8.19)¹ which suggested that the surface was exerting an appreciable vapour pressure above this temperature. Reference to the data of Hilderbrand & Potter

	A.R. Sodium sulphate w/w%	Typical sample of upstream deposit w/w%
Sodium	31.5	31.8
Potassium	0.2	0.0
Sulphate	66.9	67.9
Chloride	0.2	0.0

TABLE 8.6

Comparative analysis of injected salt and deposit

(1963) showed that at the concentrations of salt used, the deposit should not exert an appreciable vapour pressure until a temperature of 900°C was reached. The anomaly between these differing results was explained on analysis of the deposits which were found to be a mixture of calcium carbonate, sodium chloride and a small amount of calcium chloride. Typical chemical analysis of the anions and cations present are shown in Table 8.7. The compounds in the deposit were obtained by X-ray analysis.

Rigorous tests were then carried out to find the source of the sodium chloride. These tests were in two stages, firstly runs were made without salt injection and it was found that no salt deposit formed on the target ring. Secondly, the salts used in previous tests were injected individually in consecutive runs and each deposit was analysed. The deposits were only found to contain the injected salt. Hence it was concluded that the sodium chloride must have been released by an exchange reaction between the calcium chloride and the salt glaze which had formed on the combustor as a result of the sodium chloride tests.

1. No correction has been made for variation in concentration and velocity between runs.

Run No.	Temperature at forward Stagnation point, °C	Deposit analysis				
		%CO ₃	%H ₂ O	%Cl	%Na	%Ca
F36	620	20	13.4	17	12	34
F37	600	19	7.2	13	15	33
F38	550	25	7.1	27	12	27
F39	520	26	12.4	19	10	31

TABLE 8.7

Analysis of Deposits from Injection of Calcium Chloride
into Combustor

SECTION 9

Discussion of Results

9.1 Deposition of Sodium Chloride and Potassium Chloride

As the results obtained with these salts were similar, they will be discussed together.

9.1.1 Deposition by Impaction and Diffusion

These tests formed part of the proving trials for the combustor and were only carried out using sodium chloride. Comparison of the deposition curves for partial and complete vaporisation of the salt are depicted in Figs. 8.2 and 8.11. From these figures it can be seen that the collection by impaction which occurs under conditions of incomplete vaporisation caused deposit formation beyond the dew-point of the salt. It is thus possible for deposits of a given salt to form at surface temperatures above the condensation point as calculated from vapour diffusion theory. Under such conditions, droplets of salt impact at a rate which exceeds the rate of evaporation. In boiler practice, similar processes may account for the presence of a salt in a boiler tube deposit at high surface temperatures and hence complicate the formulation of a theory of deposition.

9.1.2 Deposition by Diffusion

The observed rates of deposition of sodium chloride and potassium chloride for the area within the laminar boundary layer were respectively 4% and 8% higher than the theoretical deposition rates in the plateau range of surface temperature. At these temperatures the deposited salt does not exert an appreciable vapour pressure. In the theoretical calculations it was assumed that vapour diffusion was the sole mechanism of transport to the surface and so the discrepancy between the

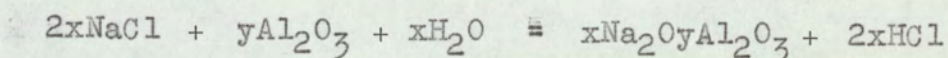
two rates could be due to thermal diffusion. It has been estimated in Appendix 5 that this second mechanism could introduce a maximum increase of 6% for sodium chloride and 9% for potassium chloride of the amount which would deposit as a result of vapour diffusion only.

As the surface temperature was raised, the vapour pressure exerted by the surface deposit became greater, hence the driving force for mass transfer and the theoretical deposition rate decreased. The vapour pressure exerted by the surface deposit was calculated using previous workers data of vapour pressure of the salt as a function of temperature. Zimm & Mayer (1944) measured the vapour pressure of sodium chloride 'in vacuo' as a function of temperature while a second set of data obtained by Jackson & Duffin (1963) in the presence of water appeared to show that the effective vapour pressure of the salt was increased. As the water vapour content of the present system is approximately the same as in Jackson & Duffin's system, it might be expected that the experimental results would be closer to the theoretical curve calculated using their data. However it was found that the results were closer to the theoretical curve calculated using Zimm & Mayer's data. It was also found that the experimental results with potassium chloride were in good agreement with the theoretical curve which made use of vapour pressure data measured 'in vacuo' (Wartenberg & Albrecht 1921). There were no data for the vapour pressure exerted by potassium chloride in the presence of water vapour. Jackson & Duffin (1963) explained the differing vapour pressure results between a system 'in vacuo' and one containing moisture by postulating that the water vapour reacts with sodium chloride to form

sodium hydroxide. However, as in the present system, there is reasonable agreement between experimental and theoretical results using the data of Zimm & Mayer (1944), this reaction does not seem to occur.

A more detailed comparison between the two systems reveals an alternative explanation for the discrepancy. Jackson & Duffin (1963) measured the vapour pressure exerted by sodium chloride in a similar system to the current one. The salt was evaporated from a platinum crucible in the hottest part of the combustion chamber and the concentration of it was varied by adjusting the temperature of the crucible, and determined from its loss in weight. The sodium chloride was condensed onto a platinum/rhodium target tube, the temperature of which was controlled by cooling air as in the present system. The Reynolds number of the flow based on tube diameter was only 21 so the temperature around the tube was uniform; this, together with the fact that there was a slight temperature gradient along the tube, meant that the dew-point line appeared circumferentially around the ring. The temperature at this point was estimated by interpolation between measured values. The dew-point experiments were carried out with atmospheres of nitrogen, the nitrogen containing 8% v/v water vapour and flue gas from the combustion of both benzene and propane. The results from the three series of experiments with water vapour present were similar, and differed from the results 'in vacuo'. Jackson & Duffin (1963) concluded that there was a reaction between the sodium chloride and water vapour on the platinum/rhodium tube surface and the resultant hydroxide evaporated immediately. Since no sodium hydroxide was analysed in the deposits, a more likely

explanation is that a reaction occurred between the sodium chloride, the water vapour and the lining of their combustor which was alumina, resulting in the formation of sodium aluminate. Clews (1925) found that this reaction occurs at an appreciable rate above a temperature of 830°C according to the equation:-



At $1,000^{\circ}\text{C}$ it was found that 99% of the chloride was converted after passing moist air over a mixture of equal weights of sodium chloride and alumina for 5 hours. The lining of the present combustor is a complex mixture of alumino-silicates which will contain a certain amount of free silica. This silica will react with both sodium chloride and potassium chloride forming sodium silicate and potassium silicate respectively. However, Clews & Thompson (1922) found that the reaction for sodium chloride was extremely slow as only 18.7% of the salt in a mixture of equal weights of sodium chloride and silica was converted to the silicate after 36 hours in a moist gas stream at $1,000^{\circ}\text{C}$.

The reaction between the alumina combustor walls and the sodium chloride also explains why the experimental results of Jackson & Duffin (1963) were 30% below the theoretical deposition rate.

The rate of deposition at the rear of the tube beneath the turbulent wake was one half to one third of the rate within the laminar boundary layer when the surface deposit did not exert an appreciable vapour pressure. Therefore it can be concluded that as more deposition occurs on the area beneath the laminar boundary layer so corrosion will be greater in that region. This phenomena has been observed in boilers

and an example of a cross-section through a corroded boiler tube from a front row of a tube bank is shown in Fig. 2.2. However, theoretically it was to be expected that the mass transfer rate would be similar to that under the laminar boundary layer because at the order of Reynolds number used, the heat transfer around the target tube is approximately uniform, and, as mass transfer rates were low, the heat and mass transfer should be analogous. An explanation for the discrepancy is that nucleation of the diffusing salt vapour will begin before it reaches the surface of the target tube because the temperature gradient across the turbulent wake will be considerably smaller than across the laminar boundary layer. Therefore the diffusivity of the vapour will decrease and, consequently, the mass transfer rate will be less.

In the area beneath the laminar boundary layer it is concluded that nucleation begins on the surface of the tube as there is good agreement between experimental and theoretical results.

9.1.3 Physical Characteristics of Deposited Salt

The fused appearance of the deposits of sodium chloride and potassium chloride collected at temperatures up to 190°C and 212°C respectively, below the melting points of the salts, is of particular interest. The presence of a molten phase, although transient, on a boiler tube would increase both corrosion and the cementing of particles together (bridging). Microscopic examination and X-ray diffraction analysis showed that such deposits after cooling were crystalline. As the temperatures at which this supercooling effect occurred were well below the melting points of the salt, and as there were no visible flow marks around the ring, persistence of a molten

phase was unlikely. Hence it can be concluded that the supercooled matter deposits in a molten form and then proceeds to crystallise from the melt.

Nucleation of solid salt from either the vapour or liquid phase occurs at a temperature which is at or below the melting point of the salt. The latter case is referred to as supercooling. Nucleation can be considered as homogeneous because the concentration of salt in the vapour phase is so low that the bulk material is effectively divided into minute samples, so any foreign matter which could act as a catalytic nuclei will be confined to a small fraction of the vapour.

Rapid cooling delays the spontaneous appearance of a condensed phase until a critical temperature, known as the freezing threshold, is reached (Buckle & Ubbelohde 1960). The interval between the threshold temperature and the normal melting point decreases as the rate of cooling is decreased. The nature of the condensed phase is also influenced by the rate of cooling. Thus, whereas a low to moderate rate of cooling allows salt to condense in the sequence, vapour/liquid/solid, a rapid rate can induce a direct vapour/solid transition (desublimation). Buckle & Ubbelohde (1960) observed that with initial and final cooling rates of $50,000^{\circ}\text{Cs}^{-1}$ and $600^{\circ}\text{Cs}^{-1}$ respectively, crystals of sodium chloride and potassium chloride did not form until 632°C and 601°C respectively. These temperatures were considered to be the freezing threshold temperature of the two salts. In the current tests, the transition from a fully crystalline to a fully fused deposit occurred over the temperature range $610^{\circ}\text{C} - 640^{\circ}\text{C}$ for sodium chloride, and $560^{\circ}\text{C} - 585^{\circ}\text{C}$ for

potassium chloride. Although the environment for condensation was more dynamic involving velocities of between 10 m/s and 30 m/s these temperatures agree approximately with the threshold temperatures observed by Buckle & Ubbelohde (1960). The average cooling rate in the present system was approximately $23,000^{\circ}\text{Cs}^{-1}$ which is similar to that in Buckle & Ubbelohde's experiments, if a linear gradient is assumed (see Table 9.1).

Jackson & Duffin (1963) did not observe a supercooling effect when studying the condensation of sodium chloride onto a cooled tube. A comparison between the flow conditions of Jackson & Duffin's tests and the present ones (Table 9.1) shows that the cooling rate in the neighbourhood of their target tube was only $500^{\circ}\text{Cs}^{-1}$. So it appears there is a critical cooling rate between $500^{\circ}\text{Cs}^{-1}$ and $23,000^{\circ}\text{Cs}^{-1}$ at which supercooling of the salts begin.

At temperatures below the lower limit of supercooling the degree of supersaturation is high and desublimation occurs to give a similar dendritic deposit for both salts (Figs. 8.4 and 8.9). The dendrites of potassium chloride, however, seemed to be larger. With increasing temperature the degree of supersaturation decreases and supercooling begins to become significant at temperatures which are associated with the formation of elongate crystals (Figs. 8.5 and 8.10).

The elongate crystals of sodium chloride were smaller and grew more uniformly than those of potassium chloride. Signs of dendritic growth were always visible among the elongate crystals of potassium chloride.

Elongate crystals of sodium chloride have been grown by Turchanyi, Horvath & Tarjan (1963) at low supersaturations of the salt. They explained this crystal growth in terms of an

	Gas Velocity m/s	Tube diameter cm	Reynolds number (based on tube diameter)	Conductance, $\text{g cm}^{-2}\text{s}^{-1}$	Thickness of boundary layer at an angle of 60° from the forward stagnation point, mm.	Cooling rate, deg. C s^{-1}
Work of Jackson & Duffin (1963)	0.3	1.0	21	2.6×10^{-4}	7	500
Present Work	(1) 10.5	5.1	3,700	3.4×10^{-3}	2	(4) 23,000

- (1) A low velocity is used for this comparison in order to give the lowest rate of cooling.
- (2) Calculated from the heat transfer correlation $N_{Nu} = 0.821 (N_{Re})^{0.385}$ (McAdams 1954b).
- (3) As the Reynolds number is low, the pressure distribution will be almost constant around the target tube and the thickness of boundary layer can be calculated from the standard formula for a laminar boundary above a flat plate.
- (4) Calculated by multiplying the average salt velocity through the boundary layer by the cooling rate in terms of distance across the layer at a surface temperature when supercooling started to occur. A linear temperature gradient was assumed in calculating the cooling rate.

TABLE 9.1

Comparison with the Results of Jackson & Duffin

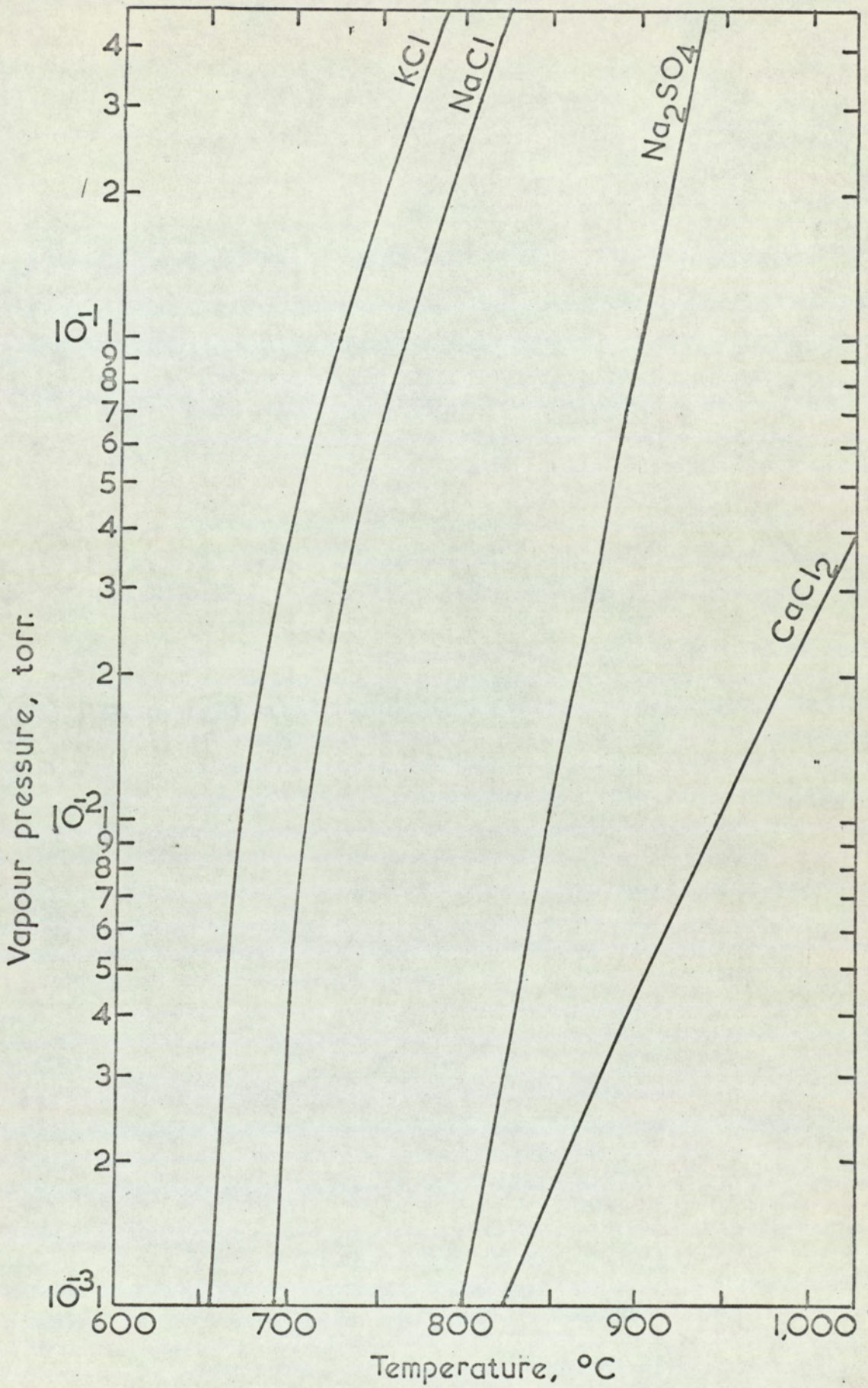


FIG. 9.1 VAPOUR PRESSURE OF THE FOUR SALTS INVESTIGATED AS A FUNCTION OF TEMPERATURE

axial screw dislocation which emerges as a growth step in the growing crystal face.

9.2 Deposition of Sodium Sulphate

9.2.1 Difficulties of Vaporisation

Sodium sulphate was found to be much more difficult to vaporise than either sodium chloride or potassium chloride. An indication of this difficulty can be obtained from Fig. 9.1 which compares the vapour pressure/temperature relationships of the four salts - sodium chloride, potassium chloride, sodium sulphate and calcium chloride.

At the lowest velocity possible in the combustor, namely 10.5 m/s, and concentrations of sodium sulphate vapour above 0.100 torr, noticeable impaction occurred. Below this value of concentration an even deposit formed containing no crystals greater than 10 microns, which suggested that the salt was fully vaporised and therefore vapour diffusion and thermal diffusion were the only mechanisms of collection. However the rate of deposition was found to increase proportionally upon a decrease of the concentration when the surface deposit did not exert an appreciable vapour pressure until the level of 0.011 torr was reached. On further reduction of the concentration level, it was found that the deposition rate was proportional to the concentration gradient. Therefore it can be concluded that between concentrations of 0.100 torr and 0.011 torr, particles of sodium sulphate smaller than 10 microns exist in the flue gas and transfer to the surface by particle diffusion. As the resistance of small particles is far greater than that of vapours, the rates of deposition by particle diffusion will be less than by vapour diffusion.

9.2.2 Deposition by Diffusion

For the area within the laminar boundary layer on the front of the tube at surface temperatures at which the salt exerted a negligible vapour pressure the deposition rates were, on average, 30% higher than the theoretical deposition rates. It was calculated in Appendix 5 that the maximum discrepancy introduced by thermal diffusion would be only 11%. The remaining difference of 19% between theoretical and experimental results could be accounted for by the errors in evaluating the density of sodium sulphate at its boiling point which involved extrapolation from only five experimental points. The boiling point density of sodium sulphate is required in the calculation of the diffusivity of the salt.

At average surface temperatures above 720°C , the vapour pressure exerted by the deposited salt became increasingly significant, and the theoretical curve of deposition rate descended. The experimentally observed values followed a similar pattern to the theoretical curve. However as only a few points were obtained due to the high temperature of the surface, a close comparison cannot be made. The observed condensation points were in good agreement to the values found using the vapour pressure data of Halstead (1967) which was measured 'in vacuo'.

The rate of deposition at the rear of the tube beneath the turbulent wake was only a fifth of the upstream deposition when the salt was fully vaporised. This ratio was greater than was observed with either sodium chloride or potassium chloride, and suggests that the salt was nucleating further from the tube surface.

9.2.3 Physical Characteristics of Deposited Salt

As with the two previous salts investigated the fused

appearance of deposits, collected at temperatures up to 350°C below the melting point of the salt, was the main interest. Microscopic examination and X-ray diffraction again showed that the deposits after cooling were crystalline.

The main difference between the supercooling of sodium sulphate, sodium chloride and potassium chloride was the dependence on concentration even when the salt was fully vaporised. Therefore the nucleation of sodium sulphate vapour appears to be a function of concentration as well as rate of cooling. Whether the dependence upon concentration is because of heterogeneous nucleation due to impurities in the system is impossible to discern.

At temperatures below the lower limit of supercooling desublimation occurred to give a dendritic crystal growth. These dendrites were not as well defined as the dendrites of sodium chloride and potassium chloride which is possibly due to the transition from one form of sodium sulphate to another on cooling the deposit. Five forms of sodium sulphate are known to exist (Table 9.2); the deposits being entirely composed of type III. Hence it is postulated that on initial deposition, sodium sulphate I or II was formed and both being unstable transformed to sodium sulphate III on cooling. Small, Strawson & Lewis (1963) also found that sodium sulphate III appeared in a deposit which was formed from the vapour phase and subsequently cooled.

9.3 Calcium Chloride

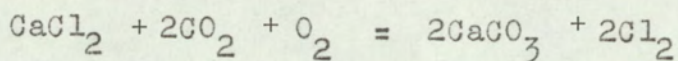
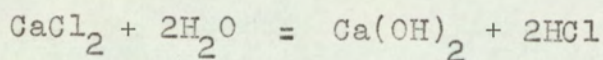
Previous experimenters have shown that at temperatures above 700°C calcium chloride will react at an appreciable rate with both water vapour (Robinson, Smith & Briscoe 1926) and carbon dioxide (Mellor 1923) according to the reactions:-

Decreasing temperature	High temperature form (stable above 141°C)	Na_2SO_4 - I
	Unstable	Na_2SO_4 - II
	Metastable at room temperature	Na_2SO_4 - III
	Unstable	Na_2SO_4 - IV
	Low temperature form (stable at room temperature)	Na_2SO_4 - V

The phase changes occur over the small range of temperature 190°C - 240°C and the proximity of the transition temperatures and associated hysteresis effects have made it difficult to measure the actual transition temperatures.

TABLE 9.2

The Crystalline Forms of Sodium Sulphate



As there is a high percentage of carbon dioxide in the flue gas from the combustion of propane, the second reaction explains why calcium carbonate was found in the deposit. The reason for the absence of calcium hydroxide in the deposit is that its vapour pressure in the main gas stream was too low for condensation to occur at tube temperatures above 530°C . At the highest concentration of calcium chloride used, 0.060 torr, if 50% of the salt was converted to the hydroxide, a surface temperature of less than 530°C would be necessary for the calcium hydroxide to condense onto the tube.

It is proposed that the occurrence of sodium chloride in the deposits is due to the reaction between the calcium chloride and the slight salt glaze of sodium silicate which was present on the combustor walls. The salt glaze appeared during the sodium chloride test runs over a period of several weeks.

At low surface temperatures the growth of the deposit was dendritic. As with sodium sulphate, the dendrites were not well defined, which was most likely due to a mixture of compounds being present. As the surface temperature was raised the crystals gradually became smaller until above a temperature of 590°C , the deposit was fully fused. This fusion temperature would be dependent on the eutectic reaction between the calcium carbonate and sodium chloride as well as the freezing threshold temperatures of both compounds.

SECTION 10Conclusions

The specific conclusions drawn from this work can be summarised as follows :-

(1) Under conditions normally prevailing, a laminar boundary layer will be formed in the front row of a boiler tube bank.

(2) In the region within the laminar boundary layer the deposition rates of sodium chloride and potassium chloride are proportional to:

(a) The concentration difference of the salt vapour between the bulk gas stream and the tube surface.

The concentration difference is only dependent upon surface temperature at values at which the deposits exert an appreciable vapour pressure.

(b) The square root of the main gas stream velocity.

(3) The deposition rate of fully vaporised sodium sulphate within the laminar boundary layer is proportional to the concentration difference of the vapour between the bulk gas stream and tube surface. The concentration difference is again only dependent upon the surface temperatures at values at which the deposits exert an appreciable vapour pressure.

It can be inferred that the deposition rate is also proportional to the square root of the main stream velocity, but this could not be verified over a range of velocities due to experimental difficulties in vaporising the salt.

(4) Theoretical calculations using a heat/mass transfer analogy adequately predicted the experimental results of sodium chloride and potassium chloride and the agreement may be improved by estimating the effect of thermal diffusion.

Similar theoretical calculations for sodium sulphate

which included the effect of thermal diffusion, gave values of deposition rates which were 19% below the experimentally observed results. It is concluded that the discrepancy is due to the paucity of experimental data required to calculate the density of sodium sulphate.

- (5) Failure to vaporise the injected sodium chloride completely led to deposition at temperatures beyond the condensation point. This is because material will deposit onto the tube by inertial impaction at a faster rate than at which it will evaporate from the surface.
- (6) Fused deposits of sodium chloride, potassium chloride and sodium sulphate were found at temperatures of 190°C , 212°C and 350°C respectively below their normal melting points.
- (7) The fusion points of sodium chloride and potassium chloride are dependent only upon the rate of cooling while the fusion point of sodium sulphate is also dependent upon the concentration of vapour in the bulk gas stream. The dependence upon concentration could be due to nucleation of sodium sulphate vapour being affected more by any impurities in the system (heterogeneous nucleation) than with the other two salts.
- (8) Theoretical calculations indicate that the vapour pressure observed 'in vacuo' gives a best prediction of deposition rate.
- (9) The dendritic crystals of sodium chloride, potassium chloride and sodium sulphate, and the elongate crystals of sodium chloride and potassium chloride are formed by desublimation, while the fused deposits of all three salts are formed in the sequence vapour/liquid/solid.
- (10) The deposition rates of sodium chloride, potassium

chloride and sodium sulphate in the turbulent wake are less than in the region beneath the laminar boundary layer, which explains why less corrosion occurs on the rear part of a boiler tube.

(11) A heat/mass transfer analogy cannot be used in predicting the rates of deposition in the turbulent wake because of nucleation of the salt before the tube surface.

(12) Calcium chloride reacts appreciably with carbon dioxide and water vapour at a temperature of 1000°C , forming calcium carbonate and calcium hydroxide respectively. Due to these reactions, calcium chloride is not important in the corrosion of boiler tubes or in causing deposit build up on them.

From these twelve specific conclusions, three general ones can be made regarding the corrosive and bridging characteristics, in particular of high alkali content coals, as follows :-

(1) The rate of boiler tube corrosion will increase as the transfer of alkalis to the tube surface increases. The mass transfer rate will be greater on areas beneath a laminar boundary layer than beneath a turbulent wake.

(2) The appearance of fused deposits at temperatures well below the dew point of the salt will lead to larger corrosion rates than expected at low tube surface temperatures.

(3) The onset of fusion will increase the rate of bridging between boiler tubes by cementing the fly-ash particles together with resultant loss of heat transfer and increase in the pressure drop across the tube bank.

REFERENCES

- Albrecht, F. (1931), *Physikalische Zeitschrift*, 32, 48.
- Abernathy, R. F., Gibson, F. H., and Frederic, W. H., (1965), U.S. Bur. of Mines, Rep. 6579.
- Anderson, G. H., and Diehl, E. K., (1955), A.S.M.E. Preprint 55-A-200.
- Arthur, J. R., and Wadsworth, K. D., (1950), *Progress in Coal Science*, ed. D. H. Bangham, 1, 396, Butterworths.
- Barnhart, D. H. and Williams, P. C., (1955), A.S.M.E. Preprint 55-A-193.
- Baron, J. R., (1958), M.I.T. NSL. TR. No. 160, 71.
- Bird, J. G., Stewart, W. E. and Lightfoot, E. N., (1960), *Transport Phenomena*, 160, J. Wiley and Sons, Inc.
- Bishop, R. J., (1966), Ph.D. Thesis, University of London.
- Bishop, R. J., (1967), Private Communication, B.C.U.R.A.
- Bishop, R. J., Gliffe, K. R. and Langford, T. H., (1967), Private Communication, B.C.U.R.A.
- Bishop, R. J., Cutler, E. and Valance, A., (1963), Private Communication, B.C.U.R.A.
- Boll, R. H. and Patel, H. G., (1960), A.S.M.E. Paper No. 60-WA-182.
- Boulton, G. and Taylor, J.J., (1963), *J. Inst. Fuel*, 36, 463.
- Brinkley, S. R., (1947), *J. of Chem. Phys.*, 15, (2).
- Brown, T. D., (1966), Ph.D. Thesis, University of Sheffield.
- Buckle, H. R. and Ubbelohde, A. R., (1960), *Proc. Roy. Soc.A.*, 259, 325.
- Carlile, J. H., (1952), *J. Inst. Fuel*, 25, 256.
- Chapman, S., (1912), *Philos. Trans. A.* 211.
- Chapman, S., (1962), *Progress in International Research on Thermodynamics and Transport*, 24, New York.
- Chapman, S. and Cowling, T. G., (1952), *The Mathematical Theory of Non-Uniform Gases*, 1-431, Cambridge.
- Chapman, S. and Mason, E. A., (1962), *J. of Chem. Phys.*, 36, 627.
- Chen, C. Y., (1955), *Chem. Rev.*, 55, 595.
- Clews, J. L., (1925), *J.C.S.*, 126, 735.

- Clews, J. L. and Thompson, G., (1922), J.C.S., 122, 1142.
- Cliffe, K. R., (1967), Unpublished Work, B.C.U.R.A.
- Comings, E. W., Clapp, J. T. and Taylor, J. F., (1948),
Ind. Eng. Chem., 40, 1076.
- Crone, H. G., (1945), Coal Research, B.C.U.R.A., 86.
- Crossley, H. E., (1948), Trans. Inst. Chem. Eng., 26, 131.
- Crossley, H. E., (1952), J. Inst. Fuel, 25, 224.
- Crossley, H. E., (1955), A.S.M.E. paper 55-A-153.
- Crossley, H. E., (1963), J. Inst. Fuel, 36, 228.
- Crumley, P. H., Fletcher, A. W. and Wilson, D. S., (1955),
J. Inst. Fuel, 28, 117.
- Crumley, P. H. and McCamely, W. (1958), Proc. of the
Conference on Science in the Use of Coal, Inst. of
Fuel, Paper 32.
- C.S.I.R.O., (1966), Coal Res. in C.S.I.R.O., 28, Feb., 11.
- Cutler, E., (1963), Private Communication, B.C.U.R.A.
- Daybell, G. N., (1967), J. Inst. Fuel, 40, 3.
- Douglas, W. J. M., and Churchill, S. W., (1958), C.E.P.
Symposium Ser. No. 18, 52, 23.
- Durie, R. A., (1963), Fuel (London), 40, 407.
- Edwards, A. M., Jackson, P. J. and Howes, L. S., (1962),
J. Inst. Fuel., 35, 121.
- Einstein, A., (1905), Ann. Phys. Lpz., 17, 549.
- Enskog, D., (1911), Phys. Z., 12, 56.
- Epstein, P. S., (1924), Phys. Rev., 23, 710.
- Epstein, P. S., (1927), Z. Physik., 27, 1.
- Evans, H. L., (1961), Int. J. Heat Mass Transfer, 3, 321.
- Fells, I. and Harker, J. H., (1967), J. Inst. Fuel, 40, 477.
- Gabler, H., (1963), Brennot-Warme-Kraft, 15, 431.
- Galloway, T. R. and Sage, B. H., (1967), A.I.Ch.E.Jl., 13,
(3), 563.
- Geidt, W. H., (1951), J. Aero. Sci. 18, 725.
- Gluskter, H. J. and Rees, O. W., (1964), Ill. Geol. Surv.
Circ., 372.

- Goldberg, S. A., Gallagher, J. J. and Orning, A. A., (1967),
Trans. A.S.M.E., 90 ser. A (2), 193.
- Green, H. L. and Lane, W. R., (1964), Particulate Clouds,
E. and F. N. Spon.
- Grew, K. E., (1944), Phil. Mag. 35 (7), 30.
- Griffith, E. and Awberry, J. H., (1933), Proc. Inst. Mech.
Engrs., 125, 319.
- Haase, H., (1962), Chemie-Ingr-Tech., 34, 632.
- Halstead, W. D., (1967), C.E.R.L. Report RD/L/N73.
- Hegge Zijnen, B. G., (1958), Appli. Sci. Res. Section A, 7, 149.
- Hilderbrand, D. L. and Potter, N. D., (1963), J. Phys. Chem.,
67, 223.
- Hilpert, R., (1933), Forsch. Ing. Wes., 4, 215.
- Hirschfelder, J., Curtiss, F. and Bird, B., (1954),
Molecular Theory of Gases and Liquids, Wiley and Sons,
New York.
- Jackson, P. J. and Duffin, H. G., (1963), C.E.G.B. Conf.,
Mechanism of Corrosion by Fuel Impurities, 427,
Butterworths.
- Jackson, P. J. and Ward, J. M., (1956), J. Inst. Fuel, 29, 446.
- Jonakin, J., Rice, G. A. and Reese, J. T., (1959), A.S.M.E.
Paper 59-Fu-5.
- Kestin, J., Maeder, P. F. and Wang, O., (1961), Int. J. Heat
Mass Transfer, 3, 133.
- Kestin, J., Maeder, P. F. and Sogin, H. H., (1961),
J. Appli. Math. Phys., 12, 115.
- Knudsen, M. S. and Weber, S., (1911), Ann. Phys. Lpz., 36, 982.
- Knudsen, J. G. and Katz, P. L., (1958a), Fluid Dynamics and
Heat Transfer, 500, McGraw-Hill.
- Knudsen, J. G. and Katz, P. L. (1958b), Fluid Dynamics and
Heat Transfer, 248, McGraw-Hill.
- Langmuir, I., (1942), O.S.R.D. Rep. No. 940, Washington D.C.:
Office of Technical Services.
- Langmuir, I. and Blodgett, K. B., (1944), G.E.C. Lab.
Rep. R. L. 225, Schenectady.
- Lin, C. C., (1957), Proc. 9th Intern. Congress Appl. Mech.,
Brussels, 4, 155.
- McAdams, W. H., (1954a), Heat Transmission, 272, McGraw-Hill.

- McAdams, W. H., (1954b), Heat Transmission, 260, McGraw-Hill.
- McPhail, D. C., (1944), R. and M., 2437.
- Marskell, W. G. and Miller, J. M., (1956), J. Inst. Fuel, 29, 380.
- Mason, E. A., (1957), J. of Chem. Phys. Part I, 27, 75.
Part II, 27, 782.
- Maltauch, J. (1925), Z. Phys., 32, 439.
- Mellor, J. W., (1923), A Comprehensive Treatise of Inorganic and Theoretical Chemistry, 3, 714, Longmans.
- Millikan, R. A., (1923a), Phys. Rev., 21, 217.
- Millikan, R. A., (1923b), Phys. Rev., 21, 1.
- Min, K., Chao, B. T. and Wyman, M. E., (1963), Rev. Scient. Inst., 34, 529.
- Monch, G., (1923), Phys. Z, 34, 77.
- Nelson, W. and Cain, C., (1959), A.S.M.E. Preprint 59-A-89.
- Ounstead, D., (1958), J. Inst. Fuel, 31, 474.
- Pankhurst, R. C. and Holder, D. W., (1953), Wind Tunnel Technique, 86, Sir Isaac Pitman and Sons Ltd.,
- Pereles, E. G., (1958), Res. Rep., S.M.R.E. No. 144.
- Perkins, H. C. and Leppert, G., (1964), Int. J. Heat Mass Transfer, 7, 143.
- Pope, A., (1954), Wind Tunnel Testing, 46, New York.
- Proctor, N. A. A. and Taylor, G. H., (1966), J. Inst. Fuel, 39, 284.
- Ranz, W. E. and Wong, J. B., (1952), Ind. Eng. Chem., 44, 1371.
- Raynor, D., (1964), R. A. E. Maths. Computing Note Series C, 327.
- Robinson, W., Han, S. L., Essig, R. H. and Heddleson, C. F., (1951), Ohio State University Research Foundation, Report 41.
- Robinson, P. L., Smith, H. C. and Briscoe, H. V. A., (1926), J.C.S., 129, 836.
- Rosenblatt, P. and La Mer, V. K., (1946), Phys. Rev., 70, 385.
- Samms, J. A. C., and Watt, J. D., (1966), B.C.U.R.A., Monthly Bull., 30 (7), 232.
- Saxton, R. L. and Ranz, W. E., (1952), Jnl. Appl. Phys., 23, 917.

- Schlichting, H., (1960), Boundary Layer Theory, 330, McGraw-Hill.
- Schmidt, K., (1959), Staub, 19, 416.
- Schmidt, E. and Wenner, K., (1947), N.A.C.A. Tech. Mem., 1147.
- Seban, R. A., (1960), Trans. A.S.M.E., 82 ser. C, 101.
- Sell, W., (1935), V.D.I. - Forsch - H., 347.
- Sherwood, J. and Woertz, A. L., (1939), A.I.Ch.E., J1., 35, 1034.
- Shotter, J., (1965), Private Communication, B.C.U.R.A.
- Shuttleworth, A., (1964), Ph.D. Thesis, University of Sheffield.
- Small, N. J. H., Strawson, H. and Lewis, A., (1963), C.E.G.B. Conf. Mechanism of Corrosion by Fuel Impurities, 238, Butterworths.
- Sogin, H. H. and Subramanian, V. S., (1961), Trans. A.S.M.E. 83, ser. C, 483.
- Spalding, D. B., (1951), Ph.D. Thesis, University of Cambridge.
- Spalding, D. B., (1960), Int. J. Heat Mass Transfer, 1, 192.
- Spalding, D. B., (1961), Int. J. Heat Mass Transfer, 2, 15.
- Spalding, D. B. and Evans, H. L., (1961), Int. J. Heat Mass Transfer, 2, 314.
- Spalding, D. B. and Chi, S. W., (1963), Int. J. Heat Mass Transfer, 6, 263.
- Spalding, D. B. and Patanker, S. V., (1967), Heat and Mass Transfer in Boundary Layers, Morgan-Grampian.
- Squire, H. B., (1938), Modern Developments in Fluid Dynamics, 2, Oxford University Press.
- Stairmand, C. J., (1950), Trans. Instn. Chem. Engrs., 28, 130.
- Sykes, C. and Shirley, H. T., (1952), Iron and Steel Institute Special Report No. 43, 153.
- Talmor, E., (1966), A.I.Ch.E.J1., 12, 1092.
- Taylor, G.I., (1940), N.G.T.E., Memo No. R.M. 2024.
- Thorne, D. J. and Watt, J. D., (1962), B.C.U.R.A., I.C. No. 265.
- Turchanyi, Gy., Horvath, T. and Tarjan I., (1963), Magyar Fiz. Foly., 11, 197.
- Vliet, G. C. and Leppert, G., (1961), Trans. A.S.M.E., 83 ser. C, 163.

Waldmann, L., (1959), Zeitschrift fur Natur-Forschung, 14a, 589.

Waldmann, L., (1962), Proc. of the Second International Symposium on Rarefied Gas Dynamics, Berkely, 301, Academic Press.

Wartenberg, A. and Albrecht, K. H., (1921), Z. Elektrochemie, 27, 162.

Wilke, K. R. and Lee, C., (1955), Ind. Eng. Chem. 47, 1253.

Zapp, G. M., (1950), M. S. Thesis, Oregon State College.

Zimm, B. H. and Mayer, J. E., (1944), J. Chem. Phys. 12 (9), 362.

APPENDIX 1Calculation of the Range of Velocities
possible in the Target Section

If it is assumed that all gases passing into the combustor are initially raised to the flame temperature of $2,200^{\circ}\text{C}$, then it is possible to calculate the nett heat input into the combustor from the equation :-

$$\begin{aligned} \text{Nett heat, } i_{\text{gas}} &= \text{Heat content of propane for} \\ &\quad \text{stoichiometric combustion} \\ &\quad - \text{Heat required to raise excess air} \\ &\quad \text{to flame temperature} \end{aligned}$$

(This equation assumes perfect mixing). A.1.1

Graphs of velocity of flue gases in the target section versus nett heat input with propane feed rate and excess air as parameters are shown in Fig. A.1.1. The equations of these curves were derived as follows :-

Two basic equations can be written expressing velocity and enthalpy of the combustion gases in terms of propane feed rate and percentage excess air.

These are:-

$$u_{\infty} = a_n \left[a_j Q_{\text{Prop}} (1 + e_x) + Q_{\text{Prop}} \right] \quad \text{A.1.2}$$

(As the volume increase on the combustion of propane is only 4% it is considered as negligible).

$$i_{\text{gas}} = Q_{\text{Prop}} (a_g - a_i a_j e_x) \quad \text{A.1.3}$$

where,

i_{gas} = Nett heat content of combustion gases, W.

u_{∞} = Velocity of gases in target section, m/s.

e_x = Percentage excess air.

Q_{Prop} = Feed rate of propane, m^3/hr .

a_g = Calorific value of propane

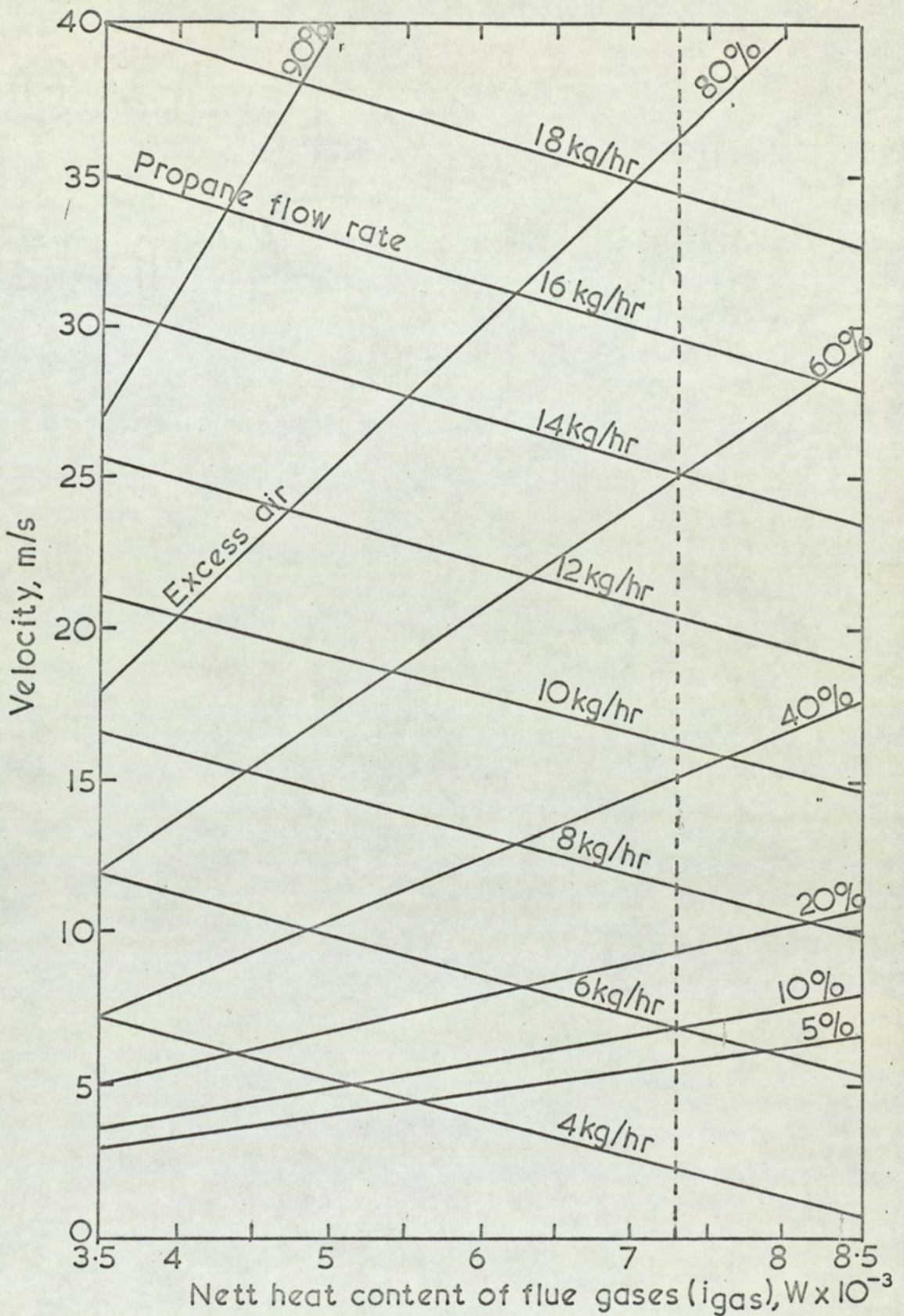


FIG. A.1.1 VELOCITY OF FLUE GASES IN THE TARGET SECTION AT 1,100°C AGAINST NETT HEAT WITH EXCESS AIR AND PROPANE FEED RATE AS PARAMETERS

$$= 9.38 \times 10^4 \text{ kJ/m}^3$$

a_h = Conversion factor for volume flow at S.T.P. to velocity in target section at 1100°C

$$= 9.3 \times 10^{-2} \text{ m}^{-2}$$

a_i = Heat content of air at 1100°C based on that at 15°C

$$= 3.34 \times 10^3 \text{ kJ/m}^3$$

a_j = Theoretical air required for combustion ($\text{m}^3_{\text{air}}/\text{m}^3$)

$$= 24$$

Feed Rate as Parameter

Substituting for e_x in Equation A.1.2

$$u_\infty = a_h a_j Q_{\text{Prop}} \left(1 - \frac{a_g Q_{\text{Prop}} - i_{\text{gas}}}{a_j a_i Q_{\text{Prop}}} + \frac{1}{a_j} \right) \quad \text{A.1.4}$$

$$= a_m Q_{\text{Prop}} - a_k i_{\text{gas}} \quad \text{A.1.5}$$

where,

$$a_k = \frac{a_h}{a_i} \\ = 2.82 \times 10^{-5} \text{ m/kJ}$$

and,

$$a_m = a_h a_i + \frac{a_g a_h}{a_i} + a_h \\ = 49 \text{ m}^{-2}$$

Excess Air as Parameter

Equation A.1.2 can be written as:-

$$u_\infty = a_h Q_{\text{Prop}} [a_j(1 + e_x) + 1] \quad \text{A.1.6}$$

Eliminating Q_{Prop} in Equations A.1.6 and A.1.3

$$i_{\text{gas}} = \frac{u_\infty (a_g - a_i a_j e_x)}{a_h [a_j(1 + e_x) + 1]} \quad \text{A.1.7}$$

As $\frac{1}{a_j}$ is small, approximately 0.05, it can be ignored.

Rearranging Equation A.1.7

$$u_\infty = i_{\text{gas}} \left(\frac{1 + e_x}{a_h - e_x a_o} \right) \quad \text{A.1.8}$$

where,

$$\begin{aligned} a_n &= \frac{a_g}{a_h a_j} \\ &= 4.21 \times 10^4 \text{ kJ/m} \end{aligned}$$

and,

$$\begin{aligned} a_o &= \frac{a_i}{a_h} \\ &= 3.56 \times 10^4 \text{ kJ/m} \end{aligned}$$

As mentioned previously, Bishop's heat input figure forms the basis of estimating the range of velocities possible. The heat input into his combustor was 7,300 W and this value is indicated in Fig. A.1.1.

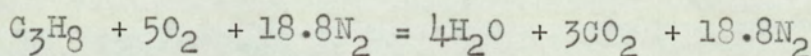
The minimum velocity was controlled by the fact that for safety a minimum oxygen content of 3% is required which corresponds to an excess air factor of 15%. From the graph it can be seen that this gives a minimum value of 8 m/s.

The maximum velocity of the flue gases is determined by the amount of propane available. From Fig. A.1.1 it can be seen that a minimum flow rate of propane of 16 kg/hr. is required so that the heat content of 7,300 W and the maximum velocity of 30 m/s are obtained. It was therefore decided to set the limit on the propane flow rate just above this at 18 kg/hr., because at a greater flow rate, storage of propane would become a problem.

APPENDIX 2Formulae for Computer Programme

The computer programme for evaluating the flow rates, oxygen content of the flue gas and the partial pressure of the salt involves a series of algebraic expressions in which values of the unknowns are obtained from the measured data. Due to the introduction of the S.I. system of units mid-way through the present project, quantities are expressed in both this and the English system.

The formulae for the programme are as follows:-

Chemical EquationCorrected Oxygen (%), dry basis

The oxygen content of the flue gas is measured by a Kent Oxygen Recorder (Section 5.1.7.3) and the value obtained is corrected for the carbon dioxide content of the flue gas and atmospheric pressure using the formulae:-

$$\text{Corrected oxygen \%} = \frac{O_2 \times 100E}{(100 + CO_2)}$$

where E is a correction factor for atmospheric pressure, defined by:-

$$\log_e E = -2 \log\left(\frac{P}{10}\right) + 2.1644$$

P = atmospheric pressure, mm.Hg

O₂ = observed oxygen (%)

CO₂ = observed carbon dioxide (%)

Calculated Oxygen (%), dry basis

$$\text{Calculated oxygen} = \frac{\text{Flow rate of oxygen in flue gas}}{\text{Flow rate of dry flue gas}} \times 100$$

As propane needs 23.8 times its own volume of air for combustion, the flow rate of excess air is ($Q_{\text{air}} - 23.8Q_{\text{Prop}}$). Oxygen is 21% v/v of air, so the flow rate of oxygen becomes:-

$$(Q_{\text{air}} - 23.8 Q_{\text{Prop}}) \times \frac{21}{100}$$

21.8 molecules of dry gas are produced when 1 molecule of propane is burned in the stoichiometric amount of air (23.8 molecules). Therefore the flow rate of dry combustion gases is:-

$$Q_{\text{Total, dry}} = Q_{\text{air}} - 2Q_{\text{Prop}}$$

Substituting in the original equation, calculated oxygen

$$= \frac{21Q_{\text{air}} - 500 Q_{\text{Prop}}}{Q_{\text{air}} - 2Q_{\text{Prop}}}$$

Propane Input

The propane feed rate is measured by a flow-rator calibrated for standard conditions, hence the measured values have to be corrected by applying the ideal gas law as follows:-

$$\frac{P_b Q_I}{T_b} = \frac{P_a}{T_a} \cdot Q_{\text{Prop}}$$

where Q_I = Indicated reading of propane flow-rate, ft³/min.

Q_{Prop} = Corrected reading of propane flow-rate, ft³/min.

P_a = Pressure at which flow-rate is calibrated,
= 421 in. wg. absolute.

P_b = Measured pressure, in. wg. absolute.

T_a = Temperature at which flow-rator is calibrated
= 278°K

T_b = Measured temperature, °K.

Therefore $Q_{\text{Prop}} (\text{Std m}^3/\text{min}) = 2.83 \times 10^2 Q_{\text{Prop}} (\text{Std ft}^3/\text{min})$.

Air Input

The air input to the burner is measured by a sharp edged orifice plate of 1.5 in. or 1 in. diameter dependent on flow rate. The actual flow rate is calculated from the formula:-

$$Q_{\text{air}} = \text{Constant} \times \left(\frac{P_c}{T_c} \Delta h \right)^{\frac{1}{2}}$$

where the constant takes into account the coefficient of discharge, the area ratio, viscosity of the air and diameter of orifice. It can be evaluated using graphs and tables given in B.S. 1042.

For the 1.5 in. diameter orifice, the constant = 216.

For the 1 in. diameter orifice, the constant = 82.2.

The other symbols in the equation are as follows:-

Q_{air} = Flow rate of air, Std ft³/min.

P_c = Measured air pressure, in. wg. absolute

T_c = Measured air temperature, °K

Δh = Water differential across orifice, in. wg.

Flow rate of air, $Q_{\text{air}}(\text{Std m}^3/\text{min}) = 2.83 \times 10^{-2} Q_{\text{air}}(\text{Std ft}^3/\text{min})$

Calculated True Velocity, wet basis

The difference between the flow of wet and dry flue gas is equal to the amount of water vapour produced from the injected salt solution and that produced as a result of the combustion of the propane.

Let the injection rate of the salt solution be Q_{solvent} ml/min. and, as 1 lb. mole of a gas occupies 378 Std ft³/min. at S.T.P. so the resultant flow of water vapour can be written:-

$$\frac{Q_{\text{solvent}} \times 378}{453.6 \times 18} = 0.0464 Q_{\text{solvent}} \text{ Std ft}^3/\text{min.}$$

The amount of water vapour produced from the combustion of propane is four times the propane input, so the resultant flow of combustion gases is:

$$Q_{\text{Total, dry}} + 4 Q_{\text{Prop}}$$

Therefore $Q_{\text{Total, wet}} = Q_{\text{Total, dry}} + 4 Q_{\text{Prop}} + 0.0464 Q_{\text{solvent}}$

where $Q_{\text{Total, wet}}$ is the total flue gas flow rate (Std ft³/min).

The velocity in the duct can be obtained by dividing the flow rate $Q_{\text{Total, wet}}$ by the cross-sectional area, taking into

account the temperature of the gas in the target section. The area of the target section is 24 in.^2 so the actual velocity in the vicinity of the target tube is:-

$$\text{True velocity (ft/s)} = 3.67 \times 10^{-4} (273 + T_{\infty}) Q_{\text{Total, wet}}$$

$$\text{True velocity (m/s)} = 1.04 \times 10^{-5} (273 + T_{\infty}) Q_{\text{Total, wet}}$$

where T_{∞} is the main stream gas temperature in the neighbourhood of the target tube.

Salt Input

The mass flow rate of the salt (g/min) = $0.001 \cdot Q_{\text{solvent}} C$
where C = Concentration of solution (g.salt/litre).

Therefore the volume flow rate,

$$Q_{\text{salt}} (\text{Std ft}^3/\text{min}) = \frac{378 \times 0.001 \cdot Q_{\text{solvent}} \times C}{453.6 \times M_{\text{salt}}}$$

where M_{salt} is the molecular weight of the salt

Volume flow rate of the salt (Std m^3/min) = 2.83×10^{-2}

Q_{salt} (Std ft^3/min).

Calculated Volume Fraction of Salt Vapour in Wet Flue Gases

$$V_{\text{salt}} = \frac{Q_{\text{salt}}}{Q_{\text{Total, wet}}}$$

Calculated Partial Pressure of Salt Vapour in Flue Gases (Torr)

As 1 atmosphere is 760 mm.

$$P_{\text{salt}} = 760 V_{\text{salt}}$$

APPENDIX 3Method for Calculating the Dimensions of the
Laminar Boundary Layer

Spalding (1961) derived the following differential equation expressing the rate of boundary layer growth:-

$$u_g^x \frac{d \delta_b^x}{dx^x} = F_b \left(\delta_b^x \frac{du_g^x}{dx^x}, v_o^x \delta_b^x \right) \quad A.3.1$$

where $\delta_b^x = \delta_b \left(\frac{u_\infty}{r_c v} \right)^{\frac{1}{2}}$

$$x^x = \frac{x}{r_c}$$

$$v_o^x = v_o \left(\frac{r_c}{u_\infty v} \right)^{\frac{1}{2}}$$

As Evans (1960) showed that graphs of $\delta_b^x \left(\frac{du_g^x}{dx^x} \right)$ versus F_b with $v_o^x \delta_b^x$ as a parameter were approximately linear (Fig. A.3.1) a quadrature procedure can be used to solve equation A.3.1.

Spalding considers that the most suitable substitution is of the form:-

$$E_b = F_b + e \delta_b^x \left(\frac{du_g^x}{dx^x} \right) - j \quad A.3.2$$

where e and j are constants. Equation A.3.2 then becomes:-

$$u_g^x \frac{d \delta_b^x}{dx^x} + e \delta_b^x \left(\frac{du_g^x}{dx^x} \right) = E_b + j \quad A.3.3$$

E_b is a non-linear function of $\delta_b^x \left(\frac{du_g^x}{dx^x} \right)$ and of $v_o^x \delta_b^x$, and is a measure of the error involved in the straight line approximation.

If equation A.3.3 is multiplied throughout by u_g^{e-1} it becomes 'exact' and can be written in the integrated form, as follows:-

$$\delta_b^x u_g^{xe} = \int_0^x (j + E_b) u_g^{x(e-1)} dx^x \quad A.3.4$$

when the boundary condition u_g^x is known as a function of x^x then part of this equation, i.e.

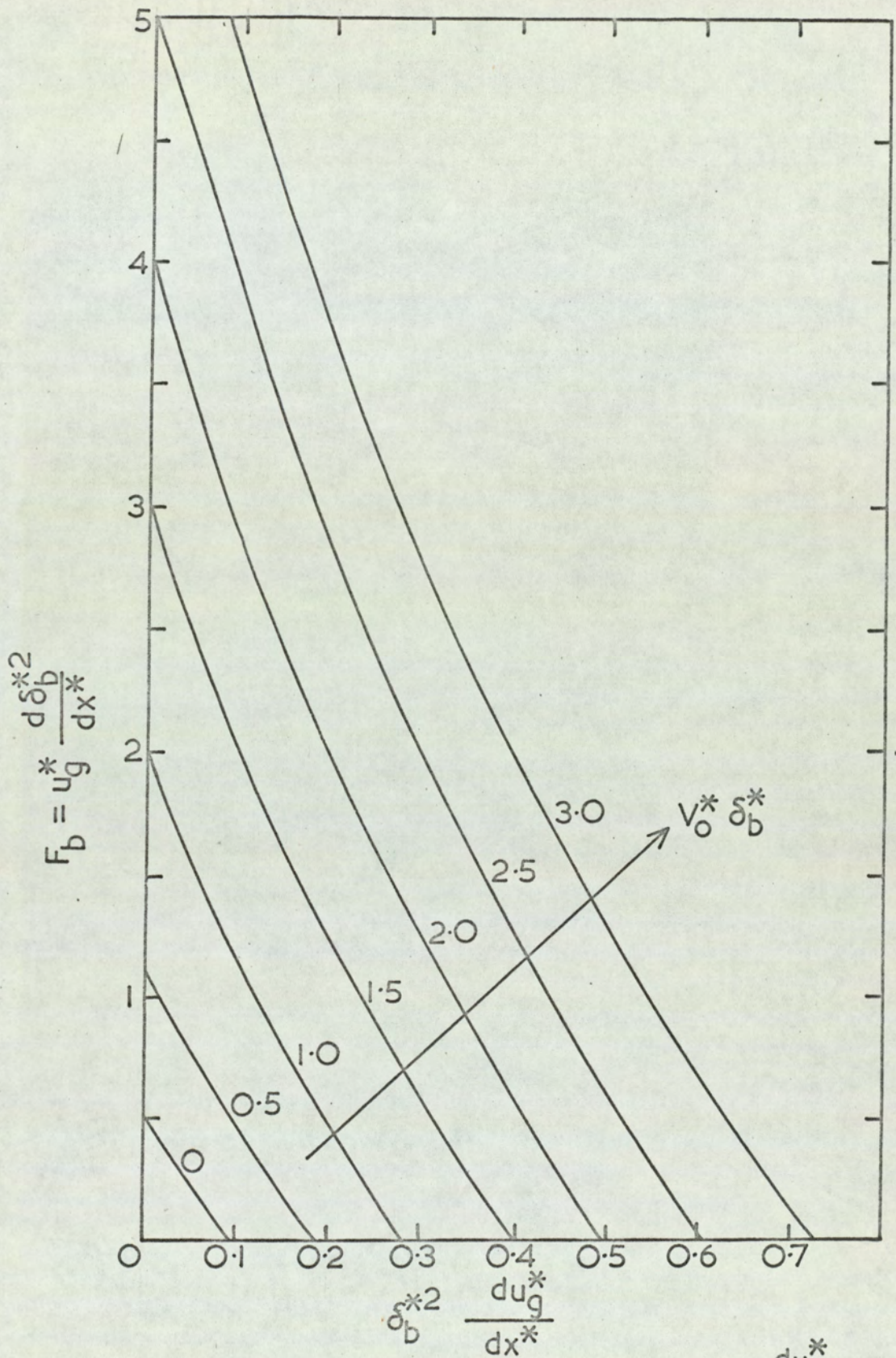


FIG. A. 3.1 THE FUNCTION F_b VERSUS $\delta_b^{*2} \frac{du_g^*}{dx^*}$

WITH $V_0^* \delta_b^*$ AS PARAMETER

(EVANS 1960)

$$\int_0^{x^*} j u_g^{*2} e^{-1} dx^*$$

can be solved by graphical integration. The remaining part of the equation can then be determined by an iterative procedure in which a first approximation to δ_b^* , namely $\delta_{b,I}^*$ is evaluated from equation A.3.4.

$$\delta_{b,I}^* = \left[\frac{\int_0^{x^*} j u_g^{*2} e^{-1} dx^*}{u_g^* e} \right]^{\frac{1}{2}} \quad \text{A.3.5}$$

The derived value of δ_b^* is then used to give a first approximation to the value of E_b at each value of x^* by reference to tables compiled by Evans (1960) and quoted by Spalding (1961). A second approximation $\delta_{b,II}^*$ can then be evaluated from the equation:-

$$\delta_{b,II}^* = \left[\frac{\int_0^{x^*} j u_g^{*2} e^{-1} dx^* + \int_0^{x^*} E_{b,I} u_g^{*2} e^{-1} dx^*}{u_g^* e} \right]^{\frac{1}{2}} \quad \text{A.3.6}$$

This procedure can be repeated until δ_b^* as a function of x^* has been found with sufficient accuracy.

Spalding (1958) found that the values of the constants e and j were 5.164 and 0.441 respectively. From this procedure it is not possible to calculate δ_b^* at the forward stagnation point so the value is calculated using the graph of, $\delta_b^{*2} \left(\frac{du_g^*}{dx^*} \right)$ versus F_b with $v_g^* \delta_b^*$ as parameter (Evans, 1960; Spalding, 1961). At the stagnation point of a tube, $u_g = 0$ while $\frac{du_g^*}{dx^*}$ is finite, hence it follows that $u_g^* \left(\frac{d\delta_b^{*2}}{dx^*} \right)$ and F_b

are also zero. From the graph a relationship between $\delta_b^{*2} \left(\frac{du_g^*}{dx^*} \right)$ and $v_g^* \delta_b^*$ can be obtained for $F_b = 0$. As $\frac{du_g^*}{dx^*}$ and v_g^* (which is equal to the main stream velocity at the

stagnation point) are known, the value of $\delta_b^{\mathcal{K}}$ at the stagnation point can be obtained.

The displacement thickness $\delta_a^{\mathcal{K}}$ can be calculated from the momentum thickness by using tables of Holstein & Bohlen¹ (Schlichting 1962a). The shape function Λ and the ratio of the displacement thickness to the momentum thickness $\frac{\delta_a^{\mathcal{K}}}{\delta_b^{\mathcal{K}}}$

can be found, and the displacement thickness evaluated. The boundary layer thickness can be obtained from the relationship (Schlichting 1962b),

$$\frac{\delta_a^{\mathcal{K}}}{\delta} = \frac{3}{10} - \frac{1}{120} \Lambda \quad \text{A.3.7}$$

1. It should be noted in the table that

$$K = \frac{\delta_b^2}{\nu} \left(\frac{du_g}{dx} \right) = \delta_b^{\mathcal{K}2} \left(\frac{du_g^{\mathcal{K}}}{dx^{\mathcal{K}}} \right)$$

References

- Evans, H. L. (1960) Ph.D. Thesis, Imperial College, University of London.
- Schlichting, H. (1962a) Boundary Layer Theory (McGraw-Hill) P. 249
- Schlichting, H. (1962b) Boundary Layer Theory (McGraw-Hill) P. 246
- Spalding, D. B. (1958) J. Fluid Mech. 4, 22.
- Spalding, D. B. (1961) J. Heat Mass Transfer, 2, 15.

APPENDIX 4Method of Calculating the Separation Point

The boundary layer becomes unstable and separates from the surface of the tube when a critical value of Reynolds number based on displacement thickness is exceeded. This critical value depends only upon the shape factor of the system and can be obtained from a standard graph (Schlichting 1962).

The critical Reynolds number decreases with distance around a tube as shown in Fig. 6.5. A graph of the actual Reynolds number is also included in Fig. 6.5; this Reynolds number increases steadily from the stagnation point around the tube as the displacement thickness increases. At a certain point, called the point of instability, the curves intersect and the flow will separate.

This point is reached when:-

$$\frac{u_g \delta_a}{\nu} = \left(\frac{u_g \delta_a}{\nu} \right)_{\text{crit}} \quad \text{A.4.1}$$

It should be noted that this point does not necessarily coincide with the point of minimum pressure.

Reference

Schlichting, H., (1962). Boundary Layer Theory (McGraw-Hill), 414.

APPENDIX 5The Contribution of Thermal Diffusion to the Total Mass Transfer Rate through the Laminar Boundary Layer

The equations for an incompressible two-dimensional laminar boundary layer consisting of a binary mixture are as follows (Baron 1956):-

$$\text{Continuity : } \frac{\partial u}{\partial x} + \frac{\partial v}{\partial y} = 0 \quad \text{A.5.1}$$

Component Continuity :

$$\rho u \frac{\partial m_1}{\partial x} + \rho v \frac{\partial m_1}{\partial y} = \frac{\partial}{\partial y} \left[\rho D_{1,2} \left(\frac{\partial m_1}{\partial y} + \alpha m_1 m_2 \frac{\partial (\text{Ln } T)}{\partial y} \right) \right] \quad \text{A.5.2}$$

Momentum :

$$\rho u \frac{\partial u}{\partial x} + \rho v \frac{\partial u}{\partial y} = \frac{\partial P}{\partial x} + \frac{\partial}{\partial y} \left(\mu \frac{\partial u}{\partial y} \right) \quad \text{A.5.3}$$

$$\text{and } \frac{\partial P}{\partial y} = 0$$

Energy :

$$\begin{aligned} \rho u \frac{\partial i}{\partial x} + \rho v \frac{\partial i}{\partial y} &= u \frac{\partial P}{\partial x} + \mu \left(\frac{\partial u}{\partial y} \right)^2 + \frac{\partial}{\partial y} \left(k \frac{\partial T}{\partial y} \right) \\ &+ RT \alpha \frac{\partial}{\partial y} \left[\rho D_{1,2} \frac{\partial m_1}{\partial y} + \alpha m_1 m_2 \frac{\partial (\text{Ln } T)}{\partial y} \right] \quad \text{A.5.4} \\ &+ \rho D_{1,2} \left[\frac{\partial m_1}{\partial y} + \alpha m_1 m_2 \frac{\partial (\text{Ln } T)}{\partial y} \right] \frac{\partial}{\partial y} \left[i + RT \alpha \right] \end{aligned}$$

These equations are obtained by taking mass, momentum and energy balances respectively, over a control volume of unit depth of the boundary layer and using standard boundary layer simplifications (Kays 1966).

Two further assumptions have to be made in the derivation of the energy equation namely,

- (1) There is no internal generation of heat due to chemical reactions.
- (2) No work is done by external fields.

It is assumed that heat and mass will be transferred by both the temperature gradient and concentration gradient. Transportation of mass due to a temperature gradient is termed thermal diffusion while the reciprocal process of transportation of heat due to a concentration gradient is called the diffusion-thermo or Dufour effect.

As mentioned in Section 3.3.1 these equations can only be conveniently solved for concentration diffusion. It can be shown, as follows, that in the present system the effect of thermal diffusion is small and the Dufour effect can be neglected.

By comparing the ratios of thermal diffusion with concentration diffusion, and the heat energy due to mass transfer with that due to heat transfer, the following ratios emerge respectively:-

$$|H_a| = \left| \frac{\alpha m_1 m_2 \frac{\partial (\ln T)}{\partial y}}{\frac{\partial m}{\partial y}} \right| \quad \text{A.5.5}$$

$$|H_b| = \left| \frac{RT \alpha}{i} \right| \quad \text{A.5.6}$$

Considering Equation A.5.5 first, this can be written as:-

$$H_a \approx \frac{\alpha m_1 m_2 \frac{1}{T} \frac{\Delta T}{\Delta y}}{\frac{\Delta m_1}{\Delta y}} \quad \text{A.5.7}$$

It is assumed that the temperature and mass diffusion gradients are linear, and that when the surface deposit does not exert a vapour pressure, the concentration of salt vapour at the surface is zero. These last two assumptions mean that if the concentration of salt in the bulk phase is m_1 then the average concentration in the boundary layer becomes $\frac{m_1}{2}$.

Equation A.5.7 now simplifies to:-

$$H_a \approx \frac{\alpha m_1 m_2 \left(\frac{T_\infty - T_w}{\delta} \right)}{\left(\frac{T_w + T_\infty}{2} \right) \left(\frac{m_1}{\delta} \right)} \quad \text{A.5.8}$$

Now $m_2 \rightarrow 1$ when concentrations of salt vapour are small, as in the present case, so Equation A.5.8 can be reduced to:-

$$H_a \approx \frac{\alpha (T_\infty - T_w)}{(T_\infty + T_w)} \quad \text{A.5.9}$$

Assuming that the gas mixture can be approximated to a Masonian type then α can be calculated from the relatively simple formula:-

$$\alpha = \frac{5}{16\sqrt{2}} \left(\frac{r_1}{r_2} \right) \left(\frac{M_1}{M_1 + M_2} \right)^{\frac{1}{2}} \quad \text{A.5.10}$$

This equation was derived using the Chapman-Enskog kinetic theory for a gas mixture composed of rigid molecules. From their theory the thermal diffusion factor can be written as:-

$$\alpha = \frac{15}{4} \left(\frac{K}{M_2} \right) \frac{\mu_2 T}{5 P D_{1,2} Q'} \quad \text{A.5.11}$$

where Q' is a factor dependent upon the collision pattern.

The factor can be obtained from the standard equation for diffusion derived from the kinetic theory, namely:-

$$\frac{1}{D_{1,2}} = \left(\frac{8}{3} n_2 \right) \left(\frac{2 M_1 M_2}{\pi K T (M_1 + M_2)} \right)^{\frac{1}{2}} \pi r_1^2 Q' \quad \text{A.5.12}$$

Eliminating Q' ,

$$\alpha = 2 K T \frac{\mu_2 n_2 \pi r_1^2}{5 P M_2} \left(\frac{2 M_1 M_2}{\pi K T (M_1 + M_2)} \right)^{\frac{1}{2}} \quad \text{A.5.13}$$

This can be reduced to Equation A.5.10 by substituting for viscosity using the following equation, which was derived from the kinetic theory:-

$$\mu_2 = \frac{1}{4 \pi r_2^2} \sqrt{\left(\frac{K T M_2}{\pi} \right)} \quad \text{A.5.14}$$

and the fact that the pressure $P = KnT$.

By using Equations A.5.9 and A.5.10, the thermal diffusion factor and the mass transfer effect of thermal diffusion were calculated as shown in Table 5.1. These quantities were calculated for the largest average temperature gradient used in the present experiments.

Evaluation of Equation A.5.6, in which T is the average boundary layer temperature, gives the ratio of the energy fluxes. The results are shown in Table 5.2. The value of Equation A.5.6 will only increase slightly as the surface temperature rises because the decreasing temperature difference and correspondingly high average temperature T will be counteracted by the increase in the heat capacities of the salts.

References

- Baron, J. R. (1956) M.I.T. NSL TR 160.
- Chapman, S. (1962) Progress in International Research on Thermodynamics and Transport Properties (New York), 257.
- Kays, W. M. (1966) Convective Heat and Mass Transfer (McGraw-Hill) 20-34.
- Knudsen, J. G. & Katz, D. L. (1958) Fluid Dynamics and Heat Transfer (McGraw-Hill) 500.
- Schlichting, H. (1962) Boundary Layer Theory (McGraw-Hill) 30.
- Van der Hegge Zijnen, B. G. (1958) Appli. Sci. Res. Section A, 7.

	$\frac{r_1}{r_2}$	$\frac{m_1}{m_1 + m_2}$	Thermal Diffusion	Effect of Thermal Diffusion, H_a , %
Sodium Chloride	1.200	0.669	0.216	6.0
Potassium Chloride	1.298	0.720	0.321	9.0
Sodium Sulphate	1.377	0.882	0.399	11.1

TABLE A.5.1

The amount of mass transferred by thermal diffusion compared with that transferred by concentration diffusion for the salts sodium chloride, potassium chloride and sodium sulphate.

	Specific heat capacity at 773°K, mJ/kg. °C.	Effect of energy due to mass transfer, H_b %
Sodium Chloride	3.3	3.0
Potassium Chloride	3.5	4.2
Sodium Sulphate	3.8	4.8

TABLE A.5.2

The amount of energy transferred due to mass transfer compared with that transferred due to heat transfer for the salts sodium chloride, potassium chloride and sodium sulphate.

APPENDIX 6

Solution of the Boundary Layer Equations for Mass Transfer
when Vapour Diffusion is the sole mechanism of transfer.

The calculation of the rate of mass transfer through a laminar boundary layer requires the simultaneous solution of the four boundary layer equations (Appendix 5). This procedure is very tedious. However, Spalding (1960) has shown that the diffusion and energy equations can be reduced to a single standard form under conditions of steady flow and low rates of transfer. The solution of the problem is then reduced to one involving three equations and is similar to the corresponding problem in heat transfer.

Ignoring thermal diffusion and the Dufour effect (Appendix 5), the diffusion and energy equations can be written, respectively, as:-

Mass Diffusion

$$\rho u \frac{\partial m_1}{\partial x} + \rho v \frac{\partial m_1}{\partial y} = \frac{\partial}{\partial y} \left(\rho D_{1,2} \frac{\partial m_1}{\partial y} \right) \quad \text{A.6.1}$$

and

Energy

$$\rho u \frac{\partial i}{\partial x} + \rho v \frac{\partial i}{\partial y} = \frac{\partial}{\partial y} \left(\frac{k \partial T}{\partial y} \right) + \frac{\partial}{\partial y} \left(\rho D_{1,2} \frac{\partial m_1}{\partial y} \right) + u \frac{\partial P}{\partial x} + \mu \left(\frac{\partial u}{\partial y} \right)^2 \quad \text{A.6.2}$$

Derivation of a General Expression for Heat and Mass Transfer

For the range of Reynolds number considered in this work, the pressure gradient $\frac{\partial P}{\partial x}$ is small and the term $u \frac{\partial P}{\partial x}$ in equation A.6.2 can be ignored.

The final term in the energy equation represents viscous energy and is only important at high Prandtl numbers and when the velocity approaches the speed of sound. As the Prandtl number and gas velocity are both low, this term can be ignored. Hence the energy equation A.6.2 becomes

$$\rho u \frac{\partial i}{\partial x} + \rho v \frac{\partial i}{\partial y} = \frac{\partial}{\partial y} \left(\frac{k \partial T}{\partial y} \right) + \frac{\partial}{\partial y} \left(\rho D_{1,2} \frac{\partial m_1}{\partial y} \right) \quad \text{A.6.3}$$

In both the diffusion and energy equations A.6.1 and A.6.2, it is convenient to replace the conductivity constants $\rho D_{1,2}$ and k by γ and Γc respectively, then μ , γ and Γc have the same dimensions and each can be considered as a simple transport property.

The conduction term can now be written as:

$$\frac{\partial}{\partial y} \left(k \frac{\partial T}{\partial y} \right) = \frac{\partial}{\partial y} \left(\Gamma c \frac{\partial T}{\partial y} \right) = \frac{\partial}{\partial y} \left(\Gamma \sum m_1 c_1 \frac{\partial T}{\partial y} \right)$$

If the flue gas is considered to behave as a perfect gas, which is a reasonable assumption for the present system, then

$$c_1 dT = di_1$$

$$\text{hence } \frac{\partial}{\partial y} \left(k \frac{\partial T}{\partial y} \right) = \frac{\partial}{\partial y} \left(\Gamma \sum m_1 \frac{\partial i_1}{\partial y} \right)$$

Equation A.6.3 now becomes:

$$\rho u \frac{\partial i}{\partial x} + \rho v \frac{\partial i}{\partial y} = \frac{\partial}{\partial y} \left(\Gamma \sum m_1 \frac{\partial i_1}{\partial y} \right) + \frac{\partial}{\partial y} \left(\sum \gamma \frac{\partial m_1 i_1}{\partial y} \right) \quad \text{A.6.4}$$

If it is assumed that the Lewis number is unity, then the transport terms γ and Γ are equal. In the present work this assumption is untrue (N_{Le} lies between 0.4 to 0.7 dependent on the salt being used) but a subsequent correction can be made

Substituting $\gamma = \Gamma$ in equation A.6.4

$$\rho u \frac{\partial i}{\partial x} + \rho v \frac{\partial i}{\partial y} = \frac{\partial}{\partial y} \left(\Gamma \sum m_1 \frac{\partial i_1}{\partial y} + \Gamma \sum i_1 \frac{\partial m_1}{\partial y} \right) \quad \text{A.6.5}$$

The last term can be simplified as follows,

$$\Gamma \sum \left(m_1 \frac{\partial i_1}{\partial y} + i_1 \frac{\partial m_1}{\partial y} \right) = \Gamma \sum \frac{\partial (m_1 i_1)}{\partial y} = \Gamma \frac{\partial}{\partial y} \sum (m_1 i_1) = \Gamma \frac{\partial i}{\partial y}$$

The derived energy equation which concerns the transfer of heat, now has exactly the same form as the diffusion equation for the transfer of mass and can be written,

$$\rho u \frac{\partial i}{\partial x} + \rho v \frac{\partial i}{\partial y} = \frac{\partial}{\partial y} \left(\Gamma \frac{\partial i}{\partial y} \right) \quad \text{A.6.6}$$

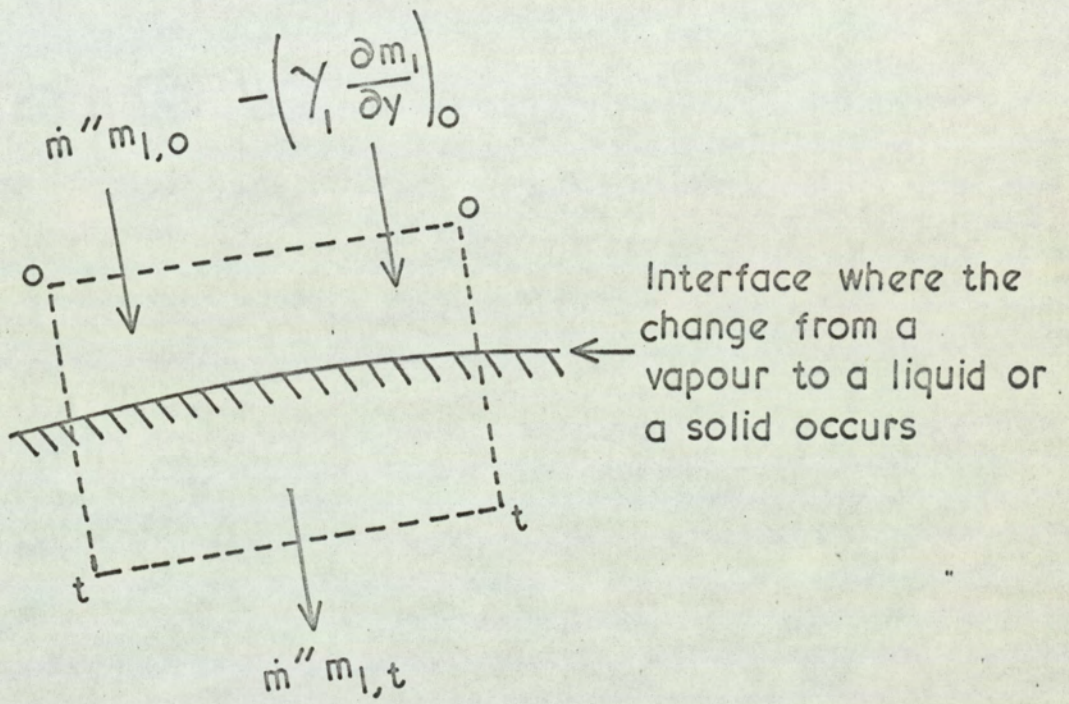


FIG.A.6.1 CONTROL VOLUME ENCLOSING THE PHASE INTERFACE

If the concept of a conserved property is now introduced such that the property b is equal to m or i , then the diffusion and energy equations can be written in the general form

$$\rho u \frac{\partial b}{\partial x} + \rho v \frac{\partial b}{\partial y} = \frac{\partial}{\partial y} \left(\rho \frac{\partial b}{\partial y} \right) \quad \text{A.6.7}$$

Consideration of Boundary Conditions

A general form of the boundary condition at the wall can be developed from the diffusion and energy equations.

Considering the steady flow of a component '1' across the phase boundary as shown in Fig. A.6.1, where 't' is the condition in the transferred state beyond the phase boundary and 'o' is the state just inside the phase boundary. In the present study 'o' is the condition of the salt in the vapour state just before it condenses and 't' is the condition just after when the liquid or solid material has been formed.

Applying a mass balance,

$$\dot{m}'' m_{1,o} - \left(\gamma_1 \frac{\partial m_1}{\partial y} \right)_o - \dot{m}'' m_{1,t} = 0$$

hence, $\dot{m}'' = \frac{\left(\gamma_1 \frac{\partial m_1}{\partial y} \right)_o}{m_{1,o} - m_{1,t}}$

A similar form can be obtained by applying an energy balance,

$$\dot{m}'' i_o - \sum_1 \left(\gamma_1 \frac{\partial m_1}{\partial y} \right) i_{1,o} - \left(\Gamma c \frac{\partial T}{\partial y} \right)_o - \dot{m}'' i_t = 0$$

hence, $\dot{m}'' = \frac{\sum_1 \left(\gamma_1 \frac{\partial m_1}{\partial y} \right) i_{1,o} - \left(\Gamma c \frac{\partial T}{\partial y} \right)_o}{i_o - i_t}$ A.6.8

Using the previous approximation that the Lewis number is equal to unity, the second term can be written as:

$$\begin{aligned} \left(\Gamma c \frac{\partial T}{\partial y} \right)_o &= \left(\Gamma \frac{\partial T}{\partial y} \right)_o \left(\sum_1 m_1 c_1 \right)_o = \Gamma \sum_1 \left(m_1 c_1 \frac{\partial T}{\partial y} \right)_o \\ &= \Gamma \sum_1 \left(m_1 \frac{\partial i_1}{\partial y} \right)_o \end{aligned}$$

$$\begin{aligned} \text{Therefore } \dot{m}'' &= \frac{\left[\Gamma \sum_1 \left(i_1 \frac{\partial m_1}{\partial y} + m_1 \frac{\partial i_1}{\partial y} \right) \right]_o}{i_o - i_t} = \frac{\Gamma \sum_1 \frac{\partial (m_1 i_1)}{\partial y}}{i_o - i_t} \quad \text{1/44.} \\ &= \frac{\left(\Gamma \frac{\partial i}{\partial y} \right)_o}{i_o - i_t} \quad \text{A.6.9} \end{aligned}$$

Equations A.6.8 and A.6.9 can now be written in a general form representing the boundary conditions as:

$$\dot{m}'' = \frac{\varphi \left(\frac{\partial b}{\partial y} \right)_o}{b_o - b_t} \quad \text{A.6.10}$$

The resulting mathematical problem is to obtain solutions to the b-equation A.6.7 for various boundary conditions of b (equation A.6.10). The velocity components u and v are obtained from a solution of the corresponding momentum and continuity equations.

The situation can be simplified if the 'b' equation is linear, in this case

$$\left(\varphi \frac{\partial b}{\partial y} \right)_o \propto (b_g - b_o)$$

This equation assumes that the transport term φ , and that mass flow rates within the boundary layer, ρu and ρv , are independent of the concentration gradient. As the mass transfer rates are small in the present work, both of these assumptions should be valid. It will be shown later that the effect of the first assumption can be estimated and is negligible.

It is now convenient to define a mass transfer conductance, g , such that

$$\begin{aligned} \left(\varphi \frac{\partial b}{\partial y} \right)_o &= g_i (b_g - b_o) \\ \text{or } g_i &= \frac{\left(\varphi \frac{\partial b}{\partial y} \right)_o}{b_g - b_o} \quad \text{A.6.11} \end{aligned}$$

Combining equations A.6.10 and A.6.11

$$\dot{m}'' = g_i \left(\frac{b_g - b_o}{b_o - b_t} \right) \quad \text{A.6.12}$$

If a mass transfer driving force 'B' is defined such that:

$$B = \frac{b_g - b_o}{b_o - b_t} \quad \text{A.6.13}$$

then equation A.6.12 becomes

$$\dot{m}'' = g_i B \quad \text{A.6.14}$$

Therefore 'B' can be evaluated for given values of 'b' which in this case are the concentrations in the 'o', 't' and 'g' states. The conductance 'g_i' is obtained from an appropriate solution of equation A.6.7.

As low mass transfer rates are involved, a heat/mass analogy can be used to solve equation A.6.7. Appropriate data has been obtained from model tunnel experiments (section 7) and the solution of the momentum, continuity and energy equations (Pun 1967).

The use of heat transfer data makes it necessary to define another conductance term, g_h, for the case in which the concentration gradient tends to zero.

$$g_h = \lim_{B \rightarrow 0} \left(\frac{\dot{m}''}{B} \right) \quad \text{A.6.15}$$

g_h has to be expressed as a function of a heat transfer coefficient, the term usually employed in the reporting of heat transfer data. As 'T' is the conserved property, equation A.6.11 can be written as,

$$g_h = \frac{\left(\Gamma \frac{\partial T}{\partial y} \right)_o}{T_g - T_o} \quad \text{A.6.16}$$

Heat transfer conductance is defined by the equation,

$$\dot{q}''_o = h(T_g - T_o) = \left(\frac{k \partial T}{\partial y} \right)_o = \left(\Gamma c \frac{\partial T}{\partial y} \right)_o \quad \text{A.6.17}$$

Combining equations A.6.16 and A.6.17

$$g_h = \frac{h}{c}$$

This relation is obtained in a non-dimensional form by dividing by ρu_∞ to give,

$$\frac{g_h}{\rho u_\infty} = \frac{h}{\rho u_\infty c} = N_{St,h}$$

Hence if the heat/mass transfer analogy is correct, equation A.6.14 expressing the mass transfer rate can be written as,

$$\dot{m}'' = N_{St,h} G_\infty B \quad \text{where } G_\infty = \rho u_\infty \quad \text{A.6.18}$$

Corrections have to be made for earlier assumptions that are not wholly valid.

The earlier assumption that the Lewis number was equal to unity can be corrected as follows:

Heat transfer to a tube in cross-flow can be written as,

$$N_{St,h} = C N_{Re}^b N_{Pr}^{-a} \quad \text{A.6.19}$$

As the Lewis number is not equal to unity, the Prandtl number will have a different value to the Schmidt number for the same system, when mass transfer is occurring.

If $N_{St} = y$ then the value of the Prandtl number corresponding to a Lewis number of unity would also be 'y'. However, in practice, the Lewis number is not equal to unity, so the Prandtl number will have a value x .

By substituting in equation A.6.19 the correction to the Stanton number for conditions of mass transfer can be found.

If the Lewis number equals unity (assumed in the derivation of $\dot{m}'' = g_1 B$), then:

$$N_{St,i} = C N_{Re}^b y^{-a}$$

However $N_{Pr} = x$, hence for heat transfer alone,

$$N_{St,h} = CN_{Re}^b x^{-a}$$

$$\text{Dividing } \frac{N_{St,i}(N_{Pr} = y)}{N_{St,h}(N_{Pr} = x)} = \frac{y}{x}^{-a}$$

$$\begin{aligned} N_{St,i}(N_{Pr} = y) &= N_{St,h}(N_{Pr} = x) \frac{y}{x}^{-a} \\ &= N_{St,h}(N_{Pr} = x) N_{Le}^a \end{aligned} \quad \text{A.6.20}$$

Evans (1962) found for laminar boundary layer flows for Reynolds numbers less than 80,000 that 'a' could be taken as $2/3$.

Hence equation A.6.18 may be modified:-

$$\dot{m}'' = (N_{Le})^{2/3} (N_{St,h}) G_{\infty} B \quad \text{A.6.21}$$

Considering the assumption that the transport term, ϕ , is dependent upon the concentration gradient, Spalding (1951) and Evans (1961) showed that this dependence followed the same pattern for most cases, namely $N_{St,i}$ falls below $N_{St,h}$ when B is positive (evaporation) and rises above it when B is negative (condensation).

From these results, Spalding & Evans (1961) proposed the following correction factor,

$$\frac{N_{St,i}}{N_{St,h}} = (1 + B)^{-0.4} \quad \text{A.6.22}$$

As driving force B is only of the order of 10^{-3} , in the present work, this correction can be ignored.

The small magnitude of the driving force B also indicates that the dependence of the velocity field within the boundary layer upon concentration is also likely to be negligible.

References

Evans, H. L. (1961) Int. J. Heat Mass Transfer 3, 321.

Evans, H. L. (1962) Int. J. Heat Mass Transfer 5, 35.

Pun, W. M. (1967) Private Communication, Imperial College,
London.

Spalding, D. B. (1951), Ph.D. Thesis, University of Cambridge.

Spalding, D. B. (1960), Int. J. Heat Mass Transfer, 1, 192.

Spalding, D. B. & Evans, H. L. (1961) Int. J. Heat Mass
Transfer, 2, 334.

APPENDIX 7

Theoretical Calculation of the Mass Transfer Rate for Sodium Chloride, Potassium Chloride and Sodium Sulphate

The ohmic-type equation for mass transfer, which was derived in Appendix 6, forms the basis of the calculations, that is :-

$$\dot{m}'' = g_i B \quad \text{A.7.1}$$

(a) Evaluation of Conductance Term, g

$$g_i = N_{st,h} (N_{Le})^{2/3} G \quad \text{A.7.2}$$

First, it is necessary to calculate the Stanton Number where

$$N_{st,h} = \frac{N_{Nu}}{N_{Pr} N_{Re}} = \frac{N_{Nu}}{0.7 N_{Re}}$$

According to Pun (1967), the $\frac{N_{Nu}}{N_{Re}}$ relationship for the tube

across the combustor duct is given by :-

$$\frac{N_{Nu}}{(N_{Re})^{1/2}} = 1.139 - 0.0985 \left(\frac{x}{dc}\right)^2 - 0.9618 \left(\frac{x}{dc}\right)^4 \quad \text{A.7.3}$$

This equation was derived using the static pressure measurements obtained in model studies (Section 6), and is valid for angles of up to 100° from the forward stagnation point of the tube.

Accordingly, Equation A.7.3 can be rewritten :-

$$N_{st,h} = \frac{1}{(N_{Re})^{1/2}} \left[1.63 - 0.1141 \left(\frac{x}{dc}\right)^2 - 1.38 \left(\frac{x}{dc}\right)^4 \right] \quad \text{A.7.4}$$

An average Stanton number was evaluated by integration over the area between angles of $0-100^\circ$ measured from the forward stagnation point.

$$N_{st,h,m} = \frac{1.43}{(N_{Re})^{1/2}} \quad \text{A.7.5}$$

All transport properties of the system are evaluated at mean film temperatures (Douglas & Churchill 1958). Thus at a

particular main stream gas velocity and temperature, the Reynolds number for the flow decreases slightly as the surface temperature increases.

$$\text{The Lewis number} = \frac{\rho D_{1,2}}{\frac{k}{c}}$$

where the diffusivity can be evaluated from the following correlation given by Gilliland (1934),

$$D_{1,2} = \frac{0.0043T^{3/2}}{P(V_1 + V_2)} \sqrt{\left(\frac{1}{M_1} + \frac{1}{M_2}\right)}$$

Subscript 2 refers to the flue gases assumed to have the same physical properties as air, and subscript 1 refers to the salt vapour. This equation refers to ideal gas conditions. The molar volume of sodium chloride V_1 was obtained by dividing the molecular weight by the density at the normal boiling point which was estimated by extrapolating high temperature density data. The values obtained are as follows :-

Sodium chloride :	51.5 cm ³ /g.mole.
Potassium chloride :	65.3 cm ³ /g.mole.
Sodium sulphate :	78 cm ³ /g.mole.

Other terms in the equation are :-

$$P = 1 \text{ atmosphere.}$$

$$M_2 = 29$$

$$V_2 = 29.9 \text{ cm}^3/\text{g.mole.}$$

The calculated values of diffusivity for the temperature range 600°C to 1,400°C are shown in Table A.7.1.

It was found that for each salt the Lewis number was constant over the range of average surface temperatures investigated which was 500°C - 900°C, giving mean film temperatures from 800°C - 1,000°C for a main stream gas temperature of 1,100°C.

The final term in Equation A.7.2, the mass flow rate G ,

Temperature, °C	Diffusivity of sodium chloride cm ² /s	Diffusivity of potassium chloride cm ² /s	Diffusivity of sodium sulphate cm ² /s
600	0.54	0.48	0.42
800	0.74	0.65	0.57
1,000	0.95	0.83	0.77
1,200	1.19	1.04	0.91
1,400	1.44	1.26	1.06

TABLE A.7.1

Diffusivities of the three salts as a
function of Temperature

was calculated from volumetric flow rate and density (assumed to be $2.57 \times 10^{-4} \text{g/cm}^3$) at the main stream temperature of $1,100^\circ\text{C}$. Values of g as a function of mean film temperature and Reynolds number are given in Table A.7.2.

(b) Evaluation of Driving Force B

The conserved property is mass, hence Equation A.7.2 becomes :-

$$B = \frac{m_g - m_o}{m_o - m_t} \quad \text{A.7.6}$$

A single phase is condensing, hence $m_T \rightarrow 1$. Concentrations of the salt vapour in the main stream are only in the order of 10^{-4} torr so if condensation is to occur, $m_o < 10^{-4}$.

Therefore $m_o - m_T \rightarrow -1$ and,

$$B = m_g - m_o \quad \text{A.7.7}$$

To obtain the driving force in terms of partial pressure, the following substitutions are used:-

$$m = \frac{n_1 M_1}{n_2 M_2}$$

Substituting in Equation A.7.7 :-

$$B = \left(\frac{n_1 M_1}{n_2 M_2} \right)_g - \left(\frac{n_1 M_1}{n_2 M_2} \right)_o \quad \text{A.7.8}$$

As $\frac{P_2}{P_1} = \frac{n_2}{n_1}$

Equation A.7.8 becomes :-

$$B = \frac{M_{\text{salt}}}{M_{\text{air}}} \left[\left(\frac{P_1}{P_2} \right)_g - \left(\frac{P_1}{P_2} \right)_o \right] \quad \text{A.7.9}$$

Average values of the driving force B as functions of the average upstream surface temperature were now calculated for the salt concentrations in the main stream gases. The principal steps in these calculations were :-

(1) For a particular stagnation point temperature the average surface temperature was found using the peripheral temperature

Average surface temperature, °C.		500	550	600	650	700	750	800
Mean film temperature, °C.		800	825	850	875	900	925	950
Kinematic Viscosity cm ² /s.		1.305	1.365	1.42	1.475	1.53	1.596	1.665
Mass flow Rate (g cm ⁻² s ⁻¹)		0.276						
Velocity 10.5 m/s	N _{Re}	4.11 x 10 ³	3.95 x 10 ³	3.8 x 10 ³	3.66 x 10 ³	3.53 x 10 ³	3.41 x 10 ³	3.30 x 10 ³
	N _{st}	2.19 x 10 ⁻²	2.25 x 10 ⁻²	2.3 x 10 ⁻²	2.35 x 10 ⁻²	2.39 x 10 ⁻²	2.43 x 10 ⁻²	2.46 x 10 ⁻²
	g _{NaCl}	3.19 x 10 ⁻³	3.27 x 10 ⁻³	3.34 x 10 ⁻³	3.41 x 10 ⁻³	3.47 x 10 ⁻³	3.53 x 10 ⁻³	3.58 x 10 ⁻³
	g _{KCl}	2.98 x 10 ⁻³	3.04 x 10 ⁻³	3.10 x 10 ⁻³	3.16 x 10 ⁻³	3.22 x 10 ⁻³	3.29 x 10 ⁻³	3.36 x 10 ⁻³
	g _{Na₂SO₄}	2.80 x 10 ⁻³	2.84 x 10 ⁻³	2.88 x 10 ⁻³	2.94 x 10 ⁻³	2.99 x 10 ⁻³	3.04 x 10 ⁻³	3.09 x 10 ⁻³

TABLE A7.2 Evaluation of the Conductance 'g' as a Function of Surface Temperature and Gas Velocity

Cont'd

Cont'd..

Mass flow Rate (g cm ⁻² s ⁻¹)		0.475						
Velocity 18 m/s	N _{Re}	7.1 x 10 ³	6.82 x 10 ³	6.55 x 10 ³	6.3 x 10 ³	6.08 x 10 ³	5.89 x 10 ³	5.72 x 10 ³
	N _{st}	1.705 x 10 ⁻²	1.73 x 10 ⁻²	1.76 x 10 ⁻²	1.79 x 10 ⁻²	1.825 x 10 ⁻²	1.86 x 10 ⁻²	1.90 x 10 ⁻²
	g _{NaCl}	4.29 x 10 ⁻³	4.34 x 10 ⁻³	4.4 x 10 ⁻³	4.47 x 10 ⁻³	4.56 x 10 ⁻³	4.65 x 10 ⁻³	4.75 x 10 ⁻³
	g _{KCl}	3.91 x 10 ⁻³	3.99 x 10 ⁻³	4.08 x 10 ⁻³	4.15 x 10 ⁻³	4.24 x 10 ⁻³	4.32 x 10 ⁻³	4.40 x 10 ⁻³
Mass flow Rate (g cm ⁻² s ⁻¹)		0.790						
Velocity 30 m/s	N _{Re}	11.75 x 10 ³	11.3 x 10 ³	10.9 x 10 ³	10.5 x 10 ³	10.1 x 10 ³	9.75 x 10 ³	9.44 x 10 ³
	N _{st}	1.315 x 10 ⁻²	1.335 x 10 ⁻²	1.36 x 10 ⁻²	1.38 x 10 ⁻²	1.41 x 10 ⁻²	1.44 x 10 ⁻²	1.47 x 10 ⁻²
	g _{NaCl}	5.46 x 10 ⁻³	5.55 x 10 ⁻³	5.65 x 10 ⁻³	5.76 x 10 ⁻³	5.86 x 10 ⁻³	5.97 x 10 ⁻³	6.09 x 10 ⁻³

TABLE A7.2 Evaluation of the Conductance 'g' as a Function of Surface Temperature and Gas Velocity

distribution curves (Fig. 7.3).

(2) For the same temperature at the forward stagnation point, the vapour pressure exerted by the surface deposit was found at 10° intervals up to the limit of the laminar boundary layer. The following vapour pressure data were used in conjunction with Fig. 7.3 to obtain the required values.

Sodium Chloride

$$\log_{10} p = 11.093 - 12.288 \left(\frac{1,000}{T} \right) + 2 \log_{10} \left(\frac{1,000}{T} \right)$$

(Zimm & Mayer 1944)

$$\log_{10} p = 14.1 - 14.72 \left(\frac{1,000}{T} \right)$$

(Jackson & Duffin 1963)

Potassium Chloride

$$\log_{10} p = 8.1301 - \frac{8.86 \times 10^3}{T}$$

(Wartenberg & Albrecht
1921)

Sodium Sulphate

(a) For the temperature range $1,040 - 1,157^\circ\text{K}$

$$\log_{10} p = 9.071 - \frac{1.26 \times 10^4}{T}$$

(b) For the temperature range $1,157 - 1,520^\circ\text{K}$

$$\log_{10} p = 8.011 - \frac{1.14 \times 10^4}{T}$$

(Halstead 1967)

The sodium chloride data of Jackson & Duffin (1963) was measured in the presence of water vapour while the rest of the data was measured 'in vacuo'.

(3) The eleven values of vapour pressure at the surface were subtracted from the partial pressure of salt vapour in the main stream. When the value was found to be negative (indicating absence of condensation), it was taken as zero, because evaporation does not take place. The average driving force was then derived using the arithmetic mean of the eleven differences in vapour pressure.

(4) The steps 1 - 3 were repeated for various average surface

temperatures.

The results for all concentrations of the three salts are shown in Table A.7.3, a-d. Using the results of Tables A.7.2 and A.7.3, curves of theoretical mass transfer rates as a function of temperature can be drawn as shown in Figs. 8.11, 8.12 and 8.16. The points of inflexion in the negative slopes of the curves resulted from the "levelling out" of the peripheral temperatures as the extremity of the laminar boundary layer was approached, (Fig. 7.3).

References

- Cliffe, K. R. (1967) B.C.U.R.A. Document DBA/30.
- Douglas, W. J. M. & Churchill, S. W. (1958) C.E.P. Symposium Ser. No. 18, 52, 23.
- Duffin, H. C. & Hinds, D. V. (1963) C.E.R.L. Lab. note No. RD/L/N 122/63.
- Halstead, D. (1967) C.E.R.L. Lab. note No. RD/L/N 73/67.
- Wartenberg, H. & Albrecht, Ph. (1921) Zeitschrift Für Electrochemie 27, 162.
- Zimm, B. H. & Mayer, J. E. (1944) J. Chem. Phys. 12(9), 362.

$P = 0.055$ torr

Temperature at Forward Stagnation Point, °C	Average Surface Temperature, °C	(P - Po) Average torr	B Average x 10 ⁴ , atmos.
635	B regarded as constant when temp. 610°C	0.055	1.45
646	622	0.048	1.26
649	626	0.046	1.20
656	633	0.041	1.08
668	647	0.031	0.82
682	662	0.022	0.58
704	688	0.009	0.24
727	709	0.000	0.00

$P = 0.110$ torr

Temperature at Forward Stagnation Point, °C	Average Surface Temperature, °C	(P - Po) Average torr	B Average x 10 ⁴ , atmos.
644	B regarded as constant when temp. 620°C	0.11	2.9
684	662	0.091	2.39
688	667	0.083	2.18
694	674	0.069	1.82
704	682	0.051	1.32
721	702	0.024	0.63
745	728	0.000	0.00

$P = 0.250$ torr

Temperature at Forward Stagnation Point, °C	Average Surface Temperature, °C	(P - Po) Average torr	B Average x 10 ⁴ , atmos.
654	B regarded as constant when temp. 630°C	0.250	6.58
686	665	0.222	5.85
695	675	0.209	5.50
714	695	0.164	4.31
725	707	0.125	3.30
743	725	0.070	1.84
768	752	0.000	0.00

TABLE A.7.3a

Evaluation of the driving force 'B' as a function of surface temperature for sodium chloride (using data of Jackson & Duffin 1963)

P = 0.250 torr

Temperature at Forward Stagnation Point, °C	Average Surface Temperature, °C	(P - P _o) Average torr	B Average x 10 ⁴ , atmos.
660	639	0.250 regarded as constant when temp. 639	6.58
725	708	0.209	5.50
758	743	0.150	3.95
772	757	0.075	1.98
788	775	0.038	1.0
800	787	0.019	0.5
816	805	0.000	0.0

P = 0.110 torr

Temperature at Forward Stagnation Point, °C	Average Surface Temperature, °C	(P - P _o) Average torr	B Average x 10 ⁴ , atmos.
650	628	0.110 regarded as constant when temp. 628	2.9
680	660	0.100	2.63
712	694	0.083	2.19
725	708	0.073	1.92
740	725	0.053	1.40
758	743	0.021	0.55
784	770	0.000	0.00

P = 0.055 torr

Temperature at Forward Stagnation Point, °C	Average Surface Temperature, °C	(P - P _o) Average torr	B Average x 10 ⁴ , atmos.
640	617	0.055 regarded as constant when temp. 617	1.45
680	660	0.049	1.29
703	683	0.036	0.945
712	694	0.027	0.49
725	708	0.016	0.421
740	725	0.007	0.184
760	745	0.000	0.000

TABLE A.7.3b

Evaluation of the driving force 'B' as a function of surface temperature for sodium chloride (using data of Zimm & Mayer 1944)

P = 0.0110 torr

Temperature at Forward Stagnation Point, °C	Average Surface Temperature, °C	(P - P _o) Average torr	B Average x 10 ⁴ , atmos.
740	725	0.0110 regarded as constant when temp. 725	0.708
800	787	0.0094	0.605
825	815	0.0079	0.508
852	844	0.0054	0.348
862	854	0.0038	0.244
872	865	0.0020	0.129
893	888	0.0000	0.000

P = 0.0055 torr

Temperature at Forward Stagnation Point, °C	Average Surface Temperature, °C	(P - P _o) Average torr	B Average x 10 ⁴ , atmos.
710	692	0.0055 regarded as constant when temp. 692	0.354
765	750	0.0048	0.309
800	787	0.0038	0.245
825	815	0.0024	0.154
834	825	0.0015	0.096
852	844	0.0004	0.026
870	863	0.0000	0.000

TABLE A.7.3c

Evaluation of the driving force 'B' as a function of surface temperature for sodium sulphate

P = 0.250 torr			
Temperature at Forward stagnation Point, °C	Average Surface Temperature, °C	(P - P ₀) Average torr	B Average x 10 ⁴ , atmos.
590	565	0.250 regarded as constant when temp. 565	8.80
656	635	0.225	8.02
703	685	0.173	6.16
725	708	0.120	4.27
740	725	0.070	2.50
758	743	0.027	0.96
777	763	0.000	0.00

P = 0.125 torr			
Temperature at Forward Stagnation Point, °C	Average Surface Temperature, °C	(P - P ₀) Average torr	B Average x 10 ⁴ , atmos.
580	553	0.125 regarded as constant when temp. 553	4.45
656	635	0.099	3.52
682	662	0.078	2.78
703	685	0.048	1.71
712	694	0.032	1.14
725	708	0.017	0.61
750	735	0.000	0.00

P = 0.0650 torr			
Temperature at Forward Stagnation Point, °C	Average Surface Temperature, °C	(P - P ₀) Average torr	B Average x 10 ⁴ , atmos.
560	532	0.065 regarded as constant when temp. 532	2.32
610	585	0.058	2.06
656	634	0.039	1.39
682	662	0.020	0.71
703	685	0.008	0.28
712	694	0.005	0.18
725	708	0.000	0.00

TABLE A.7.3d (Continued)

Temperature at Forward Stagnation Point, °C	Average Surface Temperature, °C	(P - P _o) Average torr	B Average x 10 ⁴ , atmos.
538	503	0.0350 regarded as constant when temp. 503	1.25
610	585	0.0240	0.85
630	606	0.0175	0.62
650	628	0.0100	0.36
680	660	0.0040	0.14
703	685	0.0005	0.02
706	688	0.0000	0.00

TABLE A.7.3d

Evaluation of the driving force 'B' as a function of surface temperature for potassium chloride

APPENDIX 8RESULTS

The results for each salt are denoted by the following code letters:

- C Sodium Chloride (impaction occurring)
- D Sodium Chloride (impaction not occurring)
- E Sodium Sulphate
- F Calcium Chloride
- G Potassium Chloride

The results for an individual salt are divided into two sections, (a) and (b). The results in section (a) were obtained at temperatures when the surface deposit did not exert an appreciable vapour pressure, while results in section (b) were obtained at temperatures when the surface deposit did exert an appreciable vapour pressure.

Nominal Concentration : 0.250 torr

Nominal Velocity : 18.0 m/s

Area of Deposition : 2,200 mm²

Run No.	Weight of deposit, mg.	Run time, min.	Salt conc. torr.	Velocity, m/s	Temperature at forward Stagnation Point, °C
G32	232	30	0.272	17.80	705
G33	55	30	0.248	17.73	770
G36	270	30	0.263	17.91	565
G37	283	30	0.271	17.80	625
G38	331	30	0.263	17.85	575
G39	383	30	0.284	17.80	700
G40	334	30	0.276	18.04	675
G41	224	30	0.267	17.62	725
G42	412	30	0.262	17.66	690
G43	303	30	0.269	17.94	710
G44	301	30	0.270	17.86	600
G45	312	30	0.270	17.96	650
G46	283	30	0.239	18.06	600
G47	380	30	0.254	17.99	625
G48	234	30	0.268	18.14	765
G49	350	30	0.247	18.05	625
G51	247	30	0.263	17.89	755
G53	590	10	0.241	10.13	575
G54	351	30	0.251	17.87	635
G55	164	10	0.250	18.04	575
G56	137	10	0.252	18.09	595
G57	140	10	0.251	18.10	633
G58	139	10	0.256	18.05	638

Nominal Concentration : 0.250 torr

Nominal Velocity : 18.0 m/s

Area of Deposition : 2,200 mm²

Run No.	Weight of deposit, mg.	Run time, min.	Salt conc. torr.	Velocity, m/s	Temperature at forward Stagnation Point, °C
C59	132	10	0.237	18.01	668
C60	110	10	0.241	18.11	698
C61	113	10	0.238	18.28	735
C62	0	10	0.259	18.03	805
C63	115	10	0.255	18.03	705
C64	87	10	0.256	18.16	645
C65	62	10	0.244	17.96	755
C66	73	10	0.255	17.83	644
C67	97	10	0.260	17.81	775
C68	128	10	0.261	18.14	730
C69	120	10	0.255	18.31	675
C70	120	10	0.258	17.91	750
C72	12	10	0.267	17.85	795

Nominal Concentration : 0.055 torr

Nominal Velocity : 10.5 m/s

Area of Deposition : 2,200 mm²

Run No.	Weight of deposit, mg.	Run time, min.	Salt conc. torr.	Velocity, m/s	Temp. at forward Stagnation Point, °C	$\frac{\text{Weight}}{\text{Time} \cdot \text{Conc} \cdot (\text{Velocity})^{\frac{1}{2}}}$
(a)						
D55	34	50	0.056	10.98	570	3.66
D56	33	50	0.052	10.95	590	3.84
D58	32	50	0.054	10.83	640	3.59
D59	34	50	0.056	10.64	625	3.72
(b)						
D77	15	50	0.054	10.57	710	1.72
D75	6	50	0.052	10.71	720	0.72
D76	5	50	0.057	10.68	735	0.54

Nominal Concentration : 0.055 torr

Nominal Velocity : 18.0 m/s

Area of Deposition : 2,200 mm²

Run No.	Weight of deposit, mg.	Run time, min.	Salt conc. torr.	Velocity, m/s	Temp. at forward Stagnation Point, °C	$\frac{\text{Weight}}{\text{Time} \cdot \text{Conc.} \cdot (\text{Velocity})^{\frac{1}{2}}}$
(a)						
D105	35	40	0.050	18.8	600	4.03
D106	33	40	0.049	19.0	645	3.85
(b)						
D107	16	30	0.048	18.6	690	2.56
D109	30	40	0.047	18.8	690	3.66
D111	12	40	0.048	19.0	715	1.43
D110	5	40	0.049	18.7	725	0.59
D108	4	40	0.049	18.7	730	0.47

Nominal Concentration : 0.055 torr

Nominal Velocity : 30.0 m/s

Area of Deposition : 2,200 mm²

Run No.	Weight of deposit, mg.	Run time, min.	Salt conc. torr.	Velocity, m/s	Temp. at forward Stagnation Point, °C	$\frac{\text{Weight}}{\text{Time} \cdot \text{Conc.} \cdot (\text{Velocity})^{\frac{1}{2}}}$
D119	31	30	0.048	29.3	610	3.97
D120	30	30	0.048	30.3	640	3.78
D122	33	30	0.048	29.9	610	4.18

D121	21	30	0.048	30.0	690	2.65
D124	7	30	0.048	30.7	720	0.88
D123	2	30	0.048	30.3	730	0.25

Nominal Concentration: 0.110 torr

Nominal Velocity : 10.5 m/s

Area of Deposition : 2,200 mm²

Run No.	Weight of deposit, mg.	Run time, min.	Salt conc. torr.	Velocity m/s	Temp. at forward Stagnation Point, °C	$\frac{\text{Weight}}{\text{Time} \cdot \text{Conc.}^{\frac{1}{2}} (\text{Velocity})^{\frac{1}{2}}}$
(a)						
D14	29	25	0.083	11.0	600	4.20
D26	37	30	0.101	10.6	690	3.74
D36	39	30	0.110	10.8	560	3.60
D37	31	25	0.108	10.9	600	3.47
D38	31	25	0.106	10.9	650	3.55
D39	32	25	0.105	10.6	600	3.70
D40	32	25	0.114	10.6	650	3.46
D49	31	25	0.105	10.9	675	3.56
D51	33	25	0.106	11.0	625	3.75
D139	30	25	0.100	10.5	560	3.71
D140	38	30	0.113	9.5	635	3.63
D141	28	20	0.118	8.9	525	3.99
D142	28	20	0.107	9.6	520	4.20
D143	34	25	0.107	9.9	600	4.03
D144	47	30	0.133	9.8	630	3.77
(b)						
D47	29	25	0.108	10.7	680	3.29
D43	29	25	0.120	10.8	695	2.94
D42	23	25	0.108	10.8	700	2.59
D46	18	25	0.108	10.9	715	2.02
D50	20	25	0.109	10.7	715	2.25
D52	7	25	0.107	10.9	720	0.79

Cont'd...

Nominal Concentration : 0.110 torr

Nominal Velocity : 10.5 m/s

Area of Deposition : 2,200 mm²

Run No.	Weight of deposit, mg.	Run time, min.	Salt conc. torr.	Velocity m/s	Temp. at forward Stagnation Point, °C	$\frac{\text{Weight}}{\text{Time} \cdot \text{Conc.} \cdot \text{Velocity}^{\frac{1}{2}}}$
D53	17	25	0.114	10.7	720	1.82
D41	8	25	0.112	10.7	725	0.87
D44	8	25	0.103	10.9	725	0.94
D54	11	25	0.105	10.6	725	1.28
D45	6	25	0.106	11.0	740	0.68
D57	5	25	0.113	10.9	745	0.53
D48	2	25	0.105	10.8	750	0.23

Nominal Concentration : 0.110 torr

Nominal Velocity : 18.0 m/s

Area of Deposition : 2,200 mm²

Run No.	Weight of deposit, mg.	Run time, min.	Salt conc. torr.	Velocity m/s	Temp. at forward Stagnation Point, °C	$\frac{\text{Weight}}{\text{Time} \cdot \text{Conc.} \cdot \frac{1}{2} (\text{Velocity})}$
(a)						
D78	46	25	0.120	19.4	580	3.49
D79	50	25	0.132	18.8	590	3.51
D80	52	25	0.128	19.0	625	3.73
D81	52	25	0.132	18.9	625	3.65
D82	49	25	0.127	18.8	650	3.57
D83	52	25	0.133	18.9	645	3.62
D84	32	15	0.134	18.6	675	3.69
D86	37	20	0.117	19.2	655	3.61
(b)						
D90	34	20	0.138	18.5	700	2.85
D96	34	20	0.127	18.5	705	3.11
D93	26	20	0.121	18.9	715	2.48
D97	31	20	0.121	18.7	715	2.96
D87	24	20	0.125	19.0	725	2.20
D88	23	20	0.125	18.6	725	2.14
D89	21	20	0.119	19.0	735	2.02
D94	19	20	0.124	18.8	735	1.76
D92	15	20	0.126	18.5	740	1.38
D91	8	20	0.122	18.7	750	0.76
D95	7	20	0.127	18.8	760	0.64

Nominal Concentration : 0.110 torr

Nominal Velocity : 30.0 m/s

Area of Deposition : 2,200 mm²

Run No.	Weight of deposit, mg.	Run time, min.	Salt conc. torr.	Velocity m/s	Temp. at forward Stagnation Point, °C	$\frac{\text{Weight}}{\text{Time} \cdot \text{Conc} \cdot \frac{1}{2}} \cdot \text{Velocity}$
(a)						
D112	32	15	0.104	30.9	620	3.70
D113	32	14	0.103	31.3	640	3.95
D114	36	15	0.107	31.5	655	4.02
(b)						
D115	31	15	0.108	31.4	690	3.41
D118	12	15	0.106	31.2	730	1.35
D117	2	15	0.106	31.3	750	2.25
D116	0	15	0.102	31.5	760	0.00

Nominal Concentration : 0.250 torr

Nominal Velocity : 10.5 m/s

Area of Deposition : 2,200 mm²

Run No.	Weight of deposit, mg.	Run time, min.	Salt conc. torr.	Velocity m/s	Temp. at forward Stagnation Point, °C	Weight Time. Conc. ^{1/2} (Velocity) ^{1/2}
(a)						
D6	29	10	0.266	10.8	600	3.32
D7	31	10	0.294	10.7	650	3.16
D10	27	10	0.254	10.7	655	3.25
D22	40	15	0.241	10.8	625	3.37
D29	36	10	0.274	11.0	580	3.95
D31	33	10	0.291	10.8	590	3.45
D32	37	10	0.290	10.8	580	3.89
D60	35	10	0.288	11.3	610	3.64
D61	34	10	0.280	11.2	605	3.63
D64	32	10	0.261	11.0	630	3.71
D65	31	10	0.245	10.9	675	3.85
D67	30	10	0.247	10.8	675	3.71
D147	46	15	0.272	10.3	685	3.51
D148	47	15	0.281	9.9	685	3.35
D149	49	15	0.266	10.5	615	3.78
D150	66	20	0.271	10.3	625	3.80
D151	40	11	0.273	10.5	680	4.11
D152	68	21	0.269	10.3	580	3.74
D153	66	20	0.289	9.8	610	3.64
D154	16	5	0.277	10.4	690	3.60
D155	65	20	0.310	8.9	590	3.52
D156	51	15	0.293	9.4	615	3.79

Cont'd...

Nominal Concentration : 0.250 torr

Nominal Velocity : 10.5 m/s

Area of Deposition : 2,200 mm²

Run No.	Weight of deposit, mg.	Run time, min.	Salt conc. torr.	Velocity m/s	Temp. at forward Stagnation Point, °C	$\frac{\text{Weight}}{\text{Time} \cdot \text{Conc.}^{\frac{1}{2}}}$ (Velocity)
D157	59	25	0.195	10.0	505	3.81
D158	63	25	0.195	10.5	515	4.00

(b)						
D71	28	10	0.244	10.7	700	3.51
D70	30	10	0.263	11.2	710	3.42
D17	21	10	0.280	10.9	715	2.27
D72	28	10	0.261	10.8	715	3.25
D27	31	15	0.246	10.7	720	2.57
D74	39	15	0.248	10.9	720	3.71
D15	27	15	0.238	11.0	725	2.32
D63	14	10	0.257	11.1	730	1.63
D66	21	10	0.274	10.9	735	2.33
D62	12	10	0.248	11.0	750	1.28
D19	17	15	0.270	10.8	755	1.28
D69	7	10	0.261	10.6	770	0.82
D24	8	15	0.253	10.5	775	0.65
D68	3	10	0.270	10.7	785	0.34

Nominal Concentration : 0.250 torr

Nominal Velocity : 18.0 m/s

Area of Deposition : 2,200 mm²

Run No.	Weight of deposit, mg.	Run time, min.	Salt conc. torr.	Velocity m/s	Temp. at forward Stagnation Point, °C	$\frac{\text{Weight}}{\text{Time} \cdot \text{Conc.}^{\frac{1}{2}}}$ (Velocity) ^{$\frac{1}{2}$}
(a)						
D98	44	10	0.274	18.6	635	3.73
D99	43	10	0.275	18.5	600	3.63
D100	44	10	0.259	18.9	645	3.91
D101	37	10	0.251	19.0	695	3.10
(b)						
D103	27	10	0.263	18.9	745	2.36
D104	22	10	0.263	19.1	760	1.91
D102	4	10	0.265	18.9	785	0.35

Nominal Concentration : 0.250 torr

Nominal Velocity : 30.0 m/s

Area of Deposition : 2,200 mm²

Run No.	Weight of deposit, mg.	Run time, min.	Salt conc. torr.	Velocity m/s	Temp. at forward Stagnation Point, °C	$\frac{\text{Weight}}{\text{Time} \cdot \text{Conc.}^{\frac{1}{2}} (\text{Velocity})^{\frac{1}{2}}}$
(a)						
D125	51	10	0.245	29.9	610	3.81
D126	51	10	0.244	30.5	650	3.79
D127	48	10	0.239	30.8	645	3.55
(b)						
D128	13	10	0.238	30.7	765	0.98

Nominal Concentration : 0.0055 torr

Nominal Velocity : 10.5 m/s

Area of Deposition : 2,200 mm²

Run No.	Weight of deposit, mg.	Run time, min.	Salt conc. torr.	Velocity m/s	Temp. at forward Stagnation Point, °C	$\frac{\text{Weight}}{\text{Time} \cdot \text{Conc.}^{\frac{1}{2}} (\text{Velocity})^{\frac{1}{2}}}$
(a)						
E32	20	135	0.0055	9.9	750	8.58
E60	21	120	0.0057	9.9	605	9.78
E62	19	120	0.0061	9.1	520	8.58
E63	39	210	0.0065	8.8	660	8.94
E67	37	210	0.0060	9.3	600	9.66
(b)						
E73	26	210	0.0059	10.4	835	6.72
E61	8	106	0.0058	9.8	850	2.52

Nominal Concentration : 0.0110 torr

Nominal Velocity : 10.5 m/s

Area of Deposition : 2,200 mm²

Run No.	Weight of deposit, mg.	Run time, min.	Salt conc. torr.	Velocity m/s	Temp. at forward Stagnation Point, °C	$\frac{\text{Weight}}{\text{Time} \cdot \text{Conc.}^{\frac{1}{2}}}$ (Velocity)
(a)						
E29	41	120	0.0106	9.7	650	10.32
E31	39	120	0.0106	9.6	605	9.96
E33	35	120	0.0106	9.6	755	8.88
E52	28	90	0.0099	10.1	650	9.90
E54	30	75	0.0098	10.9	800	12.24
E55	21	75	0.0106	9.9	710	8.40
E57	27	90	0.0101	9.9	525	9.48
E58	26	90	0.0099	10.7	825	8.94
E59	22	75	0.0107	10.1	800	8.76
(b)						
E53	18	90	0.0107	9.6	850	6.00
E51	14	120	0.0107	9.8	870	3.48
E56	16	120	0.0103	10.4	880	4.02

Nominal Concentration : 0.0250 torr

Nominal Velocity : 10.5 m/s

Area of Deposition : 2,200 mm²

Run No.	Weight of deposit, mg.	Run time, min.	Salt conc. torr.	Velocity m/s	Temp. at forward Stagnation Point, °C	$\frac{\text{Weight}}{\text{Time} \cdot \text{Conc.} \cdot \text{Velocity}^{\frac{1}{2}}}$
(a)						
E25	41	70	0.0254	10.0	550	7.20
E27	28	50	0.0270	9.6	705	6.72
E28	36	50	0.0268	9.6	650	8.52
E30	30	50	0.0268	9.6	588	7.26
E44	27	45	0.0273	9.7	600	7.14
E65	50	75	0.0260	10.2	650	7.74
E69	46	75	0.0252	10.6	620	7.98
E71	40	60	0.0259	10.1	700	8.10
(b)						
E50	20	60	0.0268	9.5	830	4.02
E47	29	60	0.0276	9.6	850	5.64
E26	24	70	0.0270	9.8	880	4.08
E45	15	45	0.0254	10.6	880	4.02
E46	12	60	0.0270	9.7	900	2.40

Nominal Concentration : 0.100 torr

Nominal Velocity : 10.5 m/s

Area of Deposition : 2,200 mm²

Run No.	Weight of deposit, mg.	Run time, min.	Salt conc. torr.	Velocity m/s	Temp. at forward Stagnation Point, °C	Weight Time · Conc. ^{-1/2} (Velocity) ^{1/2}
(a)						
E1	39	25	0.100	10.3	585	4.89
E2	40	25	0.100	10.6	700	4.92
E3	34	25	0.102	10.0	555	4.26
E7	39	25	0.106	10.1	600	4.67
E8	38	25	0.104	9.8	655	4.71
E9	38	25	0.101	10.2	705	4.77
E10	41	25	0.108	9.6	755	4.92
E11	38	25	0.102	10.0	555	4.77
E12	36	25	0.107	9.6	700	4.37
E13	37	25	0.107	9.7	605	4.45
E14	36	25	0.101	10.1	650	4.53
E15	40	25	0.106	9.8	675	4.83
E16	41	25	0.109	9.7	700	4.88
E17	38	25	0.104	10.0	575	4.67
E19	41	25	0.110	9.6	750	4.24
E20	38	25	0.106	9.7	545	4.66
E22	42	25	0.109	9.7	800	5.00
E64	37	25	0.101	10.0	655	4.63
E66	39	25	0.100	9.9	695	4.92
E68	39	25	0.108	9.5	720	4.68
E70	40	26	0.103	9.9	775	4.77
E72	49	30	0.100	10.3	590	5.10

Cont'd...

Nominal Concentration : 0.100 torr

Nominal Velocity : 10.5 m/s

Area of Deposition : 2,200 mm²

Run No.	Weight of deposit, mg.	Run time, min.	Salt conc. torr.	Velocity m/s	Temp. at forward Stagnation Point, °C	$\frac{\text{Weight}}{\text{Time} \cdot \text{Conc.} \cdot \frac{1}{2}}$ (Velocity)
(b)						
E23	32	25	0.107	9.7	855	3.84
E49	19	25	0.105	10.4	900	2.29
E24	13	25	0.109	9.3	955	2.11

Nominal Concentration : 0.0070 torr

Nominal Velocity : 10.5 m/s

Area of Deposition : 2,200 mm²

Run No.	Weight of deposit, mg.	Run time, min.	Salt conc. torr.	Velocity m/s	Temperature at forward Stagnation Point, °C
F9	15	165	0.0069	9.8	540
F10	16	180	0.0072	9.3	565
F12	4	150	0.0070	10.0	625
F13	10	150	0.0070	9.4	600
F14	11	150	0.0068	9.8	580
F15	5	150	0.0071	9.5	680
F16	5	150	0.0072	9.5	645
F17	7	120	0.0061	10.2	545
F18	10	180	0.0069	9.4	575
F19	2	135	0.0063	10.3	655
F20	13	150	0.0075	8.8	550
F29	9	180	0.0070	9.2	650
F30	32	180	0.0065	9.9	520
F31	25	180	0.0069	9.2	550
F33	9	180	0.0055	12.3	605
F35	9	180	0.0067	9.8	610

Nominal Concentration : 0.0140 torr

Nominal Velocity : 10.5 m/s

Area of Deposition : 2,200 mm²

Run No.	Weight of deposit, mg.	Run time, min.	Salt conc. torr.	Velocity, m/s	Temperature at forward Stagnation Point, °C
F21	15	105	0.0130	10.2	575
F22	3	120	0.0147	9.2	655
F23	7	150	0.0142	9.5	650
F24	8	120	0.0140	9.5	625
F25	12	120	0.0139	9.3	600
F26	3	60	0.0140	9.3	635
F27	8	120	0.0143	9.3	615
F28	15	120	0.0146	8.6	560
F40	30	125	0.0182	9.9	585

Nominal Concentration : 0.0300 torr

Nominal Velocity : 10.5 m/s

Area of Deposition : 2,200 mm²

Run No.	Weight of deposit, mg.	Run time, min.	Salt conc. torr.	Velocity, m/s	Temperature at forward Stagnation Point, °C
F1	27	50	0.0262	10.1	540
F2	19	50	0.0321	8.0	615
F3	26	50	0.0274	9.7	560
F6	14	50	0.0270	9.9	620
F8	18	50	0.0293	9.1	560
F32	20	45	0.0264	9.7	535
F34	7	45	0.0258	10.3	610
F36	27	120	0.0317	10.2	620
F37	31	120	0.0346	9.1	600
F38	48	120	0.0335	9.0	550
F39	50	120	0.0341	9.1	520

Nominal Concentration : 0.0560 torr

Nominal Velocity : 10.5 m/s

Area of Deposition : 2,200 mm²

Run No.	Weight of deposit, mg.	Run time, min.	Salt conc. torr.	Velocity, m/s	Temperature at forward Stagnation Point, °C
F4	28	30	0.0582	9.1	555
F5	21	30	0.0553	9.6	600
F7	23	30	0.0538	9.7	570
F11	16	30	0.0542	9.9	655

Nominal Concentration : 0.035 torr

Nominal Velocity : 18.0 m/s

Area of Deposition : 2,200 mm²

Run No.	Weight of deposit, mg.	Run time, min.	Salt conc. torr.	Velocity m/s	Temp. at forward Stagnation Point, °C	$\frac{\text{Weight}}{\text{Time} \cdot \text{Conc.} \cdot \frac{1}{2}}$ (Velocity)
(a)						
G21	13	20	0.035	17.6	595	4.45
G22	25	40	0.036	17.1	595	4.20
G23	28	40	0.036	17.3	555	4.75
G72	19	30	0.035	17.6	520	4.33
G73	18	30	0.034	18.5	580	4.15
G74	20	30	0.034	18.2	620	4.83
G75	18	30	0.034	18.3	580	4.11
G76	18	30	0.034	18.7	640	4.03
G80	20	30	0.034	18.5	580	4.59
(b)						
G79	15	30	0.032	19.3	640	3.57
G77	8	30	0.032	19.1	670	1.93
G25	3	33	0.034	17.8	685	0.69
G78	5	30	0.033	19.0	685	1.17

Nominal Concentration : 0.065 torr

Nominal Velocity : 10.5 m/s

Area of Deposition : 2,200 mm²

Run No.	Weight of deposit, mg.	Run time, min.	Salt conc. torr.	Velocity m/s	Temp. at forward Stagnation Point, °C	$\frac{\text{Weight}}{\text{Time} \cdot \text{Conc.}^{\frac{1}{2}}}$ (Velocity) ^{$\frac{1}{2}$}
(a)						
G1	39	45	0.065	9.8	580	4.32
G2	42	45	0.064	9.9	595	4.63
G5	43	45	0.062	10.2	630	4.86
G7	40	45	0.070	8.8	550	4.33
G11	40	45	0.068	9.8	525	4.19
G13	42	45	0.065	9.9	600	4.68
G53	30	30	0.059	10.2	570	5.04
G55	28	30	0.063	9.7	580	4.71
G68	27	30	0.062	9.9	550	4.60
G69	29	30	0.063	9.7	510	4.86
G70	28	30	0.063	9.7	540	4.74
(b)						
G71	23	30	0.063	9.9	640	3.87
G3	41	45	0.065	9.8	665	4.35
G9	25	45	0.064	10.1	675	2.71
G4	26	45	0.065	10.1	700	2.83
G12	11	45	0.065	9.8	700	1.21
G54	3	30	0.062	10.1	700	0.50
G56	8	45	0.060	10.2	700	0.94
G57	3	40	0.061	10.5	710	0.38

Nominal Concentration : 0.065 torr

Nominal Velocity : 18.0 m/s

Area of Deposition : 2,200 mm²

Run No.	Weight of deposit, mg.	Run time, min.	Salt conc. torr.	Velocity m/s	Temp. at forward Stagnation Point, °C	$\frac{\text{Weight}}{\text{Temp. Conc.}^{\frac{1}{2}} (\text{Velocity})^{\frac{1}{2}}}$
(a)						
G24	28	20	0.071	17.3	555	4.77
G26	26	20	0.072	17.5	635	4.41
G28	28	20	0.069	18.4	645	4.78
G31	25	20	0.069	18.5	645	4.23
G32	29	20	0.068	18.2	590	5.01
G34	41	30	0.067	18.9	625	4.71
G35	33	30	0.070	18.2	620	3.77
(b)						
G27	15	20	0.070	17.4	680	2.60
G33	17	20	0.068	18.8	690	1.92
G30	15	30	0.070	18.9	700	1.66
G29	4	20	0.069	18.7	705	0.67
G36	7	30	0.068	18.6	710	0.80

Nominal Concentration : 0.125 torr

Nominal Velocity : 10.5 m/s

Area of Deposition : 2,200 mm²

Run No.	Weight of deposit, mg.	Run time, min.	Salt conc. torr.	Velocity m/s	Temp. at forward Stagnation Point, °C	Weight
						Time. Conc. $\cdot \frac{1}{2}$ (Velocity) $\frac{1}{2}$
(a)						
G14	41	20	0.139	8.9	520	4.92
G15	38	20	0.125	10.0	600	4.83
G16	38	20	0.125	10.1	575	4.81
G17	38	20	0.124	10.1	570	4.89
G18	39	20	0.120	10.6	620	5.04
G20	38	20	0.123	10.5	640	4.80
G38	56	30	0.124	10.3	600	4.74
G42	39	20	0.126	9.5	550	5.04
G46	37	20	0.129	9.5	520	4.65
G50	39	20	0.131	9.3	545	5.07
G51	42	20	0.132	9.1	555	5.28
G66	50	25	0.120	10.0	550	5.30
G67	52	25	0.121	10.2	590	5.40
(b)						
G47	50	30	0.122	10.5	655	4.21
G40	54	30	0.130	9.9	670	4.41
G48	46	30	0.124	10.3	675	3.87
G43	37	30	0.123	10.6	690	3.07
G49	41	30	0.122	10.1	690	3.53
G41	24	30	0.128	9.6	700	2.02
G37	25	30	0.124	10.4	710	2.08
G45	24	30	0.125	10.2	715	2.00
G39	19	30	0.127	10.2	720	2.16
G19	6	20	0.122	10.5	725	0.76
G44	8	30	0.121	10.5	730	0.68

Nominal Concentration : 0.250 torr

Nominal Velocity : 10.5 m/s

Area of Deposition : 2,200 mm²

Run No.	Weight of deposit, mg.	Run time, min.	Salt conc. torr.	Velocity m/s	Temp. at forward Stagnation Point, °C	$\frac{\text{Weight}}{\text{Time} \cdot \text{Conc}^{\frac{1}{2}} (\text{Velocity})^{\frac{1}{2}}}$
(a)						
G84	39	10	0.259	9.5	625	4.88
G85	38	10	0.257	9.2	520	4.89
G86	43	10	0.261	9.5	560	5.34
G87	40	10	0.259	9.4	605	5.04
(b)						
G88	31	10	0.252	9.8	680	3.93
G58	20	15	0.242	10.0	720	1.74
G59	15	15	0.255	9.8	735	1.26
G60	12	15	0.235	10.7	745	1.04
G61	17	20	0.243	10.6	745	1.07